Analysis of Multipath Channel Reduction Models for the Testing of Realistic GNSS Receivers

Florian Ribaud

To cite this version:

Florian Ribaud. Analysis of Multipath Channel Reduction Models for the Testing of Realistic GNSS Receivers. Networking and Internet Architecture [cs.NI]. Institut National Polytechnique de Toulouse - INPT, 2016. English. NNT : 2016INPT0105 . tel-01692083v2

HAL Id: tel-01692083
https://hal.science/tel-01692083v2

Submitted on 26 Oct 2023

THÈSE

En vue de l'obtention du

DOCTORAT DE L'UNIVERSITÉ DE TOULOUSE

Délivré par :

Institut National Polytechnique de Toulouse (INP Toulouse)

Discipline ou spécialité :

Réseaux, Télécommunications, Systèmes et Architecture

Présentée et soutenue par :

M. FLORIAN RIBAUD
le lundi 5 décembre 2016

Titre :

Analysis of Multipath Channel Reduction Models for the Testing of Realistic GNSS Receivers

---

Ecole doctorale :

Mathématiques, Informatique, Télécommunications de Toulouse (MITT)

Unité de recherche :

Département d'Ingénierie de Systèmes Complexes (DISC-ISAE)

Directeur(s) de Thèse :

M. OLIVIER JULIEN
M. FERNANDO PEREZ FONTAN

Rapporteurs :

M. CLAUDE OESTGES, UNIVERSITE CATHOLIQUE DE LOUVAIN
M. TERRY MOORE, THE UNIVERSITY OF NOTTINGHAM GB

Membre(s) du jury :

M. CLAUDE OESTGES, UNIVERSITE CATHOLIQUE DE LOUVAIN, Président
M. FERNANDO PEREZ FONTAN, UNIVERSIDAD DE VIGO, Membre
M. OLIVIER JULIEN, ECOLE NATIONALE DE L'AVIATION CIVILE, Membre
M. SEBASTIEN ROUGERIE, CENTRE NATIONAL D'ETUDES SPATIALES CNES, Membre

Remerciements

Bien des personnes ont joué des rôles importants durant les trois dernières années que je viens de passer en tant que doctorant de l'ONERA, au service DEMR. Dans un premier, il faudra remercier toutes les personnes impliquées de près ou de loin dans la rédaction du présent manuscrit et dans le travail de thèse qu'il contient. Egalement, le support moral assuré par nombre de personnes de mon entourage devra être gratifié.

Dans un premier temps, j'aimerais remercier toute l'unité RCP du service, pour son accueil et son environnement de travail cent pour cent compatible avec la recherche, à travers M. Laurent Castanet (chef de l'unité RCP) et M. Florent Christophe (directeur du service DEMR). J'aimerais également accorder une mention spéciale à Mme Corinne De Pablo, secrétaire du service DEMR, dont les compétences et la patience m'ont soustrait à bien de misères administratives. Enfin, je ne dois pas oublier de citer Xavier Boulanger, qui a accepté de recueillir un doctorant dans son bureau dès le début de ma thèse, et durant les trois années suivantes dans une ambiance très agréable.

En ce qui concerne le travail de thèse, il est très important de remercier toute mon équipe d'encadrement, à commencer par mon directeur de thèse M. Olivier Julien de l'ENAC pour ses précieuses recommandations techniques ou administratives. Egalement, je remercie M. Joël Lemorton, mon encadrant ONERA, pour sa patience et ses conseils durant les trois années. Sans oublier mon co-directeur de thèse, M. Fernando Perez-Fontan de l'université de Vigo, avec qui il a été très agréable de travailler durant ses séjours à Toulouse.

Enfin, c'est à Mehdi Ait-Ighil et à Sébastien Rougerie que je dois l'aide la plus précieuse. Mehdi a pris part à l'encadrement de la thèse en tant que spécialiste du simulateur SCHUN (qu'il a lui-même implémenté). Sans ses conseils très avisés et sa patience tout au long des trois ans, cette thèse n'aurait peut-être jamais vu le jour. Sébastien a joué son rôle d'encadrant côté CNES à merveille, et bien plus encore. Je dois le remercier particulièrement pour ses indications concernant l'algorithme d'optimisation SAGE. Egalement, je remercie Mehdi et Sébastien pour la patience qu'ils ont mise dans la relecture de mon manuscrit. Il me faut également remercier M. Frédéric Lacoste (CNES) pour l'encadrement de la première année, et de m'avoir donné l'idée et l'envie de me lancer dans une thèse durant mon PFE effectué au CNES.

J'ai bénéficié d'un soutien moral considérable de la part de mes collègues doctorants, en particulier ceux qui m'ont aidé à rythmer les activités extra-professionnelles, à coups de matchs de foot, bars et paillotes (le week-end et pas seulement …). Les vrais se reconnaitront. Enfin, qu'auraient été ces trois ans sans mes fidèles colocs, qui ont partagé la vie de tous les jours d'un thésard. Grâce à Geoffrey C., Ghislain R., Jean-Elie D. et Hugo J., les bons comme les mauvais moments étaient toujours festifs. Merci bien sûr à tous nos amis qui ont partagé ces longues soirées, que je ne citerai pas de peur d'oublier quelqu'un.

Enfin, merci à mes parents, pour leur soutien permanant durant mes études. Merci également à mes frères, en particulier ceux qui se sont déplacés pour assister à ma soutenance.

Merci infiniment à tous !!

Allez le RC Strasbourg !

Florian

Table of contents

List of Figures

List of Tables

List of Abbreviations

3CM	Three Components Model
BOC	Binary Offset Carrier
CDF	Cumulative Density Function
CRIME	Channel Reduction by Independent Markov Process
CS	Chip Spacing
DLL	Delay Lock Loop
DOA	Direction of Arrival
EMLP	Early Minus Late Power
ESPRIT	Estimation of Signal Parameters via Rotational Invariance Techniques
GNSS	Global Navigation Satellite System
GO	Geometrical Optic
GPS	Global Positioning System
LHCP	Left Handed Circular Polarization
LMS	Land Mobile Satellite
LOS	Line Of Sight
ML	Maximum Likelihood
MOM	Method of Moments
MUSIC	Multiple Signal Classification
NLOS	Non Line of Sight
PDF	Probability Density Function
PLL	Phase Lock Loop
PO	Physical Optic
RHCP	Right Handed Circular Polarization
RNG	Random Number Generator
SAGE	Space Alternating Generalized Expectation Maximization
SCHUN	Simplified Channel for Urban Navigation
TDL	Tap Delay Line
UTD	Universal Theory of Diffraction

Introduction

a. PhD thesis background and motivations

The need of an unmasked and accurately synchronized signal to provide navigation information takes a major advantage of the large areas covered by the satellites in MEO (*Medium Earth Orbit*). Recently, the innovative steps in the navigation domain mainly concern the design of more complex signal models. They aim at improving the accuracy of the navigation information and improving the robustness of the system to signal perturbations, like interferences, noise or multipath for example. The GALILEO European project has been conducted in that prospect. It is supposed to be fully deployed by 2020.

Nowadays, the satellite navigation development is challenged by the increasing interest in high precision positioning in urban areas. The density of obstacles may lead to signal perturbations of the signal through the possible loss of LOS (*Line Of Sight*) or superposition of multipath to the useful signal. Many applications could benefit from improved urban positioning. They include LBS (*Location Based Services*), ITS (Intelligent Transport Systems), augmented reality, vehicle lane control, advanced rail signaling and navigation for the blind. Therefore, the multipath issue for GNSS receivers (in particular for future Galileo or multi-constellation receivers) is of utmost interest. The use of this kind of receivers in more and more challenging environments (for example urban areas) necessitates to deeply investigate the GNSS performances of the system in real environment, as well as assessing the adequate mitigation techniques.

The multipath phenomenon is indeed one of the most serious threats to accuracy in GNSS navigation. Multipath is the phenomenon whereby a signal arrives at a receiver with multiple paths due to reflection and diffraction of the electromagnetic waves. The multipaths take longer paths to the antenna than the direct signal, resulting in the distortion of the carrier and code of the GNSS signal. Hence a degradation of the performance in the navigation accuracy. Multipath effect is predominant in constrained environments such as urban canyons, as the user's GNSS antenna is surrounded by many reflecting structures (walls, trees, other vehicles, etc.). Therefore, multipaths will degrade the performances related to the GNSS applications. In addition, for pedestrian or vehicular receivers, the multipath channel is mainly caused by the environment and is then totally unpredictable and hard to model. In some cases, the multipath can be due to the reflections around the platform the GNSS antenna is located on. This is the case for sensor stations. Other specific configurations may occur, where the characteristics of the direct path or the predominant multipaths vary. This is also the case for GNSS receivers located under a vegetation layer, where the direct path is attenuated by the canopy. Some of the characteristics of multipaths may also depend on the type of users (static or dynamic), as it is the case for Doppler properties. In all these cases, the multipath channel is described by the impulse response that consists in the combination of several echoes characterized by their amplitude, phase, delay, Doppler shift and direction of arrival.

Therefore, wide-band channel models have been implemented in parallel to the development of the GNSS sector. They aim at synthesizing realistic environments and put the new receivers to test. Two major channel modelling approaches have been designed, namely statistical and deterministic approaches. As many multipath configurations may be encountered, it remains difficult to draw statistical or empirical models versatile and accurate in the same time. Furthermore, the geometry of the environment can be complex (for example in urban areas or for sensor stations) which results in high computation loads if deterministic models are used. More recent hybrid models mixing statistical and physical modules showed to be a good tradeoff between practical computational effort and realistic multipath channels. In particular, the SCHUN simulator (Simplified Channel for Urban

Navigation), developed at the ONERA by Mehdi Ait-Ighil and its PhD supervising team [AIT 12] has shown to be able to model the LOS and multipath channel through the virtual city concept. Its accuracy is close to purely physical models, with computational performance close to real-time.

However, the large number of echoes synthesized by the model (several thousand per impulse response snapshot) limits its utilization for the testing of navigation systems. Indeed, these models are used to assess the performance of GNSS receivers in multipath environment. In particular, the Galileo system is assessed to test the specificities of the signal (BOC/MBOC modulation, long and tiered codes) for multi-constellation and diversity techniques. Today, multi-frequency techniques as well as diversity antenna techniques provide the GNSS positioning with high precision in urban areas. The introduction of Galileo and the modernization of the GNSS constellation give rise to new opportunities for the development of these mitigation techniques which take advantage of multi-frequency characteristics. Nevertheless, the definition of new algorithms using several frequencies requires a good knowledge of the parameters of the channel in order to take benefit of possible information redundancies.

Then, the multipath models have to be integrated either in software or hardware simulators. The testing of both software and hardware receivers suffer from large impulse responses. For software simulators, the computing time may be critical. For hardware simulators, the generation of each multipath signal requires an additional channel, then increasing the complexity and cost of the equipment. This is the reason why the models have to be simplified. The reduction techniques have to be applied to the channel model in order to limit the number of echoes without decreasing too much the representativeness of the channel in terms of receiver’s performance.

b. PhD thesis objectives

For that reason, it has been decided to focus this thesis on the analysis of solutions to decrease the number of echoes in the channel impulse responses, all by preserving the original accuracy of SCHUN to model the effect of realistic environments on the pseudo-range error of the receiver. In the scope of [AIT 13], it has been decided to implement a reduction technique making the SCHUN model adaptable to the constraints of hardware signal emulation, respecting these accuracy specifications, with practical implementation facilities (in terms of computation time essentially).

The approach chosen to address this problem can be divided in two main steps. On one side, different reduction methods will be designed and implemented. On the other side, they will be compared through the criterion of the preservation of the pseudo-range error. Three different reduced channel models have been considered. Among these models, two main approaches can be identified. Indeed, the two methods referred to as Weighted Clustering and Statistical method are dedicated to the preservation of the channel characteristics in terms of power-delay profile and/or Doppler spectrogram. They rely on the aggregation of multipaths and the statistical selection of multipaths respectively. Both methods are low demanding in terms of computational resource. The parametric optimization approach is dedicated to the conservation of the open loop discriminator error. It relies on an optimization process, heavier in terms of computational costs. The comparison of these approaches according to the pseudo-range error preservation compares the performance of low demanding methods relatively to heavier optimization processes.

c. PhD thesis outline

Chapter 1 introduces the problem of modelling the multipath channel. The first section presents different channel models extracted from the literature. They are divided in three approaches: statistical, deterministic and physical-statistical models. Then, a section has been dedicated to the presentation and the validation of a specific hybrid model, namely SCHUN (*Simplified Channel for Urban Navigation*). This simulator will be used as the reference channel model in the following of this thesis. Finally, the limitations to adapt these channel outputs to the testing of GNSS receivers motivates the channel reduction.

Chapter 2 focusses on the reduction of the multipath channel by aggregating multipaths. The question addressed all along this chapter is: “which parameters have to be taken into account to aggregate the echoes?”, and “which algorithm would be the most efficient in terms of preservation of the characteristics of the original channel and in terms of computation time”. As a preliminary study, a simple selection method on the multipath power has been performed. Then, in order to optimize the preservation of the delay spread, different Tap Delay Line models have been implemented. In the following sections, the Doppler shift criterion has been added to the aggregation process. Different clustering techniques have been implemented for that purpose. Finally, the method referred to as Weighted Clustering has been proposed. It aims at preserving the characteristics of the original channel with a low computational effort. It consists in aggregating the closest multipaths in terms of delay and Doppler shift, so as to improve the stability of the echoes of the reduced channel.

Chapter 3 presents the implementation of a parametric optimization process. It aims at optimizing the parameters of the reduced channel (delay, complex amplitude and Doppler shift of the multipaths) so as to conserve the channel correlation function. After introducing the cost function related to this process, the general architecture of the SAGE algorithm chosen to address this problem is presented. A particular attention is brought to the Doppler resolution of the algorithm, which has a strong impact on its performance. More specifically, the optimal tradeoff between Doppler resolution and number of echoes in the reduced channel is investigated, in order to implement an optimal parameterization method.

Chapter 4 investigates the possibility to draw multipaths of the reduced channel from their statistical distribution. It will be considered that each echo follows a first-order Markov process. A critical analysis of the method CRIME presented in [Schu 14] is performed. In particular, the technique used compute the amplitudes and delays is criticized. In that scope, an innovative semi-statistical reduction method is proposed. According to this new method, the delays of the echoed are drawn statistically, while the complex amplitude is deduced from the impulse response continuous power-delay profile.

Chapter 5 performs the comparison of the reduction methods presented in chapters 2, 3 and 4 in terms of preservation of the pseudo-range error. The comparison process is restricted to the Weighted Clustering, the parametric optimization method and the modified statistical method. First, a state-of-the-art of the different comparison frameworks of the literature is presented. To initiate the comparison, the only impact of the reduction methods on the open loop discriminator error is considered. From these results, a hierarchy among the reduction methods is established. This simulation is transposed to different positions of the emitter satellite and different numbers of echoes in the reduced channels, in order to emphasize their possible impact on this hierarchy. Then, the impact of the tracking loops of the receiver has been investigated, using the receiver simulator GeneIQ, briefly presented in this chapter 5. From that comparison, another hierarchy is established. Different signal parameters (modulation and bandwidth) have been considered to widen the scope of these results. A particular attention is brought to the impact of the elevation of the emitter satellite on this hierarchy, which turns out to have a significant impact on the performance of the reduction methods.

Finally, the conclusion of this thesis decides which method is the most well suited to address the channel reduction problem, putting into balance the computational resource required by each approach.

d. PhD thesis contributions

This thesis investigates the most efficient method to address the channel reduction problemat. All along this study, different results will be presented:

- Implementation of the Clustering Weighted method, which shows a very good efficiency in terms of Doppler and delay conservation with low computational effort. The pseudo-range error caused by the original channel is also well preserved (almost as well as parametric optimization methods).
- Development of a method to parametrize the reduced channel multipaths so as to preserve the channel autocorrelation function, using the SAGE algorithm. Determination of the ideal tradeoff between Doppler resolution of the algorithm and number of echoes in the reduced channel to improve the algorithm's efficiency.
- Implementation of a statistical method to draw the reduced channel multipaths from a specific stochastic process, adapting the model of [Schu 14] the constraint of larger impulse responses.
- Comparison of the three aforementioned approaches according to the preservation of the pseudo-range error of the receiver. Different signal parameters and tracking configurations have been considered. The most efficient approach is identified, taking the computational load into balance.
- Implementation of the discriminator open-loop error, to investigate the efficiency of the reduction methods with a validity index easy to implement. Development of a close formula to compute it from the impulse response parameters. Validation of this criterion comparing its results to those of more elaborate models of GNSS receiver.

These results have been presented at the occasion of international workshops. The following papers have been elaborated and presented:

F. Ribaud, M. Ait-Ighil, J. Lemorton, O. Julien, F. Perez-Fontan, F. Lacoste, S. Rougerie, “Comparison of different methods to aggregate multipaths for GNSS receivers performance assessment“, ENC 2015, Bordeaux, France.

F. Ribaud, M. Ait-Ighil, S. Rougerie, J. Lemorton, O. Julien, F. Pérez-Fontan, “Reduction of the Multipath Channel Impulse Response for GNSS applications”, EuCAP 2016, Davos, Switzerland.

F. Ribaud, M. Ait-Ighil, S. Rougerie, J. Lemorton, O. Julien, F. Pérez-Fontan, “Reduced multipath channel modelling preserving representative GNSS receiver testing”, ION GNSS+2016, Portland, USA.

Chapter 1

1. Modeling of the LMS channel and introduction to the problem of channel reduction

This chapter has been designed to introduce the channel reduction problem addressed in this thesis and to present the different concepts useful to lead this study. The first section will present the channel models of the literature, focussing on urban environments. Both statistical and deterministic approaches will be presented with a critical analyse of each method, in order to justify the use of hybrid (both statistical and physical) approaches. The second section will be devoted to the presentation of the SCHUN (Simplified CHannel for Urban Navigation) channel simulator. It has been used all along this thesis to generate the reference channels (the reduction methods will be applied on these impulse responses). Finally, the third section will illustrate the constraints caused by the large number of multipaths synthesized by SCHUN, from the point of view of a GNSS receiver. This section will introduce the necessity to implement reduction methods to reduce the reference impulse responses, which is the main work of this thesis.

1.1. Different approaches to model the LMS channel

A significant number of urban channel models have already been proposed. They can be grouped in three major families, namely the statistical, deterministic and hybrid physical-statistical models. The presentation of these different families will constitute the three subsections of this section. The major difference between statistical and deterministic approaches relies in the trade-off between accuracy, versatility and computational load of the methods. The hybrid physical-statistical approaches try to take benefit of the advantages of both approaches, while erasing their drawbacks.

The following sub-sections will distinguish the modelling of the environment itself from the computation of the interactions between the signal and the environment. Indeed, some channel models mix statistical distribution of the environment and deterministic computation of the channel parameters and vice-versa.

1.1.1. Statistical approaches

The statistical channel approaches consist in fitting empirical models on experimental data obtained during measurement campaigns. As a first approach of the problem, it can be mentioned the narrow-band models, which aim at reproducing the time-series of signal attenuation. However, such approaches can be shortcoming to simulate the shadowing effect. Therefore, the state oriented models have been introduced in the literature. They mainly rely on the Markov chain theory. The Markov states represent the different shadowing levels of the signal. However, the only consideration of the narrow band channel characteristics is not enough in GNSS navigation contexts. The multipaths have a strong impact on the positioning performance of the receiver. The modeling of the multipath amplitude, phase, delay and Doppler shift is of utmost interest for GNSS applications. Therefore, wide-band models have been implemented.

1.1.1.1. The narrow-band statistical models

The environment of the receiver has two major impacts on the channel narrow-band power: the shadowing and fast fading effects. It was already mentioned that the shadowing constitutes the signal blockage by canonical objects of the environment whereas the fast fading effect is due to the constructive or destructive combination of multipaths at the receiver antenna.

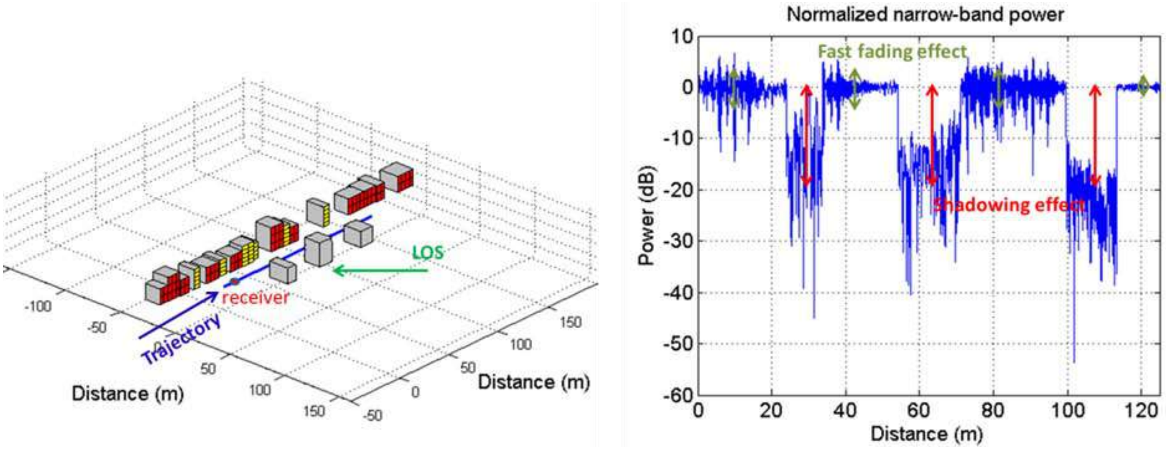

Figure 1.1 : Illustration of the shadowing and fast fading effects on the narrow-band power

Fig. 1.1 illustrates the impact of the fast fading and shadowing effects on the narrow-band power of the channel. The right plot represents the narrow-band power received by the GNSS receiver along its trajectory. This power is normalized by the nominal LOS power. The left plot represents the environment corresponding to this scenario. The narrow-band power has been computed by the SCHUN model, which will be detailed in section 1.2. The shadowing effect causes the power fading segments extended in time. They have been spotted by the red arrows and are due to the presence of buildings between the receiver and the incident signal. The three buildings in question are apparent on the left plot of Fig. 1.1. The fast fading effect causes the high-frequency attenuation. It has been spotted by green arrows.

The shadowing and the fast fading have distinct impacts on the time-series. Therefore, it is difficult to define a statistical distribution simulating jointly the shadowing and the fast fading. The merging models, like [Pere 01], consider the probability to be in LOS (Line Of Sight) or NLOS (Non Line of Sight) on one hand and the distribution of the fast fading effect on the other hand. This distribution depends on the LOS or NLOS condition. Among the most commonly used statistical models of the narrow-band channel, the Rayleigh and Rice distributions can be cited:

- The **Rayleigh** distribution is used to model the fast fading in NLOS conditions. The multipaths distorting the narrow-band channel power are supposed to be statistically independent in terms of delay and phase. Eq. 1.1 displays the density function associated to the Rayleigh distribution. It depends on the fast fading standard deviation σ, which is estimated from experimental data in a given environment. The variable r is referred to as the Rayleigh variable and corresponds to the norm of a complex vector whose real and imaginary parts are Gaussian distributions of mean 0 and standard deviation σ.

$$f(r) = \frac{r}{\sigma^2} e^{-r^2/2\sigma^2} \tag{1.1}$$

- The **Rice** distribution is used to model the fast fading effect on one side and the LOS component on the other side. Therefore it is used to model the effects of a multipath environment considering that a certain proportion of the direct path reaches the receiver. It is characterized by the Rice factor noted K, which represents the ratio between LOS and multipath power. Several methods have been developed to estimate this parameter from experimental data [Tepe 03]. Eq. 1.2 displays the density function of the Rice distribution, considering the Rice factor K and the standard deviation σ for the fast fading. Note that I_0 corresponds to the modified Bessel function of first kind and order zero.

$$f(r) = \frac{2(K+1)r}{\sigma^2} e^{-K-\frac{(K+1)r^2}{\sigma^2}} I_0(2r\sqrt{\frac{K(K+1)}{\sigma^2}}) \tag{1.2}$$

Those two distributions have been presented in this section because they are commonly used to model the narrow-band channel. However, other distributions can be used. Two examples will be cited hereafter to simulate the shadowing and fast fading effects according to a statistical approach (and eventually the design of the environment).

- The **Loo** distribution gives the possibility to tune both LOS and multipath components, using a lognormal distribution characterized by its mean and standard deviation (α, φ) and a Rayleigh distribution [Pere 01] respectively.

- The **log-normal** distribution is commonly used to characterize the environment, and more specifically the dimensions of the buildings or streets of the virtual cities. Such models allow the simulation of both LOS/NLOS and multipaths from a deterministic point of view. It will be detailed in the following sections.

As a conclusion, those models are designed to predict the coherent and incoherent fading effects considering a given state of LOS blockage. However, they are inadequate for environments with fast fading variations. Therefore, state-oriented models have been introduced.

1.1.1.2. The state oriented statistical models

The Markov chain approach has been developed because it is well suited to model the switch from one state of shadowing to another. The probability of transition defines a Markov chain with discrete time and discrete states. It means that the probability of fading at a given instant is influenced by the fading at the predecessor instant. The number of discrete states defines the number of diverse shadowing levels of the environment. Usually 2 or 3 states are considered. Note that the slow fading effect of the complex envelope is fully characterized by the state vector P and the transition probability matrix Q of the Markov chain.

The fast fading fluctuations are modeled by various probability distributions that are specific to each state. Therefore, the narrow-band channel is fully characterized by P, Q and the parameters of the fast fading statistics inside each state. These parameters are usually estimated from measurement campaigns. Three examples of state-oriented channel models are mentioned hereafter:

- The Lutz model has been proposed in [Lutz 91]. It considers two shadowing levels referred to as ON and OFF states. The ON state corresponds to the pure LOS condition whereas the OFF state corresponds to total signal blockage (NLOS). The Rice and Log-normal distributions are used to model the fast fading effect in LOS and NLOS states respectively.

- A 3-states Markov model has been proposed in [Pere 05]. In that case, three distinct shadowing levels are considered. State 1 corresponds to pure LOS conditions. State 3 corresponds to pure NLOS conditions. State 2 is an intermediate shadowing level between State 1 and State 3. Typically, State 3 can be linked to the signal blockage by buildings, whereas State 2 corresponds to softer attenuations, like trees for example.

- The model referenced under ITU-R P681 may also be mentioned as a 2-states Markov model, with a statistical shadowing distribution inside each state [ITU 15].

Fig 1.2 illustrates a 2-states Markov chain of the first order. As it is represented on the left plot, such a model is well suited to represent the time series of Fig. 1.1. The fast fading variations can be modeled by a Rice distribution in LOS state and a Rayleigh distribution in NLOS state.

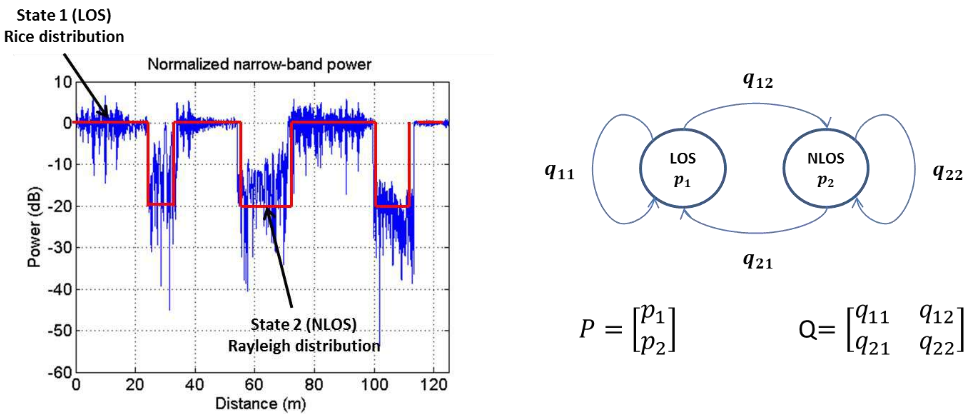

$$P = \begin{bmatrix} p_1 \\ p_2 \end{bmatrix} \qquad Q = \begin{bmatrix} q_{11} & q_{12} \\ q_{21} & q_{22} \end{bmatrix}$$

Figure 1.2 : Illustration of a 2-states Markov chain

Both fading and fast fading effects can be modeled by Markov chains. Therefore, it is an improvement to the distributions presented in sub-section 1.1.1. However, it can be noted that only the narrow-band characteristics of the channel were considered so far. In the present thesis, the channel modeling problem is dedicated to the calibration of the receiver pseudo-range error. Therefore, the wide-band parameters of the channel, such as multipath delays and Doppler shifts, have a major interest. Thus, the narrow-band channel models are shortcoming, and the wide-band models have to be investigated.

1.1.1.3. The wide-band statistical models

Most of the literature dealing with the statistical modeling of the wide-band channel relies on the WSSUS assumptions (*Wide-Sense Stationarity for Uncorrelated Scatterers*), which are developed in [Bell 63]. Those assumptions are fulfilled only if the channel autocorrelation remains constant and if the delay and Doppler of the Scatterers remains uncorrelated. Due to the possible non-uniform distribution of the scatterers in the azimuthal plane, those assumptions tend to restrain the field of application of such approximations. However, a few models based on the WSSUS have been developed. Some of the most worth mentioning are cited in the following. This list of models does not aim at making the reader fully familiar with these approaches, but at giving an overview of the different techniques that have been considered so far. More complete descriptions and other models can be found in [Ait 13], [Satn 08] and [COST 02].

- The model of Saleh and Velenzuela [Sale 87] was designed for indoor propagation modeling. It proposes to group the multipaths of the wide band channel in clusters, according to observations made on a measurement campaign [Sale 87]. The delays of the clusters are characterized by a Poisson distribution, as well as the delays of the multipaths inside each cluster (with different λ parameters). The amplitudes of the multipaths are determined by Rayleigh distributions, whose standard deviation decreases with the delays of the multipaths.

- The model introduced by Jahn [Jahn 96] relies on the same measurement campaign as [Sale 87]. The LOS component is modeled using Rice or Rayleigh distributions, depending on the shadowing level. The multipaths are divided in two delay zones, corresponding to near and far delay echoes. Among the near delay multipaths, the number of echoes is given by a Poisson law. Their delays are scaled using a Tap Delay Line technique and their amplitudes decrease according to an exponential law. Among the far echoes, their number is given by a Poison law as well but their amplitudes follow a Rayleigh distribution.

- The model of Perez-Fontan introduced in [Pere 01] was already mentioned and comprises a wide-band component. From an overall point of view, it is constituted of both wide-band and state-oriented approaches. The Markov states are used to characterize the different shadowing levels of the LOS component, completed with a log-normal distribution to create low LOS fluctuations. In what concerns the multipaths channel, the principle of this model is to simulate the main contributions of the delay line, constituted by the LOS and the major rays (generated by specular reflection). These components are followed in delay by a cluster of multipaths whose delays follow an exponential distribution. The amplitude of the multipaths decreases according to linear decays whose slope depends on the Markov state.

In this non-exhaustive list of models, no generation of virtual environment was considered. It must be mentioned that this limitation is likely to lead to unrealistic multipath modeling in some cases.

1.1.1.4. Synthesis on the statistical channel models

The presentation of the different statistical channel models allowed identifying the major advantages and drawbacks of this approach. They are discussed hereafter. Those different points motivated the development of other types of channel models.

The statistical methods give the possibility to apply simple statistical distributions to different types of scenarios, in order to simulate the narrow-band and wide-band characteristics of the LMS channel. Therefore, the main advantage of the statistical models is their ease of implementation and the low computation load. Moreover, the different statistical distributions that were described all along the previous sub-sections are easily adaptable from one scenario to another. Indeed, only few parameters have to be tuned in order to transpose it to other navigation situations.

However, it was mentioned that the parameters of those different models are extracted from experimental data. Therefore, it can be expected that various experimental data are required to fit the parameters to specific navigation situations. In order to take into account the specific features of a given environment, some data corresponding to a close environment have to be available. The more accurate the statistical channel model is, the more data are required to make it versatile. In order to consider every possible environment type, signal angle of arrival, polarization and frequency band, modulation and trajectory, very extensive measurement campaigns are required. Some other types of approaches have to be investigated in order to increase the channel accuracy.

1.1.2. Deterministic channel models

1.1.2.1. General principle

The deterministic channel approaches consist in computing the LMS channel narrow-band or wide-band parameters by modeling physically the different interactions of the impinging wave front with the environment surrounding the receiver. It requires the knowledge of the canonical elements composing the LMS channel and the characteristics of the wave, such as polarization and angle of arrival. From these data, the resulting electromagnetic wave reaching the receiver is computed. Note that such methods are possible thanks to the recent improvements of the computing tools allowing sufficient computational effort to perform such calculations.

The deterministic methods all rely on the resolution of the Maxwell's equations on the physical representation of the environment of the receiver. However, the deterministic models differ in the different assumptions and simplifications made to perform suitable computations. From that perspective, the deterministic methods can be divided in two families, namely full-wave methods and asymptotic methods.

The full-wave methods consist in solving the EM problem with no simplification assumption, which makes it adaptable to any scenario with a suitable knowledge of the physical composition of the environment (i.e. material EM properties). However, such methods are not applicable to large scenarios, because of the fast augmentation of the computational effort with the size of the environment as it will be explained in section 1.2.2.

The asymptotic methods regroup different simplifications of the original full-wave method. Such considerations generally imply some assumptions on the structure of the environment and on the position of the receiver. Nevertheless, these methods have the advantage to be applicable to a wide range of scenarios, contrary to full-wave methods. The most worth mentioning approaches will be briefly presented in section 1.2.3.

1.1.2.2. The full-wave methods

The full-wave methods are also considered as exact methods because they do not rely on any assumption. As mentioned in the previous sub-section, the drawback of the exact methods is the computational effort required. Indeed, in order to ensure the numerical convergence to the solution of the problem, the environment has to be meshed in objects whose size is typically between λ/5 and λ/10, which increases the number of unknowns in the Maxwell equations.

The full-Wave methods regroup different techniques, which differ in the formalism considered to solve the Maxwell's equations. One of these methods is referred to as MoM (*Method of Moments*). It consists in computing the EM wave reaching the receiver from the radiation of the currents induced on the physical environment by the impinging wave. This method requires to take into account boundary conditions on each considered object, leading to high computation load. Only recent improvements on matrix inversion capacities allowed sufficient computing skills to realize such calculations. Also worth mentioning as full-Wave methods are the FEFD (*Finite Element in Frequency Domain*) and FDTD (*Finite Difference in Time Domain*). They address the Maxwell's equations from a differential point of view and in the temporal domain respectively.

Despite the augmentation of the computation resources, such methods require a prohibitive computation time and computer memory, increasing rapidly with the complexity of the environment. Generally, the dimensions of the scenario are limited to a magnitude of several tens of wavelengths. This thesis deals with the modeling of wide environments. Therefore these methods are remote from the field of applications of this study and do not intervene in the following chapters.

However, being given the accuracy of these methods to model the electromagnetic field and its adaptation capacities, the full-wave methods have been implemented in different applications, such as antenna radiation modeling or RCS (Radar Cross Section) computation. An example of such an implementation is the Elsem3D software in the Electromagnetic and Radar department at the ONERA, which relies on the MoM theory.

1.1.2.3. The asymptotic methods

The asymptotic methods regroup different approaches to model the electromagnetic field. They are characterized by the different simplifications and assumptions simplifying the resolution of the electromagnetic problem. Therefore, these models differ from the exact methods of the previous sub-section insofar as the Maxwell equations are not addressed rigorously but on larger surfaces (large compared to the wavelength), on which the surface currents are considered uniform. In order to satisfy this approximation, different assumptions can be made, which lead to different asymptotic solutions to the electromagnetic problem. They can be divided in two major families: optical-ray and current based methods.

- The optical-ray approach relies on the modeling of electromagnetic rays according to the Fermat's principle with different assumptions like GO (*Geometrical Optics*) or UTD (*Universal Theory of Diffraction*) for example. The GO approach is constituted of two major ray modelling methods: the SBR (*Shooting and Bouncing Ray*) and RT (*Ray Tracing*) methods. The SBR methodology consists in emitting EM rays in every direction around the transmitter, computing the interaction of each of these rays with the environment (reflection, diffraction or scattering) and combining the resulting rays reaching the receiver. The RT method consists in the recursive formation of the image of the signal sources by every object of the environment. A more complete presentation of these methods can be found in [COST 02]. Note that SBR and RT both require a complete knowledge of the environment of the receiver. The UTD consists in modelling the electromagnetic field resulting of the wave diffraction by edges of the environment along a single ray. The point of origin of this ray is located along the considered edge and is positioned according to the geometry of the scenario (relative position emitter-edge-receiver). The complex amplitude of the diffracted field along the different polarization axis are deduced from those of the incident field, the physical composition of the element considered and the geometry of the scenario. This formalism is presented in [McNa 90]. Note that this model considers infinite edges (and thus no corners), which is a major simplification.

- The current based method consists in the resolution of the EM problem using integral formulations of the Maxwell's equations, occulting the harmonics of the surface current of order higher than 1. In order to satisfy this assumption, only objects larger than three times the wavelength can be involved in the model. Two main approaches can be cited following this approach: PO (*Physical Optics*) for scattering surfaces and PTD (*Physical Theory of Diffraction*) for edges.

1.1.2.4. Presentation of the SE RAY-EM Fermat software

The SE RAY-EM FERMAT (*Fonctionnalités pour l'Electromagnétisme et le Radar par les Méthodes Asymptotiques*) is a software relying on the deterministic modeling of the electromagnetic field. It was developed jointly by ONERA and OKTAL companies (France). It relies on the same assumptions as asymptotic methods to address the EM problem on complex 3-dimensional scenarios. It has been decided to present the main characteristics of this software because it is a typical illustration of the deterministic methods (more specifically the asymptotic methods). Moreover, it was a major validation tool for the implementation of the SCHUN hybrid model, widely used along this thesis. The field of applications of SE RAY-EM FERMAT can be extended to bistatic RCS, SAR and antenna modeling.

In order to compute the signal echoes reaching the receiver antenna, SE RAY-EM FERMAT applies the SBR (Shooting and Bouncing Ray) to the 3-dimensional virtual environment. Note that both geometrical and physical designs of the environment are performed by the SE-Physical-Modeler module of the software. The complex amplitude of these echoes are computed by the SE RAY-EM module using PO (*Physical Optics*) and ECM (*Equivalent Current Method*) composed of reflection, diffraction and scattering. The originality of such a tool relies on the coupling of optical ray methods (SBR) for far field zones and current based methods for far near zones. However, the use of PO limits the size of the objects to more than few times the wavelength. Fig. 1.3 was extracted from [Ait 13] and illustrates the hybridization of the different approaches to compute the electromagnetic field near the receiver. The GO has been illustrated through the specular reflection of the facets in near field zones and the PO through the scattering by small elements of the surface.

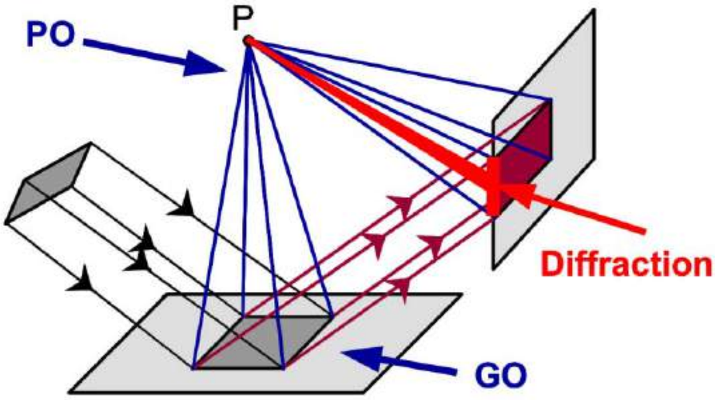

Figure 1.3 : Illustration of the PO, ECM and GO coupling in the SE-RAY-FERMAT module

In the context of modeling the LMS channel, the outputs of the simulators are the channel impulse responses, which contain the delay, phase, Doppler, DOA (*Direction of Arrival*) azimuth and elevation and amplitude along the different polarization axes of the rays reaching the receiver (echoes and LOS). Due to the wide and complex scenarios faceted at small scale, several millions of echoes are generated for each impulse response snapshot. This constraint has been solved by the use of a Tap Delay Line approach, which will be further commented in chapter 2. It must also be mentioned that the computational effort required by the simulator is significant, which is a common limitation to all deterministic channel models.

1.1.2.5. Synthesis on the deterministic channel models

Different deterministic models were presented, including exact and non-exact methods. They allowed identifying the advantages and limitations of this physical approach.

The main advantage of these methods is their global accuracy to model the physical interactions of the impinging electromagnetic wave with a given environment. Indeed, contrary to the statistical approaches, the deterministic models are able to compute the impulse response of a specific environment, taking into account all its characteristics. It makes easier the parametrization of the EM scenario, and therefore increases the application possibilities (for example to any frequency).

However, two major drawbacks can be drawn from this presentation. The globally important computation time required by these methods has already been mentioned. Even if the asymptotic methods and their simplifications limit the computational load, it remains critical in the case of GNSS applications for example. This constraint increases quickly with wide scenarios.

Moreover, in order to take benefit of the exactness of the deterministic methods, the environment must be designed geometrically and physically with accuracy, including material EM properties. This statement can be problematic for complex scenarios since large 3D database will be needed.

Therefore, hybrid methods, which mix characteristics of the statistical and deterministic approaches, have been developed. Some of them will be presented in the following section.

1.1.3. Hybrid channel models

Different channel models comprising both statistical and deterministic components have been implemented so far. This section inventories four of them, classified according to their narrow-band/wide-band characteristic. However, note that the hybrid model SCHUN, which is a major tool of this thesis, is presented separately in section 1.2.

1.1.3.1. Narrow-band hybrid models

Among the most worth mentioning narrow-band models, the model of Abele (2009) and the model of Li (2010) may be mentioned.

- It was already underlined that the **model of Abele** [Abel 09] consists in narrow-band channel modelling, considering an environment composed of buildings and trees. Depending on the accuracy required and the computational effort allowed, two modules have been implemented to compute the narrow-band channel power. The first one is deterministic and the second one empirical. This environment is typically designed as two parallel building rows, between which a receiver is moving.

Therefore, two components have to be modelled in order to take into account all the interactions of the signal with the environment: one coherent component (LOS) and one incoherent (multipath). Those two contributions are modelled separately.

The shadowing caused by the buildings is modelled as a diffracted ray using the Kirchhoff integrals on parallelepipeds. It allows an accurate prediction of the shadowing (it is a 3-dimensional model). Moreover, the shadowing variations are smoother than in the case of Markov chains. However, the polarization of the EM wave is not taken into account. The impact of the vegetation can be computed either deterministically or stochastically. The deterministic model uses the RET (*Radiative Energy Transfer*), which consists in a scalar attenuation of the signal depending on the geometry of the canopies. It is referenced by ITU under the recommendation ITU-R 833-6 [ITU 07]. The stochastic model consists in an exponential distribution of attenuation depending on the canopy geometry and signal frequency.

The multipaths can also be modelled either deterministically or statistically. A distribution of Rice is used to compute the time series of narrow-band power attenuation, whose Rice factor depends on the environment and on the shadowing level. In that case, both the buildings and the vegetation are characterized by the Rice distribution. In the case of a deterministic model, the narrow-band power scattered by the vegetation is computed using the RET and the multipath power scattered by the façades of the buildings is computed using a specific equivalent RCS model presented in [Abel 08].

- The model proposed by **Li** in [Li 10] combines stochastic and deterministic approaches to model the narrow-band power in a virtual 3D city. The deterministic component is applied to the coherent component only, to estimate the shadowing level, whereas a stochastic process is applied to compute the impact of the multipaths on the narrow-band time series. Concerning the LOS component, it is modelled using the optical-ray approach knowing the positions of the emitter and receiver with respect to the geometry of the virtual city. It is composed of GO and UTD diffraction. The shadowing is divided in three states, corresponding to clear LOS, NLOS and an intermediate state. The stochastic process modelling the impact of the multipaths on the narrow-band time series is tuned depending on the state of shadowing. A distribution of Nakagami is used in LOS and intermediate LOS states, whereas a log-normal distribution is used in NLOS state.

1.1.3.2. Wide-band hybrid models

Two hybrid wide band models are worth mentioning: the model of Oestges (2000) and the model of Lehner (2007).

- **The model of Oestges** presented in [Oest 00] relies on the virtual city concept. More specifically, the model designs a virtual environment using statistical distributions of the dimensions of the buildings, trees and streets. The channel resulting of the interaction of the impinging wave with the virtual city is computed deterministically. The wide-band parameters of the channel are computed using an optical-ray approach, whereas the narrow-band time series are modelled by a Rice distribution whose parameters are set by the wide-band characteristics of the channel. The LOS is modeled using ray-tracing and UTD-ECM diffraction whereas multipaths are computed using GO reflections. However, it must be mentioned that the number of echoes that can be generated by the model is limited, compromising its accuracy.

- **The model of Lehner** is referred to as LMMC (*Land Mobile Multipath Channel Model*) in [Lehn 07]. It is a hybrid physical statistical approach to model the wide-band parameters of the LMS channel. It must be mentioned that this model is referenced by ITU under the recommendation ITU-R P.681-8. In order to design the statistical module of the model, a wide measurement campaign has been performed, within different environments (urban, suburban, rural and highways). The emitter satellite was represented by a Zeppelin emitting a 1510 MHz signal (close to the GPS L1 signal frequency), allowing different angle of arrival configurations. All the collected data have been used to model virtual scenarios with respect to the type of environment considered. It must be mentioned that the measurements are composed of wide-band data, estimated thanks to the ESPRIT algorithm (*Estimation of Signal Parameters via Rotational Invariance Techniques*).

According to the configuration of the scenario set by the user, the LOS component is modelled using deterministic methods: simple and double knife edge methods for the diffraction by buildings, trunks and lamp posts and linear attenuation coupled to a random attenuation for the canopy shadowing.

Some scatterers are distributed along the environment. Their quantity and position is estimated from the measurement data, as well as their power, motion and life span. Their delays, Doppler shifts and phases are computed geometrically according to their position. The full version of LMMC includes the possibility to generate multiple satellite scenarios. However, as the model does not model the environment, different satellite positions lead to different distributions of scatterers and uncorrelated coherent components.

1.1.3.3. Synthesis on the hybrid models

Four hybrid deterministic-statistical models have been presented in this section. Two of them are narrow-band approaches and the two others are wide-band approaches. It was already mentioned that this thesis focusses on the channel modelling for GNSS applications. Therefore, the critical comparison of the models will put the emphasis on the wide-band approaches.

The interest of hybrid models is the possibility to take advantage of both statistical and deterministic models and to encounter their drawbacks:

- The model of Lehner considers a statistic distribution of point-like scatterers. It limits the number of echoes to simulate rich environments and thus the computational effort. On the other hand, the lack of accuracy of the statistical model is compensated by the deterministic computation of the coherent component, which has a major impact on the receiver tracking error.

- In what concerns the model of Oestges, the difficulty to implement specific scenarios to run deterministic models has been bypassed by the virtual city concept, with the statistical design of the environment. On the other hand, the lack of accuracy of the statistical models is compensated by the deterministic computation of the wide-band parameters of the channel.

Therefore, the hybrid models have shown to be an interesting trade-off between the advantages and drawbacks of the different modelling approaches. However, these models still present a few limitations. For example, the virtual city generated by the model of Oestges only simulates a few echoes, which can impact the accuracy of the model. Also, the Lehner model distributes the multipath sources according to the experimental data corresponding to a specific measurement scenario. Therefore, two different simulation configurations lead to different multipath environments, which is not physically relevant. In order to improve these models, the SCHUN software has been implemented and presented in [Ait 13].

1.2. The SCHUN simulator

This section is dedicated to the presentation of the model SCHUN, which plays a major role in the following chapters of this thesis. It was already mentioned that it is a hybrid physical-statistical channel simulator. Therefore, after presenting the general architecture of the simulator and its major possibilities, the statistical and deterministic components of the model will be described separately in the third and fourth sub-sections.

1.2.1. General presentation of the simulator

The channel simulator SCHUN has been implemented to compute the wide-band parameters of the LMS channel corresponding to the motion of a receiver in an urban canyon. It is dedicated to the testing of GNSS and LMS systems, as the signal carrier frequency can be tuned in L-band or C-band. Therefore, the virtual city is designed to be realistic and versatile, in order to allow extensive and realistic testing of future GNSS systems. Moreover, the implementation of the statistical and deterministic modules optimize the trade-off between accuracy and computational resource, running almost real-time channel simulations.

Prior to the implementation of the simulator, a study has been conducted in [Ait 13], [Ait 12] and [Ait 11], to analyze the level of details of the environment necessary to be representative of realistic scenarios. The metric of this comparison was the power scattered by different façades, with various details. The architecture of the virtual city has been designed according to the conclusions of this study, and is further documented in section 1.2.3. Therefore, the channel building model can be considered as realistic and representative of the pseudo-range error caused by urban environments on the GNSS receivers. No specific model has been implemented for the vegetation in the initial version of the simulator validated in [Ait 13]. Therefore, this thesis is focused on environments constituted of buildings only. However, it must be mentioned that pre-existing vegetation models have been implemented in the simulator in the meantime.

The versatility of the model relies in the diversity of the scenarios that can be designed. Indeed, the size and position of the buildings, as well as the different façades considered can be either distributed statistically or set by the user. A wide library of façades is available to fit very specific types of buildings. Moreover, the orientation and length of the trajectory can be designed by the user, as well as the speed of the receiver and the position of the different emitter satellites. The diversity of polarization and frequency are also ensured.

1.2.2. Architecture of the model

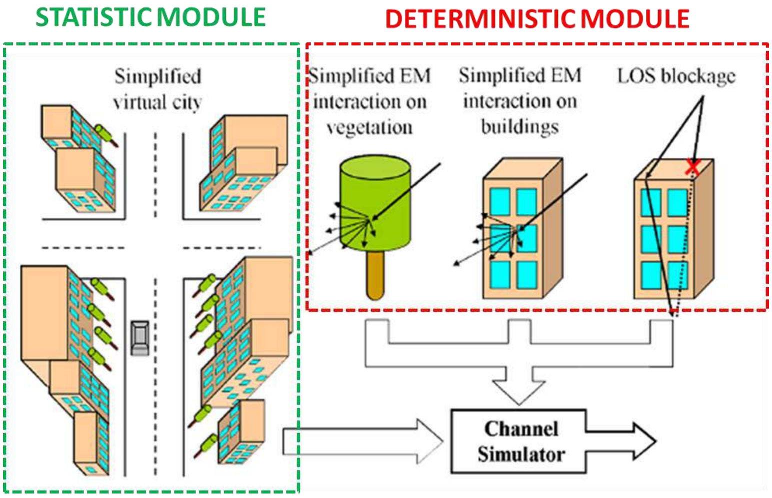

Figure 1.4 : Architecture of SCHUN, with statistical and deterministic components

As a hybrid model, the SCHUN simulator can be divided in two components, one statistical and the other deterministic. Fig. 1.4 illustrates the macro-architecture of SCHUN, on which the two components have been identified. The statistical module of the simulator is dedicated to the generation of the virtual city, which depends on the specifications set by the user. Further explanations about the virtual city will be displayed in section 1.2.3. The deterministic component of SCHUN is dedicated to the computation of the wide-band parameters of the channel. A typical application of such channel models is the testing of GNSS systems. Therefore, the output parameters of SCHUN are composed of both coherent (LOS) and incoherent contributions (multipaths) of the channel. The wide-band parameters are displayed as the discrete delay, power, phase, Doppler shift, azimuth and elevation of arrival of the echoes and direct path, along the different polarization axes.

1.2.3. The statistical module: the virtual city

First of all, the specifications of the trajectory and satellite constellation define the first step of the scenario definition. The total length of the trajectory, as well as the speed of the receiver and the sampling frequency of the channel impulse response are set by the user. The geometry of the trajectory can be generated statistically, by tuning the minimum and maximum of the length and orientation of the street segments, which are supposed to be uniformly distributed. Note that the trajectory is defined in Cartesian coordinates in the horizontal plane, as represented on Fig. 1.7. The diversity and position of the satellites are defined by the user, in spherical coordinates. The parameters of the front wave must also be tuned: polarization (linear or circular) and frequency (L-band, S-band and C-band).

After the definition of this pre-scenario, the virtual city simulated by SCHUN is distributed, typically in the form of an urban canyon, composed of two parallel building rows, surrounding the trajectory. Depending on the position of the satellite considered, one row is involved in the LOS blockage and the other row is responsible for the scattering of the signal echoes. It has already been mentioned that the dimensioning of the buildings and streets can be generated statistically, as well as their position. The buildings are modelled as parallelepipeds. As a consequence, six parameters have to be defined, which are the depth, width and heights of the parallelepipeds and their position in Cartesian coordinates in the referential of the urban canyon. The dimensioning parameters are distributed according to log-normal laws, whose means and standard deviations are set by the user. It must also be mentioned that the height and width of the buildings are rounded in order to match the size of the façades, which are predefined. Fig. 1.5 represents an example of virtual city, corresponding to 1.5 km trajectory length. The straight segments are between 200 m and 400 m long, and the street orientations between 60° and 120°. It can be noted that the urban canyon is generated independently on each segment which can lead to inconsistent building overlap around the street crossing points.

The building density must also be defined. It corresponds to the percentage of the skyline occupied by buildings. Fig. 1.6 represents the urban canyons corresponding to two building densities (75% and 25%). Note that the building density of each row of the canyon can be defined independently.

The front side of the buildings is composed of adjacent façades. These façades are broken up into small facets, which constitute the point-like scatterers of the model. Although the size of these facets can also be tuned, it must be noted that their dimension must satisfy the far field assumption, considering a receiver located at minimum a few meters away. This assumption also depends on the frequency of the wave front. In the GNSS context, typical facets are squares with 50 cm sides. The SCHUN physical model considers three types of facets which correspond to three types of interaction of the signal with the buildings: specular (reflection on smooth surfaces), double bounce effect (dihedral reflection on edges or corners) and diffusion (incoherent scattering of the wave front by protruding or receding elements small as compared to the wavelength). More details will be given about the physic of these interactions in the following sub-section. However, it can already be mentioned that the disposition and relative proportion of these facets define different types of buildings. Indeed, the SCHUN simulator proposes different types of façades in the façade library in order to be representative of the architecture diversity of different types of urban areas (recent and ancient buildings).

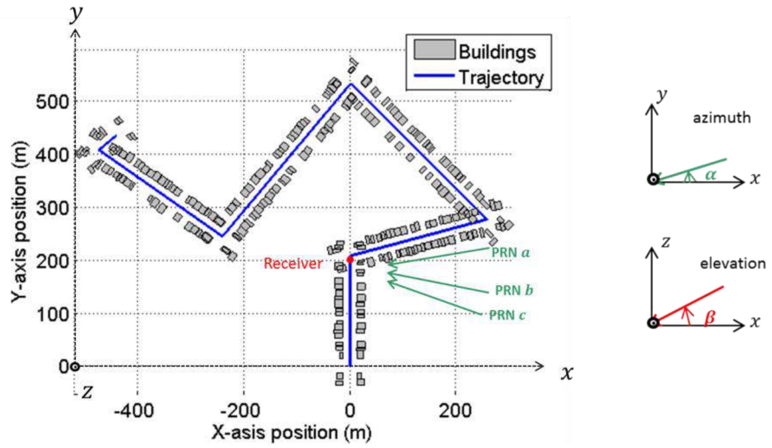

Figure 1.5 : Illustration of an urban canyon

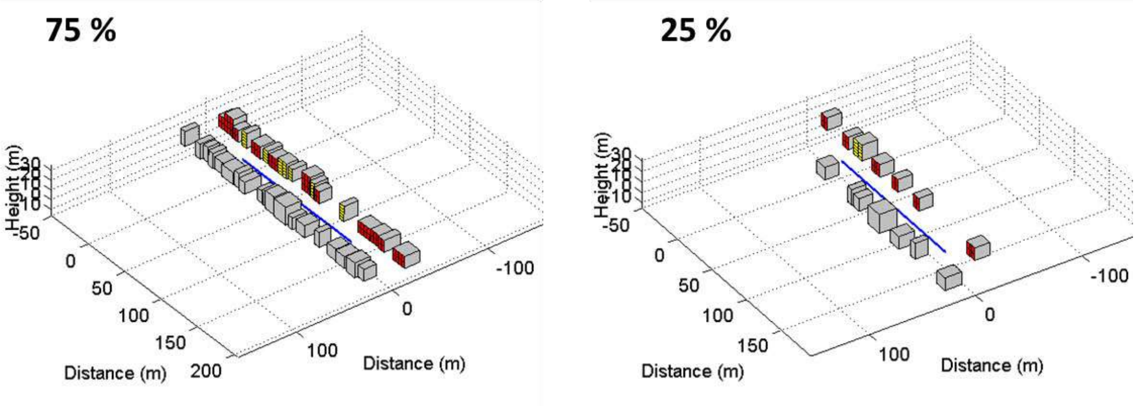

Figure 1.6 : Illustration of two urban canyons with 75% (left) and 25% (right) building density

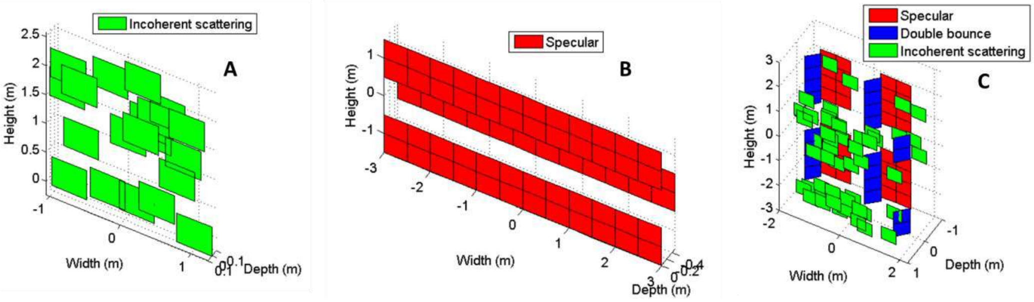

Figure 1.7 : Three examples of building façades

Fig. 1.7 represents three types of façades, extracted from the façade library of SCHUN. The façade referred to as Façade A is constituted only of incoherent scattering facets. It means that the building is mainly rough, composed of many protruding elements small compared to the signal wavelength. It may correspond to uniformly rough walls for example. Façade B is composed only of specular elements. This is typical of modern architectures, composed mainly of windows and smooth surfaces. Façade C is composed of specular, double bounce and incoherent scattering facets. This represents more complex façade types, composed of windows, edges, balconies and small features.

1.2.4. The deterministic module

The deterministic module computes the interaction of the wave front with the virtual city described above. Therefore, it can be considered that the deterministic module is involved in the channel modelling as a second step, after the generation of the virtual city by the statistical module. It was already mentioned that both LOS and multipath are synthesized deterministically. The LOS contribution is estimated using an optical ray approach, whereas the echoes are generated using the 3CM model (*Three Components Model*) developed for the specific needs of the SCHUN simulator.

1.2.4.1. The coherent contribution

The SCHUN simulator allows two possibilities to compute the wide-band parameters of the direct path: a simple ON/OFF LOS model and UTD diffraction. Note that they both rely on the optical-ray approach.

The simple ON/OFF model consists in defining at each instant the blockage of the direct path, according to the relative position receiver-satellite, and according to the geometry of the virtual city using a GO approach. The blockage is a simple ON/OFF model. If the wave front encounters a building along the direct emitter-receiver path, the LOS is OFF and the wave front is attenuated by 20 dB. If no obstacle is encountered, the LOS status is ON and no correction is applied to the direct path amplitude. Note that the buildings are considered as parallelepipeds. All three dimensions are considered in the signal blockage estimation, including the depth.

In order to improve the accuracy of the coherent component, SCHUN proposes a more complex model of signal attenuation relying on the UTD method, to compute building edge diffraction. The diffraction is considered for the buildings located between the receiver and the satellite only. For each of these buildings, the three edges facing the receiver are considered as diffracting edges. For a given edge, the point of origin of the diffracted ray is computed according to the position of the edge relatively to the satellite and the receiver. The precise calculation of the scattering point location may be found in [Ait 13], which takes back the model of [NcNa 90]. If the point of origin of the diffracted ray is located out of the edge bounds, the diffraction problem has no solution and no diffracted ray is generated. The amplitudes of the diffracted rays are computed using an optical-ray approach and depend on the geometry of the scenario. The precise formalism is also detailed in [Ait 13].

The top plot of Fig. 1.8 represents an example of urban canyon, considering a 150 m trajectory. The bottom plot of Fig. 1.8 represents the corresponding narrow-band power of the direct path, in both cases of simple LOS/NLOS model and UTD diffraction. For the clarity of this illustration, no multipath is considered (there is no scattering building row). The emitter satellite is located 30° azimuth and 35° azimuth on the same side as the building row. It can be observed that the UTD model allows a smoother transition from LOS to NLOS states. Moreover, it creates additional fluctuations of the total narrow-band power within a given LOS/NLOS state.

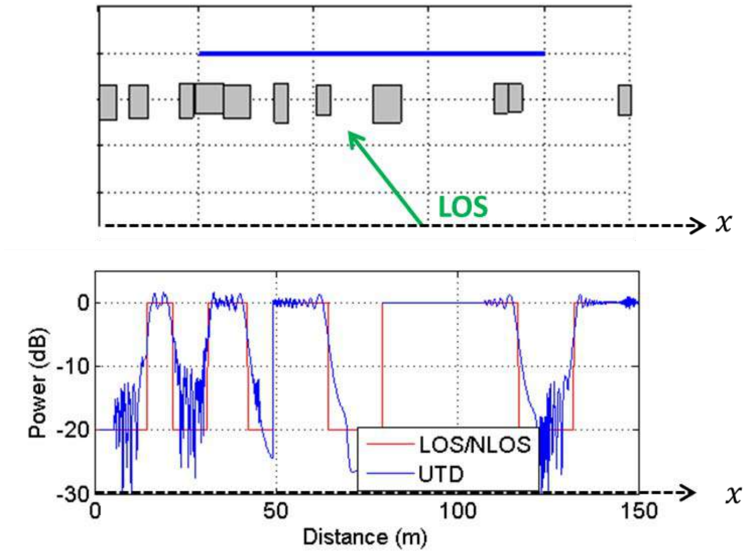

Figure 1.8 : Illustration of the LOS/NLOS and UTD models for direct path blockage

1.2.4.2. The multipath

From observations made on the full-Wave method Elsem-3D (described in section 1.2.4) and on measurement campaigns in urban areas, it has been concluded in [Ait 13] that three major interactions take place on the surface of the buildings, which leads to multipath scattering. They are identified on Fig. 1.9, which represents the density function of the position of the scatterers along the x-axis and y-axis, which corresponds to an impulse response snapshot of the measurement campaign of [Lehn 08]. Note that the receiver is moving along the vector $\vec{v}$. The multipaths whose contribution is symmetric to the LOS with respect to the x-axis (parallel to the trajectory) correspond to the specular reflection of the signal wave front. The multipaths whose contribution is opposite to the LOS is caused by the double bounce effect of the wave front on edges. Moreover, some additional multipath contribution is spread all along the x- and y-axis, corresponding to incoherent scattering by small elements.

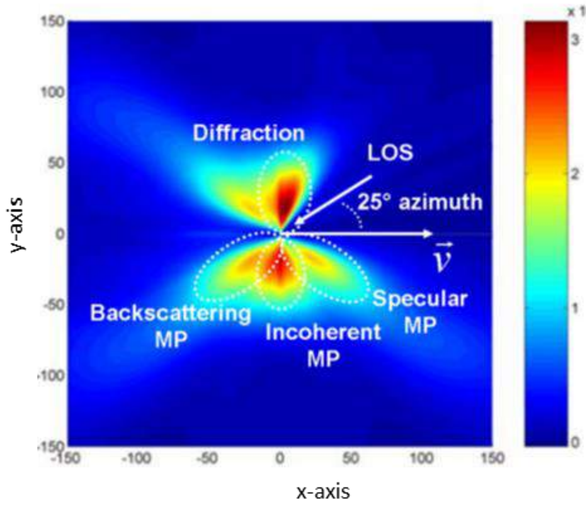

Figure 1.9 : Density function of the scatterers positions from the measurements of [Lehn 08]

Therefore it has been decided in [Ait 13] to divide the multipath modelling problem in three components, forming the scattering model referred to as 3CM in [Ait 13]. The physical nature of these three components is summed up on the scheme of Fig. 1.10. It has already been mentioned that the façades are broken up into small facets (typically 50 cm wide to satisfy the far field assumption), which are all assigned to a particular type of interaction. Each facet emits one multipath in the direction of the receiver. The delay, phase and Doppler shift of the considered multipath is computed using GO and its power using PO. Note that all facets are supposed to have the same size and the same orientation (collinear normal vectors) in order to minimize the complexity of the 3CM model.

Each type of interaction can be identified to physical elements of the facades, which allows designing realistic façades using the facets of the 3CM, as represented on Fig. 1.7. Indeed, the clusters of facets on the façades define architectural elements, like windows, window edges, smooth or rough surfaces.

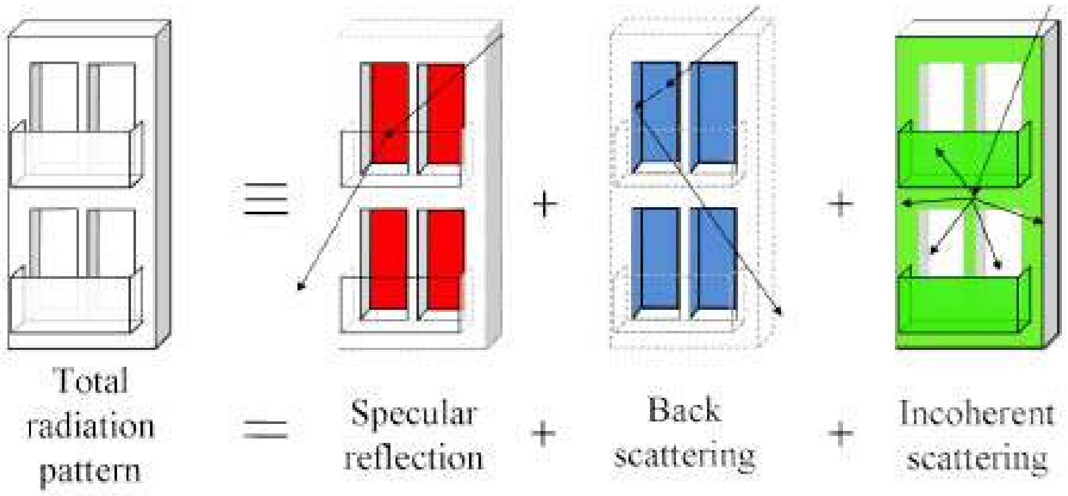

Figure 1.10 : Schematization of the 3CM in [Ait 13]

All three components of the 3CM have been developed for the purpose of the implementation of the SCHUN simulator. They all rely on the PO approach, according to different assumptions minimizing of the computational effort. They will be detailed in the following of this section.

The implementation of the 3CM is a major point of this chapter, being given the fact that it will be used as a reference channel model all along this thesis, to perform the comparison of the reduction methods.

- **The specular reflection component:**

The specular facets are used to model the reflection of the wave front on smooth surfaces. It relies on the resolution of the EM problem on each facet, using PO (*Physical Optics*) and far field assumptions. The problem is addressed by the resolution of the integral form of the Maxwell's equations on the surface of the facets. The power radiated by the surface currents of the facets is computed in every scattering direction. The phase, Doppler shift and delay of the multipaths are deduced of the position of the facets using GO. The physical base of the specular component is further detailed in [Ait 13] and is inspired from [Bala 89].

The tangential field is computed as the difference between the incident and the reflected EM fields, considering the facets as perfect dielectric materials. The electric and magnetic currents induced on the facet by the tangential field is deduced from the passage equations. An integral formulation of these equations allows computing the amplitude of the radiated field in every scattering direction. Moreover, the fact to consider only square facets decreases significantly the computational effort of the problem. All the equations corresponding to this EM formulation are available in Appendix B of [Ait 13]. Note that the polarization of the wave front is taken into account by projecting the radiation currents on the polarization axes of the receiver.

Fig. 1.11 represents the RCS (*Radar Cross Section*) of the radiated field corresponding to a perfect dielectric conductor plate estimated by the 3CM [Ait 13]. θ represents the elevation of the scattered wave and ϕ its azimuth. This scenario models the specular interaction of the wave front with a specular facet. The angle of arrival is 18° azimuth and 35° elevation.

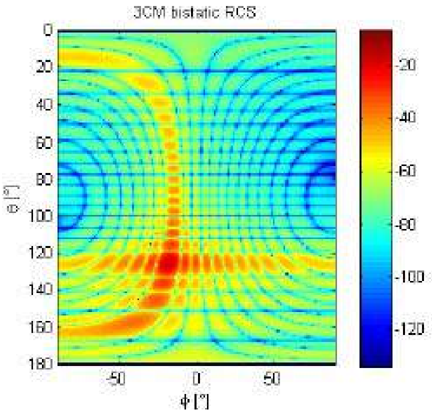

Figure 1.11 : RCS of a perfect dielectric plate using the 3CM specular model [Ait 13]

- **The backscattering component:**

The backscattering model is used to represent the double bounce reflection of the wave front on the façades (typically on window contours). The principle of the 3CM backscattering model is to use the same PO as the specular model on an equivalent plate, whose orientation and dimension is adapted to the angle of arrival of the incident wave. The orientation of the equivalent plate is opposed to the incident wave. In the 3CM formalism, the rotation of the equivalent plate is only performed in the azimuthal plane, since only second order bound effects are considered (no trihedral effects). The width of the equivalent plate is adapted to both azimuths and elevations of the incident wave [Ait 13], in order to add a weighting factor to the radiation pattern. Fig. 1.12 illustrates the positioning and sizing of the equivalent plate, considering two different azimuths of arrival.

The RCS of the equivalent plate is computed using PO. Note that the amplitude attenuation due to the reflection on a dielectric material has to be considered at the second order, because of the double reflection effect. As well, the polarization of the scattered field is computed as if the EM wave impinges a perfect electrical conductor before impinging the equivalent plate.

Fig. 1.13 represents the RCS of a backscattering type facet computed by the 3CM model. θ represents the elevation and ϕ the azimuth of the field. Note that no backscattering power is scattered beyond -50° azimuth, in order to avoid scattering in non-physical directions.

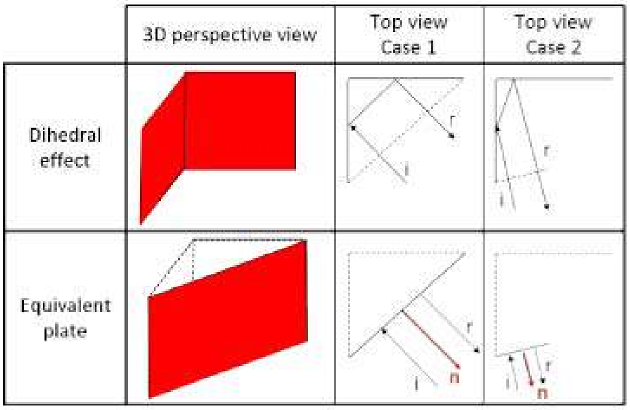

Figure 1.12 : Dimensioning and positioning of the equivalent plate to model the backscattering component of the 3CM

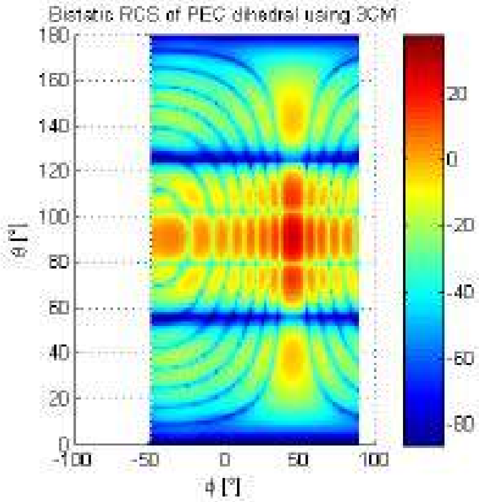

Figure 1.13 : RCS of a backscattering echo using the 3CM model [Ait 13]

- **The incoherent scattering component:**

The incoherent scattering is used to model the diffusion of the wave front by small surface elements. Typically, the incoherent scattering is generated by rough walls. Because of the diversity of the building surfaces depending of the urban scenario, different models of surfaces have been implemented, namely rough surfaces and slightly rough surfaces.

The slightly rough surfaces are composed of small roughness heights, small surface slopes and isotropic roughness. The roughness of a given facet is characterized by the distribution model of the protruding and receding elements (Gaussian or exponential), as well as the standard deviation and correlation length of their heights. Depending on the exponential or Gaussian distribution of the roughness, the scattering pattern of the facet is given by analytic formula extracted from [Ruck 70] (chapter 9). Note that the radiated field amplitude along the θ and ϕ polarization axes depend on the polarization of the receiver antenna, plus a weighting coefficient that also depends on the relative emitter-receiver polarization (vertical or horizontal). Those formulas are displayed in [Ait 13]. A third slightly rough scattering model has been implemented in [Ait 13] in the case of slightly rough surfaces, namely specular slightly rough surface. It corresponds to a sub-division of the scattering facets in micro-facets, on which specular reflections occur. A random phase is assigned to each micro-facet which leads to non-coherent scattering. Fig. 1.14 represents the RCS corresponding to Gaussian, exponential and specular slightly rough surfaces. In that case, the incident wave has an azimuth of 18° and an elevation of 35°.

The very rough surfaces consist in higher roughness heights. However, other assumptions have to be fulfilled in order to apply the analytic formulas of [Ruck 70]: big surfaces radius compared to the wavelength, isotropic roughness and smaller correlation lengths of the heights than the facet dimensions. In such conditions, similar analytic formulas as for slightly rough surfaces are applied, in order to compute the radiated field corresponding to very rough facets. Fig. 1.15 represents the RCS corresponding to the exponential and Gaussian roughness distributions, considering the same angles of arrival as Fig. 1.14.

In all cases, the wide-parameters like phase, delay and Doppler shift of the corresponding echoes are computed using GO, depending on the geometrical position of the facet.

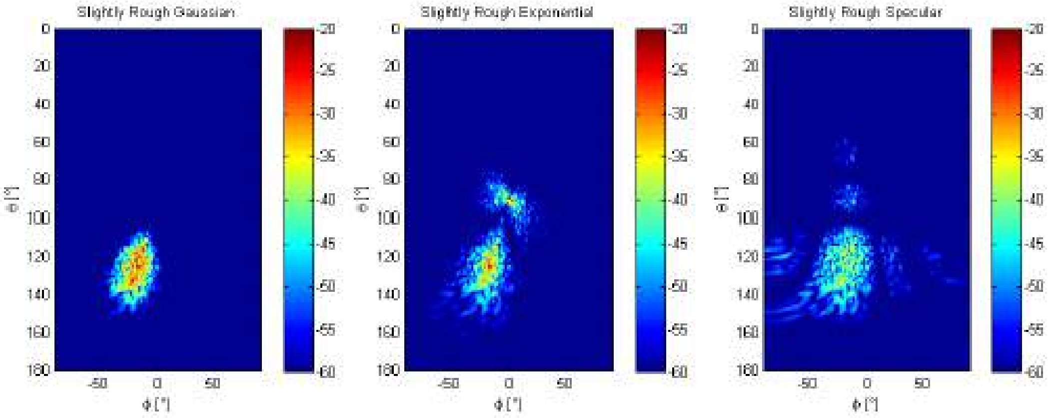

Figure 1.14 : RCS corresponding to the different slightly rough surface models

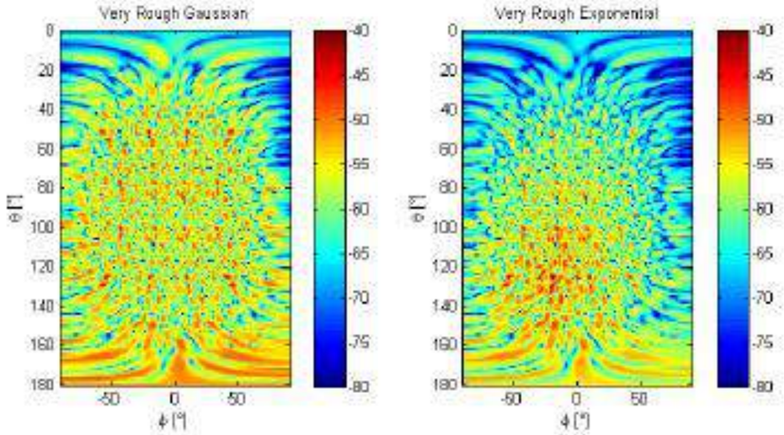

Figure 1.15 : RCS of the incoherent scattering echo considering a very rough facet with Gaussian and exponential distributions [Ait 13]

1.3. Validation of the SCHUN simulator and introduction to the channel reduction problem

1.3.1. Validation of the SCHUN simulator

- **The 3CM model:**

The validation of the 3CM model for multipath scattering in urban environments has been presented in [Ait 13] and [Ait 12]. This section relates the validation of the model on a single façade. It consists in the comparison of the narrow-band power computed by the 3CM model with the one computed by another method, referred to as Elsem3D. The latter is a deterministic solver, based on exact methods and more specifically the IEFD (*Integral Equations in the Frequency Domain*) using MoM (*Methods of Moments*). It has been presented in [Soud02] and has been considered as a reference model in [Ait 13] and [Ait 12]. Indeed, it relies on exact methods, thus privileging the accuracy of the channel model at the expense of a bigger computational effort.

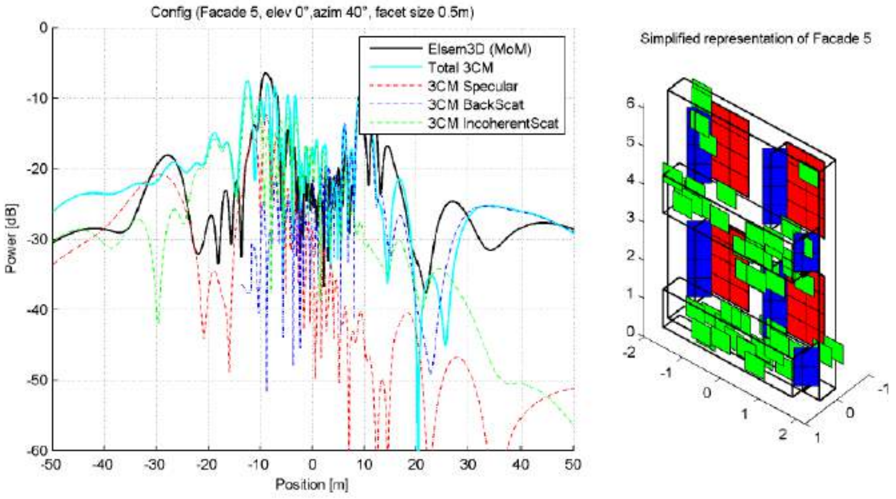

Figure 1.16 : Validation of the 3CM model on a single canonical façade

The left plot of Fig. 1.16 represents the comparison of the narrow-band channel considering the 3CM (global and separate components) and ELSEM 3D models. The façade considered on this scenario is represented on the right plot. The impinging wave has 0° elevation and 40° azimuth. It can be observed that the 3CM narrow-band model fits the exact model in a significant measure in the 0-20 dB interval, which is the critical validation zone.

Other validation elements are available in [Ait 13], including wider scenarios, different emitter positions, other types of façades and wide-band comparisons.

- **The coherent component:**

The LOS model of the SCHUN simulator has been validated separately from the 3CM model in [Ait 13]. Therefore, the UTD model of SCHUN has been compared to the PTD (*Physical Theory of Diffraction*) and ECM (*Equivalent Current Method*) of the SER-EM FERMAT model, presented in section 1.2.4. This comparison on a wide scenario has been illustrated on Fig. 1.17, considering 35° elevation and 0° azimuth of the emitter satellite. The top plot represents the urban canyon and the bottom plot the nominal power of the LOS component, which is alternatively blocked by the buildings of the scenario.

It can be observed that the overall aspect of the LOS power is respected by the UTD model. However, a few fluctuations are not reproduced, which is due to the assumption of infinite edges by the UTD model, as well as the absence of corner diffraction model.

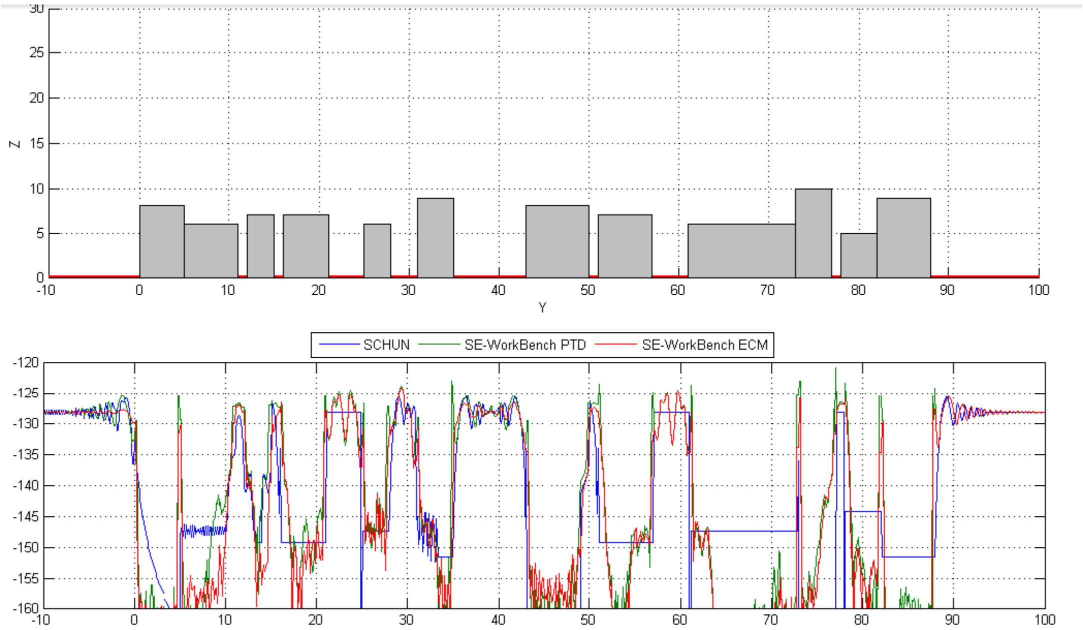

Figure 1.17 : Validation of the UTD model with the SCHUN simulator

- **Validation campaigns:**

It must also be mentioned that the SCHUN simulator has been validated through two measurement campaigns, realized in Toulouse city center and in the Saint-Lary village [Laco 10]. In the case of Saint-Lary, the environment has been synthesized using the virtual city of SCHUN. The narrow-band time series of the channel were modelled by the deterministic component of SCHUN, and compared to the measurements results. The SCHUN model showed to reproduce the narrow-band characteristics of the channel well. In the case of the Toulouse City center, a real GNSS receiver was embedded in the measurement campaign in order to assess the pseudo-range error caused by the environment. In parallel, the wide-band channel parameters have been estimated by the SCHUN simulator. They have been given as an input to a software channel receiver to estimate the tracking error caused by the synthesized environment. The comparison of the measured and simulated tracking errors showed a good correspondence, which validates the use of the SCHUN model in the GNSS context.

- **Validation**

For being a hybrid physical-statistical model, the simulator circumvents the major drawbacks of both approaches. The fact to implement virtual cities allows a good versatility of the model, able to reproduce very diverse types of urban scenarios without requiring the exact knowledge of the environmental constitution. On the other hand, the fact to compute the wide-band and narrow-band parameters of the channel using the PO allows a good accuracy of the model, as it was related by the different validation campaigns. Moreover, the implementation of the 3CM model to address the EM problem has significantly reduced the computational effort of other deterministic models, leading to almost real-time channel modelling. To finish, the Toulouse city center validation campaign has shown that such a channel simulator was well suited for the assessment of GNSS systems in dense urban scenarios. Therefore, it has been assumed in this thesis that the SCHUN model can be considered as a reference model for the realistic testing of GNSS receivers.

1.3.2. The channel reduction problem

The major originality of the SCHUN approach is the fact to break down the virtual city model in elementary facets, minimizing the computational effort while satisfying the PO and far-field assumptions. In particular, the facets have to be small enough to be able to consider that the receiver is in the far-field zone of each facet of the scenario, that is to say inferior to 50 cm approximately.

In the case of wide scenarios, this constraint leads to a high quantity of multipaths generated by the simulator (this would also be the case with any deterministic model). Fig. 1.18 represents an example of wide scenario, with 1 km trajectory. The bottom plot represents the number of multipaths synthesized by the SCHUN model depending on the position on the trajectory. The multipath influence length has been set to 50 m, which means that the facets located more than 50 m far away from the receiver do not emit any multipath to the receiver. The satellite is 30° azimuth and 35° elevation. Note that this scenario has been used for the reduction models comparison in chapter 5. Therefore, more details about the parameters of this simulation can be found in section 5.2.

It can be observed on Fig. 1.18 that the number of multipaths generated by the model is of the order of magnitude of thousands of multipaths. Moreover, the increase of the multipath influence length would increase proportionally the number of echoes. Such a high number of contributions can be problematic for the GNSS applications:

- If the channel models are used to test software simulators, the wide-band parameters of the channel are given as an input for calculating the tracking error. This requires the modelling of either the signal code or the code autocorrelation functions, whose definition can be time consuming with a high quantity of multipaths.

In order to give an idea of the computational effort required for a typical software GNSS receiver, the receiver simulator referred to as GeneIQ has been used to compute the tracking error along the 1 km trajectory of the scenario represented Fig. 1.18. GeneIQ relies on the modelling of the channel autocorrelation function to estimate its tracking error. More details about this receiver model can be found in section 5.4. The number of multipaths in the reduced channel has been limited to different quantities of echoes, from few ones to several thousands in order to illustrate the increase of the computational effort with the number of multipaths in the channel. This profile is displayed on Fig. 1.19. The blue curve represents the time needed to compute the tracking error all along the 1 km scenario, in minutes. It clearly shows that the computational effort is proportional to the number of discrete echoes in the channel. The red marker represents the real duration of the scenario, corresponding to 5 m.s^{-1} speed. It can be observed that with more than 50 echoes in the channel impulse responses, the tracking error cannot be assessed in real time. Therefore, the number of multipaths in the impulse responses has to be reduced to perform more realistic GNSS software simulations.

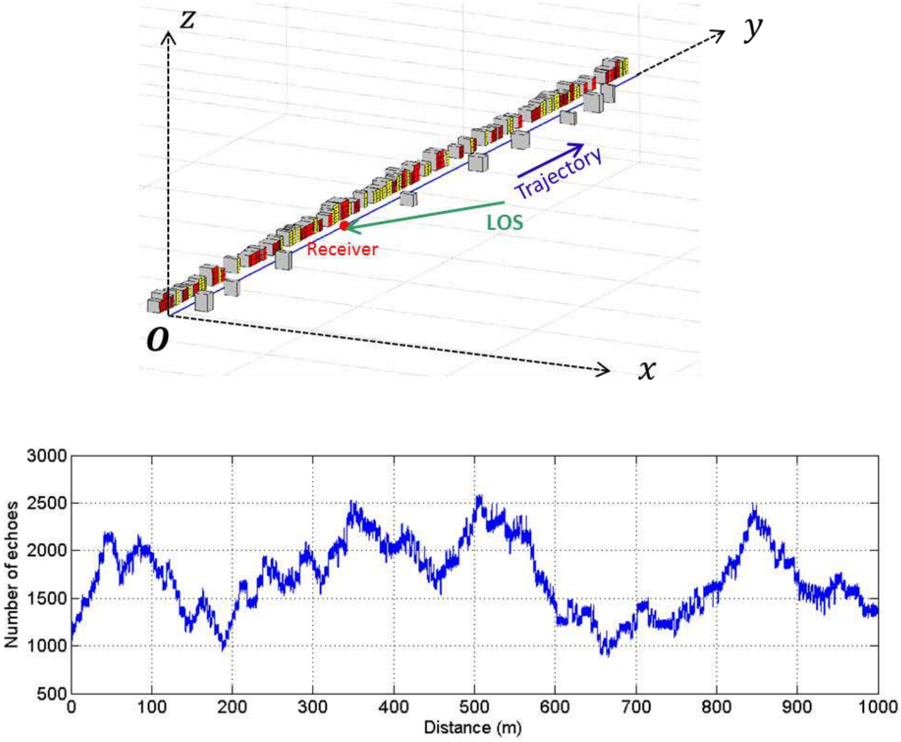

Figure 1.18 : Number of multipaths in the impulse response along the receiver's trajectory

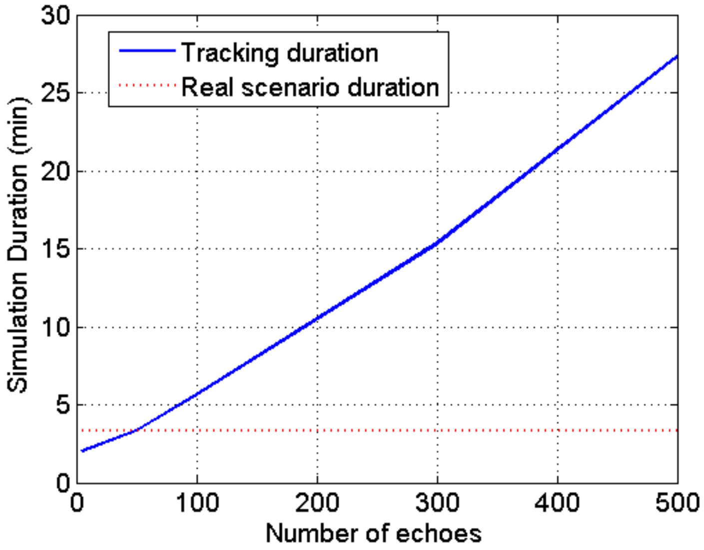

Figure 1.19 : Duration of the tracking error computation along the 1 km trajectory using GeneIQ

- Another possible application of the wide-band channel models is the use of hardware channel emulators, in order to generate physically the signal echoes. This is the case of the GNSS multi-constellation simulator NAVYS for example, developed by engineers from Thales Alenia Space, Elta and CNES [Arta 10], [Arta 08]. This GNSS signal synthesizer is dedicated to the test of real GNSS systems, on realistic scenarios. Multiple modules are available for the generation of different signals in parallel, each one assigned to one specific satellite, allowing very diverse configurations (satellite diversity, frequency, position and modulation). In addition to the modelling of the atmospheric effects on the synthesized signals, each module is divided in different channels dedicated to the generation of signal replicas, which take into account the delays, phases, amplitude and Doppler shifts of the echoes. These parameters may be provided by external channel models, like SCHUN for example (in the right format). An overview of the architecture of NAVYS is displayed on Fig. 1.20.

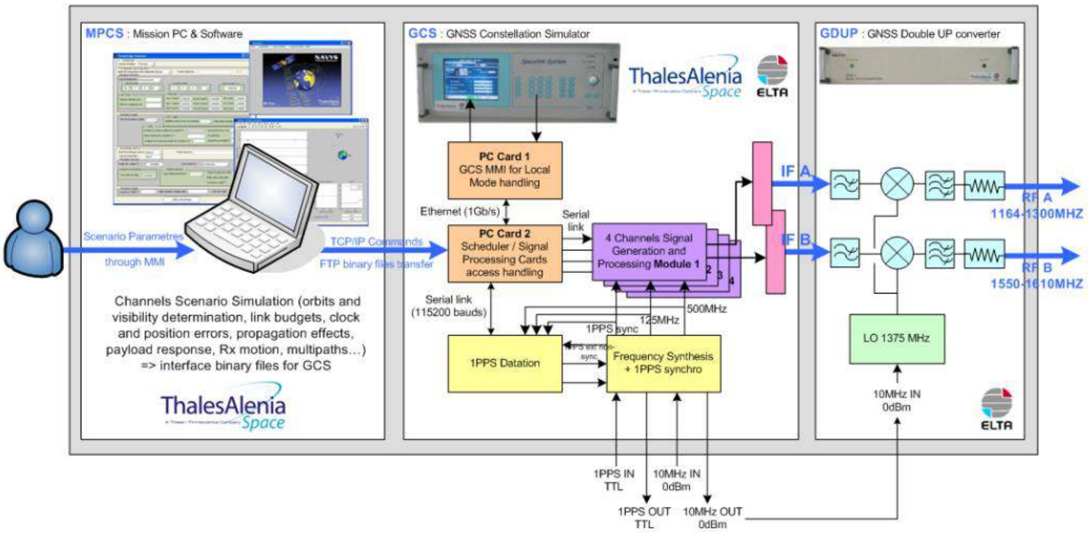

Figure 1.20 : Overview of the NAVYS constellation simulator

The NAVYS simulator showed very good performances in terms of realistic signal generation [Arta 10]. Therefore, it can be expected that its association to realistic channel models like SCHUN could be promising. However, the hardware design of such simulators is limited in terms of quantity of multipaths, as compared to the number of echoes modelled by SCHUN. In the case of NAVYS for example, the number of available signal tracks is normally set to 8 units (including the LOS). Therefore, the SCHUN channel model needs to be post-processed in order to be adaptable to such hardware simulators.

These observations motivated the focus of this thesis, that is to say the implementation of methods to reduce the number of multipaths of the impulse responses, without loss of information provided by the SCHUN model, and without impacting the representativeness of the testing of GNSS receivers.

1.4. Conclusion

This chapter provided an overview of the different possibilities to model the LMS channel. The three major approaches were confronted in the first section, namely statistical, deterministic and hybrid models. The presentation of several statistical models on one hand and physical models on the other hand highlighted the advantages and limitations of each approach. The statistical models are easily adaptable from one environment to another and easily implementable, which offers a good versatility of the simulations. However, they globally suffer from a lack of accuracy as a large amount of empirical data is necessary to implement extensive scenarios. To the contrary, deterministic models are usually more accurate, as they are applied to one specific environment straightforward. However, they require a precise description of the environment and they are globally very demanding in computational resource, especially for exact methods.

The hybrid physical-statistical models showed to be a good compromise between these two approaches. Several models were presented, which differ in the trade-off between statistical and deterministic components. The fact to implement some deterministic computation in the model increases its accuracy and the statistical components make easier the adaptation from one environment to another.

In that sense, the SCHUN model has shown to be particularly well-suited. Indeed, the virtual city concept ensures the versatility of the environment, still representative of realistic scenario. Moreover, all the wide-band parameters of the coherent and non-coherent contributions of the LMS channel are computed deterministically, which allows an accurate channel representation. This statement was validated through the comparison of the 3CM multipath model with deterministic time consuming models on one hand, and with measurement data on the other hand. This also confirmed the ability of the SCHUN model to be adapted the assessment of GNSS receivers. To finish, the breaking down of the façades in regular facets assigned to specific interactions allows some practical assumptions on the PO formalism, limiting the computational effort to almost real-time simulations.

However, this thesis focusses on the adaptation of such channel models to the GNSS applications. In that context, it has been shown that too many multipaths are modeled by most of the wide-band simulators to be suited for software simulations, and even more for hardware implementations. Therefore, it has been decided to focus this thesis on the development of reduced channel models. To do so, different algorithms will be implemented in the following chapters, to reduce the number of multipaths of the SCHUN reference model, from thousands to less than 10 units. The quality of those reduced models will be assessed through their ability to preserve the channel characteristics (delay, power, Doppler spectrogram) on one hand and their ability to preserve the pseudo-range errors in a given scenario on the other hand.

Chapter 2

2. Implementation of an optimal method to reduce the channel impulse response by aggregating or selecting multipaths

All along this chapter, reduction methods using the multipath aggregation or eventually multipath selection will be presented. All these methods will be applied to the impulse response snapshots, considering a reference scenario presented in section 2.1. The outline is organized as follows: the methods will be presented the one after the other from the most trivial to the most elaborate. This chapter will aim at covering all the different approaches mentioned in the literature. For each method, the preservation of the reference channel Power-delay profile and Doppler spectrogram will be assessed. From these results, the advantages and limitation of the methods will be provided to the reader. Three main reduction approaches will be investigated using this outline: selection methods in section 2.3, Tap Delay Line approaches in section 2.4 and clustering models in section 2.5. Two preliminary sections will present the challenge of the study and the reference scenario on which the reduction methods will be applied.

2.1. Introduction of the study: goal of the reduction methods and literature overview

The reduction methods aim at reducing the number of multipaths from thousands to less than 10. In this chapter, the aggregation methods will be applied to the different impulse responses. It means that the methods can be applied at each epoch of the scenario independently from the previous or following instants. To perform this study, the SCHUN software [Ait 13] was chosen, for the reasons mentioned in chapter 1, to compute the impulse response of the multipath channel all along the trajectory of a reference scenario presented in section 2.2. The parameters displayed are the delay, Doppler, complex amplitude (power and phase) on co- and cross-polarizations, angle of arrival (azimuth and elevation) of the echoes. Depending of the reduction method, different multipath distances over the impulse response will be defined using some of these parameters. These distances are used to form clusters of multipaths. It is important to note that in chapters 2, 3 and 4, the reduction methods will be applied to the multipaths only, regardless of the diffraction rays produced by building edges. In other terms, the simple ON/OFF mode has been chosen to model the LOS.

Fig. 2.1 illustrates a snapshot of impulse response with the plot of the power of the multipaths in terms of their delay and Doppler (left plot) and in terms of their angle of arrival (right plot). It was drawn from the reference scenario (y =25 m), which is represented on Fig. 2.3. On Fig. 2.2, the discrete multipaths are spotted, on the power-delay and Doppler-delay profiles. The power and delays are always represented with respect to the open sky LOS power and the delay of the direct path. Therefore, the LOS contribution can be easily identified, with a delay of 0 ns. In that case, the LOS is masked by the building row on the right side, hence the 20 dB power loss.

The reduction methods presented from section 2.3 to 2.5 are all adapted from various approaches found in the literature. Note that the channel reduction is necessary for various applications, including navigation, telecommunications and channel sounding. All the modifications brought to these methods will be detailed from section 2.3 to section 2.6, improving the performance of the aggregation approach all along this chapter.

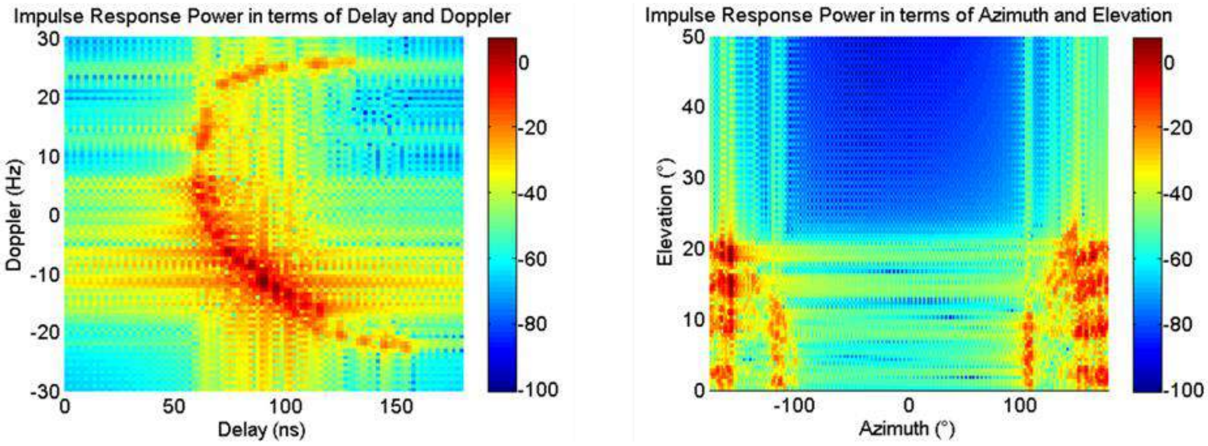

Figure 2.1 : Example of channel impulse response power in terms of delay, Doppler and angle of arrival

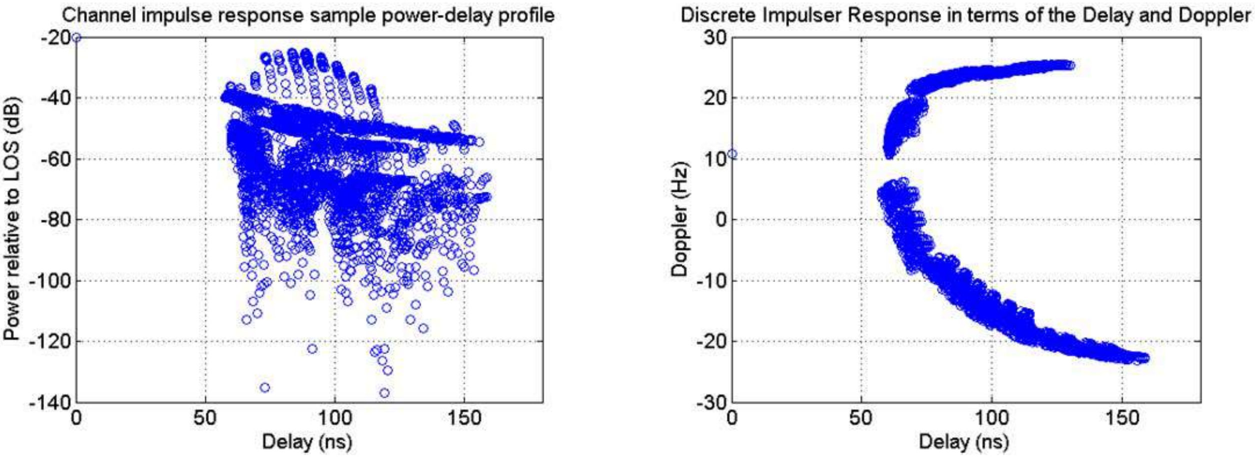

Figure 2.2 : Example of channel impulse response power-Delay and Doppler-Delay profile

2.2. Presentation of the reference scenario and impulse response samples

2.2.1. Presentation of the reference scenario

The SCHUN simulator was used to generate an urban canyon around the trajectory of the receiver. We consider the receiver in motion to investigate the channel dynamic. The speed of the receiver is 5 m.s^{-1}. The trajectory has been chosen to be sufficiently long to assess the reduction techniques properly (150 m - 6000 impulse response samples). The channel is sampled to the frequency 200 Hz. This sampling rate has been chosen according to the channel stationarity length. This characteristic has no impact on this chapter, since each sample of impulse response is reduced independently. Nevertheless, it has a strong impact on the tracking performance of the receiver, which is investigated in Chapter 5. Therefore, the study of the channel stationarity has been postponed to Chapter 5.

The receiver is moving next to a row of buildings, meaning that the trajectory is strictly parallel to the façades. The building density (70 %) and building height (15 m in average) have been chosen large enough to generate many multipaths at every instant (between 2000 and 3000) and challenge the reduction methods as much as possible. Moreover, the influence of the environment has been set to 50 m, meaning that only the multipaths caused by the façades located less than 50 m far from the receiver (in front and behind) are considered. In this scenario, the environment is composed of buildings only, in order to focus the comparison of the methods on a specific type of environment. Trees and poles for example are outs of the study.

A RHCP (right hand circular polarized) signal is emitted by a single satellite located α=30° azimuth and β=35° elevation, from the GPS constellation, as indicated on Fig. 2.3, in the L1 frequency band. The emitter is located 20000 km far away the receiver. Note that the azimuth angle is considered with respect to the x-axis as represented on Fig.2.3 and the elevation relatively to the horizontal plane.

Two different types of façades have been used on this scenario, façade A and B, in the same proportion. They are represented on Fig. 2.4. Façade A is composed mainly of specular type facets, with a few incoherent scatterers in the middle. This type of facades represents recent architecture, with smooth surfaces around the windows. To the contrary, façade B represents older architectures, with no large smooth surfaces apart windows (specular reflection), large edges materialized by backscattering facets and rough surfaces (incoherent scattering facets).

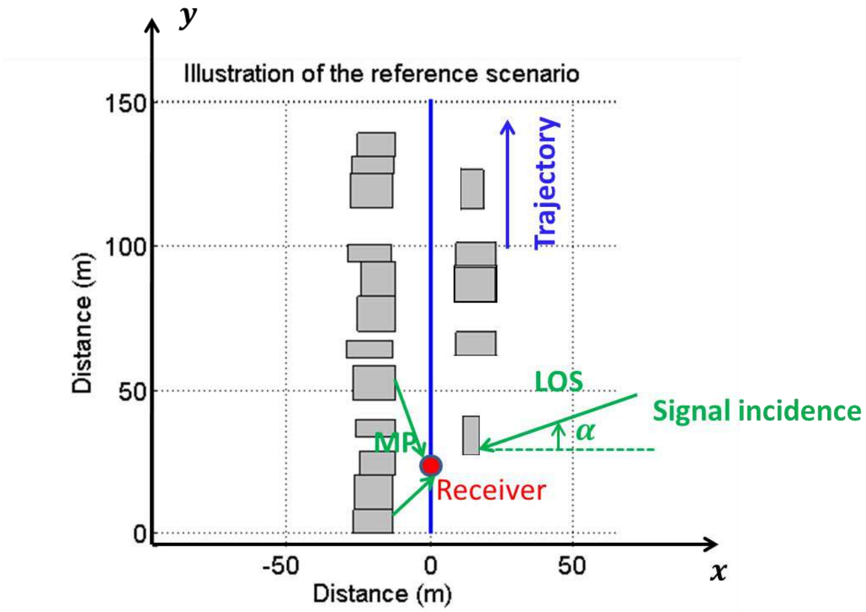

Figure 2.3: Virtual city of the reference scenario and emitter-receiver configuration

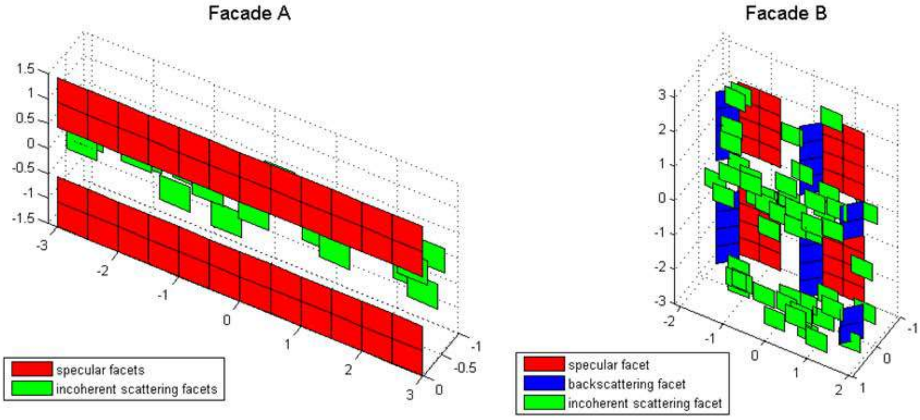

Figure 2.4: Illustration of the reference scenario virtual city façades

2.2.2. Computation of the impulse response

2.2.2.1. Power--delay spread of the impulse response

The reference impulse response was computed by SCHUN all over the reference scenario. Fig. 2.5 represents the power of the multipaths in terms of their delay along the trajectory.

As it can be remarked from Fig. 2.2 and Fig. 2.5, the channel impulse response is represented continuous. To do so, each discrete impulse response sample $h_d(t,\tau)$ has been convoluted with a sinc function in order to form the impulse response $h_c(t,\tau)$ with continuous delays. The convolution with a sinc function reproduces the frequency band limitation induced by the sampling of the signal by receivers. Eq. 2.1 and 2.2 displays the link between $h_d(t,\tau)$ and $h_c(t,\tau)$.

$$h_d(t,\tau) = \sum_{l=1}^{L(t)} \gamma_l(t).\, e^{j\varphi_l(t)} \delta(t - \tau_l(t)) \tag{2.1}$$

$$h_c(t,\tau) = h_d(t,\tau) * sinc(\pi B \tau) \tag{2.2}$$

Where

- $L(t)$ denotes the total number of discrete multipaths in the impulse response at time t.
- γ_l , φ_l and τ_l the amplitude module, phase and delay of multipath l.
- B is the pseudo-frequency of the sinc function, corresponding to the RF filter of the receiver.

Note that the delay resolution of the plot is defined by B. The larger the bandwidth, the better the resolution. Note that the value of B is purely theoretical as there is no receiver involved in this study and thus no bandwidth limitation. In order to make the comparison as easy as possible, it has been chosen to set a large bandwidth: B=100 MHz. In such conditions, the sinc function pseudo-period is 10 ns; meaning that the continuous power-delay profile is plotted with 10 ns resolution.

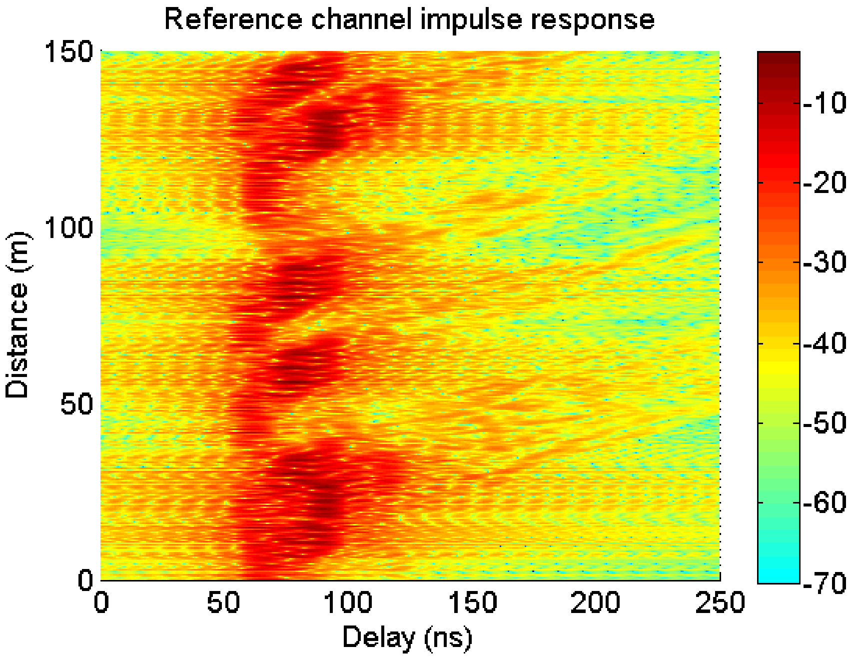

Figure 2.5: Evolution of the power-delay spread along the trajectory

It can be noticed from Fig. 2.5 that the LOS has not been taken into account in $h_c(t,\tau)$. Indeed, the reduction methods will be applied to the multipath channel only, keeping the LOS unchanged. Therefore, only the multipath channel will be plotted to provide a better visualization of the effect of the reduction methods on the multipath channel. Moreover, it has to be mentioned that the impulse response is normalized with respect to the open sky LOS power.

First, Fig. 2.5 shows high power peaks for low delay values, corresponding to the combination of coherent specular multipaths, which are caused by the specular and backscattering facets of which the receiver is in the specular zone. Secondly, it can also be observed lower multipath power all along the delay line, originated from incoherent scatterers.

2.2.2.2. Doppler spectrogram of the impulse response

The second parameter that will be investigated along chapters 2, 3 and 4 of that study is the Doppler shift of the multipaths, depending of their power. The Doppler spectrogram of the impulse response has been computed along the trajectory. To do so, the Bello dispersion function has been used as defined in [Bell 63]. It is the Fourier transform of the narrow-band power of the impulse response along the time dimension, as expressed by Eq. 2.3 and 2.4. To compute the dispersion function at time t, the following process was applied: first, the total narrowband power of the multipath channel has been computed by summing the complex amplitudes of all the multipaths at time t. Secondly, the Doppler shifts of the multipaths were used to propagate their phase and compute the evolution of the narrowband power at the times $t+\frac{m}{M}T$, where $m=1,\ldots,M$ and T is the duration of the propagation. The dispersion function is the Fourier transform of the narrowband channel $P(t+\frac{m}{M}T)$ along the time dimension. Therefore, its literal expression is given by 2.3 and 2.4.

$$S(t,f_d)=\sum_{m=1}^{M}P(\,t+\frac{m}{M}T)e^{-j2\pi f_d\frac{m}{M}T} \tag{2.3}$$

Where

$$P(t+\Delta t)=\sum_{l=1}^{L}\gamma_l(t).\,e^{j\varphi_l(t)}.\,e^{j2\pi\vartheta_l\Delta t} \tag{2.4}$$

- f_d denotes the Doppler frequency.
- $\gamma_l(t)$ and $\varphi_l(t)$ are the amplitude and phase of multipath l and Δt is the propagation instant.

In that case, the Doppler resolution is given by T and the maximum Doppler shift is given by M/T. This time again, there is no theoretical constraint on M and T. Indeed, the Doppler spectrum is computed for each impulse response sample independently. Then, there is no need to consider any coherency time of the channel as all the parameters used to compute the narrowband channel (amplitude, phase and Doppler shift) are considered at instant t to compute the dispersion function at instant t. A propagation duration T=200 ms has been chosen to reach 5 Hz Doppler resolution. The sampling period of the narrowband power was set to 5 ms to be able to observe Doppler shifts up to 100 Hz.

Like for the power-delay, the LOS Doppler is not represented on the Doppler spectrogram to focus on the multipath Doppler characteristics. Moreover, the Doppler spectrogram is represented relatively to the LOS power. It is also important to remark that only the Doppler due to the motion of the receiver is considered. The Doppler due to the motion of the satellite is the same for every multipath at a given time and is not of interest in the channel reduction context. Figure 2.6 illustrates the Doppler spectrogram along the trajectory on the reference scenario. Two major multipath contributions can be observed, one in the negative Doppler between *-20 Hz* and *0 Hz*, corresponding to the backscattering multipaths reaching the receiver from behind (the emitter satellite being located in front of the receiver) and one in the positive Doppler between *0 Hz* and *20 Hz* corresponding to the specular multipaths reaching the receiver from front. The incoherent scatterers radiate lower power all along the Doppler line.

It can be noted that the backscattering multipaths are the most powerful. Indeed, all along this thesis, only the co-polar component of the power is represented. The signal is RHCP polarized on this scenario, which implies a switch of polarization at each reflection of the signal on dielectric surfaces. The specular multipaths undergo one reflection only whereas the backscattering multipaths undergo two reflections, hence the stronger power on the co-polar component.

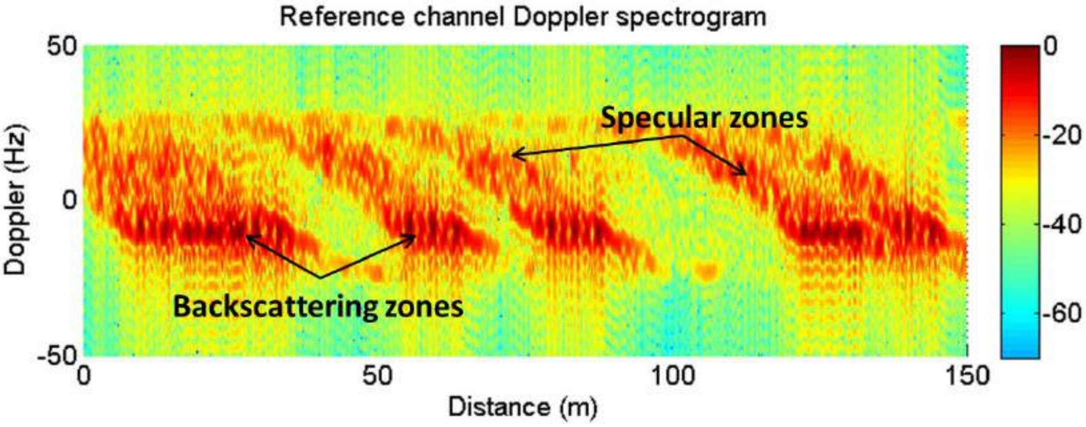

Figure 2.6: Doppler spectrogram of the multipath channel along the trajectory of the reference scenario

2.3. Preliminary test: performance of the selection methods

2.3.1. Literature overview

The principle of the methods referred to as “selection methods” is to reduce the number of multipaths by keeping only the most important ones, according to various criteria, cutting away the others. A few works in the literature investigated the performance of this kind of methods. In [Kolu 03], the author discusses this possibility, emulating the echoes of the reduced channel using a hardware channel generator. Therefore, this problem is close to the one of this thesis, even if the scope of the study is different. First, in [Kolu 03], the channel is measured using a channel sounder coupled to the SAGE maximum-likelihood algorithm to estimate the multipaths, with 25 ns delay resolution, which leads to sampled impulse responses. Secondly, the empirical channel presented in [Kolu 03] is dedicated to telecommunications, which leads to other constraints than navigation issues. Indeed, the delay profile of the impulse responses presented in [Kolu 03] are approximately 10 times longer in delay than the ones of this thesis. In the satellite navigation context, multipaths with $\tau > T_c + C_s/2$ have no effect on the tracking performance (T_c denotes the chip duration and C_s the chip spacing). Therefore, they are not considered. Another difference between telecommunication and navigation is the comparison of the BER (*Bit Error Rate*) in [Kolu 03] to assess the reduction methods, contrary to the comparison of the pseudo-range errors in this thesis.

Nevertheless, the best selection method according to the conclusions of [Kolu 03] will be used in this section to assess the impact of this approach on the original channel. Three approaches were presented in [Kolu 03]: cut off multipaths from the impulse response by minimizing the energy error, the delay spread error or frequency error. It concluded that the minimization of the energy error had similar results than the minimization of the delay spread error, better than the minimization of the frequency error. Therefore, it has been decided to implement a selection method preserving the total power of the channel as best as possible.

It should be mentioned that [Krac 08] also investigated a selection method, cutting off the lowest power multipaths. In that case, the field of application is also navigation. Moreover, the comparison of the methods involves the pseudo-range error preservation as well. However, the size of the original impulse responses is significantly lower than in this thesis [Jul 13] (less than one hundred multipaths).

2.3.2. Implementation and assessment of the selection methods

According to the recommendations found in the literature, it has been decided to select the multipaths with the highest power, in order to reduce the original impulse response. A basic algorithm has been implemented: the most powerful multipaths are selected and remain unchanged in the reduced channel; the other ones are cut off. Figure 2.7 illustrates the power-delay profile of an impulse response snapshot before and after reduction, in the case of 10 multipaths in the reduced channel. The right plot shows that the multipaths of the reduced channel are close terms of delay. Therefore, Fig. 2.8 zooms on the multipaths of the power-delay profile presented on Fig. 2.7.

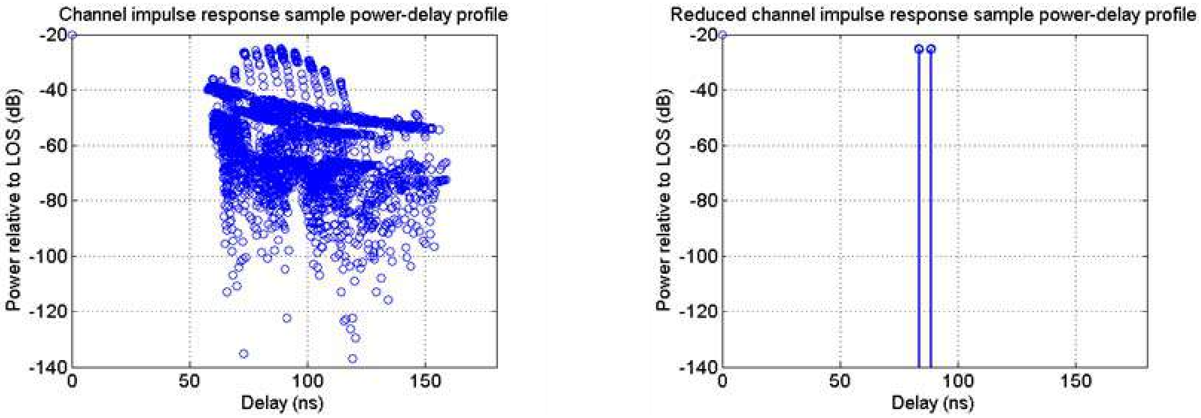

Figure 2.7: Illustration of impulse response reduction using the minimum energy error selection method at distance d=25 m of the reference scenario

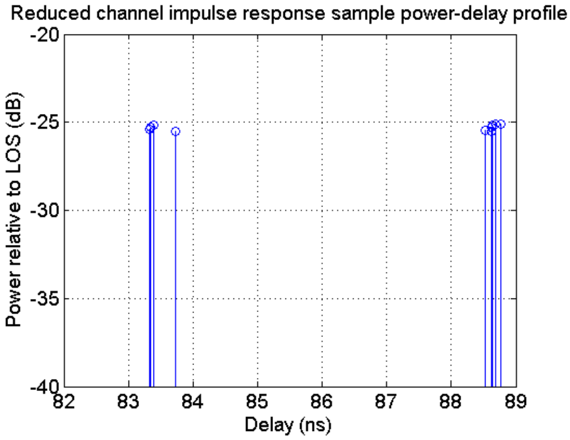

Figure 2.8: Zoom on the reduced channel impulse response of Fig. 2.7

Fig. 2.7 and Fig. 2.8 show that the selection method has a strong impact on the impulse response delay spread. Indeed, on this example corresponding to d=25 m on the reference scenario, the original impulse response shows a delay spread superior to 100 ns. On the reduced channel, this delay spread is decreased to 10 ns. Only two multipath sources are conserved by the reduction algorithm. The right plot of Fig. 2.9 displays the power of the reduced impulse response depending on the multipath elevation and azimuth. Two multipath sources are clearly identifiable, but all others have been cut off by the algorithm, as compared to the reference impulse response on the left plot. This observation proves the strong impact of this specific reduction method on the original channel.

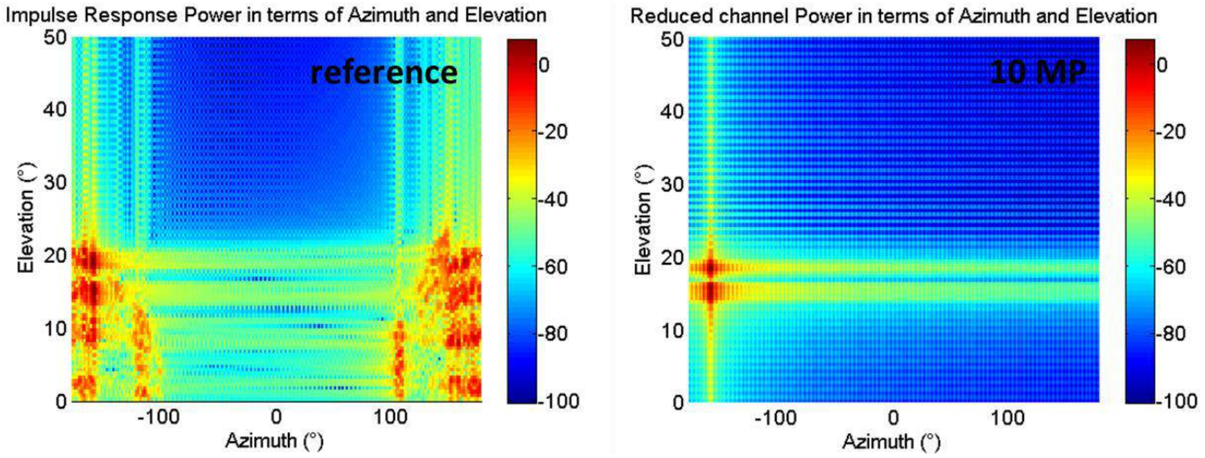

Figure 2.9: Comparison of the reference channel impulse response power in terms of angle of arrival with the selection method reduced one

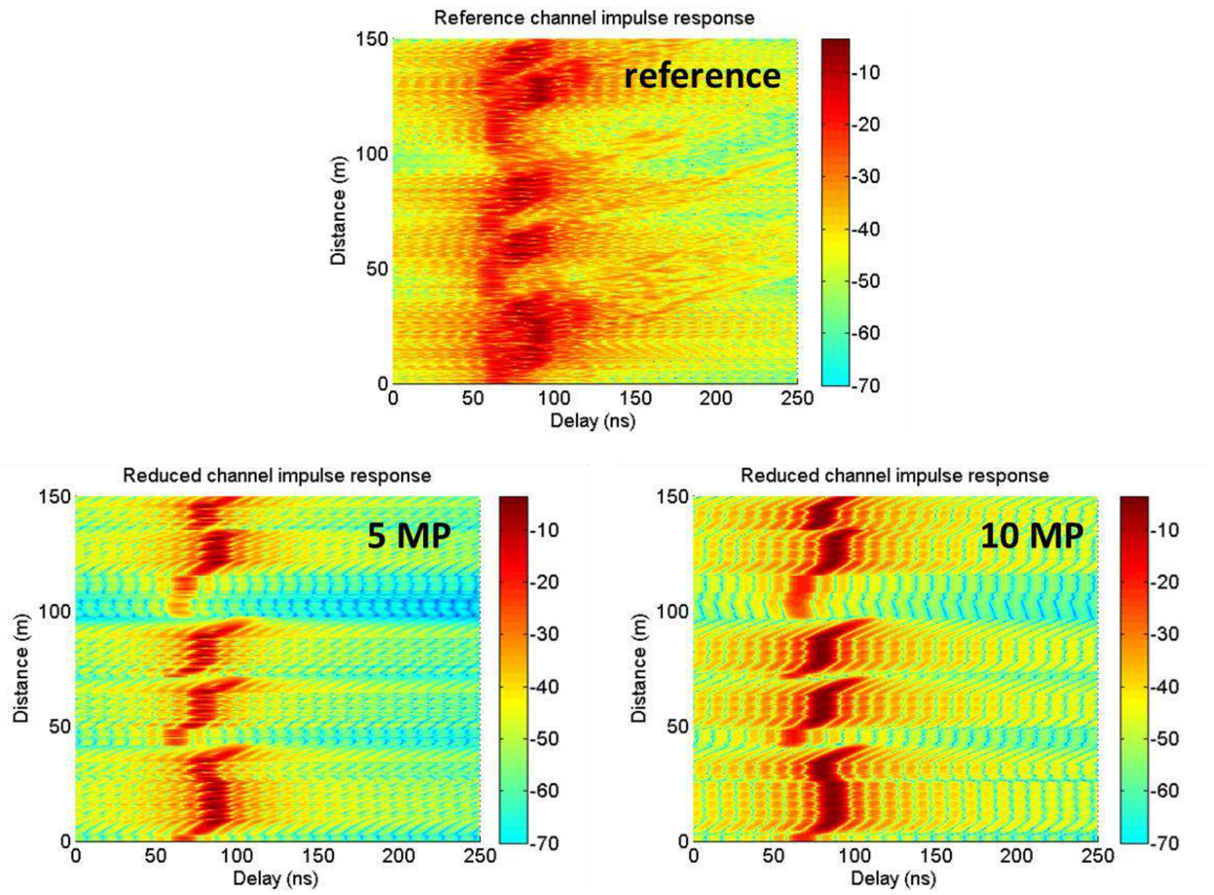

Figure 2.10: Reduced power-Delay profile along the trajectory with 5 and 10 contributions in the reduced channel (bottom) compared with the reference channel (on top)

Fig. 2.10 illustrates the evolution of the channel impulse response power-delay profile all along the trajectory on the reference scenario, in the case of 5 multipaths (left plot) and 10 multipaths (right plot) in the reduced channel. The top plot recalls the reference channel power-delay profile. First, it can be observed that the two bottom plots are similar, meaning that the augmentation of the number of multipaths in the reduced channel from 5 to 10 do not improve the performance of the method. Secondly, it also illustrates the shortening of the delay spread. Indeed, the multipath power is concentrated inside a small delay interval (less than 20 ns wide) at every instant along the trajectory.

Fig. 2.11 represents the reduced channel Doppler spectrogram along the trajectory. As compared to the reference Doppler spectrum on Fig. 2.6, the Doppler spread has been significantly reduced, as well. Indeed, only one sharp power peak is preserved by the reduction method, located in the negative Doppler, whereas the reference Doppler spectrogram clearly shows some multipath power in both positive and negative Doppler zones. This is a consequence of the impairment of the multipath angle of arrival, illustrated on Fig. 2.9.

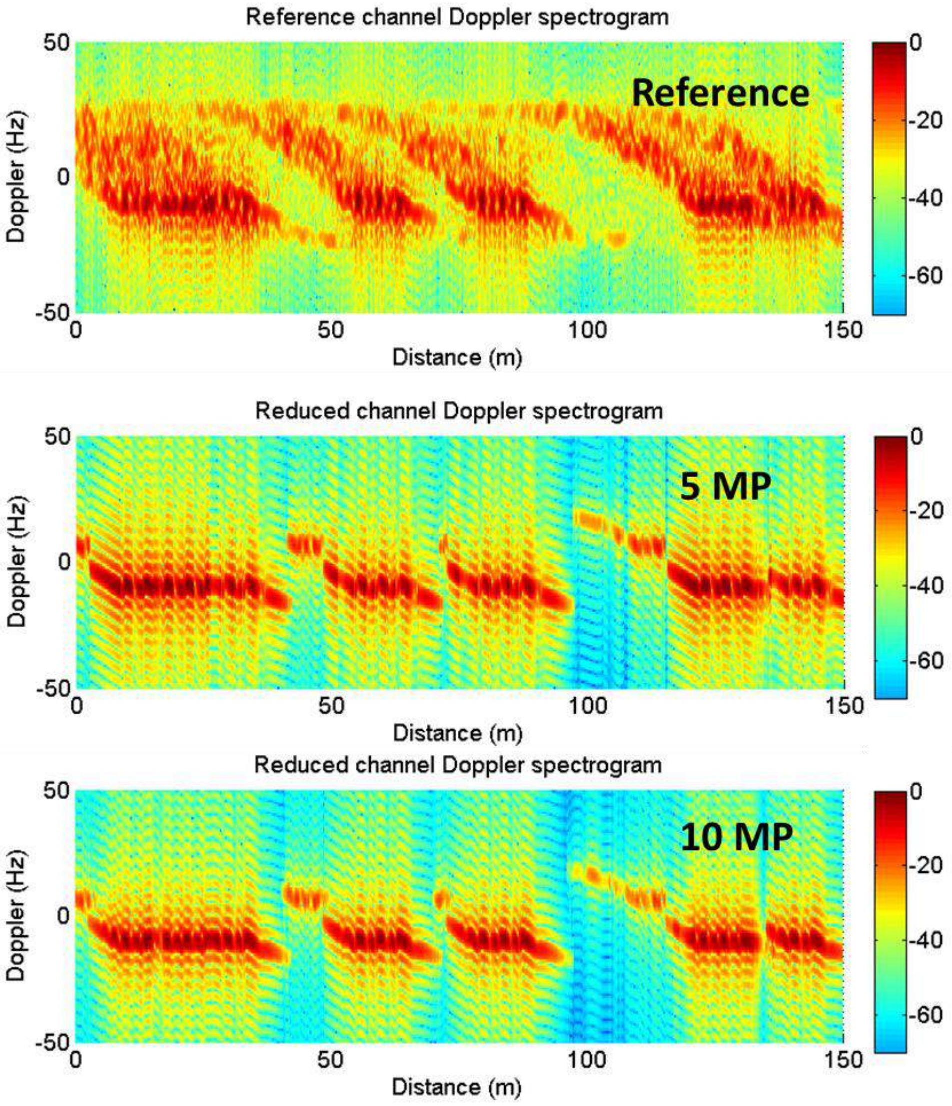

Figure 2.11: Reduced channel Doppler spectrogram along the trajectory with 5 and 10 contributions in the reduced channel

Fig. 2.9, 2.10 and 2.11 illustrated the impairment of the delay, Doppler and angle of arrival of the original channel by the selection methods. On this reference scenario presented in section 2.2, SCHUN simulates thousands of multipaths to build the reference impulse response. On Fig. 2.2 which displayed an example of power-delay profile, the multipaths can be separated in two groups, depending on their amplitude. First, some high power contributions can be identified. They are generated by specular and backscattering facets of which the receiver is in the specular zone. Nevertheless, these multipaths are not many, and are associated to facets located in a restricted geographical zone. Therefore, the selection of the multipaths among those zones lead to a cut off of the multipath diversity. On the other side, many weaker amplitude multipaths are spread all along the delay line. Their power is negligible, if considered individually, with respect to the high power multipaths. But the fact that they are many and partially coherent creates power contributions all along the delay line. Hence the difference between the reference and the reduced impulse response illustrated Fig. 2.10.

For this poor impulse response preservation, the selection methods have proved to be ineffective to reduce the multipath channel. A suitable reduction method, in order to improve the channel diversity conservation, should consider the whole delay line. These types of approach will be investigated in the following section.

2.4. Tap Delay Line channel models

2.4.1. Literature overview

The Tap Delay Line approach is commonly used to reduce the size of the impulse response, for different signal processing applications. This section focuses on these methods, based on a delay scaling approach. The common point of these methods is to sample the reduced channel delay line, using regular delay intervals to reduce the number of discrete contributions in the channel. Contrary to the selection methods presented in the previous section, the reduction algorithm considers the whole delay line to compute the parameters of the reduced channel.

As suggested by [Ait 11], the Tap Delay Line method is used in wide-band telecommunication applications to simulate the effects of the sampled multipath channel on the telecommunication systems. Its easy implementation made it very popular in the context of the wide-band channel modelling. It can be used either to reduce the multipath impulse response, like in [Ait 11], or to adapt the multipath delays to specific sampling instants, like in [Silv 03].

The problem of this thesis is similar to the problem of [Ait 11]. Therefore, the emphasis will be put on the Tap Delay Line method suggested in this study. It consists in the basic Tap Delay Line model applied to the channel reduction context. A few enhancements to this basic approach will be discussed, in order to optimize the performance of the model.

Different Tap Delay Line variants are compared in [Silv 03]. This comparison is useful for this thesis in order to establish a complete assessment of the Tap Delay Line performance. Therefore, a particular interest will be brought to the different methods presented in [Silv 03], even if the field of application differs significantly from this thesis. Indeed, in [Silv 03], Tap Delay Line methods are used to change the sampling instants of the delay line. Several techniques are presented in [Silv 03], and compared through the BER preservation criteria.

In order to avoid the testing of an exhaustive set of reduction methods, it has been decided to split them in two groups. The first type regroups the methods which aim at aggregating multipaths with close delays, like the basic Tap Delay Line method used in [Ait 11] and some of the methods presented in [Silv 03]. The second type of methods consists in sampling the continuous power-delay profile, referred to as channel re-sampling in [Silv 03] and [Mehl 08]. In order to find an optimal Tap Delay Line method, this section will compare a simple Tap Delay Line approach to the channel re-sampling techniques.

2.4.2. Tap Delay Line approach

First, the performance of the basic Tap Delay Line method will be assessed. This method is built as follows:

- First, the Delay scale is sampled, divided in regular delay intervals. Each tap is represented by a single multipath at its center. Fig. 2.12 illustrates the delay line scaling used to run the Tap Delay Line algorithm.

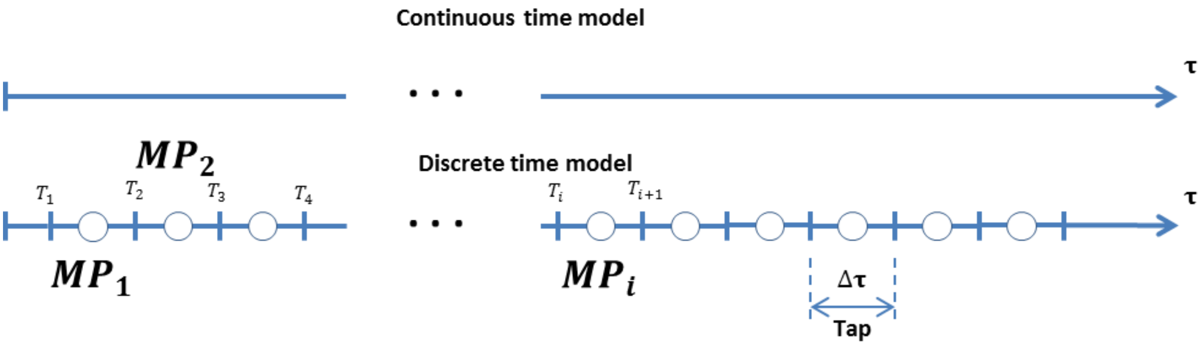

Figure 2.12: Illustration of the delay line scaling process

- Then, all the multipaths reaching the receiver within the same tap are coherently summed (considering multipath amplitude module and phase), to compute the complex amplitude of the multipath at the center of the Tap. Eq. 2.5 displays this calculation:

$$\tilde{\gamma}_i(MP_i) = \sum_{l,\ \tau_l \epsilon [T_i, T_{i+1}]} \gamma_l e^{j\varphi_l} \tag{2.5}$$

Where

- $\tilde{\gamma}_i(MP_i)$ denotes the complex amplitude of the multipath MP_i of the tap i.
- $[T_i, T_{i+1}]$ denotes the delay interval of tap i.
- $\tau_l, \gamma_l, \varphi_l$ denote respectively the delay, amplitude module and phase of multipath l, so that $\tau_l \epsilon [T_i, T_{i+1}]$.

The Tap Delay Line channel is constituted of the multipaths MP_i, located at the center of the taps. It should be mentioned that the size of the taps $\Delta\tau$ has a major impact on the performance of the algorithm. Indeed, the smaller the tap width, the more multipath on the reduced impulse response, and the better the performance. Fig. 2.13 illustrates the impact of the Tap Delay Line algorithm on the power-Delay profile, at the same point of the trajectory as Fig. 2.7. For this example, the tap width of 20 ns has been chosen. Note that with a constant tap size, the number of multipaths in the reduced channel depends on the impulse response delay spread. There are two major consequences to this.

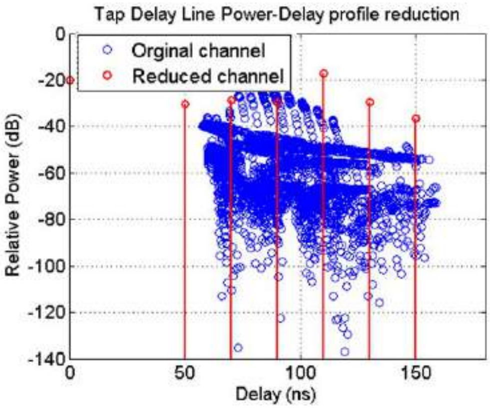

Figure 2.13: Illustration of the Tap Delay Line reduction effect on the power-delay profile at time t=5s, with $\Delta\boldsymbol{\tau}$=20 ns tap width

First, the delay spread of the channel is likely to change along the trajectory, leading to a non-constant number of multipaths in the reduced channel. The evolution of the number of multipaths in the channel along the time is theoretically acceptable. Indeed, the variation of the environment along the course creates rays appearance and disappearance, normally at a low power level. The Tap Delay Line model is able to reproduce this phenomenon, when the number of multipaths of the original channel in a given tap increases or fades away. Fig. 2.14 represents the evolution of the multipath delays and power of the Tap Delay Line reduced channel, on a segment of the reference scenario. Along the trajectory, 3 multipaths appear. It confirms that the power of the multipaths at the time of their appearance is low relatively to the other contributions, which is physically acceptable.

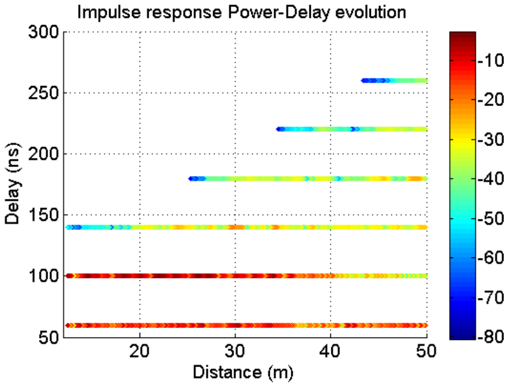

Figure 2.14: Evolution of the multipath delays and power (color) along the [12 m, 50 m] segment of the reference scenario with $\Delta\boldsymbol{\tau}$=40 ns tap width

Secondly, the Tap Delay Line method presents some practical limitations. Indeed, it is impossible to set the number of multipaths in the reduced channel. The only parameter that is scalable is the size of the taps. Therefore, the user can not know a priori the number of multipaths generated by the reduction algorithm. In order to compare the performance of a given reduction method to the performance of the Tap Delay Line method without bias, the number of multipaths in both reduced channels has to be the same (because their performance increase with the number of echoes). This statement can possibly impede the following of this study, which consists in assessing the modifications brought to the Tap Delay Line elementary method, by comparing the preservation of the original channel power-delay and Doppler spectrogram. For that reason, a systematic technique to adjust the number of multipaths to the desired value has been implemented and will be presented in the following.

From these ascertainments, a few improvements have been brought to the elementary Tap Delay Line method, listed hereafter:

- First, as mentioned in section 2.2, the Tap Delay Line method is applied to the multipaths only. The LOS ray stays clear from any modification. Aggregating the LOS with multipaths would generate interferences, severely impairing the reduction performance. In the following of the study, the LOS contribution will always be separated from the multipath components, on which the reduction algorithms will be applied.

- The second improvement concerns the position of the taps. In the presentation of the elementary Tap Delay Line algorithm, it was only mentioned that the delay scale had to be sampled, without detailing the position of the center of those taps. It has been decided in that study to keep the delay of the strongest multipath of the impulse response unmodified (classically the one generated by a specular reflection on the façade). That means that the tap containing this strongest multipath is centered on this ray, in order to avoid moving it to the center of the Tap. Therefore, for each impulse response snapshot, the most powerful multipath has been identified and the position of the taps has been adapted to its delay, as illustrated on the simplified example of Fig. 2.15, on which it can be observed that the first tap is centered on the maximum power multipath.

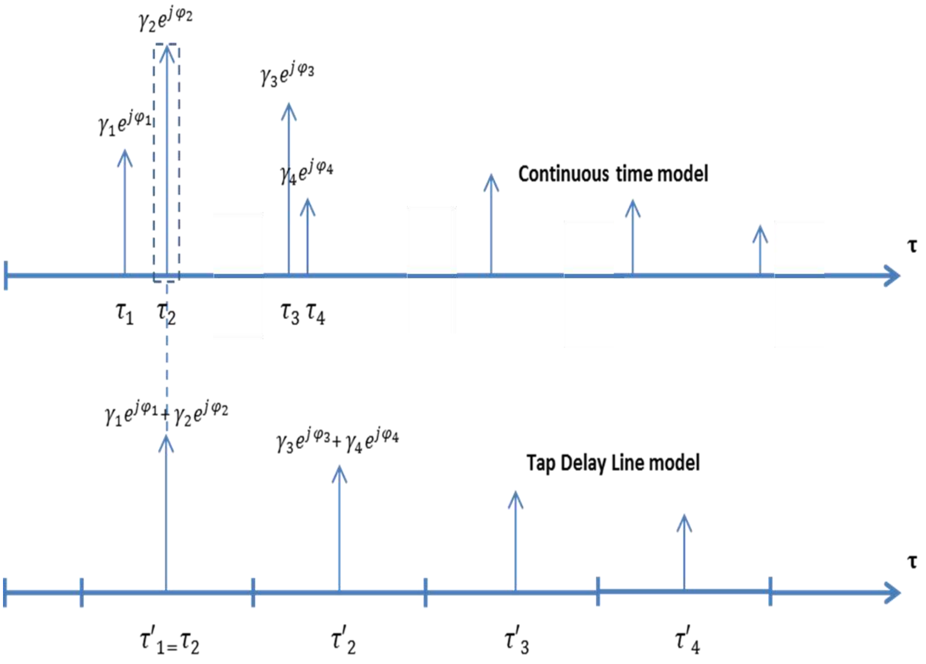

Figure 2.15: Illustration of the Tap Delay Line reduction process

- To finish, as previously stated, an algorithm has been implemented in order to control the number of multipaths in the reduced channel. First, the user chooses a given number of multipaths L and a tap size $\Delta\tau$, small enough so that at every epoch the number of non-0 multipaths generated by the Tap Delay Line channel is bigger than L (knowing approximately the maximum delay spread). Then, in order to reduce the number of multipaths down to L, the lowest power multipath is merged with the multipath of closest delay. This process is repeated as many times as necessary to have L multipaths in the reduced channel.

This reduction process has been applied to the reference impulse response described in section 2.2. As in the previous section, two reduced impulse responses have been computed, one containing 5 multipaths and the other 10 multipaths (less restrictive). In both cases, the size of the delay taps has been set to 10 ns, which corresponds to the delay resolution of the continuous impulse response represented Fig. 2.16.

The top plot of Fig. 2.16 represents the evolution of the channel power-delay profile, along the 150m of the trajectory in the reference scenario. The same plot was already displayed on Fig. 2.5. The two bottom plots represent the evolution of the Tap Delay Line channel power-delay profile, in the case of 5 multipaths (left) and 10 multipaths (right) in the reduced channel.

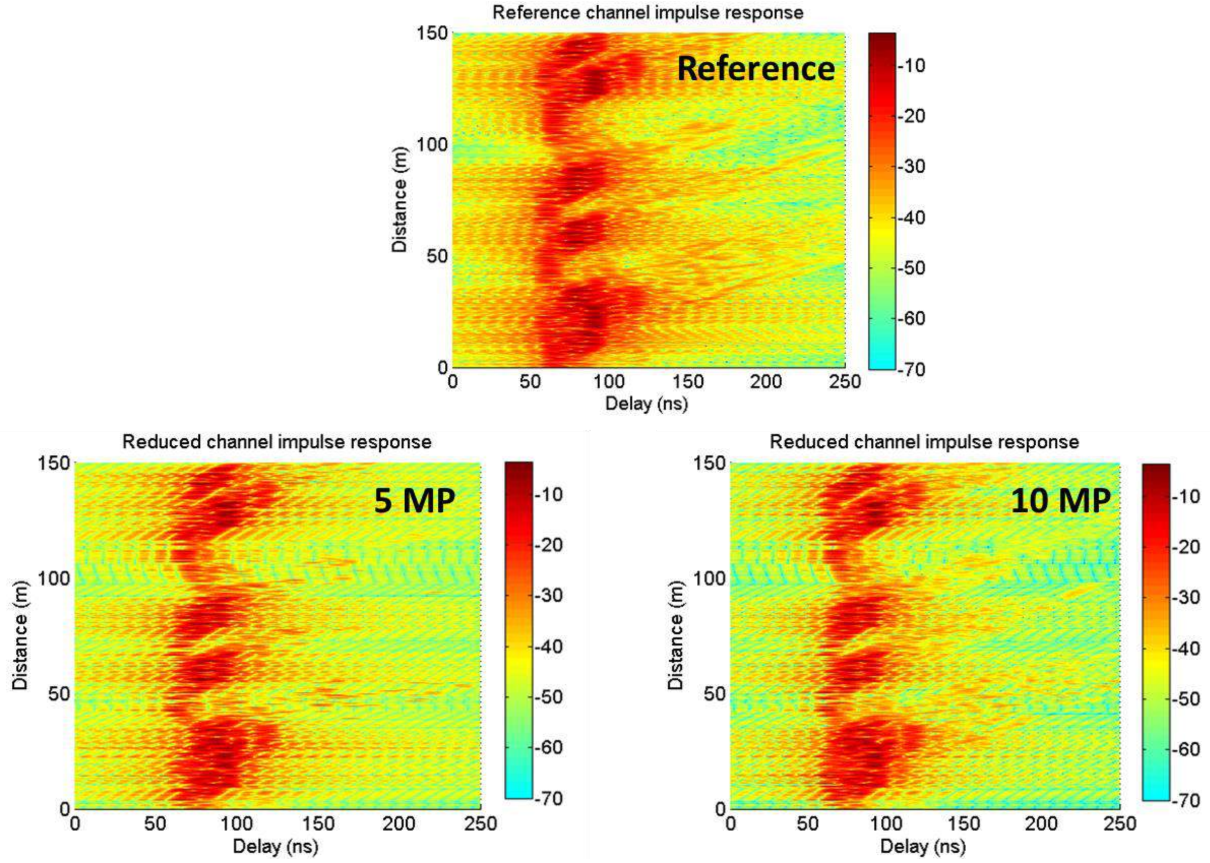

Figure 2.16: Comparison of the reduced channel impulse responses (bottom) with the reference (on top) for 5 and 10 multipaths using the Tap Delay Line

First, it can be observed that contrary to the selection methods, the Tap Delay Line preserves the delay spread of the impulse response. Indeed, the power peaks are clearly identifiable and then the multipath delay spread can easily be read through the power-delay profiles on Fig. 2.16. When observing this delay spread epoch per epoch on the reference channel, it appears to vary from 30 ns to almost 100 ns. The same variation is displayed by both 5-multipath and 10-multipath reduced channels. This improvement is clearly induced by the fact to consider the whole delay line to aggregate the multipaths, and not only focus on the major contributions.

Moreover, the power-delay profile of the 5-multipath Tap Delay Line channel and the one of the reference channel seem to overlap, even if a few minor power peaks shown by the reference channel are not reproduced by the 5-multipath reduced channel (incoherent scattering). It can be observed on the right plot that the fact to limit the reduction process to 10 multipaths in the reduced channel increases the power-delay preservation performance. Indeed, more power contributions are observable in the high delay zones (corresponding to remote facets).

It has to be mentioned that the choice of 10 ns tap size has a strong influence on the performance. As explained in section 2.2, the continuous impulse responses represented on the plots of Fig. 2.16 are drawn with 10 ns delay resolution. Therefore the impact of the sampling process on the power-delay profile is not observable on these plots. With larger tap widths, a decrease of the performance would have been observed.

As a partial conclusion, the Tap Delay Line technique improves the performance of the multipath reduction methods as compared to the selection methods, especially concerning the preservation of the delay spread. It showed to be able to conserve the original channel power-delay profile reasonably well, at condition to set a small tap width, leading to a larger reduced impulse responses, which can be compensated by the reduction algorithm that has been presented. Nevertheless, the fact to move the multipaths to the center of the delay taps can imply a mismatch between the power peaks of the reference channel as compared to those of the reduced channel. Therefore, it has been decided to explore the other possibilities of channel reduction, still in the Tap Delay Line type. Note that the preservation of the Doppler spectrogram by the Tap Delay Line method has not been mentioned yet. It will be investigated below in section 2.4.4.

2.4.3. Channel re-sampling techniques

It was suggested in [Silv 03] an alternative Tap Delay Line approach: the channel re-sampling method. The general idea of this second type of reduction process is to make the discrete multipath channel continuous, and then to re-sample it with the desired sampling rate and position of the samples. In [Silv 03], the original discrete channel was not given by a channel synthesizer as in this thesis but by real channel sounding measurements. In that case, the channel re-sampling method is used to adjust the delays of the original channel samples to another sampling rate.

A few variants of this general approach are presented in [Silv 03], which differ essentially in the way to make the discrete impulse response continuous. For the current study, it has been decided to use the model consisting in the convolution with a sinc function, as suggested in [Mehl 08]. Convoluting the delay dimension with a sinc function is the temporal consequence of the limitation of the signal frequency band as it is sampled by the receiver. The sinc function model has been chosen for this purpose and its pseudo-frequency is identified to the RF bandwidth of the receiver. Note that this technique has already been presented in section 2.2, and was used to plot the impulse response power-delay profiles. Eq. 2.6 is obtained by combining Eq. 2.1 and 2.2, where $h_c(\tau)$ denotes the continuous impulse response, at the time t:

$$h_c(\tau) = \sum_{l=1}^{L} \gamma_l . e^{j\varphi_l} sinc(\pi B(\tau - \tau_l)) \tag{2.6}$$

In Eq. 2.6, $\tau_l, \gamma_l, \varphi_l$ denote respectively the delay, amplitude module and phase of the multipath l . To apply the channel re-sampling model to the reference impulse response of this study, this specific convolution process will be applied to the reference channel, at each epoch. *B* denotes the signal bandwidth, which has been set to B=100 MHz in this chapter. This bandwidth value has been chosen large compared to the actual capacities of a hardware receiver, whose bandwidth does not often exceed 20 MHz. However, in order to increase the delay resolution of the continuous impulse response, 100 MHz bandwidth has been considered, which implies 10 ns sinc function lobe width. Fig. 2.17 illustrates the channel convolution with the sinc function on a simplified channel with 4 multipaths.

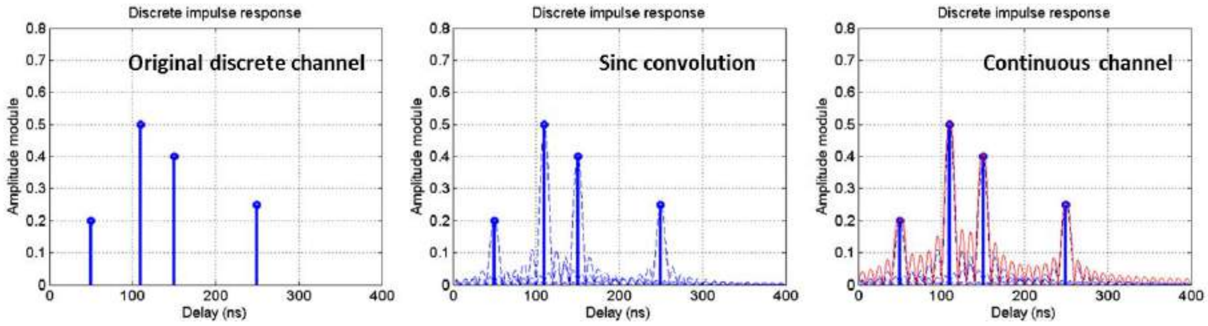

Figure 2.17: Illustration of the continuous channel construction

Once the impulse response is continuous, it is resampled to the sampling period τ_e. As a consequence, the channel impulse response has been reduced, and the number of multipaths in the reduced channel depends on the sampling rate. Therefore the value of the sampling period has a strong impact on the reduced channel. Nevertheless, it has been decided to set the value of τ_e so as to optimize the conservation of the transfer function. This process will be detailed hereafter. Fig. 2.18 illustrates the continuous channel sampling process.

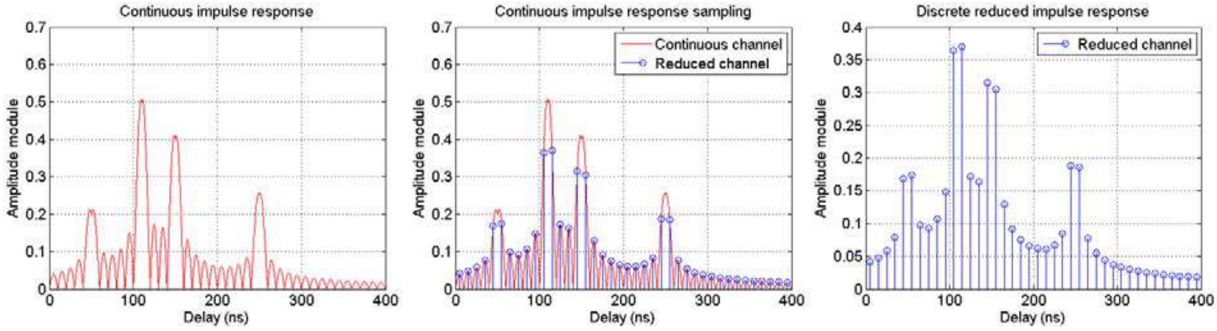

Figure 2.18: Illustration of the continuous channel sampling process

As it can be observed on Fig. 2.18, the reduced impulse response is composed of regularly spaced multipaths along the delay line. The improvement brought by this method is the fact that the multipaths are samples of the reference impulse response. Contrary to the elementary Tap Delay Line approach, the multipaths are not moved to the center of the taps and the contribution of every multipath of the channel is considered.

The most important parameter of the algorithm is the delay line sampling rate, which has already been mentioned. To choose the ideal sampling period, the Fourier transform of the impulse response, referred to as the channel transfer function in [Bell 63], has been investigated on the reference and reduced channels. Eq. 2.7 displays the literal expression of the transfer function of the channel at the time t, computed as the Fourier transform of the impulse response along the delay dimension:

$$H(f) = \int_{-\infty}^{+\infty} h(\tau) e^{j2\pi f\tau} d\tau \tag{2.7}$$

In Eq. 2.7, $H(f)$ denotes the Fourier transform of the discrete impulse response $h(\tau)$ described in Eq. 2.1. By developing $h(\tau)$:

$$H(f) = \int_{-\infty}^{+\infty} \sum_{l=1}^{L} \widetilde{\gamma_l}\, \delta(\tau - \tau_l) e^{j2\pi f\tau} d\tau \tag{2.8}$$

According to the integral properties of the Dirac function, Eq. 2.8 becomes:

$$H(f) = \sum_{l=1}^{L} \widetilde{\gamma_l} e^{j2\pi f\tau_l} \tag{2.9}$$

In Eq. 2.8 and 2.9, $\widetilde{\gamma_l}$ and τ_l denote the complex amplitude and delay of multipath l. Fig. 2.19 illustrates an example of transfer function, with the corresponding temporal impulse response at time t=5 s on the reference scenario. The frequency band chosen to investigate the transfer function is B=100 MHz. Note that the Transfer Function is not necessarily a pair function of the frequency. Indeed, as revealed by Eq. 2.9, the transfer function is complex, and the relative phases of the multipaths create this dissymmetry around the frequency f=0.

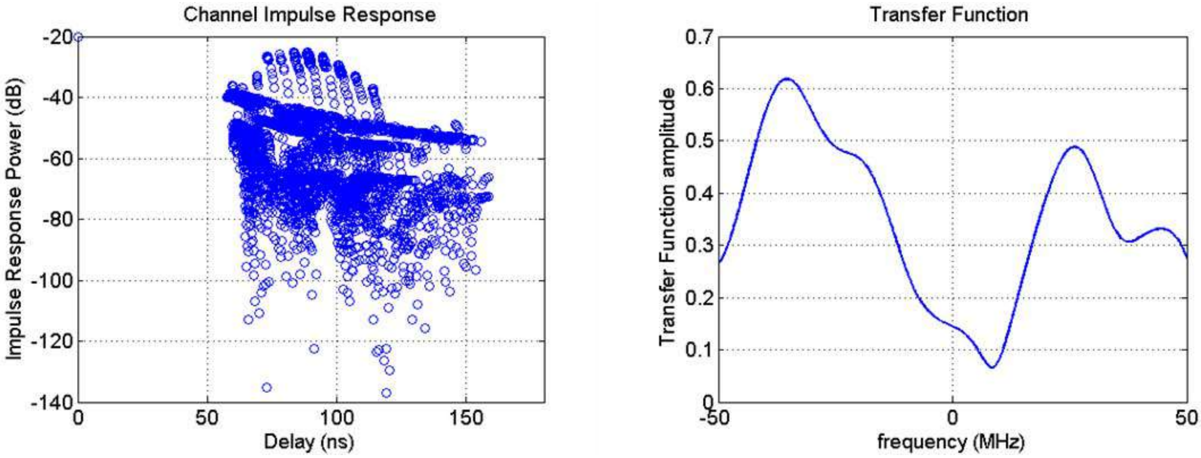

Figure 2.19: Example of channel transfer function, at t=5 s on the reference scenario

The continuous channel sampling period of the re-sampling technique has been chosen so as to optimize the similarity between the reference channel transfer function and the reduced one. This study will be developed hereafter. $h(\tau)$ denotes the impulse response in the delay dimension at a given epoch and $H(f)$ the corresponding transfer function computed using Eq. 2.9. $h_{red}(\tau)$ will be the reduced channel impulse response and $H_{red}(f)$ its transfer function. In the following, $III_{\tau_e}(\tau)$ will denote the Dirac comb, with delay τ_e between the Dirac impulses, as specified by Eq. 2.10:

$$III_{\tau_e}(\tau) = \sum_{k=-\infty}^{+\infty} \delta(\tau - k\tau_e) \tag{2.10}$$

If B denotes the signal bandwidth, the reduced channel impulse response is given by:

$$h_{red}(\tau) = \left(h(\tau) * sinc_{\frac{1}{B}}(\pi B\tau)\right).III_{\tau_e}(\tau) \tag{2.11}$$

Eq. 2.12 is obtained by applying the Fourier Transform to both parts of Eq. 2.11:

$$H_{red}(f) = \left(H(f).\frac{1}{B}rect_B(f)\right) * \frac{1}{\tau_e}III_{\frac{1}{\tau_e}}(f) \tag{2.12}$$

The element $rect_B(f)$ denotes the rectangle function of width B, which is the Fourier transform of the sinc function. Moreover, the Fourier transform of the Dirac comb is a Dirac comb in the frequency domain, according to the Poisson summation formula. Eq. 2.12 shows that $H_{red}(f) = H(f)$ on the frequency bandwidth B if and only if $\tau_e = \frac{1}{B}$. Therefore, when applying the channel re-sampling method to reduce the multipath channel, the sampling period has been chosen the same as the sinc function pseudo-period , as represented on Fig. 2.18, that is to say τ_e=10 ns.

This reduction process has been applied to the reference impulse responses. A few complements have been brought to this algorithm, listed hereafter:

- It can be observed from Fig. 2.18 and Eq. 2.11 that the continuous impulse response power-delay profile is extended to negative delays. Therefore, in order to preserve the total impulse response power, some multipaths of the reduced channel must have negative delays. It consists in echoes with a lower travel time than the direct path, which has no physical sense. That is why it has been decided to aggregate these negative delay multipaths with the multipath of smallest positive delay. It means that the complex amplitude of every multipath with a negative delay is coherently added to the amplitude of the multipath with lowest positive delay, to preserve the narrow-band channel power.

- Moreover, this continuous power-delay profile is infinite in theory. Therefore, some multipaths have to be cut off in order to obtain a finite discrete impulse response. A delay threshold has been set, in order to decrease the number of multipaths, avoiding any significant loss of total channel power. It has been decided that all the multipaths whose power is under 1 % of the total narrow-band channel power are cut off.

- To finish, the same issue as with the Tap Delay Line method is encountered: the user of the algorithm has no control on the number of multipaths in the reduced channel, which depends here on the delay spread of the reference power-delay profile. Therefore, the same method as the one proposed for the Tap Delay Line reduction process has been applied: the smallest power multipaths are moved and aggregated with the closest multipaths in terms of delay.

Fig. 2.20 displays an example of the channel re-sampling process applied to the reference channel, at time t=5 s of the reference scenario. As for the Tap delay Line power-delay profile, the reduced channel delays are sampled. In that study, the sampling rate τ_e=10 ns has been chosen. Even if an algorithm has been proposed previously to tune the number of multipaths in the reduced channel, it is possible to adjust the tap size, with an approximate knowledge of the delay spread and of the final number of multipaths. The bigger the delay spread, the bigger the tap size. If the tap size is too small compared to the delay spread, a small number of multipaths in the reduced channel leads to the reduction of the delay spread. This will be illustrated by Fig. 2.22.

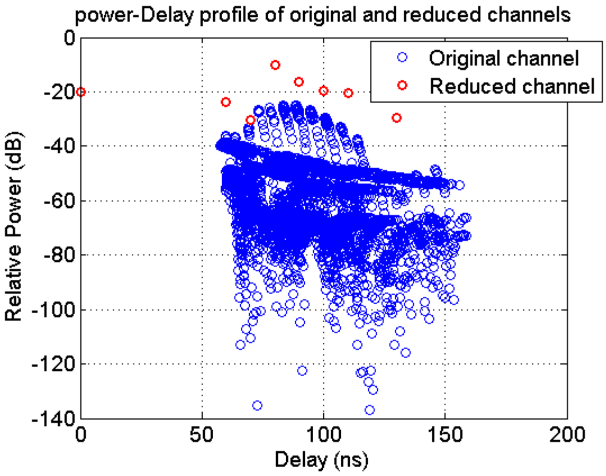

Figure 2.20: Example of reduce channel Power-Delay profile at time t=5s

Fig. 2.21 shows a sample of the comparison between reference and reduced impulse responses in the frequency domain, through the transfer function comparison at the time t=5 s. As stated previously, this re-sampling method aims at preserving the best the impulse response in the frequency domain. It can be observed on Fig. 2.21 that the reduced channel impulse response matches the original channel almost perfectly, which is an illustration of the good functioning of the algorithm. Note that theoretically, the transfer functions of the original and reduced channels should overlap perfectly, as shown by Eq. 2.12. This would be the case if the whole infinite delay line had been considered in the reduced channel. The fact of having cut off the low power delays and moved the negative delays to the positive delay zone creates a slight incoherency, observable on Fig. 2.21.

Fig. 2.22 represents the evolution of the channel impulse response power-delay profile along the trajectory. The top plot represents the reference channel impulse response. The bottom plots represent the re-sampled channels. It can be observed that the impulse response in the delay domain is preserved by the channel re-sampling technique better than by the Tap Delay Line technique, both with 5 and 10 multipaths in the reduced channel. This is due to the fact that the channel re-sampling technique does not move the multipaths to the center of the taps, but considers a continuous multipath power all along the delay line to determine the total multipath power at the center of each delay tap. It was the major enhancement brought by the channel re-sampling method, which is justified by the illustration of Fig. 2.22. A slight decrease of the impulse response delay spread is observable on the 5-multipath reduced channel, which illustrates the previous statement stating that small tap sizes combined with too few multipaths in the reduced channel can lead to the delay spread diminution. Indeed, this lack of delay spread is no more observable on the 5-multipath reduced channel.

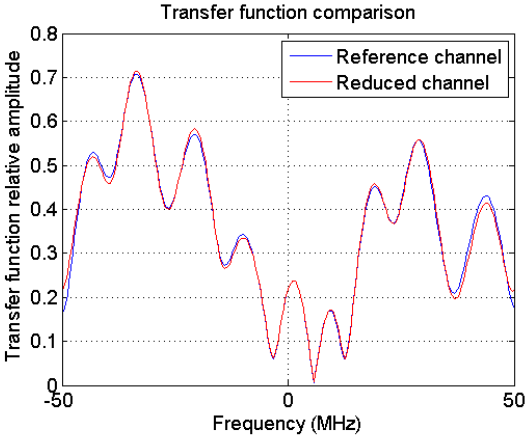

Figure 2.21: Example of T=transfer function comparison at time t=5s

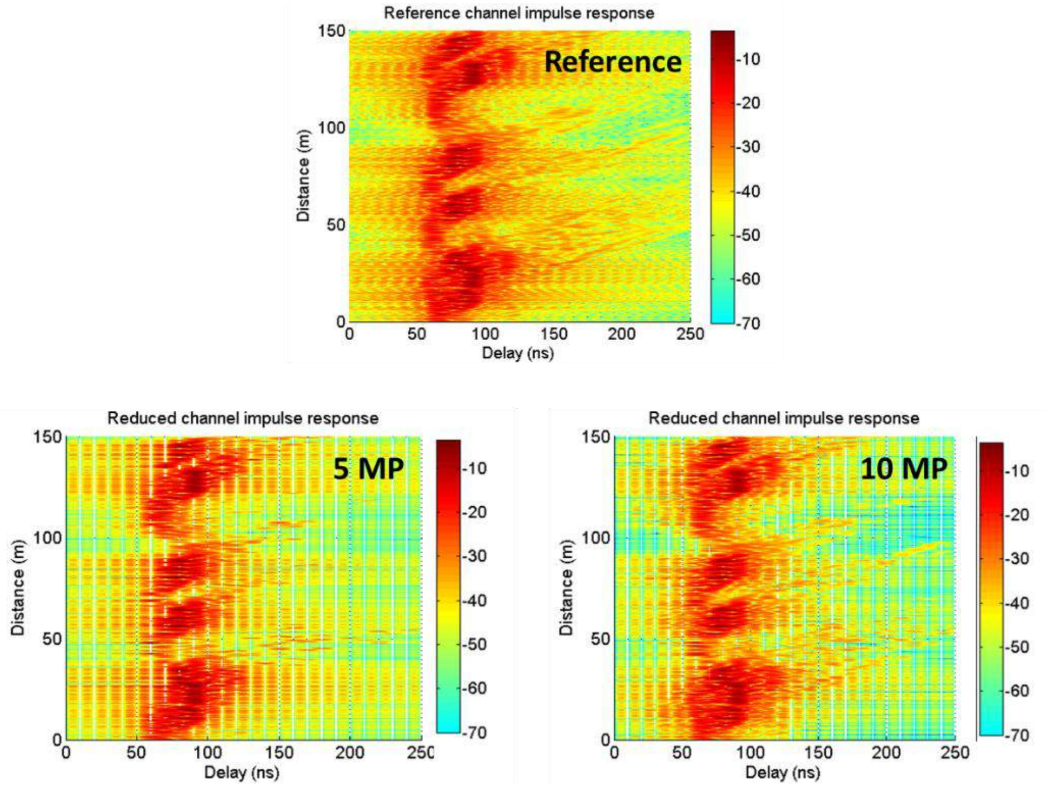

Figure 2.22: Evolution of the Power-delay profile along the trajectory with 5 and 10 multipaths in the re-sampled channel

The performance of the channel re-sampling technique in terms of impulse response preservation is slightly better than the Tap Delay Line technique. However, this amelioration is not significant enough to consider that the re-sampling technique has really improved the Tap Delay Line technique, from the only comparison of the impulse response preservation. Nevertheless, the channel re-sampling approach optimizes the preservation of the channel transfer function, as illustrated by Fig. 2.21. Therefore, the preservation of the channel impulse response in the frequency domain is expected to be better with the re-sampling technique than with the Tap Delay Line technique. This is confirmed by Fig. 2.23, which illustrates an example of comparison of the channel transfer function using the Tap Delay Line reduction approach and the channel re-sampling approach, with 10 multipaths in the reduced channel. The re-sampled channel function fits the reference channel transfer function better than the Tap Delay Line, especially in the high frequency zones.

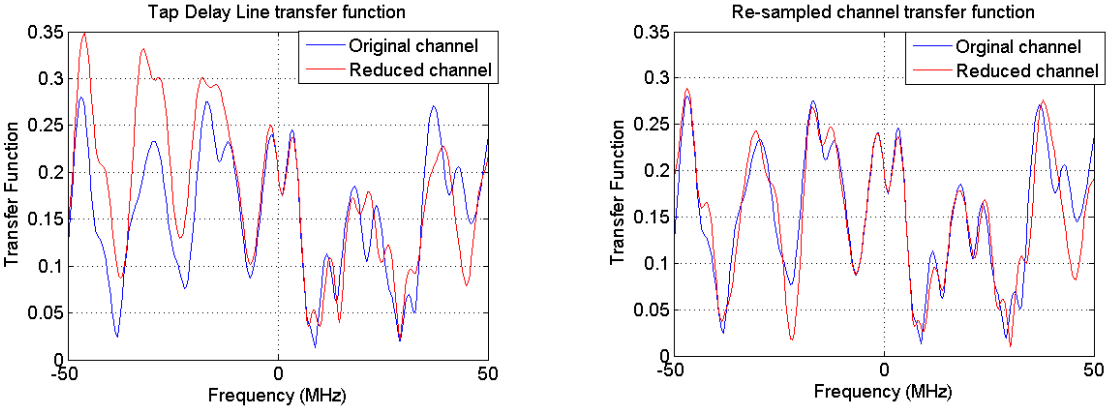

Figure 2.23: Comparison of the Tap Delay Line reduced channel (left plot) and resampled channel (right plot) transfer function with the reference transfer function at time t=10 s

2.4.4. Doppler spectrum of the reduced channels

In the subsections 2.4.2 and 2.4.3 concerning Tap Delay Line and channel re-sampling processes, the construction of the Doppler distribution of the reduced channel has not been mentioned. These two approaches perform the channel reduction along the delay dimension and do not take into account the Doppler shifts of the multipaths. However, the specifications of the reduced channels that will be computed all along this thesis require the Doppler parameter of each multipath. Therefore, an algorithm has been added to the previous section to compute the mean Doppler shift of each tap. The Doppler of the multipath at the center of a tap of the reduced channel is the average Doppler of all the multipaths of the reference channel reaching the receiver within this delay tap, weighted by their amplitude module.

Finally, Eq. 2.13 displays this Doppler calculation, for the tap l, at the time t. $\tau_l \in [T_i, T_{i+1}]$ refers to the multipath delays belonging to the Tap l and $\widetilde{\gamma_l}$ the corresponding complex amplitude.

$$\vartheta_i(t) = \frac{\sum_{l,\tau_l \in [T_i,T_{i+1}]} |\widetilde{\gamma_l}| \, \vartheta_l(t)}{\sum_{l,\tau_l \in [T_i,T_{i+1}]} |\widetilde{\gamma_l}|} \tag{2.13}$$

Fig. 2.24 represents the comparison between the Doppler spectrum of the reference and re-sampled channels, with 5 and 10 multipaths in the reduced channels. Fig.24 shows clearly a mismatch between reference and reduced impulse responses, in the case of 5 multipaths as well as 10 multipaths. First, the multipath power peaks appear discontinuous along the Doppler line, instead of following the facets along the trajectory. The specular and backscattering contributions are not clearly identifiable anymore. Secondly, some power peaks appear on non-physical Doppler locations. For example, the major contribution all along the trajectory seems to be located at Doppler 0 Hz, corresponding to scatterers located beside the receiver. In the reference scenario, the emitting satellite is located 30° azimuth. As a consequence, the major power contributions are the specular and backscattering facets located 30° or -30° toward the receiver. No power peak is observable in these Doppler zones on the reduced channels.

Therefore, the re-sampling channel reduction approach impairs the Doppler spectrogram of the environment. Fig. 2.25 illustrates the same comparison as Fig. 2.24 with the Tap Delay Line reduced channel. It shows exactly the same lack of Doppler spectrum preservation. This observation could be expected being given the fact that the same technique was used for both Tap Delay Line and channel re-sampling methods to compute the Doppler shift of the reduced channel echoes.

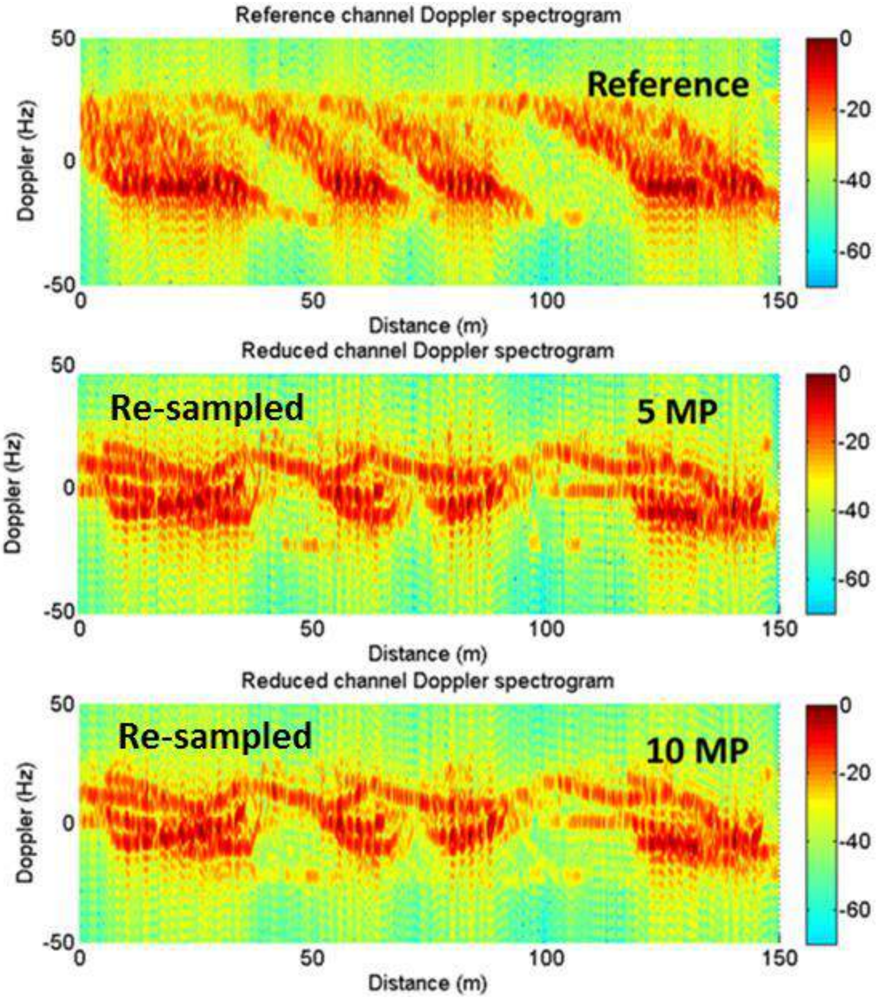

Figure 2.24: Comparison of the reference channel Doppler spectrum (top plot) with the re-sampled channel Doppler spectrum along the trajectory

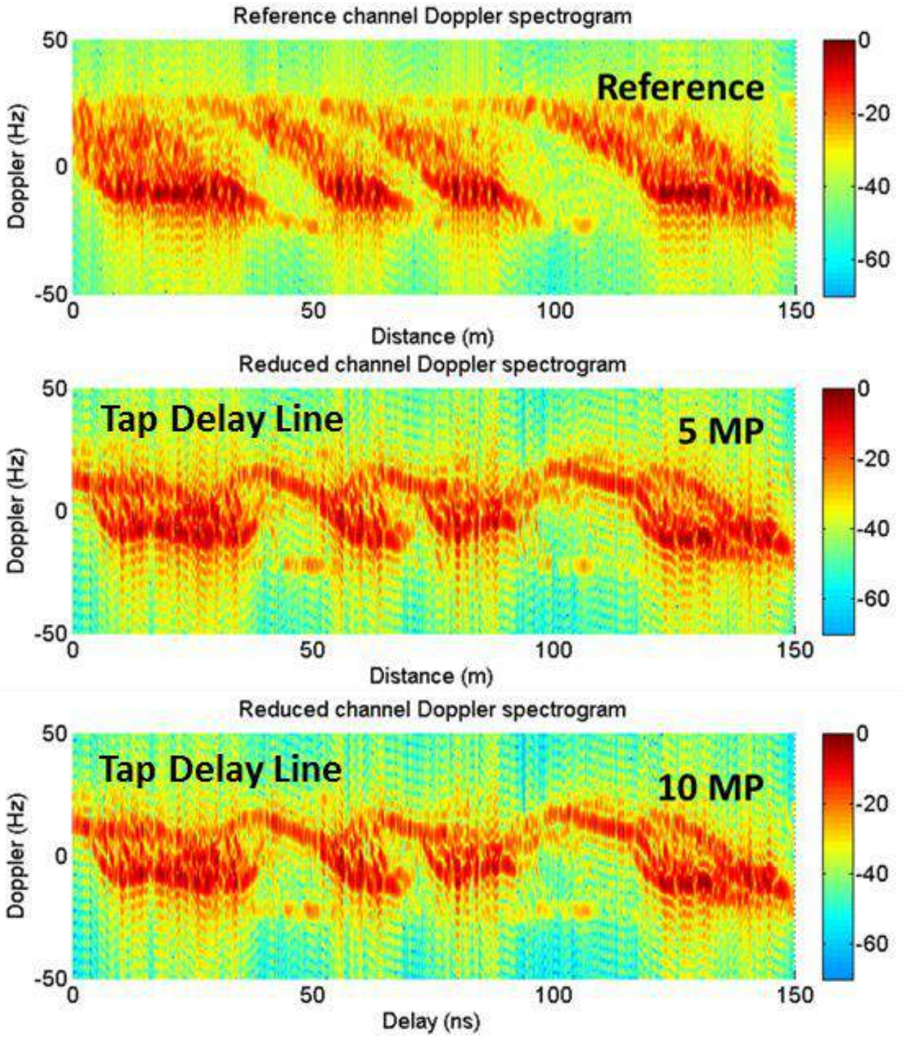

Figure 2.25: Comparison of the reference channel Doppler spectrum (top plot) with the Tap Delay Line reduced channel Doppler spectrum along the trajectory

Fig. 2.26 shows an example of the impact of the reduction process on the Doppler-delay profile at the time t=10 s on the trajectory using the Tap Delay Line technique. During the reduction process, the multipaths contained in the same tap are aggregated. The Doppler parameter of the resulting multipath is calculated using the weighted average technique described in Eq. 2.13. The red spots represent the Doppler and delay coordinates of the reduced channel multipaths on the Doppler-delay profile at time t=10 s. The Taps A, B and C have been framed on the plot in order to illustrate the fact that a single tap can contain multipaths with very different Doppler shifts. For example, Tap C consists of multipaths with high positive Doppler $\vartheta_l > 20$ Hz and negative Doppler $\vartheta_l <$-20 Hz. The multipaths of Tap C are originated by facets located far in front of the receiver or far behind it. This mixing of angles of arrivals results in a multipath with delay τ_i= 125 ns and ϑ_i=-10 Hz in the reduced channel. No multipath with similar Doppler-delay coordinates is observable on the reference impulse response, hence the non-physical Doppler spectrogram.

Two major issues arise from this Doppler inhomogeneity within the different taps:

- First, the Doppler diversity among the multipaths in the same tap causes differences in the variation of the phases of these multipaths along the time. This can lead to a discontinuity of the phase of the reduced channel multipaths. This physical aberration scrambles the information about the multipaths life span, which can be of interest for some applications.

- Secondly, the abnormal Doppler values in the reduced channel can be problematic from the receiver point of view. The Doppler parameter is generally used to propagate the multipath phases to compute their complex amplitude at different times apart from the channel sampling instants. Moreover, the Doppler shift impacts the multipath amplitude module because of the demodulation frequency error as it will be described in chapter 5.

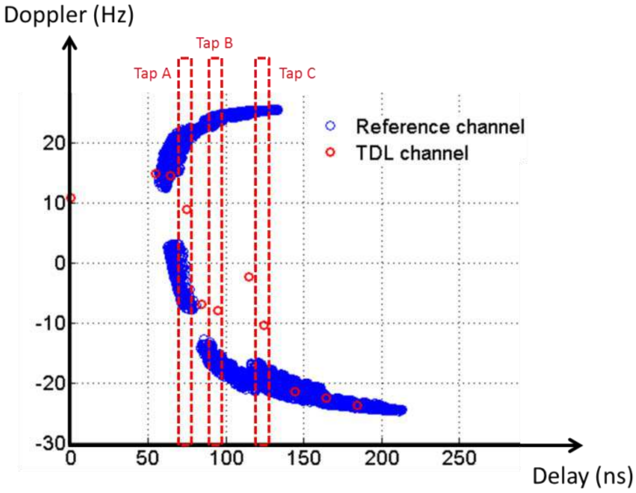

Figure 2.26: Illustration of the Doppler diversity of the multipaths in three taps of the reference Doppler-delay profile

Several techniques have been considered in order to overcome the problem of Doppler diversity in one tap. In what concerns the Tap Delay Line technique, the possibility to sample the Doppler line as well as the delay line has been investigated. Then, the reference channel Doppler-delay profile is gridded along the dimensions of delay and Doppler, with 2-dimensional Doppler-delay taps, of size $\Delta\tau$ x $\Delta\vartheta$. The multipaths reaching the receiver in the same delay and Doppler interval are coherently summed. The multipaths of the reduced channel are located at the center of the delay taps and at the center of the Doppler taps. The major drawback of such an approach is the resulting number of contributions in the reduced channel. Indeed, the final number of multipaths depends on the size of the taps as presented in the one-dimension Tap Delay Line approach. Except that in the 2-dimensional Tap Doppler-Delay Line approach the number of multipaths corresponds to the number of delay taps multiplied by the number of Doppler taps. As a consequence, the size of the reduced impulse response is much larger than the classic Tap Delay Line impulse response. This study aims at decreasing the multipath channel to less than 10 contributions, as mentioned in section 2.1. The sizes of the delay and Doppler taps have to be large enough to satisfy this restriction. Such a low channel sampling rate is likely to impair the power-delay and Doppler spectrogram of the original channel. Therefore, this technique has not been further investigated.

In what concerns the channel re-sampling method, a similar approach as the Tap Doppler-Delay Line has been chosen. Instead of sampling the continuous impulse response along the delay dimension only, Doppler impulse response can be added. First the Doppler-delay profile of the channel impulse response is convoluted with a sinc function along both delay and Doppler dimensions to create a 2-dimensional continuous impulse response. Then, it is sampled along these two dimensions at the sampling rates τ_e and ϑ_e, as described in section 2.4.3. This time again, the size of the reduced impulse response corresponds to the number of delay samples multiplied by the number of Doppler samples. The 10-multipath constraint on the reduced channel requires a low sampling rate of delay and Doppler dimensions, impairing the power-delay and Doppler spectrogram as well. Therefore, this technique has not been further investigated neither.

2.4.5. Conclusion of the Tap Delay Line study

Along this section 2.4, the Tap Delay Line and channel re-sampling approaches showed to have similar performance in terms of power-delay preservation. It could be considered as satisfactory, as compared with the reference channel impulse response along the trajectory. Nevertheless, this study identified two major drawbacks of these approaches. First, the delay line is sampled, which implies a sampled reduced impulse response. The multipath delays can only take a discrete set of values, impacting the channel delay resolution. Secondly, as observed in the last sub-section, the fact of omitting the channel Doppler parameter while aggregating the multipaths leads to an abnormal reduced channel Doppler spectrogram.

For these reasons, more elaborated channel reduction methods have been investigated in the following of this chapter.

2.5. Channel clustering techniques

The principle of the methods presented in this chapter is to reduce the channel impulse response by aggregating clusters of multipaths. At the end of the previous section, two limitations concerning the Tap Delay Line approach were pointed. First, the Tap Delay Line approach samples the delay dimension, which leads to a discrete set of delays in the reduced channel. Secondly, the Doppler shift of the multipaths is not taken into account, leading to a possibly instable reduced channel. The clustering approach overcomes these two constraints. It allows the user to cluster multipaths among a multidimensional set of data (delay-Doppler for example) without any sampling limitation. This section will investigate the performances of different clustering techniques, aiming at clustering the multipath channel along the 2-dimensional space of delay and Doppler parameters. The multipaths of the same cluster will be merged in order to build the reduced multipath channel.

2.5.1. Literature overview

The possibility to cluster multipaths has already been investigated in different context of telecommunication studies. In particular, most of these works concern the indoor channel sounding problem. In that case, the presence of a multipath cluster in a given measured data set denotes the existence of an object reflecting or diffracting the direct signal. Therefore, an accurate clustering of the multipath channel in the 3-dimensional space is the major challenge to be able to estimate the composition of the environment. As in the previous section, this problem found in the literature is remote from the scope of this thesis, which is the development of channel reduction techniques. Nevertheless, those clustering methods seem to be well suited for the channel reduction problem also. Therefore, it has been decided to take advantage of the recommendations available in the works related to the indoor multipath channel in order to implement the clustering techniques of this chapter.

Different clustering techniques have been considered in the literature. From the different studies available, three clustering approaches have been identified. Most of these studies considered that the usual *K-means* clustering method is the best way to cluster the multipaths, considering different parameters. This is the case of [Czin 06a], [Czin 05], and [Mota 11]. They all perform the clustering of measured MIMO channel data. The wide-band parameters (delay, amplitude and angle of arrival) are estimated using parametric methods such as SAGE or MUSIC. The *K-means* algorithm is then applied to these data along the dimensions of delay and angle of arrival. Note that the *K-Means* algorithm belongs to the *partitional class* of clustering techniques. The performance of such an algorithm, applied to the channel reduction problem, will be studied in section 2.5.4.

Other methods have been proposed in different studies, also applied to the indoor channel sounding issues, including the *Single Linkage Method* in [Maul 12] and [Salo 05]. The *Single Linkage Method* is a non-iterative method, belonging to the *hierarchical class* of clustering techniques, based on the progressive reduction of the number of clusters. It consists in merging successively the two closest clusters (considering a multipath distance), until reaching the desired number of clusters. The ability of this algorithm to reduce the multipath channel will be investigated in section 2.5.3.

A stochastic clustering method has been presented in [Shut 04]. The clusters constitute the discrete states of a Markov channel process. From one instant to another, data samples move from a cluster to another according to a transition probability matrix. This type of clustering method is related to the statistic channel evolution approaches that will be investigated as way of reducing the multipath channel in chapter 4. Therefore, this clustering technique will not be considered in this section.

Some studies assessed the performance of those different clustering techniques such as [Maul 12] or [Mota 13]. Nevertheless, the data sets on which the clustering algorithms are applied are very different from impulse responses considered in this thesis. Therefore, this section will investigate the performance of these techniques as well, applying them to the impulse responses of SCHUN. Moreover, a few validity indices have been presented in [Mota 13] like *Calinski-Harabasz Index*, *Generalized Dunn's Index*, *Xie-Benni Index* or *PBM Index*. They all aim at estimating the number of clusters in a given data set, by comparing the performance of the clustering process with different numbers of clusters. These indices have not been used in this thesis because the mathematical efficiency of the clustering methods is not of interest in this study. It has been decided to assess the different clustering techniques in terms of power-delay and Doppler spectrogram conservation, so as to sustain the continuity with the previous sections.

2.5.2. Multipath distance

Both *Single Linkage* and *K-means* techniques cluster the data samples according to their proximity in the global data set. Like any clustering technique, this process requires an appropriate metric to quantify this proximity. To establish such a metric, a distance over the multi-dimensional multipath space (delay, Doppler, …) has been defined. The *Multipath Component Distance* introduced in [Stei 02] has been chosen. The *Multipath Component Distance* is the generalization of the *Euclidian Distance* to multi-dimensional vectors [Czin 06b]. An example of *Euclidian Distance* is displayed on Eq. 2.14. In that example, $d_{i,j}$ represents the distance between the two multipaths i and j depending on their delays τ_i and τ_j.

$$d_{i,j} = (\tau_i - \tau_j)^2 \tag{2.14}$$

Other parameters can be added to the *Multipath Component Distance*. Thus, this distance is challenged by the combination of parameters with different units. For that matter, the different terms of the *Multipath Component Distance* are normalized Euclidian distances along different parameters. Eq. 2.15 displays the distance between two N-dimensional vectors i and j, according to the *Multipath Component Distance* model. $\Upsilon_1, \dots, \Upsilon_N$ represent different multipath parameters, which are also the different dimensions of vectors i and j. $\Delta\Upsilon_{1_{max}}, \dots, \Delta\Upsilon_{N_{max}}$ normalize the different terms of the distance in order to make it homogeneous, without unit. These values are chosen with respect to the extreme values of these different parameters ($\Delta\Upsilon_{max} = \Upsilon_{max} - \Upsilon_{min}$). This normalization of the dimensions scales the parameters between 0 and 1. $\zeta_1, \dots, \zeta_N$ are additive scaling factors allowing the user to give more importance to some parameters with respect to the others.

$$d_{i,j} = \sqrt{\zeta_1.(\frac{\Upsilon_{1_i} - \Upsilon_{1_j}}{\Delta\Upsilon_{1_{max}}})^2 + \zeta_2.(\frac{\Upsilon_{2_i} - \Upsilon_{2_j}}{\Delta\Upsilon_{2_{max}}})^2 + \dots + \zeta_n.(\frac{\Upsilon_{N_i} - \Upsilon_{N_j}}{\Delta\Upsilon_{N_{max}}})^2} \quad (2.15)$$

As introduced in this section, the clustering techniques have been chosen for their ability to cluster multipaths according to different parameters. In the previous section, the Doppler of the multipaths had been identified as a major clustering parameter. Aggregating a group of multipaths with various Doppler shifts impairs the Doppler spectrogram. Therefore, according to the study presented in section 2.4, two major multipath parameters have to be taken into account while aggregating multipaths: delay and Doppler shift. Note that in that study, the angle of arrival is almost redundant with the multipath Doppler shift. Indeed, the Doppler parameter ν_l depends on the angle of arrival of the multipath according to the equation displayed on Eq. 2.16, where α_l and β_l denote its azimuth and elevation of arrival, s the speed of the receiver, f_0 the carrier frequency and c the speed of light. The receiver is supposed to move along the y-axis as represented on Fig. 2.3, whereas the emitter is assumed to be motionless.

$$\nu_l = -s.sin(\alpha_l)\cos(\beta_l)\frac{f_0}{c} \quad (2.16)$$

As a conclusion, the clustering process may be applied the 2-dimensional space delay-Doppler instead of the 3-dimensional delay-angle of arrival. This is likely to improve the performance of the clustering for a given number of multipaths in the reduced channel. Indeed, with a limitation of 5 multipaths for example, there is less than 2 multipaths per dimension, which is likely to impair the performance of the clustering. Therefore, it has been decided to limit the clustering process to the 2-dimensional delay-Doppler impulse response profile. In other terms, multipaths will be aggregated according to their delay and Doppler proximity only.

Two remarks have to be made concerning the fact to assimilate the angle of arrival parameter to the multipath Doppler. First, the Doppler shift depends on azimuth and elevation. Therefore an angular ambiguity arises, because two different couples (azimuth, elevation) can lead to the same Doppler ν. Yet, as described in section 2.2, the reference scenario is composed of 15 m height buildings in average, located at minimum 10 m far from the receiver. Then, the elevation of the multipaths varies from 0° to 56°. As 50 m environment influence is considered, the azimuth varies from 102° to -102° (+180°). The azimuth diversity is 3 times larger than the elevation diversity, which limits this angular ambiguity.

Secondly, the SCHUN software computes the multipaths generated by one building row only, whose façades are opposed to the emitter satellite. But in the case of other channel simulators, the impulse response can contain multipaths from both sides of the urban canyon. It can be deduced from Eq. 2.16 that two multipaths with the same elevation β and azimuths α and $\alpha+\frac{\pi}{2}$ have the same Doppler. As mentioned, this second ambiguity does not exist with SCHUN but can impact other channel models.

In conclusion, the aggregation of the multipaths according to the Doppler parameter leads to a slight loss of information about the reference channel azimuth and elevation, but allows limiting the clustering to two dimensions only, increasing the clustering performance. In other terms, the emphasis has been put on the delay impulse response and Doppler spectrogram preservation, accepting a possible ambiguity concerning the multipath angle of arrival. Eq. 2.17 denotes the multipath distance chosen to process the clustering method described in the following sections.

$$d_{i,j}=\sqrt{\frac{1}{2}(\frac{\tau_i-\tau_j}{\Delta\tau_{max}})^2+\frac{1}{2}(\frac{\vartheta_i-\vartheta_j}{\Delta\vartheta_{max}})^2} \tag{2.17}$$

τ_i, τ_j, ν_i and ν_j denote the delay and Doppler of multipaths i and j. The scaling factors have been chosen $(\frac{1}{2},\frac{1}{2})$ to give as much importance to the delay as to the Doppler. It aims at preserving the Doppler spectrum as well as the impulse response power-delay profile. The value of $\Delta\tau_{max}$ is computed as the difference between the maximum theoretical delay and the LOS delay. As mentioned in chapter 1, the delays are computed geometrically according to the optical path of the ray from the emitter to the receiver. Therefore, the maximum delay has been determined geometrically considering the trajectory of a ray from the most remote facet (with 50 m environmental influence) to the receiver. The maximum delay is then estimated $\Delta\tau_{max}$ = 280 ns approximately. The value of $\Delta\nu_{max}$ is computed as twice the maximum theoretical Doppler (to consider the positive and negative segments of the Doppler line). The maximum theoretical Doppler was estimated as the maximum value of ν in Eq. 2.16 in terms of the couple (α,β), assuming a speed of 5 m.s^{-1}. Finally, $\alpha=\frac{\pi}{2}$ and $\beta=0$ give $\Delta\nu_{max}=$ 55 Hz.

2.5.3. Reduction of the impulse response using the Single Linkage Approach

2.5.3.1. General presentation of the Single Linkage Clustering

The *Single Linkage* clustering belongs to the *hierarchical class* of clustering techniques [Tou 74], [Jain 88], as it consists in building a hierarchy of clusters, according to their proximity. The *Single Linkage* is an agglomerative type of hierarchical clustering technique: initially, each sample starts in its own cluster. After successive cluster agglomerations, merging the closest clusters depending on the chosen metric, the number of clusters is reduced to the desired number of clusters *k.* Some variants of the *Single Linkage* algorithm can be found in the literature but the most common approach has been chosen to be adapted to the channel reduction problem in this study. Therefore, the clustering algorithm will process as described hereafter.

Let us consider the initial data set $X(0)$ composed of the following *n* data samples of dimension *p*:

$$X(0)=(x_1,x_2,\dots,x_n),\ x_i\in\ \mathbb{C}^p$$

The *Single Linkage* algorithm consists in merging successively the two closest samples of X until reaching the desired number of clusters *k.* The following equations describe in detail the first iteration process:

Iteration 1:

1) The initial data set is *X=X (0)*. The distance d denotes the distance chosen to evaluate the proximity between two clusters. The first action of the algorithm is to compute the distance between each cluster of the initial data set. This information is contained in matrix D, where $D\ (i\ ,j)$ is the distance between samples i and j among $\mathbb{C}^p$ according to distance $d.$

$$D = \ (d_{i,j})_{(n\ \times n)} \tag{2.18}$$

2) The algorithm identifies the two closest samples I and J in terms of distance $d.$ It corresponds to the minimum of matrix $D.$

$$[I\ ,J] = \min_{i,j}\ (d_{i,j})_{(n\ \times n)} \tag{2.19}$$

3) The two closest samples x_I and x_J are merged to form the cluster $x_I{}'$. Those two samples are aggregated using the function F, presented in Eq. 2.21. It is applied to the p dimensions of the space $\mathbb{C}^p$, in order to create a new cluster $x_I{}' \in \mathbb{C}^p$, homogeneous to the other samples.

$$x_I{}' = F(x_I\ ,\ x_J\ ) \tag{2.20}$$

$$F: \qquad \begin{array}{ccc} & \mathbb{C}^p \times \mathbb{C}^p \longrightarrow \mathbb{C}^p & \\ \begin{pmatrix} x^{(1)}, y^{(1)} \\ x^{(2)}, y^{(2)} \\ \vdots \\ x^{(p)}, y^{(p)} \end{pmatrix} & \longmapsto & \begin{pmatrix} f_1(x^{(1)}, y^{(1)}) \\ f_2(x^{(2)}, y^{(2)}) \\ \vdots \\ f_p(x^{(p)}, y^{(p)}) \end{pmatrix} \end{array} \text{(2.21)} \tag{2.21}$$

4) The two samples x_I and x_J are replaced by the cluster $x_I{}'$ in the original data set. The original data set becomes *X= X(1)*, with:

$$X(1) = (x_1, x_2, \dots, x_{I-1}, x_I', \dots, x_{j-1}, x_{j+1}, \dots, x_n) \tag{2.22}$$

As it can be observed from Eq. 2.18 to 2.22, there is one cluster less in the data set after each iteration. This process is repeated until reaching *k* samples in the final set $X(n-k)$. Fig. 2.27 illustrates the *Single Linkage* clustering method on a canonical 2-dimensional data set.

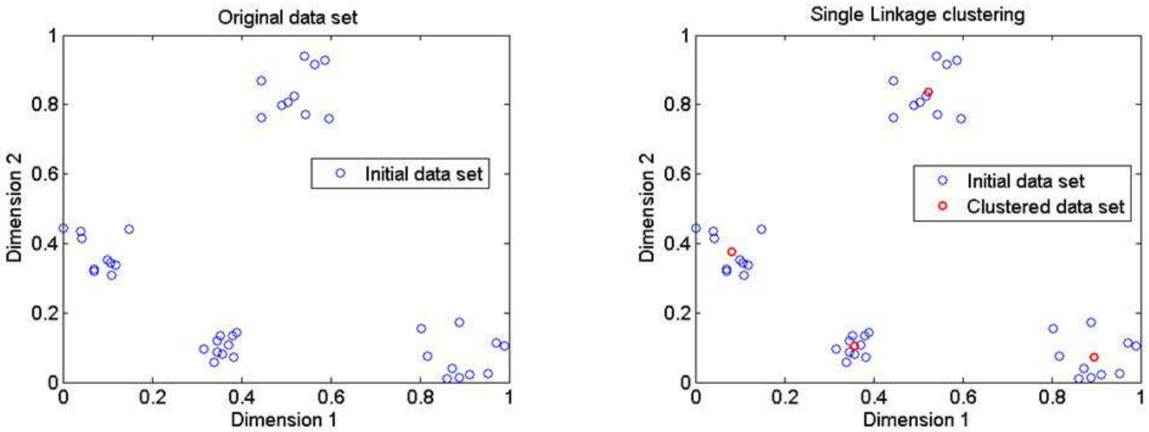

Figure 2.27: Illustration of the *Single Linkage* clustering performance

2.5.3.2. Application to the channel impulse response reduction and results

The *Single Linkage* algorithm has been applied to the impulse response samples, to evaluate the ability of such a method to reduce the multipath channel. In that case, the original data set is composed of the multipath samples of an original impulse response snapshot. As mentioned in section 2.5.2, the channel parameters considered while performing the clustering algorithm are the multipath delays and Doppler shifts. Nevertheless, note that the complex amplitude of the clusters has also to be taken into account to preserve the multipath power and phase information. The multipaths are clustered within the 2-dimensional space $\mathbb{C}^2$, using the distance described in section 2.5 ($d\colon \mathbb{R}^2 \longrightarrow \mathbb{R}$).

Concerning the third phase of the algorithm, some precisions have to be brought to the function F(as referred to in Eq. 2.21), used to agglomerate the clusters. Being given the 3-dimensional multipath space (delay, Doppler, amplitude), Eq. 2.23 defines F. In that case, $(\tau_I, \upsilon_I, \widetilde{\gamma_I})$ and $(\tau_J, \upsilon_J, \widetilde{\gamma_J})$ are respectively the delay, Doppler and complex amplitudes of multipaths I and *J:*

$$F\colon \quad \begin{array}{c} \mathbb{C}^3 \times \mathbb{C}^3 \longrightarrow \mathbb{C}^3 \\ \begin{pmatrix} \tau_I, \tau_J \\ \upsilon_I, \upsilon_J \\ \widetilde{\gamma_I}, \widetilde{\gamma_J} \end{pmatrix} \longmapsto \begin{pmatrix} f_1(\tau_I, \tau_J) \\ f_2(\upsilon_I, \upsilon_J) \\ f_3(\widetilde{\gamma_I}, \widetilde{\gamma_J}) \end{pmatrix} \end{array} \tag{2.23}$$

Eq. 2.24 to Eq. 2.26 detail the functions f_1, f_2, f_3 to compute the delay, Doppler and amplitude parameters of the cluster resulting of the aggregation of *I* and *J,* denoted as $(\tau_I', \vartheta_I', \widetilde{\gamma_I}')$*:*

$$\tau_I' = \frac{|\widetilde{\gamma_I}|\tau_I + |\widetilde{\gamma_J}|\tau_J}{|\widetilde{\gamma_I}| + |\widetilde{\gamma_J}|} \tag{2.24}$$

$$\vartheta_I' = \frac{|\widetilde{\gamma_I}|\vartheta_I + |\widetilde{\gamma_J}|\vartheta_J}{|\widetilde{\gamma_I}| + |\widetilde{\gamma_J}|} \tag{2.25}$$

$$\widetilde{\gamma_I'} = \widetilde{\gamma_I} + \widetilde{\gamma_J} \tag{2.26}$$

In other terms, the delay and Doppler of the cluster resulting of the combination of two previous multipaths are the weighted average of those multipaths delays and Doppler shifts. Its complex amplitude is the coherent sum of the previous multipaths complex amplitudes. Note the total power of the reduced channel is the same as the power of the original channel. Therefore, this reduction method preserves the channel total power and no amplitude adjustment is necessary.

This algorithm has been implemented and applied to the reference impulse response snapshot corresponding to t=6 s on the reference scenario of Fig. 2.3. Fig. 2.28 illustrates the reduced channel Doppler-delay profile of this snapshot compared to the original impulse response. The original channel has been reduced to 5 multipaths and 10 multipaths in parallel.

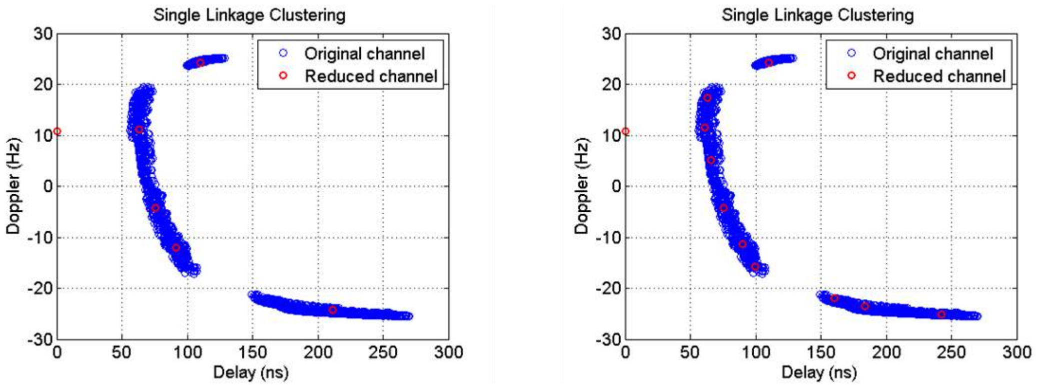

Figure 2.28: Illustration of the *Single Linkage* reduced channel with 5 and 10 multipath at time t=6 s on the reference scenario

Visually, the clustering technique seems to have succeeded in grouping the multipaths of the original channel according to their delay and Doppler. Indeed, the multipaths of the reduced channel fit perfectly the location of the multipaths of the reference. In order to have a closer look at the delay impulse response and Doppler spectrum preservation, Fig. 2.29 represents the comparison between the temporal original impulse response (Eq. 2.2) and the reduced ones at time t=6 s. Fig. 2.31 does so with the original and reduced Doppler spectrograms.

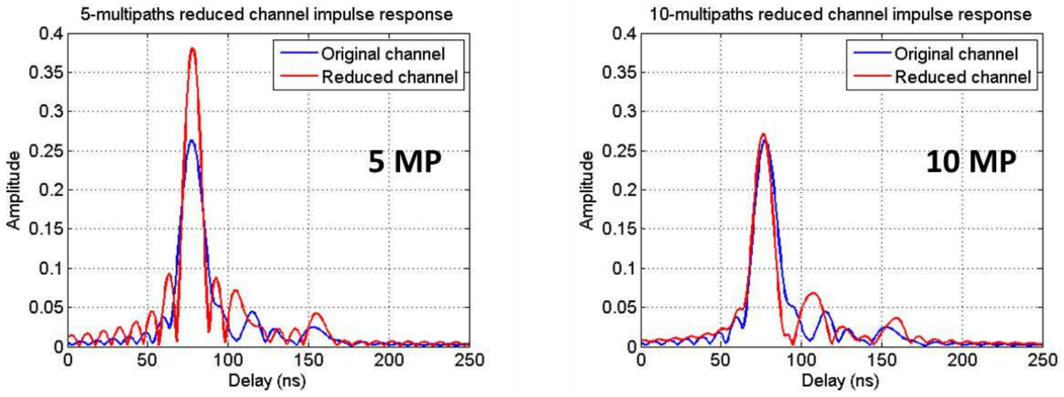

Figure 2.29: Comparison of the reference scenario impulse response with the Single Linkage reduced ones with 5 and 10 clusters, at t=6 s

From the snapshot corresponding to t=6 s, it can be observed on Fig. 2.29 that the clustering technique has preserved the total delay spread and the major power peak location at delay τ =75 ns with 5 and 10 clusters. However, the left plot shows that too much power has been attributed the major power peak; meaning that the power-delay profile is not fully conserved. For example, the secondary power peaks shown by the reference impulse response at delays τ =110 ns, τ =120 ns and τ =150 ns are not conserved in the 5-multipath reduced channel. The right plot shows that with more multipaths in the reduced channel, the preservation of the power-delay profile is improved. Indeed, the different power peaks are better conserved. However, note that the delay location of some of these peaks is shifted. For example, the secondary power peak at τ =110 ns is shifted to τ =100 ns and the power peak corresponding τ =150 ns is shifted to τ =160 ns.

Fig. 2.30 represents the comparison between the impulse response snapshot at time t=6 s and the impulse response of the Tap Delay Line reduced channel, to assess the improvement brought by the *Single Linkage* clustering technique to the power-delay profile preservation. With 5 taps only in the reduced channel, only the major power peak has been preserved by the tap delay line. This major power peak is slightly shifted, which is due to the sampling of the delay scale by the Tap Delay Line method. No secondary power peak has been reproduced. With 10 taps in the reduced channel, some power peaks are distributed along the delay line but some of them do not fit the delay location of the reference impulse response and the global proportion of the power along the delay scale has not been respected. When comparing Fig. 2.29 and Fig. 2.30, it can be deduced that the *Single Linkage* clustering technique has preserved the impulse response power-delay profile better than the Tap delay Line approach did, at least at t=6 s. As this comparison has only been studied on one impulse response snapshot, this last conclusion is only partial but motivates the further investigation of the clustering techniques.

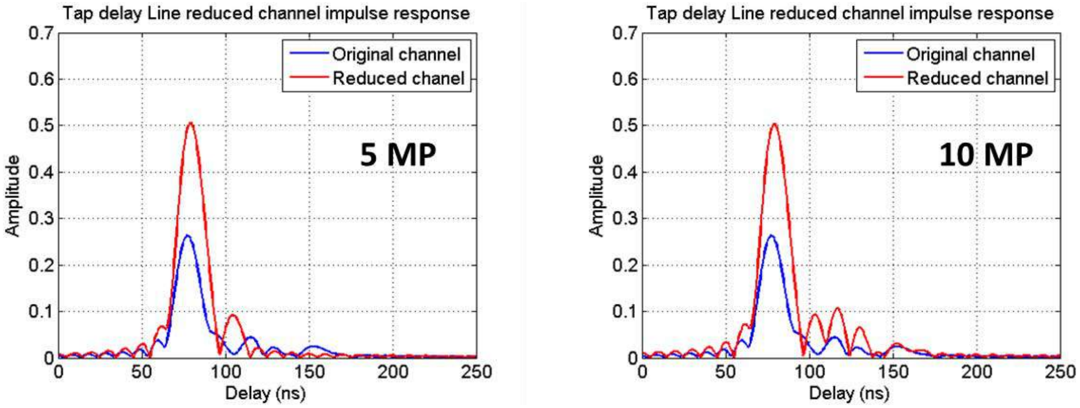

Figure 2.30: Comparison of the reference scenario impulse response with the Tap Delay Line reduced ones with 5 and 10 clusters, at t=6 s

Fig. 2.31 illustrates the preservation of the Doppler spectrogram of the *Single Linkage* technique. With both 5 and 10 multipaths in the reduced channel, the Doppler spectrograms of the reference and reduced channel overlap correctly. All significant power peaks have been preserved at the right Doppler location. Once more, this conclusion is partial being given the fact that only one snapshot has been represented. Nevertheless, it illustrates the major enhancement brought by the clustering techniques to the preservation of the Doppler parameter.

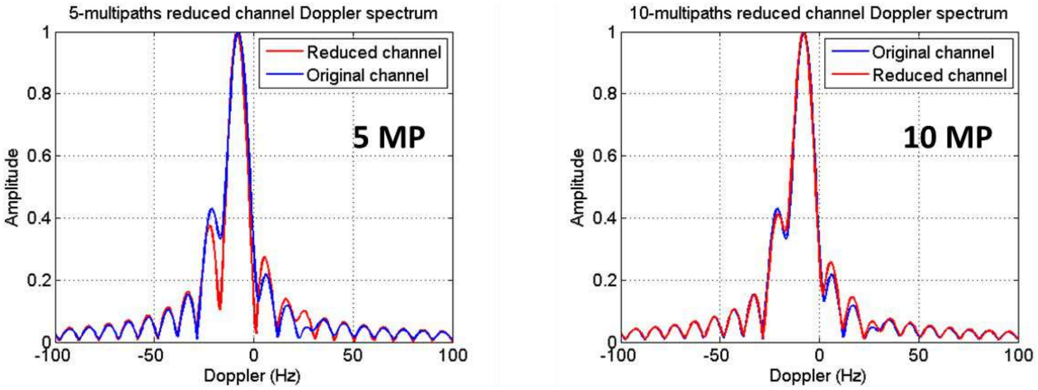

Figure 2.31: Comparison of the reference scenario Doppler spectrum with the Single Linkage reduced ones with 5 and 10 clusters, at time t=25s

2.5.3.3. Complexity of the Single Linkage technique

The complexity of the methods is of interest in the case of the *Single Linkage* method. Section 2.5.3.1 showed that many operations are necessary to decrease the number of samples from the original data set to the final number of clusters. This operations include the elaboration of the distance matrix, the identification of the closest clusters and the computation of the multipath parameters. This process is repeated so as to decrease the size of the data set sample by sample. In particular, at each algorithm iteration, the algorithm estimates the distance between each sample of the data set. As a consequence, many samples in the original data set leads to many iterations and to large distance matrices. The algorithm is composed of three major steps, repeated iteratively:

- Computation of the distance matrix.
- Selection of the minimum distance index.
- Computation of the parameters of the new clusters.

The elaboration of the distance matrix is the most consuming in terms of operations. To quantify the complexity of this step, depending on the size of original multipath channel, it has been decided to estimate the number of elementary operations processed by the algorithm. This complexity C depends on the number of multipaths in the original impulse response n and the final number of clusters K, as given by Eq. 2.27 (complexity $O(n) = n^{n+1}$).

$$C = n^n + (n-1)^{n-1} + \cdots + (K+1)^{K+1} \tag{2.27}$$

The computation time depends also on the mathematical software chosen to run the algorithm. The second step, which consists in searching the minimum value within the distance matrix, can also be time consuming, depending on the software. Classical impulse responses of SCHUN contain more than 3000 multipaths, with 50 m environmental influence. In such case, the minimum distance is sought over a 3000x3000 matrix, which leads to a long computation time. The third step is negligible as compared to the other two.

For example, this study was conducted using the Matlab software, which has the advantage to perform matrix product. In such conditions, the first step time is fast as compared to the second step. Indeed, with an appropriate vectorization of the data set, the elaboration of the distance matrix is fast as compared to the research of the minimum value over the distance matrix. The complexity displayed on Eq. 2.27 has no major impact on the total computation time in that case. However, other mathematical software approaches can possibly face the opposite scenario, that is to say long distance matrix computation or fast research of the minimum. Eq. 2.27 is given as an indication. In any case, the computation load of the algorithm increases exponentially with the number of multipaths in the reference channel.

In this context, the *Single Linkage* algorithm leads to large computation times, which severely impair the channel reduction processing performance. Indeed, with more than thousands of multipaths in the original channel impulse response, the algorithm runs over one minute to compute the reduced channel parameters of a single impulse response snapshot. As an indication, the reference scenario of this study is composed of 6000 impulse response epochs. This computation time is too large as compared to the channel computation time to be involved in most of receiver testing campaigns. Therefore, another clustering technique, less time consuming has been implemented and presented in the following sub-section.

2.5.4. Reduction of the impulse response using the K-Means clustering algorithm

2.5.4.1. General presentation of the *K-Means* clustering algorithm

The *K-Means* clustering algorithm belongs to the *partitional class* of clustering techniques [Tou 74], [Jain 88], as it consists in partitioning the data set in clusters of data. Those clusters are formed according the proximity of the data samples with respect to the distance defined in section 2.5.2. This algorithm is constituted of 2 distinct steps: *Assignment* and *Cluster update* phases. During the *assignment* phase, the data samples are assigned to the cluster with the closest centroid. During the *cluster update* phase, the centroids of the clusters are computed as an average of the cluster samples position. These two phases are repeated successively until the algorithm converges to the final position of the centroids. Let us consider a p-dimensional data set *X*, constituted of the following samples:

$$X = (x_1, x_2, \dots, x_n),\ x_i \in \mathbb{C}^p$$

The data set *X* will be partitioned in *k* clusters, using the *K-Means* algorithm. The set $K = (c_1, c_2, \dots, c_k)$, $c_i \in \mathbb{C}^p$, is composed of the centroids of the clusters. The set $L = (l_1, l_2, \dots, l_k)$, $l_i \in \mathbb{N}$ is the number of data in the different clusters. Let d be the distance over the p-dimensional data space. The following equations explains the first iteration:

- **Initialization:**

The very first step of this clustering algorithm is the initialization of the position of the centroids K_0. It is important to note that the convergence of the centroids is ensured, whatever the initial position of the centroids. Nevertheless, it can converge to a local maximum. The final distribution of the clusters is not unique and depends on the centroids initialization. Therefore, a particular attention has to be brought to this step in order to ensure the convergence of the algorithm to the global maximum, to improve the clustering performance. Let us consider that the initial centroid set K_0 is close enough to the optimal centroid distribution to ensure the convergence of the algorithm to the global maximum.

- **Assignment phase:**

For $i = 1, \dots, n$,

$$x_i \in \min_j d(x_i, c_j) \tag{2.28}$$

Each data sample is assigned to the cluster with the closest centroid, according to the distance d.

- **Centroid position update:**

For $j = 1, \dots, k$, with l_j the number of data samples in cluster c_j:

$$c_j = \frac{1}{l_j} \sum_{i, x_i \in c_j} x_i \tag{2.29}$$

The assignment phase and centroid position update phase are repeated alternatively until convergence of the algorithm.

2.5.4.2. Application to the channel impulse response reduction and results

The *K-Means* algorithm has been applied to the impulse response samples along the trajectory. In that case, the data set is composed of the multipaths in the 2-dimensional space of delay and Doppler. In other words, the *K-Means* clusters the multipaths according to their delay and Doppler proximity. The distance used for that matter is the one described in section 2.5.2. Two remarks have to be mentioned before going further in the study of the clustering performance.

- First, a slight modification has been brought to the centroid position update phase presented in section 2.5.4.1. The data samples x_i are composed of one delay and one Doppler component. In such conditions, the position of the centroid only depends on the delay and Doppler of the multipaths of the cluster. It has been decided in this study to involve the power of the multipath in the positioning of the centroids, as a weighting coefficient. Eq. 2.30 to Eq. 2.32 compute the delay τ_k, Doppler ϑ_k and amplitude module $|\widetilde{\gamma_k}|$ of the centroid *k,* as it is given by the centroid position update phase of the *K-Means* algorithm. The vector L_k regroups the index of the multipaths assigned to cluster *k* and $\tau_l, \vartheta_l$and $\widetilde{\gamma_l}$ are the delay, Doppler and complex amplitude of multipath l.

$$\tau_k = \frac{\sum_{l \in L_k} |\widetilde{\gamma_l}| \tau_l}{\sum_{l \in L_k} |\widetilde{\gamma_l}|} \tag{2.30}$$

$$\vartheta_k = \frac{\sum_{l \in L_k} |\widetilde{\gamma}_l| \vartheta_l}{\sum_{l \in L_k} |\widetilde{\gamma}_l|} \quad (2.31)$$

$$\widetilde{\gamma_k} = \sum_{l \in L_k} \widetilde{\gamma}_l \quad (2.32)$$

- Secondly, as mentioned in the previous section, a particular attention has to be brought to the initialization phase of the algorithm. In order to maximize the chances to converge to a global maximum, it has been decided to avoid choosing randomly the initial centroids. Therefore, the initialization principle presented in [Czin 07] has been applied to the channel reduction context. According to this approach, the initial centroids are built the one after the other with a focus on the wisest partitioning of the data set. To do so, the following approach has been considered:

Initialization:

1) The multipath of maximum power is chosen as the first centroid.
2) The distance of each multipath to the centroids already established is computed. The multipaths are assigned to the closest centroid.
3) The multipath with the largest distance to its respective centroid is chosen to be the following centroid.
4) Steps 2) and 3) are repeated until reaching the desired number of centroids.

This *K-Means* algorithm has been applied to the reference impulse response corresponding to t=6 s. Fig. 2.32 represents the position of the centroids on this Doppler-delay profile, considering 5 and 10 multipaths in the reduced channel.

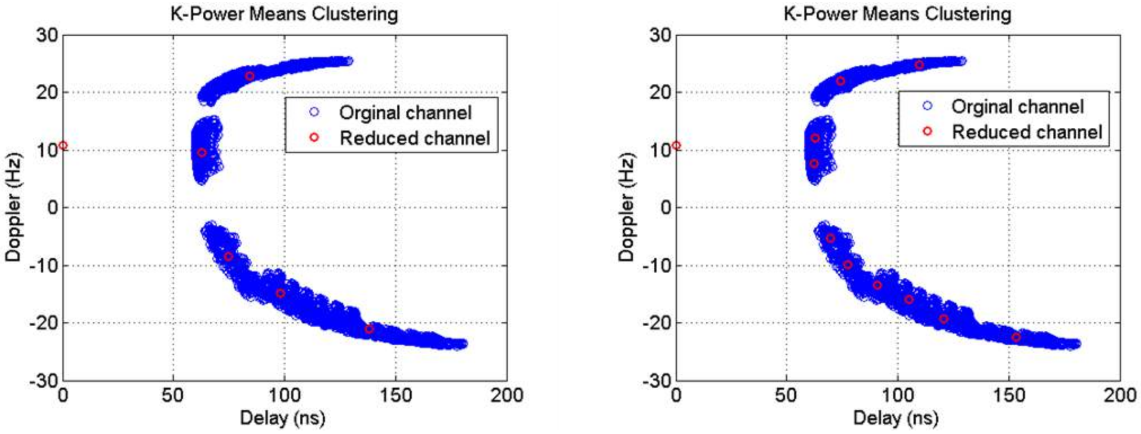

Figure 2.32: Illustration of the *K-Means* reduced channel with 5 (left) and 10 (right) multipaths at time t=6 s

It can be concluded from Fig. 2.32 that the *K-Means* clustering has succeeded in partitioning the impulse response in 5 and 10 clusters at time t=6 s. Indeed, the position of the centroids matches perfectly the Doppler-delay profile of the original channel. This clustering technique has been applied to the impulse responses all along the trajectory. The multipaths of the reduced channel are the centroids, their parameters are computed by Eq. 2.30, 2.31 and 2.32. The reduced channel impulse response along the trajectory is illustrated on Fig. 2.33 with 5 and 10 multipaths in the reduced channel.

Fig. 2.33 shows that with both 5 and 10 multipaths in the reduced channel, the reference channel delay spread is partially preserved. On the other hand, the major power peak located approximately at delay τ=80 ns has not been preserved by the 5-multipath reduced channel. Moreover, a few isolated power contributions appear at inconsistent delay locations. The 10-multipath reduced channel overlap the reference impulse response better, but in that case also, the τ=80 ns power peak is not clearly identifiable all along the trajectory. This slight impairment of the power-delay profile is due to the fact that the multipath power is concentrated at the position of the centroids. On that scenario, there is no centroid with 80 ns delay on most of the trajectory. This is why the power peak located at τ = 80 ns has not been preserved by the clustering algorithm, especially with only 5 clusters. However, it must be mentioned that the increase of the number of multipaths from 5 to 10 in the reduced channel improves the power-delay preservation.

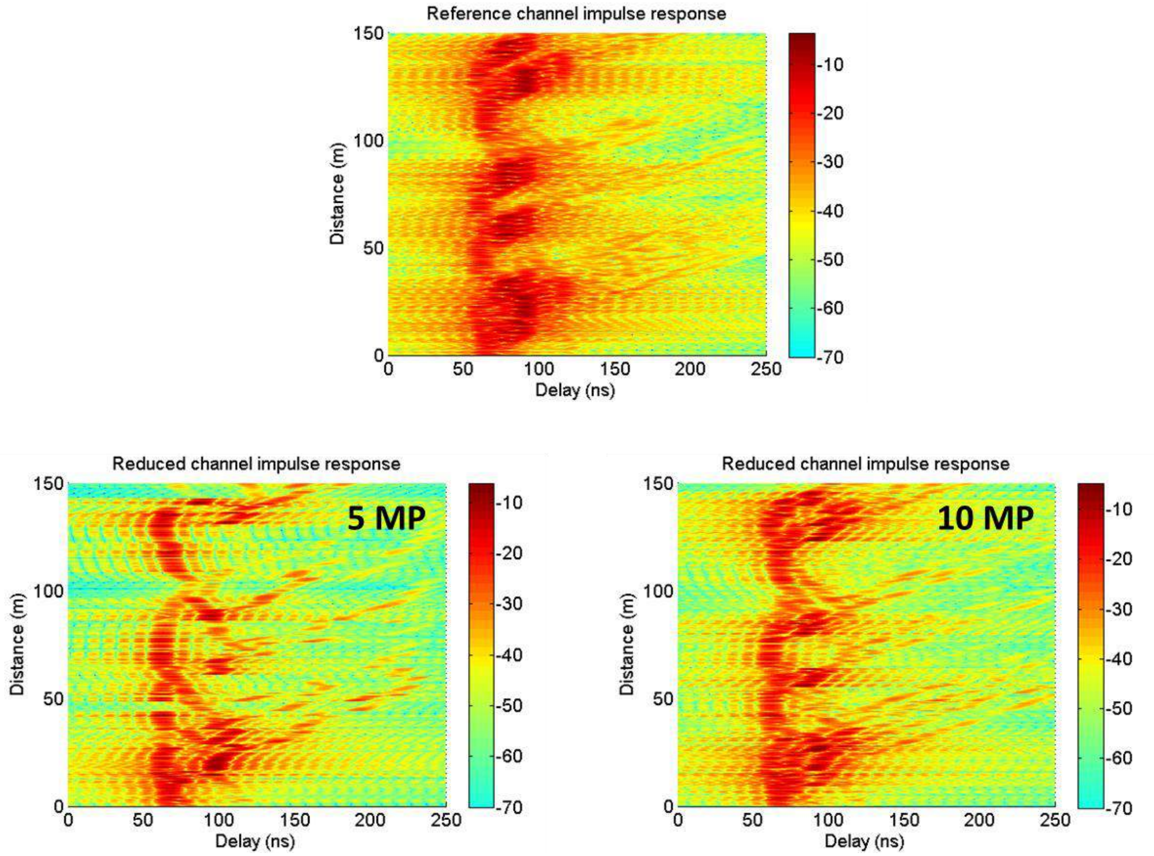

Figure 2.33: Evolution of the Power-delay profile of the reference channel (top plot) and clustering reduced ones along the receiver's trajectory

Fig. 2.34 presents the comparison between the reference channel Doppler spectrogram with the 5- and 10-multipath reduced channels Doppler spectrogram. It shows that 10 multipaths in the reduced channel are enough to preserve most of the significant power contributions along the Doppler dimension. The major power peak in the negative Doppler (which corresponds to backscattering multipaths) is clearly identifiable. The different Doppler lines decreasing from positive to negative Doppler continuously along the trajectory are caused by the motion of the receiver along the different buildings. It crosses the null-Doppler line when the receiver arrives next to the building. These lines are observable on the reference channel and are well reproduced by the 10-multipath reduced channel. Some of these are also identifiable on the 5-multipath reduced channel. Nevertheless, a few power fading zones are observable all over the 5-multipath channel Doppler spectrogram, which decrease its performance with respect to the conservation of the Doppler spectrogram. Once more, it can be remarked that the performance are well improved by the increase of the number of multipaths in the reduced channel (from 5 to 10 multipaths on this example).

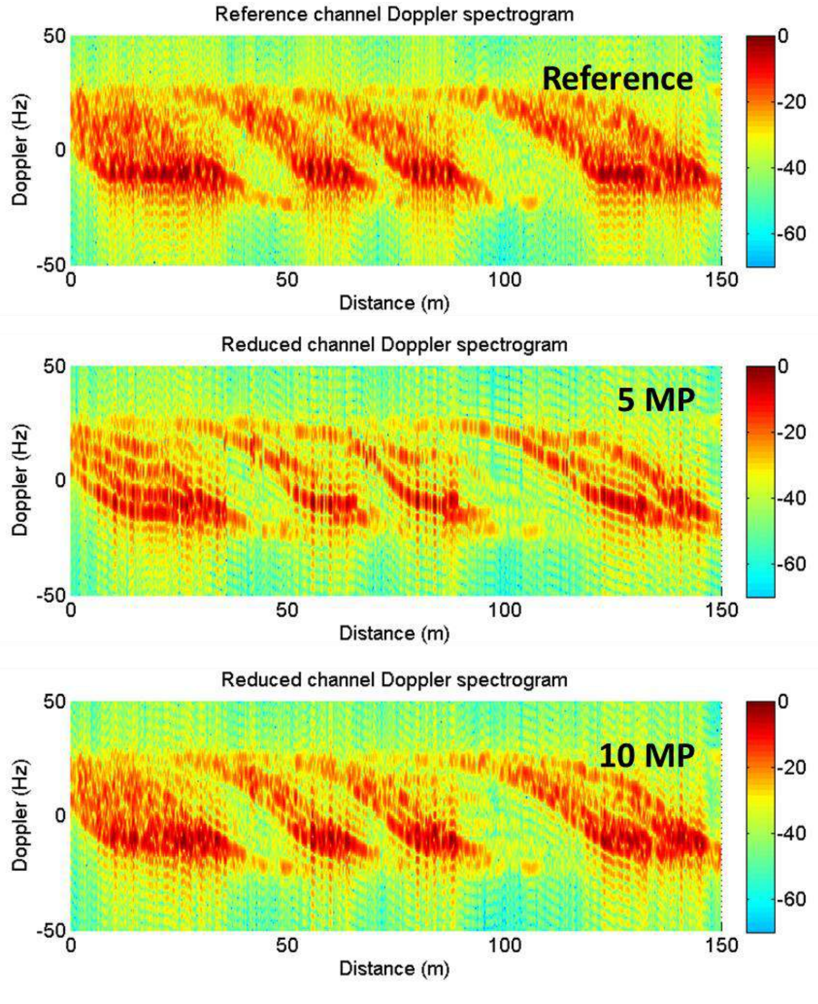

Figure 2.34: Comparison of the reference channel Doppler spectrogram (top plot) with 5- and 10-multipath reduced channel Doppler spectrogram along the trajectory

As a conclusion of the study of the *K-Means* algorithm, two major improvements and one drawback are detectable.

- The first major advantage of this algorithm was the motivation of the clustering techniques: the preservation of both delay and Doppler profiles of the channel. This enhancement was illustrated by Fig. 2.33 and 2.34. Previously, the Doppler dimension was excluded from the Tap Delay Line grouping criteria. The *K-Means* approach has allowed the separation of the multipaths with different Doppler shifts, which results in a better continuity of the phases and delays of the reduced channel, as mentioned in section 2.4.4.

- The second benefit of the *K-Means* algorithm is an improvement to the *Single Linkage* clustering approach, in terms of computational costs. Indeed, the *K-Means* algorithm simply consists in estimating the distance of each multipath to the *k* centroids. Moreover, this operation is repeated as many times as necessary to achieve the convergence of the algorithm. With the help of the pre-initialization phase presented in this section, the number of iterations did not exceed 10 loops for any of the impulse response samples of this study, considering 5 or 10 multipaths in the reduced channel. Therefore, a major decrease of the computation load has been achieved with the development of the *K-Means* clustering technique. Table 2.1 displays the computation time necessary to reduce the impulse response to 10 multipaths corresponding to 125 m sampled every 2.5 cm on the reference scenario, depending on the average number of multipaths in the reference impulse responses. Note that those durations depend on both software and hardware means used to realize the clustering process. However, it illustrates the differences between the *Single Linkage* and *K-Means* clustering techniques.

For more than a hundred multipaths in the reduced channel, the use of the *Single Linkage* clustering is critical in terms of computation load, and is likely to severely constrain the channel modeling phase.

Table 2.1 : Computation time of the different clustering algorithms for different number of multipaths in the reference channel

Clustering algorithm	50 multipaths	500 multipaths	1000 multipaths	1500 multipaths	3000 multipaths
Single Linkage	1min	120min	30h 30min	110h	1200h
K-Means	1min	2min	5min	8min	11min

- On the other hand, Fig. 2.33 illustrated the poor power-delay preservation by this algorithm, especially when the number of multipaths is limited to less than 5. As mentioned previously, the fact to restrict the delay of the multipaths to the delay of the centroids impairs the impulse response delay profile, generating inconsistent power peaks or inconsistent power fading zones. The *K-Means* algorithm only considers the multipath Doppler shifts and delays during the assignment step. Indeed, the power of the multipaths is only taken into account during the centroid position update phase and not during the assignment phase. As a consequence, the clusters constituted of low power multipaths have the same weight as the strong power clusters. The fact to modulate the multipath distance would allow the algorithm to allocate less weight to the low power clusters, and then concentrate the centroids in the stronger power multipath zones. This possibility has been investigated through the test of a new clustering technique, mentioned in [McKa 03] and presented in the following section.

2.5.5. *Enhancement of the K-Means algorithm by weighting the clusters*

The focus of this section is the enhancement of the elementary form of the *K-Means* clustering algorithm presented in the previous section. As mentioned, this enhancement will essentially concern the multipath assignment phase, by weighting the clusters depending on their amplitude. The chosen approach has been presented as a "*soft K-Means*" algorithm in [McKa 03]. It has been applied in the telecommunication context in [Abel 09], as a way of clustering the narrow-band power of channel measurements to identify different states of fading.

2.5.5.1. Presentation of the *Soft K-Means*

As presented in [McKa 03], the *Soft K-Mean* algorithm differs from the elementary *K-Mean* in the fact that the data samples do not strictly belong to one cluster, but have a degree of belonging to each cluster. In the approach explained in [McKa 03], this degree of belonging depends on the distance of the data sample to the considered centroid. In that case, the assignment phase does not only identify the centroid of minimum distance but also computes the distance of each data sample to the different centroids. These normalized distances denote the degree of belonging of the data samples to the different clusters. In the centroid position update phase, these coefficients weight the data samples average position. The following equations detail the data processing performed by the assignment and centroid position update phases. They use the same formalism as Eq. 2.28 and Eq. 2.29.

- **Assignment phase:**

The $(n \times k)$ matrix *r* containing the normalized distances of the data samples to the different centroids is given by:

$$r_i^{(j)} = \frac{\exp(-\beta d(x_i, c_j))}{\sum_{l=1}^{k} \exp(-\beta d(x_i, c_l))} \tag{2.33}$$

The coefficient β defines the degree of softening of the *K-Means* algorithm. It defines the stiffness of the algorithm, as referred to in [McKa 03]. Qualitatively, it can be remarked that the degree of belonging to the clusters as it is given in Eq. 2.33 gives more weight to the data samples located close to centroids.

- **Centroid position update**

The position of the centroids is weighted by the degree of belonging to these centroids:

$$c_j = \frac{\sum_{i=1}^{n} r_i^{(j)} x_i}{\sum_{i=1}^{n} r_i^{(j)}} \tag{2.34}$$

The assignment phase and centroid position update phase are repeated alternatively until the convergence of the algorithm.

2.5.5.2. Adaptation of the *Soft K-Means* to the multipath impulse response

The classic approach presented in [McKa 03] has been adapted to the weighted clustering focus mentioned previously. To do so, the cluster weighting coefficient has not been calculated in terms of centroid-multipath distance, but in terms of the multipath amplitude module. This adaptation leads to a modification in the formalism of the matrix r expressed in Eq. 2.35.

- **Assignment phase:**

$$r_i^{(j)} = |\tilde{\gamma}_i| \frac{\left(1/d(x_i, c_j)\right)^2}{\sum_{l=1}^{k} \left(1/d(x_i, c_l)\right)^2} \tag{2.35}$$

Two factors are identifiable in Eq. 2.35. One factor depends on the multipath distance to the centroid, normalized by the distance to the other centroids. Note that the exponential form of Eq. 2.33 has been replaced by ${}^{1}\!/_{x^2}$, to increase the influence of the distance on the clustering process. Indeed, $\lim_{d\to 0}({}^{1}\!/_{d})^2 = +\infty$ whereas $\lim_{d\to 0} e^{-d} = 1$. This distance factor is weighted by the amplitude module of the considered multipath. Note also that in the *soft K-Means* clustering presented on Eq. 2.33, the contribution of all centroids on a given data sample is 1:

$$\sum_{j=1}^{k} r_i^{(j)} = 1 \tag{2.36}$$

The contribution of the cluster is not normalized to 1 but to the multipath amplitude module:

$$\sum_{j=1}^{k} r_i^{(j)} = |\tilde{\gamma}_i| \tag{2.37}$$

- **Centroid position update:**

Considering the distance matrix of Eq. 2.35, the delay τ_j, Doppler ϑ_j and amplitude $|\tilde{\gamma}_j|$ of the centroid c_j are given by:

$$\tau_j = \frac{\sum_{i=1}^{n} r_i^{(j)} \tau_i}{\sum_{i=1}^{n} r_i^{(j)}} \tag{2.38}$$

$$\vartheta_j = \frac{\sum_{i=1}^{n} r_i^{(j)} \vartheta_i}{\sum_{i=1}^{n} r_i^{(j)}} \tag{2.39}$$

$$\tilde{\gamma}_j = \sum_{j=1}^{k} r_i^{(j)} \frac{\tilde{\gamma}_i}{|\tilde{\gamma}_i|} \tag{2.40}$$

It can be verified from Eq. 2.40 that the total narrow-band power of the channel is preserved, that is to say:

$$\sum_{j=1}^{k} \widetilde{\gamma_j} = \sum_{i=1}^{n} \widetilde{\gamma_i} \tag{2.41}$$

2.5.5.3. Application of the *Soft K-Means* clustering to the reference channel

The clustering algorithm presented in the previous section has been applied to the impulse responses of the reference scenario. Fig. 2.35 illustrates the power-delay profile of the reference channel compared to the one of the 5- and 10-multipath reduced channels using the *Soft K-Means* algorithm. As comparing Fig. 2.35 with Fig. 2.33 in the previous section, the *Soft K-Means* technique showed to preserve power-delay profile of the reference impulse response better than the elementary *K-Means* algorithm. This observation is especially obvious on the comparison of the 5-multipath reduced channels. In the case of the *Soft K-means* clustering, the power peaks are well conserved, at the right delay places. Even if the delay spread is slightly reduced on some impulse response samples, the reference channel power contributions are almost all reproduced by the reduction method. Once more, the increase of the number of multipaths to 10 increases the performance of the algorithm. In that case, the delay spread is fully reproduced along the trajectory and all multipath power contributions match the reference profile.

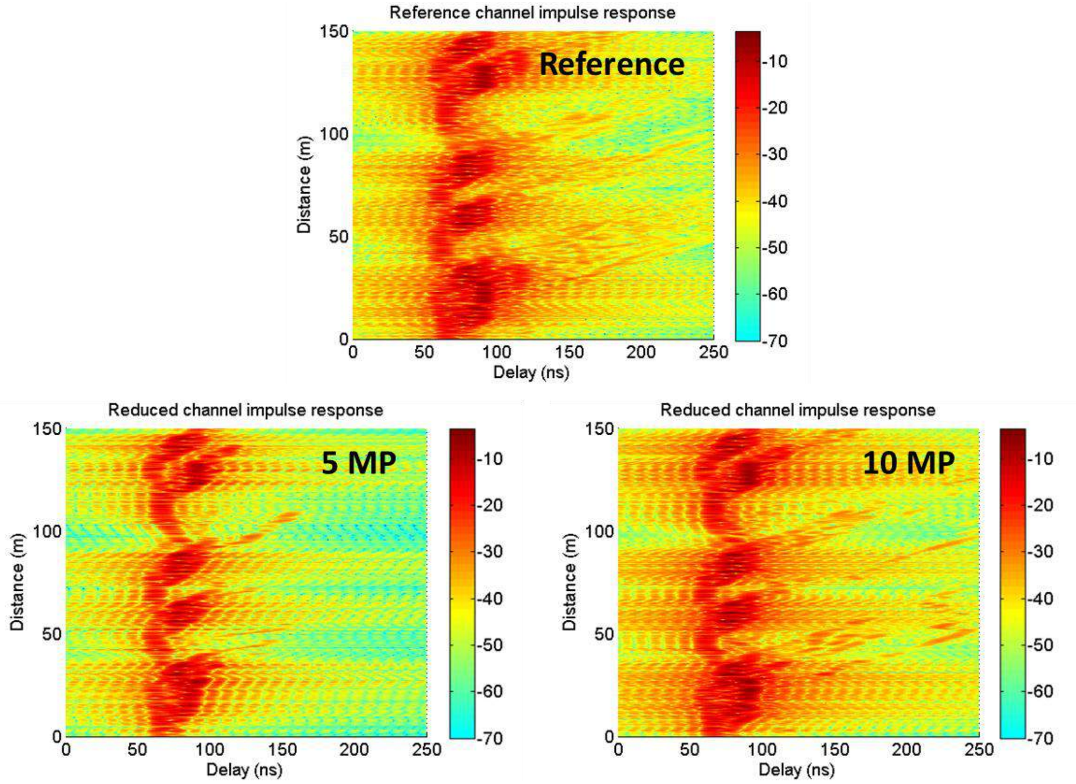

Figure 2.35: Evolution of the Power-delay profile of the reference channel (top plot) and *Soft K-Means* reduced ones along the trajectory

Fig 2.36 represents the evolution of the Doppler spectrogram along the trajectory on both reference and *Soft K-Means* reduced channels, with 5 and 10 multipaths in the reduced channel. The Doppler spectrogram shows also a better preservation of the Doppler-power profile by the *Soft K-Means* algorithm, when comparing it with the Doppler spectrogram of Fig. 2.34 corresponding to the elementary *K-Means.* The continuous Doppler lines caused by the motion of the receiver in parallel to the facades are well reproduced by the reduced channels, even with only 5 multipaths. This Doppler spectrogram preservation is improved by the increase of the number of multipaths to 10.

The performance of the *Soft K-Means* reduction technique is better than the performance of the basic *K-Means* both in terms of power-delay and Doppler spectrogram preservation. The fact to give more importance to the clusters with higher power multipaths has concentrated the centroids in the high power zones. The low power multipaths are neglected during the assignment phase which assigned more clusters to partition the high power multipaths. This led to a limitation of the Doppler and delay diversity inside the clusters of high power and then to a better conservation of the power-delay and Doppler spectrogram.

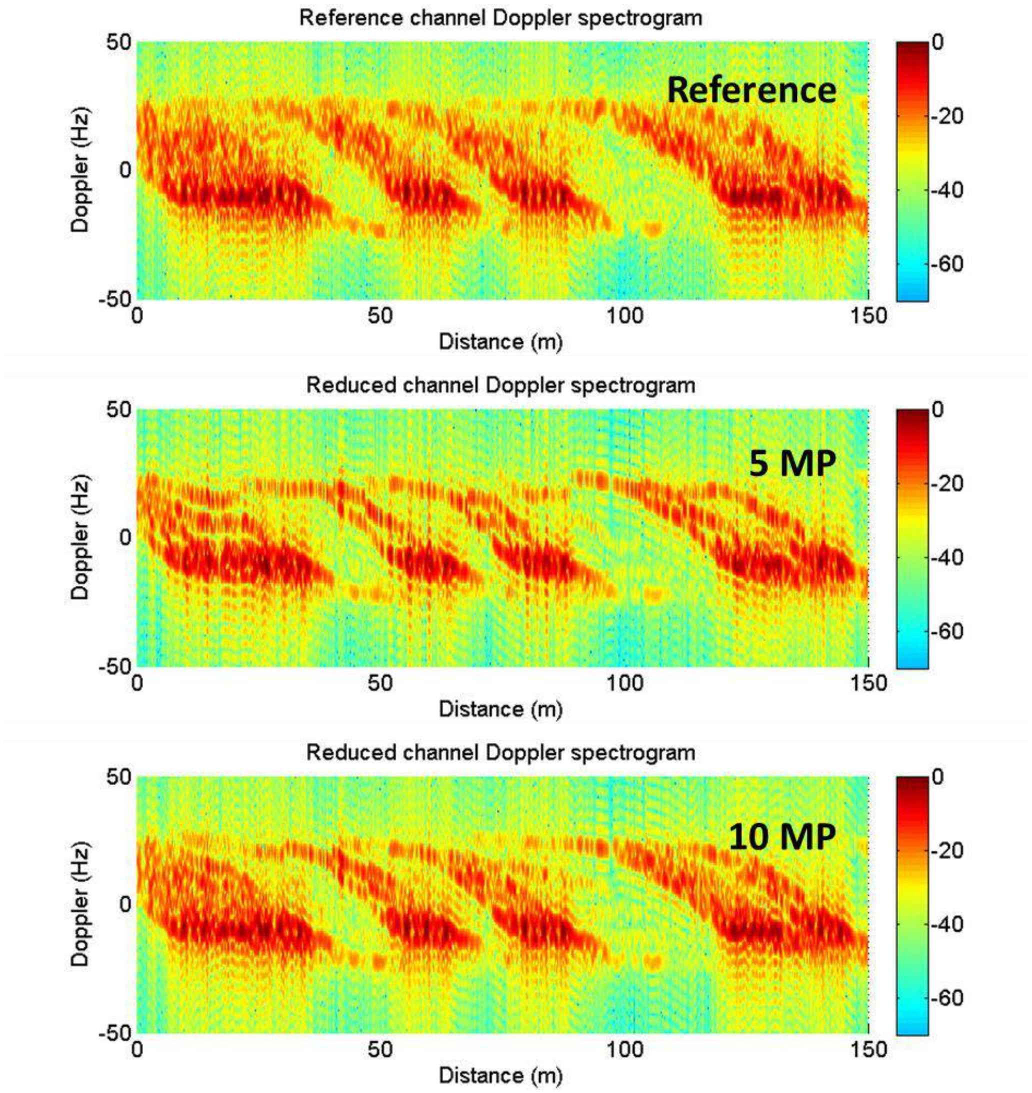
Reference channel Doppler spectrogram

Reduced channel Doppler spectrogram

Reduced channel Doppler spectrogram

Figure 2.36: Comparison of the reference channel Doppler spectrum (top plot) with the 5- and 10-multipath reduced channel Doppler spectra along the trajectory

As a first conclusion, the use of this enhanced algorithm has improved the preservation of the multipath channel parameters, which was an important criterion of success of the reduction methods, as presented in the introduction of this chapter. Moreover, its complexity is equivalent to the complexity of the *K-Means* reduction technique, which makes it the best tradeoff between computation load and channel parameters preservation.

2.5.5.4. Continuity of the multipaths

To complete assessment of the performance of the reduction techniques, it has been decided to investigate the continuity of the parameters of the reduced channel along the time. More specifically, the focus of this section will be the continuity of the delay and Doppler shifts of the reduced channel multipaths along the trajectory. The *Soft* and *Hard K-Means* clustering techniques (the elementary *K-Means* is referred to as *Hard K-Means* in [McKa 03]) will be compared.

In order to illustrate the continuity along time of the delay and Doppler parameters of the reduced channel, it has been decided to truncate the reference scenario in several segments. The length of these segments has been set to 25 m; long enough to illustrate the continuity on significant segments but short enough to observe only a limited number of events of multipath appearance/disappearance. The two relevant segments have been chosen to illustrate this focus: the segments [75m-100m] and [125m-150m].

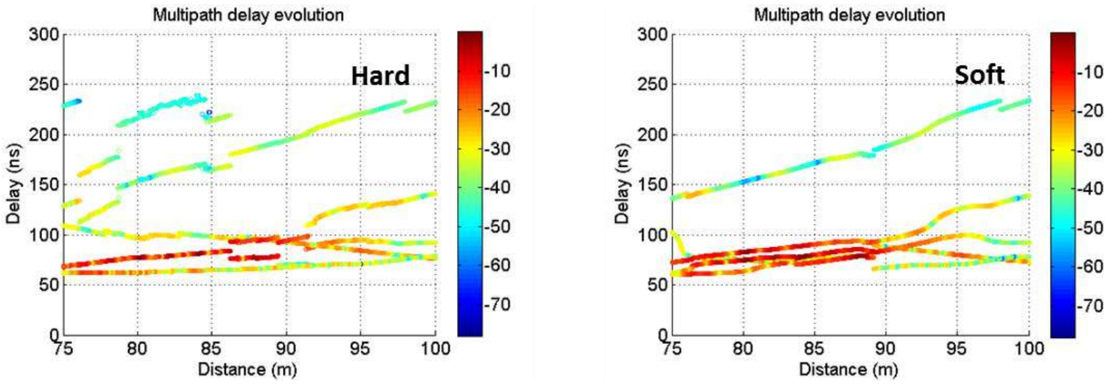

Figure 2.37: Delay evolution of the reduced channel multipaths with the *Hard* and *Soft K-Means* algorithms on the [75m-100m] segment

Fig. 2.37 illustrates the evolution of the multipath delays of the reduced channel on the segment [75m-100m]. The left plot represents the *Hard K-Means* reduced channel and the right plot represents the *Soft K-Means.* Note that the channel has been reduced to 5 multipaths in both cases. The first observation from Fig. 2.37 is that both clustering algorithms are globally continuous in delays along time. Indeed, the evolution of the delays clearly follows continuous lines, induced by the motion of the receiver along the virtual city. It proves the stability of the clusters formed by the algorithm, to such an extent that the centroids can be identified to physical multipaths (according to their continuous evolution). Nevertheless, a few discrete but severe discontinuities are observable on the *Hard K-Means* reduced channel. For example, at the distance 79 m of the trajectory, two multipaths with delays 140 ns and 180 ns disappear. At the same instant, a multipath with delay 150 ns appears. This is due to the fact that the two clusters of 140 ns and 180 ns combined because of a sudden clustering re-partition of the multipaths. These clustering re-partitions are caused by the instantaneous appearance or disappearance of groups of multipaths, modifying suddenly the Doppler-delay profile, and thus the position of the centroids.

In what concerns the *Soft K-Means* algorithm, the clusters are weighted according to the power of the multipaths. On this reference scenario, most multipath appear or disappear when the corresponding facet is far from the receiver, and thus with low power (there is no obstacle between the facets and the receiver). Therefore, the groups of multipaths who appear or disappear have no impact on the clustering process. They do not modify the partition of the multipaths; hence the better stability of the data clusters. This is confirmed by Fig. 2.37: fewer multipaths of the reduced channel disappear or appear in the case of the *Soft K-Mean* algorithm, as visible on the right plot. It is also noticeable that the centroids are concentrated in the lower delay zone, which corresponds to higher power multipaths, as expected in the presentation of the algorithm.

To observe this continuity in the Doppler dimension, Fig. 2.38 represents the reduced channel multipath Doppler shifts in the case of *Soft* and *Hard K-Means* algorithms, along the trajectory segments considered. As it could be expected, the same continuity is observable as in the case of the delays. Only a few discrete discontinuities distort the multipath evolution for both *Soft* and *Hard K-Means* algorithms. The delay variation $\Delta\tau$ of a given multipath l during the time interval Δt is given by its Doppler parameter ϑ_l according to the following relation, where f_0 denotes the carrier frequency of the incident signal:

$$\Delta\tau_l = \frac{\vartheta_l}{f_0}\Delta t \qquad (2.42)$$

The consistency of the reduced channel delays and Doppler shifts according to Eq. 2.42 is mostly verified on both *Soft* and *Hard K-Means* channels*,* as visible on Fig. 2.38. The negative Doppler multipaths have decreasing delays and the positive Doppler multipaths have increasing delays.

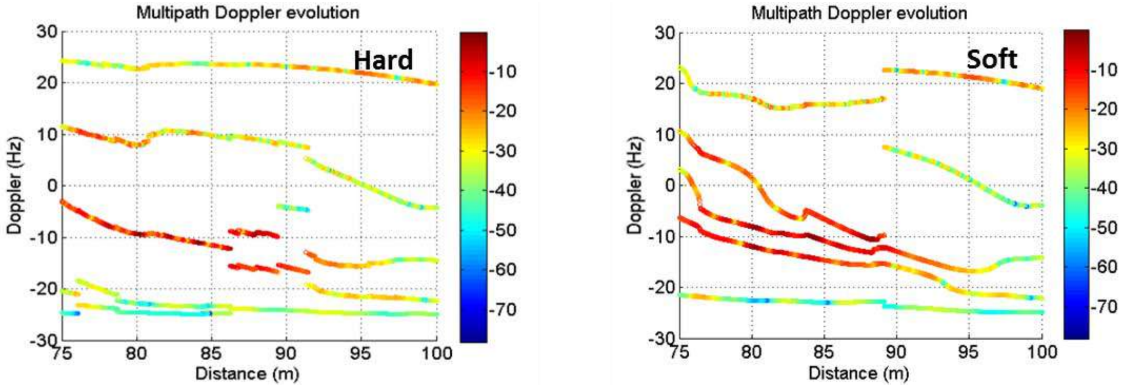

Figure 2.38: Doppler evolution with the *Hard* and *Soft K-Means* algorithms on [75m-100m]

Fig. 2.39 and 2.40 show respectively the delay and Doppler of the reduced channel multipaths on the [125m-150m] segment of the trajectory, for both *Hard* and *Soft K-Means* algorithm. The conclusions drawn on the [75m-100m] segment are confirmed by the plots of Fig. 2.39 and 2.40. The *Soft K-Means* algorithm shows a better continuity than the *Hard K-Means.*

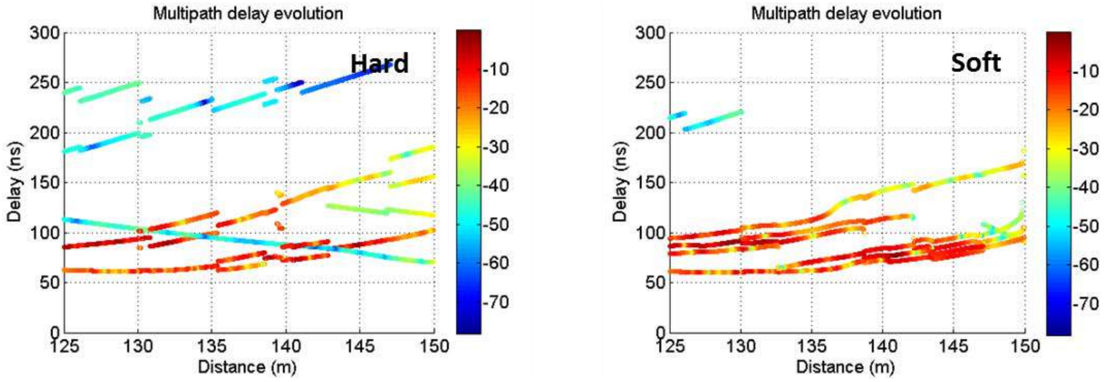

Figure 2.39: Delay evolution of the reduced channel multipaths with the *Hard* and *Soft K-Means* algorithms on the [125m-150m] segment

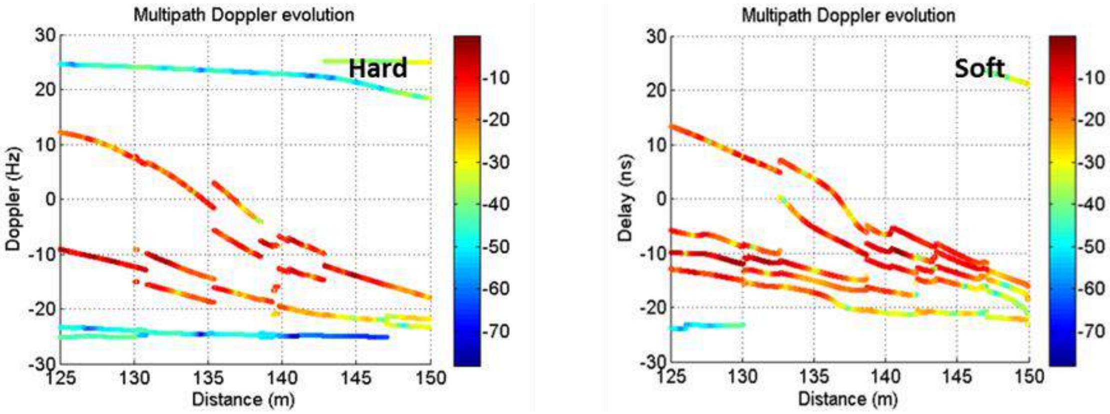

Figure 2.40: Doppler evolution of the reduced channel multipaths with the *Hard* and *Soft K-Means* algorithms on the [125m-150m] segment

2.6. Conclusion

This chapter has presented several channel reduction techniques, including selection and aggregation methods. The different aggregation methods included delay sampling techniques such as the commonly used Tap Delay Line method and the channel re-sampling method. It also presented delay-clustering techniques of the Doppler-delay space. A particular focus has been brought to the different clustering approaches to reach an optimal tradeoff complexity/accuracy. These methods were compared all along the chapter according to the preservation of the power-delay and Doppler spectrogram of the original channel, in order to establish a hierarchy among those aggregation and selection methods.

The preliminary state-of-the art works aimed at identifying all the possible approaches to address the channel reduction problem. This section had two objectives:

- Select the different reduction methods already used in order to inform the users about their impairment of the delay and Doppler characteristics of a typical multipath channel.

- Cover all the channel reduction possibilities in order to be able to consider that the method developed in section 2.5.5 referred to as *Clustering Weighted* (or *Soft K*-Means) is the best aggregation method to address the reduction problem.

In order to make an objective comparison of all the methods developed, a reference scenario has been defined in section 2.2. The methods have all been applied to the impulse response samples computed by the SCHUN software.

The first method considered was the selection method in section 2.3, which consisted in cutting of all the multipaths except the 10 most powerful. By comparing the reference impulse response to the reduced one in terms of power-delay and Doppler spectrogram, a severe limitation of the delay and Doppler spreads in the reduced channel was observed, due to the cut off of thousands of small power multipaths whose combination (partially coherent) created a significant power contribution. As a conclusion, an appropriate channel reduction method has to consider the multipaths all along the delay dimension.

It has been decided to investigate the delay line sampling possibility, using the common Tap Delay Line approach and channel re-sampling technique in section 2.4. These methods had the advantage to be easy to implement and to conserve the impulse response power-delay profile well. Nevertheless, the fact to limit the aggregation to the only delay dimension allows the algorithm to aggregate echoes with very different Doppler shifts, which can lead to phase discontinuities in the reduced channels.

Therefore, it has been decided to develop some methods taking into account both delay and Doppler dimensions of the multipaths before performing their agglomeration. The clustering approaches appeared to be an appropriate solution to this challenge, as they consist in forming groups of data according to their proximity along different dimensions. Two types of clustering algorithms were mentioned in section 2.5: *hierarchical* and *partitional*. The *hierarchical* type of clustering was considered first. It seemed to preserve both power-delay and Doppler characteristics with success but its complexity led to long computation times for scenarios with more than approximately 100 multipaths per impulse responses. Finally, the *partitional* type clustering *K-Means* has been chosen for its good ratio complexity/performance as presented in the literature. It has been decided to apply both *Hard* and *Soft* versions of the *K-Means* algorithm to the reference impulse responses. Their respective performance were investigated through the impulse response power-delay and Doppler spectrogram profiles. The best performance were obtained by the *Soft* version of the *K-Means,* which made it the best reduction method according to these criteria. Moreover, the reduced impulse responses of this method showed to be more physically consistent, with more continuous multipath delays and Doppler shifts.

As a conclusion of this chapter, the *Soft K-Means* clustering algorithm adapted to the channel reduction problematic as presented in section 2.5.5, referred to as *Clustering Weighted* in the following of this thesis, is considered as the best aggregation method. The last chapter will assess its performance in terms of preservation of the positioning error of the receiver. However, note that this conclusion is only valid for reduction methods consisting in the aggregation of multipaths. Chapter 3 and 4 will investigate totally different channel reduction approaches.

Chapter 3

3. Implementation of a parametric optimization method to preserve the channel autocorrelation function

This chapter investigates an optimization algorithm to parameterize the reduced channel multipaths so as to conserve the pseudo-range error. For having a major impact on the estimation of the signal time of arrival, the channel autocorrelation function will be regarded as the main conservation target. This study will try to take advantage of the different works related to multipath estimation using angle of arrival and/or Doppler-delay estimation. A particular focus will be brought to the Doppler-delay estimation because of the importance of these parameters on the channel autocorrelation function. A cost function will be defined to address this problem and will be minimized using the SAGE algorithm (*Space Alternating Generalized Expectation-Maximization*). The performance of this algorithm will be discussed in order to set an optimal implementation and to find a compromise between conservation of the channel power-delay and Doppler spectrogram, conservation of the channel autocorrelation function and reasonable computation time. Finally, the channel conservation will be assessed using the reference scenario (already used in the previous chapter). The performance in terms of pseudo-range error preservation will be a part of the final comparison of all the methods in the last chapter.

3.1. Introduction and literature overview

3.1.1. The channel estimation problem

Contrary to the previous chapter that was focused on the preservation of the channel power-delay and Doppler spectrogram, this study aims at preserving the impact of the multipath channel on the positioning performance. The parametric optimization methods will aim at reducing the multipath channel by estimating the best parameters of the L multipaths of the reduced channel to minimize the difference between the pseudo-range error before and after reduction.

A similar channel reduction process was already investigated in [Garc 10], which proposed to optimize the delays and complex amplitudes of the reduced channel to preserve the receiver pseudo-range and Doppler errors. Two cost functions were considered in [Garc 10], expressed as $H^{(1)}$ and $H^{(2)}$ in Eq. 3.1 and 3.2. The LOS contribution of the channel will systematically be removed from the parametric estimation. The channel that has to be reduced contains M multipaths. The function $g(\tau)$ denotes the signal code in terms of its delay of arrival and $R_{ss}(\tau)$ the autocorrelation function of $g(\tau)$. The optimization process consists in computing the L delays and amplitudes $\hat{\tau}_{l,min}$ and $\hat{\gamma}_{l,min}$to minimize $H^{(1)}$ and $H^{(2)}$.

$$H^{(1)} = \left| \sum_{l=1}^{M} \widetilde{\gamma_l} . g(t-\tau_l) - \sum_{l=1}^{L} \widehat{\gamma_l} . g(t-\widehat{\tau_l}) \right| \tag{3.1}$$

$$H^{(2)} = \left| \sum_{l=1}^{M} \widetilde{\gamma_l} . R_{ss}(t-\tau_l) - \sum_{l=1}^{L} \widehat{\gamma_l} . R_{ss}(t-\widehat{\tau_l}) \right| \tag{3.2}$$

The cost function $H^{(1)}$ is the difference between the signal convoluted with the original and reduced channels. The cost function $H^{(2)}$ is the difference between the original channel autocorrelation function and the reduced one. These two cost functions have been compared in [Garc 10] through the criterion of the preservation of the pseudo-range and Doppler errors. The conclusion of this study revealed that the pseudo-range error is preserved the best when using the cost function $H^{(2)}$, that is to say when minimizing the difference between the original and reduced channel autocorrelation functions. Therefore, it has been decided to follow this approach to define the cost function that will be used for this thesis, which will be presented in section 3.2. It can be mentioned that [Mota 10] considered another cost function which is the difference between the impulse responses in the frequency domain before and after reduction. This approach was not investigated in this thesis, as it has been decided to focus on the conservation of the autocorrelation function.

It can be observed on Eq. 3.1 and 3.2 that only the delay and complex amplitude are estimated (no Doppler shift). However, some studies in other scopes than the channel reduction problem investigated the possibility to estimate other parameters. In particular, many works dealing with the multipath mitigation issue pre-estimate the multipaths before the mitigation process. In [VanN 94], for example, multipath estimation methods showed to be 10 times more efficient than small early-late spacing techniques to decrease the error caused by the multipath channel on the carrier and code tracking errors. In that case also, only delays and complex amplitudes were estimated.

However, further works introduced the estimation of the angle of arrival to the optimization problem. Different optimization algorithms were compared in [Chun 01] and [Chun 02]. The possibility to discriminate different channel contributions according to their angle of arrival in the wireless communication context was investigated in [VanT]. Note that such approaches are strongly constrained by the antenna array architecture to estimate the azimuth of arrival of the signal contributions. Those limitations have no impact on the channel reduction problem, which considers simulated signals with known angles of arrival. Therefore, the implementation restrictions and performance limitations presented in studies like [Chun 01], [Chun 02] or [VanT 04] do not constraint this study. Joint delay and direction of arrival estimations are presented in [Mota 10]. In [Fleu 99], [Antr 08] and [Roug 12a], the delays, angles of arrival and Doppler shifts are estimated using the SAGE algorithm.

As mentioned previously, the focus of this chapter is the conservation of the positioning error. To do so, a particular attention has to be brought to the conservation of the code and carrier tracking. The delays and phase variations have a major impact on these tracking loops. The information about the phase variation of the multipaths is contained in their Doppler shift. With respect to the Doppler, the angle of arrival is almost redundant, as explained in section 2.4. Moreover, it was already mentioned in section 2.3 that the channel Doppler characteristics have to be preserved in order to avoid multiple phase discontinuities. For these reasons, it has been decided to focus the parameter optimization on the delays and Doppler shifts in this study.

3.1.2. Choice of the appropriate optimization algorithm

The maximum likelihood estimator is well known to be the best estimator, although it usually requires a significant computation load [VanT 04]. The SAGE algorithm has been proposed in order to reduce as much as possible the computation effort required to solve the maximum likelihood estimation problem [Fess 94]. In a context of multipath estimation (or mitigation), the SAGE algorithm was applied for joint DOA (Direction of Arrival), delay and Doppler estimation in time variant channels, in [Fleu 99], [Antr 08] and [Pede 97]. Still in multipath estimation domain, other estimators exist such as quadratic algorithm (Capon algorithm [Capo 69]), or sub-space algorithms (MUSIC [Schm 86], ESPRIT [Roy 89]). These estimators strongly reduce the complexity of the optimization problem, but are globally less accurate than maximum likelihood estimator. Therefore, it has been decided to adapt the SAGE approach to the channel reduction concern.

The SAGE algorithm was described in details in [Fess 94] and [Capo 69]. It consists in dividing the optimization problem in several sub-spaces, each sub-space corresponding to one path to estimate. In this thesis, each sub-space will correspond to a specific multipath of the reduced channel. However, it must be mentioned that all the aforementioned methods have been dedicated to the multipath estimation from physical measurements of the signal. In those cases, the cost function to minimize has been defined so as to isolate the useful signal from the Gaussian noise. In the channel reduction context, no noise is considered. Indeed, the received signal is simulated by the signal code convoluted with the reference multipath channel. Therefore, this algorithm has to be adapted, as it will be detailed in the following section.

3.2. Adaptation and application of the SAGE algorithm to the cost function

3.2.1. Definition of the cost function

This paragraph explains the choice of the cost function to minimize that will be considered all along this optimization problem. As already mentioned in section 3.1.1, it has been decided to focus the optimization problem on the pseudo-range error preservation. Therefore, the parametrization process will aim at minimizing the difference between the original and reduced channel autocorrelation functions, for each impulse response snapshot. Eq. 3.3 denotes the signal autocorrelation function $r(\tau)$ (equivalent to $R_{SS}(\tau)$ in Eq. 3.2).

$$r(\tau) = \int_{t=-\infty}^{+\infty} g(t) g(t-\tau) dt \tag{3.3}$$

In the urban channel context, the impinging signal is distorted by the multipath channel. The resulting signal is then the convolution of the original signal with the channel impulse response. Being given the linearity of the convolution product and of the integral, introducing the discrete impulse response expression in Eq. 3.1 results in Eq. 3.4, where $R_{c*s,s}(\tau)$ denotes the channel autocorrelation function:

$$R_{c*s,s}(\tau) = (r * h)(\tau) = \sum_{l=1}^{L} \gamma_l . e^{j\varphi_l} r(t-\tau_l) \tag{3.4}$$

It can be remarked from Eq. 3.4 that the current form of the function only depends on the reduced amplitudes, phases and delays. The Doppler shifts are not considered in this model. Thus, if a cost function based on this model is considered, the Doppler dimension could not be used in the reduction process. Therefore, it has been decided to consider N samples of the autocorrelation functions to add the Doppler dimension to the optimization problem. It corresponds to N successive correlations of the original signal with local replica spaced in time by T_e. These delayed signal replica are computed by propagating the phases and delays of the multipaths using their respective Doppler shifts along the sampling time T_e. In that case, N defines the Doppler resolution of the optimization problem, as it will be detailed in the following. The delay τ and phase φ of a given multipath at the time nT_e ($n \in [\![1, N]\!]$) are given by Eq. 3.5 and 3.6 considering its Doppler ϑ at the time nT_e:

$$\tau(nT_e) = \tau(0) + \frac{\vartheta}{f_0} nT_e \tag{3.5}$$

$$\varphi(nT_e) = \varphi(0) + 2\pi\vartheta nT_e \tag{3.6}$$

The amplitude modules and Doppler shifts are considered constant during the time NT_e. Let $\boldsymbol{R}_l(\tau_l, \vartheta_l)$ denote the autocorrelation along the delay and time of the only multipath l of delay τ_l and Doppler ϑ_l. $R_l(\tau_l, \vartheta_l)$ is built as the column vector containing the P samples of the autocorrelation function along the delay line with C_s sampling period. These correlation functions are obtained for the different correlation times nT_e and are concatenated in a column vector detailed in Eq. 3.7.

$$\boldsymbol{R}_l(\tau_l, \vartheta_l) = \begin{pmatrix} r\left(\tau_l - \frac{PC_s}{2}\right) . e^{j2\pi\vartheta T_e} \\ \vdots \\ r\left(\tau_l + \frac{PC_s}{2}\right) . e^{j2\pi\vartheta T_e} \\ r\left(\tau_l - \frac{PC_s}{2}\right) . e^{j2\pi\vartheta 2T_e} \\ \vdots \\ r\left(\tau_l + \frac{PC_s}{2}\right) . e^{j2\pi\vartheta 2T_e} \\ \vdots \\ r\left(\tau_l + \frac{PC_s}{2}\right) . e^{j2\pi\vartheta NT_e} \end{pmatrix}_{PN\times 1} \tag{3.7}$$

Eq. 3.8 denotes the computation of the original channel correlation vector X (of size $NP \times 1$), considering M multipaths in the original channel.

$$\boldsymbol{X} = \sum_{m=1}^{M} \tilde{\gamma}_m . \boldsymbol{R}_m(\tau_m, \vartheta_m) \tag{3.8}$$

Where $\tilde{\gamma}_m = \gamma_m . e^{j\varphi_m}$ is the complex amplitude of multipath m. Using the same approach, the reduced correlation vector $\boldsymbol{X}_r$ can be defined, according to the parameters of the l reduced channel multipaths.

Therefore, the cost function of the optimization process can be defined. It has been chosen to minimize the distance between the original and reduced correlation functions, which are sampled along the delay (correlator samples) and time (correlation samples) dimensions. The cost function is written J:

$$J = \|\boldsymbol{X} - \boldsymbol{X}_r\|^2 = (\boldsymbol{X} - \boldsymbol{X}_r)(\boldsymbol{X} - \boldsymbol{X}_r)^H \tag{3.9}$$

This optimization problem has $3 \times L$ unknowns: delay, complex amplitude and Doppler shift. These parameters have to be optimized for each multipath. In the following, these unknowns will be recorded in the $\boldsymbol{\Psi}$ matrix which is defined by $\boldsymbol{\Psi} = [\Psi_1 \quad \ldots \quad \Psi_L]_{3\times L}$. It can be remarked that this optimization problem is the same as the one presented in [Fleu 99], [Antr 08] and [Roug 12a]. As mentioned in [Roug 12a], a numerical method has to be used to solve this estimation problem, since it is neither linear nor quadratic. Moreover, the number of unknowns implies a heavy computation load when trying to parameterize the multipaths according to a grid search approach (meshing of the different dimensions). In [Roug 12a], a solution using the Newton algorithm is mentioned. Nevertheless, this study will focus on the SAGE algorithm, as it is presented in [Fleu 99], [Antr 08] and [Roug 12a].

3.2.2. Resolution of the optimization problem using the SAGE algorithm

3.2.2.1. Presentation of SAGE and hypothesis

As presented in section 3.1, the SAGE algorithm is an extension of the Expectation-Maximization algorithm, which relies on the sub-space sequencing of the optimization problem. In other terms, instead of addressing the minimization directly, the optimization is performed on several separated sub-spaces. Thus, the minimization of the cost function $\|\boldsymbol{X} - \boldsymbol{X}_r(\boldsymbol{\Psi})\|^2$ can be performed by sequential smaller optimization problems:

$$J_l(\boldsymbol{\Psi}) = \left\|\boldsymbol{X}_l - \boldsymbol{X}_{r,l}(\boldsymbol{\Psi})\right\|^2 \tag{3.10}$$

Where $\boldsymbol{X}_{r,l}(\boldsymbol{\Psi})$ represents one path of the reduced channel. It is defined by:

$$\boldsymbol{X}_{r,l}(\Psi_l) = \tilde{\gamma}_l . \boldsymbol{R}_l(\tau_l, \vartheta_l) \tag{3.11}$$

And verifies :

$$\boldsymbol{X}_r(\Psi) = \sum_{l=1}^{L} \boldsymbol{X}_{r,l}(\boldsymbol{\Psi}_l) \tag{3.12}$$

The vectors $\boldsymbol{X}_l$ are called “Hidden Data Spaces”. It is assumed that vector $\boldsymbol{X}$ can be approached by L disjoint sub-spaces [Fess 94]. Then, the SAGE procedure proposes one step of estimation of the “Hidden Data Spaces” (*Expectation* step), and one optimization step where the parameters Ψ_l are estimated (*Maximization* step). This process is looped on all the “Hidden Data Spaces” and repeated iteratively until the convergence of the algorithm.

The following section will detail the different steps of the algorithm, including the definition of the different sub-optimization problems and the division of the problem in “Hidden Data Spaces”. However, it has to be mentioned that the “Hidden Data Space” formalism is used in this thesis without suitable theoretical background. As developed in [Fess 94], this technique is used to solve maximum likelihood maximization, with some hypothesis on the sub-spaces of the optimization problem. In particular, it is defined in [Fess 94] that the different “Hidden Data Spaces” X_l must be fully defined by the parameter Ψ_l, which implies some assumptions on the residue of the cost function. In [Fleu 99], [Antr 08] and [Roug 12a], the SAGE algorithm is used to estimate the parameters of different signals within an impinging wave front and some additional Gaussian noise. Therefore, the residue of the cost function is expected to follow a Gaussian distribution, which allows the optimization problem to satisfy the aforementioned assumption [Roug 12a].

In this study, it has been decided to use the SAGE algorithm to address the optimization problem of Eq. 3.10 for its practical suitability to solve such a multi-dimensional problem and the similarity with the cost function to minimize of [Fleu 99], [Antr 08], and [Roug 12a]. This problem is not directly related to a maximum-likelihood maximization process, as there is no information a priori on the residue of this cost function. It has only been assumed that the optimization problem could be split in sub-optimization spaces. The ability of this method to minimize this cost function will be investigated along the following sections, to validate this approximation. However, the theoretical conclusions of [Fess 94] and [Capo 69] about the non-divergence or the local maxima of the algorithm cannot be applied to this context. Those criteria will also be studied in the following sections.

3.2.2.2. Implementation of SAGE

As mentioned in the previous section, the SAGE algorithm is composed of two major steps: the estimation of $\boldsymbol{X}_l$ called *E-STEP* and the optimization of the associated cost function $J(\boldsymbol{\Psi}_l)$ called *M-STEP*.

- **E-STEP:**

The sub-space X_l will be considered as the contribution of the multipath l (of the reduced channel) to the correlation function $\boldsymbol{X}$. It is estimated with the prior knowledge of the other sub-spaces already optimized. It aims at minimizing the residue, so as to sequence the optimization problem properly. The sub-space $\boldsymbol{X}_l$ is estimated using the Eq. 3.13:

$$\widehat{\boldsymbol{X}_l} = \boldsymbol{X} - \sum_{\substack{k=1 \\ k \neq l}}^{L} \boldsymbol{S}_{\boldsymbol{k}}(\widehat{\Psi_k}) \tag{3.13}$$

- $\widehat{\Psi_k}$ denotes the parameters estimated by SAGE for the multipath k.
- $\boldsymbol{S}_{\boldsymbol{k}}(\widehat{\Psi_k})$ denotes the correlation function of the multipath k along delay and time, depending on its delay, Doppler and complex amplitude.

- **M-STEP:**

The maximization step consists in minimizing the cost function of $\widehat{\boldsymbol{X}_l}$: $J_l(\Psi_l) = \left\|\widehat{\boldsymbol{X}}_l - \boldsymbol{X}_{r,l}(\Psi_l)\right\|^2$. This optimization process requires 3 dimensions to estimate the delay, Doppler shift and complex amplitude of the reduced channel multipath l. It is proposed in [Antr 08] and [Roug 12a] to solve this problem as 3 sub-optimization problems of dimension 1. The maximization step will estimate successively the delay, Doppler shift and complex amplitude of l:

$$\begin{aligned}
\widehat{\tau_l} &= \arg\min_{\tau_l}\left\|\boldsymbol{X}_l - \boldsymbol{S}_l(\tau_l, \widehat{\vartheta}_l, \widehat{\gamma_l})\right\|^2 \\
\widehat{\vartheta}_l &= \arg\min_{\vartheta_l}\|\boldsymbol{X}_l - \boldsymbol{S}_l(\widehat{\tau_l}, \vartheta_l, \widehat{\gamma_l})\|^2 \\
\widehat{\gamma_l} &= \arg\min_{\gamma_l}\left\|\boldsymbol{X}_l - \boldsymbol{S}_l(\widehat{\tau_l}, \widehat{\vartheta}_l, \gamma_l)\right\|^2
\end{aligned} \tag{3.14}$$

Introducing Eq. 3.10 in the cost function $J_l(\Psi_l)$ gives:

$$J_l(\Psi_l) = \|\boldsymbol{X}_l - \tilde{\gamma}_l.\boldsymbol{R}_l(\tau_l, \vartheta_l)\|^2 \tag{3.15}$$

It can be remarked from Eq. 3.15 that the cost function $J_l(\Psi_l)$ depends quadratically on the complex amplitude $\widetilde{\gamma_l}$. Thus, if $\widehat{\gamma_l}$ corresponds to an extremum of the cost function:

$$\frac{\partial J_l(\Psi_l)}{\partial \gamma_l} = 0 \tag{3.16}$$

Therefore, the development and the partial derivation of Eq. 3.15 along the amplitude dimension lead to the literal expression of $\tilde{\gamma}_l$ in terms of the other parameters:

$$\widehat{\tilde{\gamma}}_l = \frac{\boldsymbol{R}_l\left(\widehat{\tau_l}, \widehat{\vartheta}_l\right)^H \times \boldsymbol{X}_l}{\boldsymbol{R}_l\left(\widehat{\tau_l}, \widehat{\vartheta}_l\right)^H \boldsymbol{R}_l\left(\widehat{\tau_l}, \widehat{\vartheta}_l\right)} \tag{3.17}$$

By introducing the optimized complex amplitude of Eq. 3.17 in Eq. 3.15, the new cost function to maximize $\Lambda_l(\Psi_l)$ is obtained:

$$\Lambda_l(\Psi_l) = \frac{|\boldsymbol{R}_l(\tau_l, \vartheta_l)^H \times \boldsymbol{X}_l|^2}{\boldsymbol{R}_l(\tau_l, \vartheta_l)^H \boldsymbol{R}_l(\tau_l, \vartheta_l)} \tag{3.18}$$

The parameter estimation of the multipath sub-space $\boldsymbol{X}_l$ becomes Eq. 3.19. It has to be mentioned that Eq. 3.19 is solved using a grid-search approach to estimate the maximums.

$$\hat{\tau_l} = \arg\max_{\tau_l} \frac{\left|\boldsymbol{R}_l\left(\tau_l, \hat{\vartheta_l}\right)^H \times \boldsymbol{X}_l\right|^2}{\boldsymbol{R}_l\left(\tau_l, \hat{\vartheta_l}\right)^H \boldsymbol{R}_l\left(\tau_l, \hat{\vartheta_l}\right)}$$

$$\hat{\vartheta_l} = \arg\max_{\vartheta_l} \frac{|\boldsymbol{R}_l(\hat{\tau_l}, \vartheta_l)^H \times \boldsymbol{X}_l|^2}{\boldsymbol{R}_l(\hat{\tau_l}, \vartheta_l)^H \boldsymbol{R}_l(\hat{\tau_l}, \vartheta_l)} \tag{3.19}$$

$$\hat{\gamma_l} = \frac{\boldsymbol{R}_l\left(\hat{\tau_l}, \hat{\vartheta_l}\right)^H \times \boldsymbol{X}_l}{\boldsymbol{R}_l\left(\hat{\tau_l}, \hat{\vartheta_l}\right)^H \boldsymbol{R}_l\left(\hat{\tau_l}, \hat{\vartheta_l}\right)}$$

The expectation and maximization steps are alternately repeated over the different multipath sub-spaces until the convergence of the algorithm. It is suggested in [Fleu 99], [Antr 08] and [Roug 12a] that SAGE does not necessarily converge to a global maximum. As a consequence, the parameters of the different sub-spaces have to be initialized appropriately. To do so, it is proposed in [Fess 94] and [Capo 69] to do a first estimation of the different parameters, which is detailed hereafter.

- **Initialization**:

First, the reduced channel is pre-initialized to $\tau_l = 0$, $\vartheta_l = 0$ and $\tilde{\gamma_l} = 0$, $\forall l \in \{1, \dots, L\}$. Then, [Fess 94] proposes to estimate the initial parameters of the multipaths of the reduced channel using the expectation and maximization phases.

The Expectation phase is defined as follows, for a given multipath $l$of the reduced channel. $\boldsymbol{X}_l(0)$ denotes the “Hidden Data Space” estimated during the initialization process.

$$\boldsymbol{X}_l(0) = \boldsymbol{X} - \sum_{k=1}^{l-1} \boldsymbol{S_k}(\Psi_k) \tag{3.20}$$

The maximization step consists in optimizing the parameters of the different sub-spaces according to the equations of 3.19:

$$\hat{\tau_l}(0) = \arg\max_{\tau_l} \frac{|\boldsymbol{R}_l(\tau_l, 0)^H \times \boldsymbol{X}_l(0)|^2}{\boldsymbol{R}_l(\tau_l, 0)^H \boldsymbol{R}_l(\tau_l, 0)}$$

$$\hat{\vartheta_l}(0) = \arg\max_{\vartheta_l} \frac{\left|\boldsymbol{R}_l\left(\widehat{\tau_{l,0}}, \vartheta_l\right)^H \times \boldsymbol{X}_l(0)\right|^2}{\boldsymbol{R}_l\left(\widehat{\tau_{l,0}}, \vartheta_l\right)^H \boldsymbol{R}_l\left(\widehat{\tau_{l,0}}, \vartheta_l\right)} \tag{3.21}$$

$$\widehat{\gamma_{l,0}}(0) = \frac{\boldsymbol{R}_l\left(\widehat{\tau_{l,0}}, \widehat{\vartheta_{l,0}}\right)^H \times \boldsymbol{X}_l(0)}{\boldsymbol{R}_l\left(\widehat{\tau_{l,0}}, \widehat{\vartheta_{l,0}}\right)^H \boldsymbol{R}_l\left(\widehat{\tau_{l,0}}, \widehat{\vartheta_{l,0}}\right)}$$

Another solution to initialize the SAGE process has been considered in this study. This algorithm is dedicated to be applied to the impulse responses of the reference scenario along the trajectory. Therefore, it is possible to initialize the parameters of the SAGE algorithm at a given instant using the parameters estimated by SAGE at the immediate predecessor instant.

- **Algorithm stopping rule:**

It has been decided to stop the algorithm when it is close enough to its convergence point. To do so, the difference between the parameters of the different sub-spaces for two consecutive iterations i and $i+1$ is quantified. At the iteration where the parameters of every sub-space do not vary more than a given threshold, it is considered that the algorithm has converged. These thresholds can be set according to the research steps of the different parameters. In [Roug 12a], it is suggested that the following thresholds could set the convergence of the algorithm:

$$\forall l \in \{1, \dots, L\}, \qquad |\tau_l(i) - \tau_l(i+1)| \leq 0.5\, ns, \qquad |\vartheta_l(i) - \vartheta_l(i+1)| \leq 0.5\, Hz \tag{3.22}$$

- **Amplitude correction:**

The amplitude estimated by SAGE during the *M-STEP* depends on the total duration of the autocorrelation function ***X*** over time, which is given by $N.T_e$. Indeed, the narrow-band power of the channel varies during this time. In other terms, the relative amplitude and phase of the reduced channel multipaths are correctly estimated but their absolute values depend on N and T_e. Therefore, it has been decided to apply a correction to the amplitude of the multipaths, in order to preserve the original channel energy. It simply consists in multiplying the complex amplitude of each estimated echo by the complex amplitude of the original multipath channel divided by the complex amplitude of the estimated multipath channel.

Fig. 3.1 illustrates the architecture of SAGE which was described all along this section, including the initialization step, the expectation-maximization iterative process and the stopping rule.

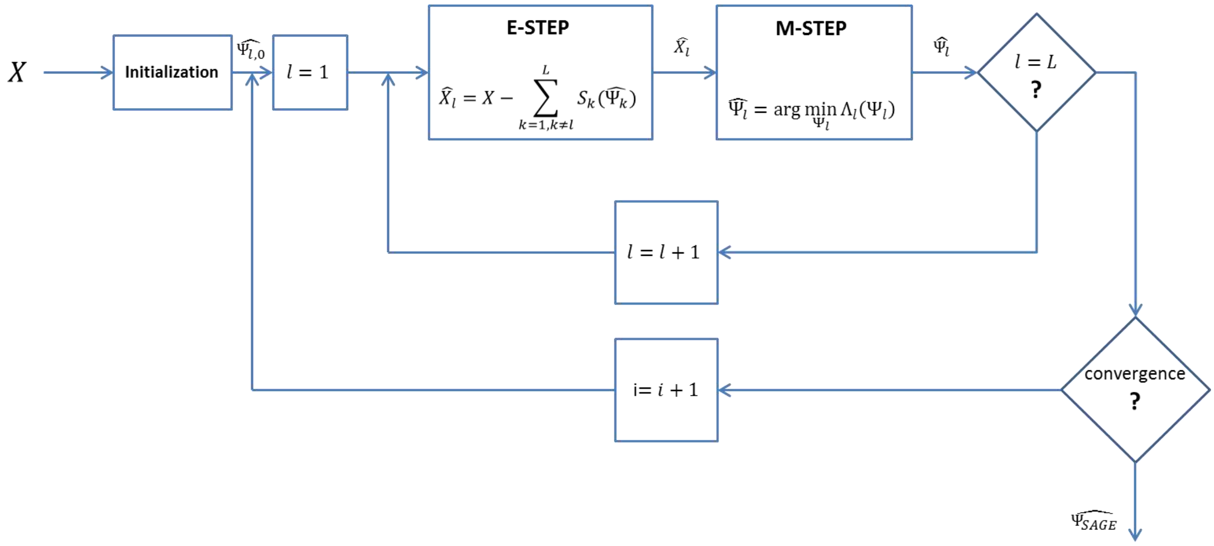

Figure 3.1 : Illustration of the SAGE algorithm architecture

3.2.2.3. Influence of the parameters of the algorithm

From the presentation of the SAGE algorithm in sections 3.2.2.1 and 3.2.2.2, three major parameters showed to have an impact on the performance. They were referred to as the delay between two correlators C_s, the number of correlation samples in time N and the temporal distance between two correlation samples T_e. The choice of these values will be discussed, because they have a major impact on the delay and Doppler resolutions of the reduced channel, as well as on the computational load.

- **Influence on the delay resolution**

The delay between two consecutive correlators C_s, and the number of correlator samples P have an impact on the delay resolution of the reduced channel. The more correlators there are, the better the resolution is. However, the more correlators there are, the bigger the complexity is and the larger the computation time is. In [Roug 12a], a study has compared the performance of the algorithm with different values of C_s and P, according to the channel RMSE (Root Mean Square Error) for different receiver RF bandwidth. It concluded that for a given bandwidth B, the maximum spacing between the correlators was given by:

$$C_{s_{opt}} = \frac{1}{B} \tag{3.23}$$

In this study, a bandwidth $B > 100$ MHz has been chosen. Therefore, the parameter C_s can be extended to approximately 200 ns. It was also suggested in [Roug 12a] that the correlator samples should cover the whole delay domain. The delay domain has been restricted to $[-T_c, T_c]$, where T_c denotes the duration of one chip of the navigation signal code. Note that it allows taking into account the contribution of every multipath likely to have an influence on the DLL tracking (the far echoes have no impact on the DLL error). The resulting value of P is given by:

$$P = ceil\left[\frac{2T_c}{C_s}\right] \tag{3.24}$$

- **Influence on the Doppler resolution**

The number of correlation samples N and the time between two samples T_e have an influence on the Doppler resolution. The number of correlator samples also has a major impact on the computation load. The more samples there are, the larger its computation time is. A compromise has to be found between this computation time and the channel Doppler resolution.

The resolution in the frequency domain of the channel autocorrelation function can be deduced from the sampled autocorrelation function in the temporal domain. Indeed, the frequency resolution is given by the total duration in the time domain. In other terms, the Doppler resolution is given by $1/NT_e$. Moreover, the sampling period defines the maximum Doppler shift identifiable by the algorithm. This maximum Doppler shift is then given by $\vartheta_{max} = 1/2T_e$.

In this study, it has been decided to set the maximum Doppler limit to 100 Hz, which corresponds approximately to the maximum multipath Doppler considering the receiver in motion at 45 km/h. The resultant sampling period is T_e=5 ms. Then, the value of N will define the Doppler resolution of the reduced channel. Its optimal value will be chosen with respect to an optimal trade-off between computation load and channel accuracy. It will be presented in the following section, which will investigate the performance of the SAGE algorithm.

3.3. Validation of SAGE and limitations

This section assesses the performance of SAGE for the needs of this thesis. It was already mentioned that SAGE has been dedicated to the conservation of the multipath channel autocorrelation function. Therefore, it can be expected that using SAGE as a reduction technique leads to a good preservation of the pseudo-range error (which will be focused in chapter 5). However, the preservation of the channel power-delay and Doppler spectrograms has also to be investigated.

Moreover, in the SAGE approach, synthetic signals are used to build the cost function to minimize, as presented on Eq. 3.3 and 3.4. It can be deduced that the optimization problem depends on several characteristics of this synthetic signal.

- First, the modulation of the signal has an influence on the impulse delay spread, thus impacting the receiver pseudo-range error. In order to build the autocorrelation functions involved in this optimization process, it has been decided to consider C/A GPS signals (BPSK(1) modulated).
- It was already mentioned that the number of correlation samples, noted N, has a major impact on the performance of SAGE. Therefore, this section will be partially devoted to the assessment of the performance in terms of power-delay and Doppler spectrogram preservation, depending on the chosen Doppler resolution.

To do so, a canonical scenario has been implemented, on which the SAGE reduction method will be applied with different numbers of multipaths in the reduced channel. This study has two targets: prove the possibility to use the SAGE algorithm to address this optimization problem in section 3.3.3 and tune N so as to find a good trade-off between computation load and delay-Doppler preservation in section 3.3.2. The canonical scenario used for this study will be briefly described in section 3.3.1.

3.3.1. Implementation of the canonical scenario

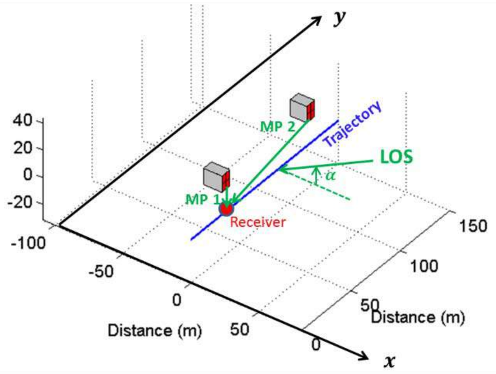

Figure 3.2: Illustration of the canonical scenario with two multipath sources

The canonical scenario is composed of two distinct multipath sources. To do so, two identical buildings have been disposed along the 150 m long trajectory. These are the only two elements constituting the environment. The other characteristics of the scenario take back the features of the reference scenario presented in section 2.2.1. The emitter is located azimuth 30° and elevation 35°. The façades composing the front of the building, from whom the multipaths are originated, are referred to as Façade B in section 2.2.1. As a consequence, multipaths of all three types reach the receiver at any time: specular contributions from the window surfaces, backscattering contributions from the window edges and corners and incoherent scattering from the small façade details (around 500 multipaths per building). The impinging wave is RHCP polarized and the receiver is moving at the speed 5m.s^{-1}. This canonical scenario has been represented on Fig. 3.2. The two multipath sources are denoted *MP1* and *MP2.*

3.3.2. Impact of the Doppler resolution on the power-delay and Doppler spectrogram

The impact of the Doppler resolution has been investigated through the conservation of the power-delay and Doppler spectrograms of the original channel. The SAGE algorithm has been run with different Doppler resolutions to highlight possible differences. Moreover, two different quantities of multipaths in the reduced channel have been tested: 2 and 5 multipaths, in order to adjust the Doppler resolution to the number of echoes to estimate.

Fig. 3.3 illustrates the power-delay profile corresponding to the original impulse response of the canonical scenario presented in the previous sub-section. Fig. 3.4 illustrates the evolution of the Doppler spectrogram corresponding to this scenario. Note that only the multipath channel is considered in both cases, the LOS is not taken into account. The power is represented relatively to the LOS power in logarithmic scale. Note that the two multipath sources are clearly identifiable on both profiles and their delay and Doppler shift are in agreement with the position of the mobile along the trajectory (considering the location of the buildings).

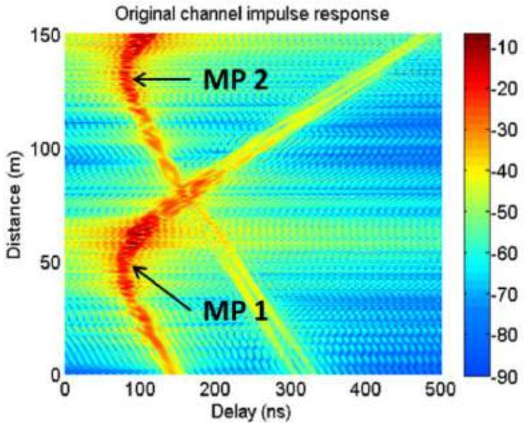

Figure 3.3: Original channel impulse response with 2 multipath sources

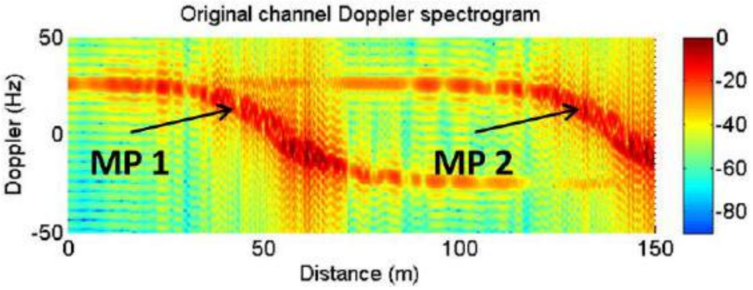

Figure 3.4: Original channel Doppler spectrogram

Fig. 3.5 displays the power-delay profile of the SAGE reduced channels, considering 50 Hz , 20 Hz, 10 Hz and 2 Hz Doppler resolutions (line 1 to 4) with 2 multipaths (left column) and 5 multipaths (right column) in the reduced channels. These plots have to be compared to the plot of Fig. 3.3 to assess the preservation of the power-delay in the different cases. Fig. 3.6 displays the Doppler spectrogram of the same reduced channels. They have to be compared to the original channel Doppler spectrogram of Fig. 3.4 to analyze the Doppler spectrogram conservation in those different cases. The different resolutions represented on both figures can be separated into three categories: high resolution (2 Hz), medium resolutions (10 Hz and 20 Hz) and low resolution (50 Hz). Three major conclusions can be drawn from these comparisons, listed below.

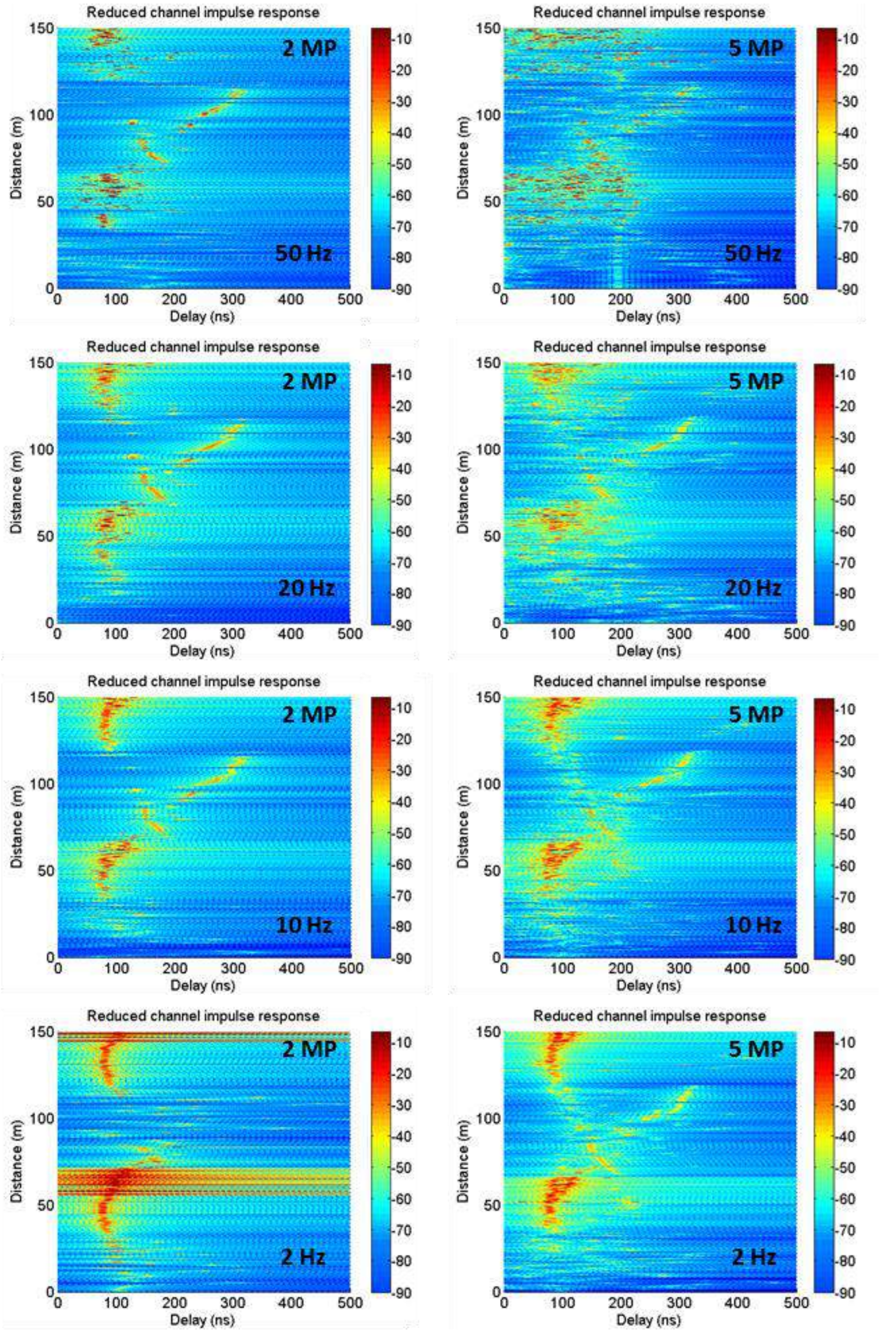

Figure 3.5: Impulse response power-delay profile of the reduced channel for different numbers of multipath and different Doppler resolutions of SAGE

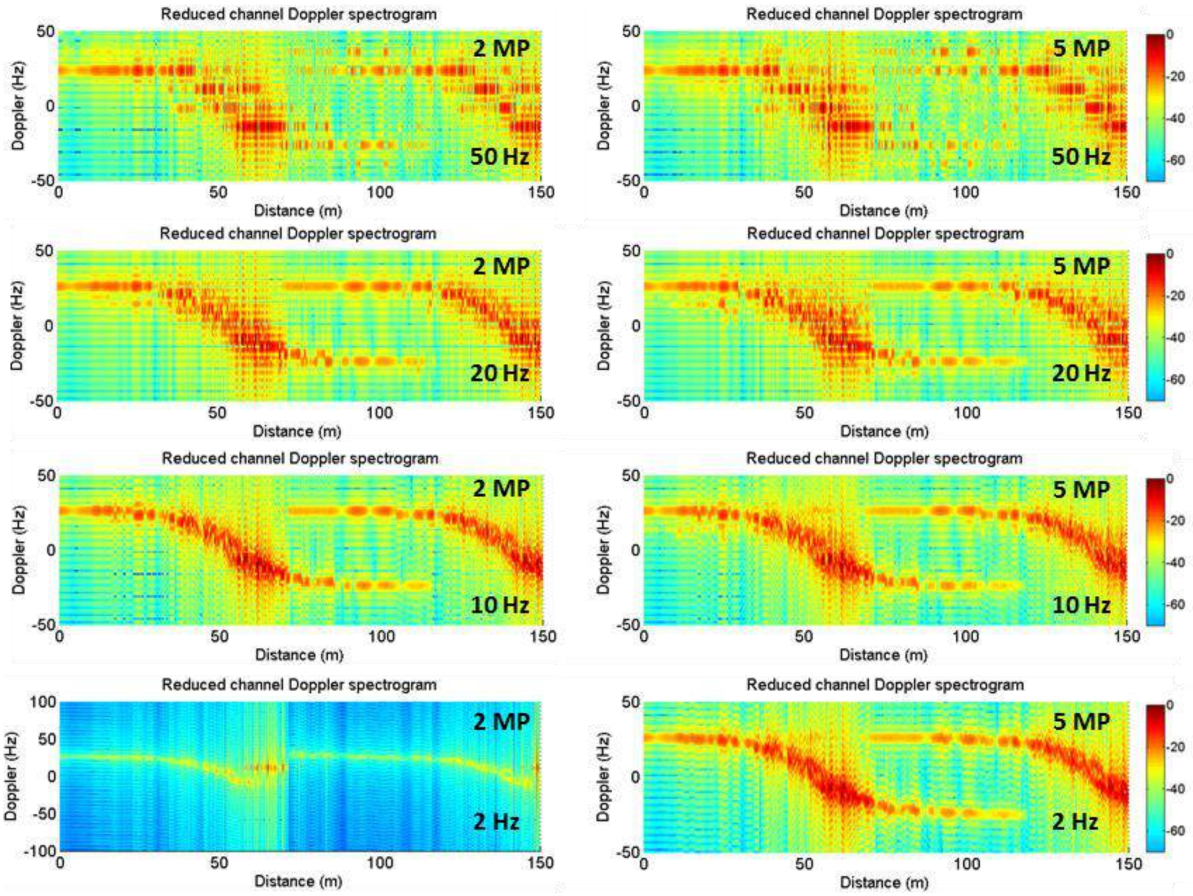

Figure 3.6: Impulse response power-delay profile of the reduced channel for different numbers of multipath and different Doppler resolutions of SAGE

- **Influence of N on the separation of the sources**

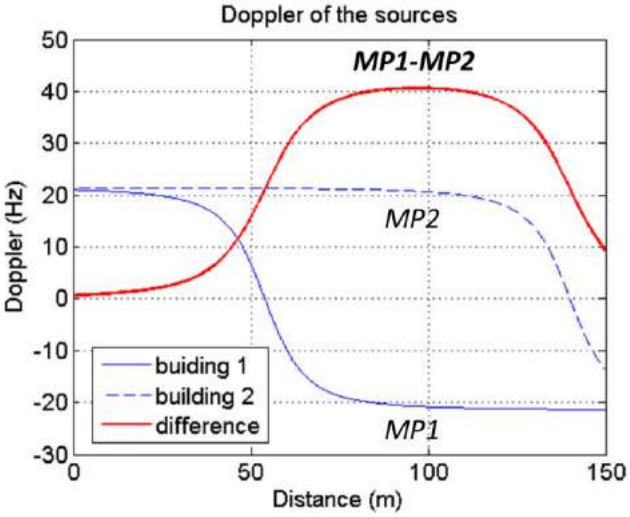

Figure 3.7: Doppler evolution of *MP1* and *MP2*

As observing the medium resolution plots of both Fig. 3.5 and 3.6 (middle lines 10 Hz and 20 Hz), it can be remarked that the two multipath sources are not well separated by SAGE along the whole trajectory. Indeed, on the segments [0m,70m] and [120m,150m], only the contributions of *MP1* or *MP2* respectively are observable. Only the [70m,120m] segment shows both contributions. This observation is due to the Doppler resolution of SAGE. Outside the segment [70m,120m], the Doppler difference between the multipaths corresponding to *MP1* and *MP2* is too low to allow SAGE to separate them during the *Expectation* step. Therefore, only one contribution is reproduced. It is important to note from Fig. 3.5 and 3.6 that this lack of Doppler resolution affects both the Doppler spectrogram and the power-delay profile. Fig. 3.7 illustrates the Doppler of *MP1* (building 1) and *MP2* (building 2) and their difference (red line) along the trajectory. It confirms that the Doppler difference between *MP1* and *MP2* is maximum on [70m,120m].

- **Impact of too many multipaths for too low resolution**

As observing the low resolution plots of Fig. 3.5 and 3.6 (top line: 50 Hz), both power-delay and Doppler spectrograms are impaired by the SAGE reduction technique, more than in the case of medium Doppler resolutions. This is also a consequence of the poor Doppler resolution impacting the *Expectation* phase of SAGE. As the multipath sources cannot be separated by SAGE, the optimization problem is not sequenced properly during the *Expectation* phase. In other terms, the sub-spaces estimated by SAGE are not the multipath sources of the reference scenario. Fig. 3.7 displays the discrete delay profile of the reduced channel impulse response with 2 multipaths all along the trajectory. This plot shows that the first multipath of the reduced channel (echo 1) corresponds to the estimation of *MP1* and *MP2*. That means that both sources are estimated within the first sub-space during the *Expectation* phase of SAGE. This leads to the strong discontinuity and inconsistency of the delay of echo 2 (negative values). Indeed, the residue from which echo 2 is estimated is devoid of echoes (as both sources are already estimated in the first sub-space). Note that the amplitude of echo 2 is low compared to the amplitude of echo 1, which is another consequence.

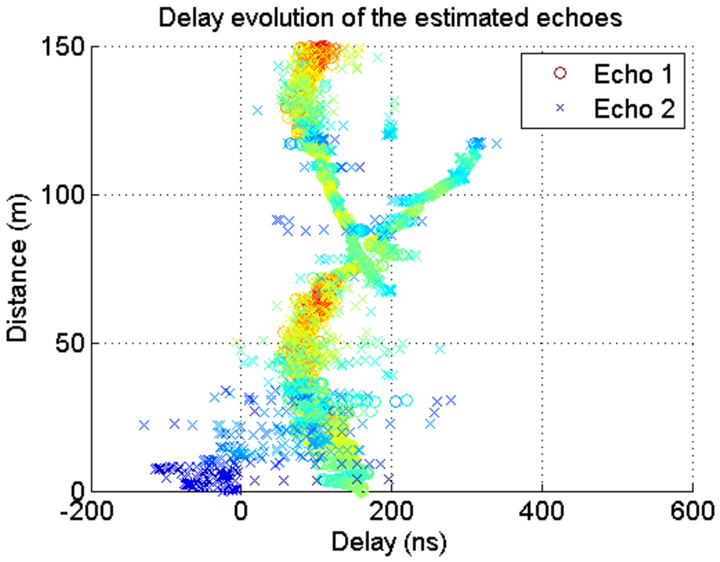

Figure 3.8: Delay evolution of the 2 paths estimated by SAGE with 20 Hz Doppler resolution

It can be observed on Fig. 3.5 ad 3.6 that the impairment of the power-delay and Doppler spectrogram of SAGE in poor Doppler resolutions is more severe with 5 multipaths in the reduced channel than with 2 multipaths. This is due to the fact that more sub-spaces are poorly estimated by the *Expectation* phase. The echoes 2, 3, 4 and 5 of the reduced channel are estimated from residues devoid of echoes, leading to many discontinuities and inconsistencies. Therefore, the wrong sub-space estimation problem is extended as increasing the number of multipaths to estimate (in low Doppler resolution). Therefore, in the case of poor Doppler resolution, the number of echoes in the reduced channel has to be limited, in order to avoid the impairment of the channel power-delay and Doppler spectrogram.

- **Impact of too few multipaths for too high Doppler resolution**

As observing the high resolution plots of Fig. 3.7 and 3.8 (bottom line: 2 Hz), it appears that the power-delay and Doppler spectrogram are more impaired than in the case of medium Doppler resolutions (10 Hz and 20 Hz). Indeed, as observing the plot corresponding to the 2-multipath reduced channel in 2 Hz Doppler resolution, it can be remarked that the two sources are not reproduced separately on any segment of the trajectory. This is due to the fact that, in high resolution, the *Expectation* phase estimates more sub-spaces than there actually are in the original channel. Instead of allocating one sub-space to echo 1 and the other sub-space to echo 2, both sub-spaces are allocated to the estimation of echo 1 or echo 2. The omission of the second echo leads to the shortening of the delay and Doppler spreads.

In the case of the 5-multipath reduced channel in high Doppler resolution (2 Hz), the power-delay and Doppler spectrograms are better preserved than with 2 multipaths in the reduced channel, as it can be observed on Fig. 3.5 and 3.6. Increasing the number of sub-spaces (number of echoes to estimate) increases the probability to allocate at least one sub-space to each echo. Therefore, the reduced channel has to contain enough multipaths to conserve the different sources of the original channel. The better the Doppler resolution is, the more multipaths are needed to take every contribution into account.

- **Synthesis**:

As a consequence, the number of multipaths in the reduced channel and the Doppler resolution of SAGE have to be balanced, in order to find the optimal trade-off between number of multipaths and Doppler resolution to conserve the power-delay and Doppler spectrogram. Indeed, it was shown that too many multipaths in poor Doppler resolution and too few multipaths in high Doppler resolution both lead to the impairment of the original channel. Moreover, it has to be mentioned that high Doppler resolutions require larger computational efforts to run the SAGE algorithm.

In the following of this chapter, it has been decided to estimate 5 multipaths in the reduced channel to investigate the conservation of the channel characteristics, considering the reference environment of section 2.2.1. Provided that the maximum Doppler spread is [-50Hz, 50Hz] with 5 $m.s^{-1}$, 20 Hz resolution is required to partition the environment properly.

3.3.3. Preservation of the channel autocorrelation function

The four plots of Fig. 3.9 represent the comparison between channel autocorrelation functions of the original and reduced channels (estimated by SAGE), with the real and imaginary parts. These examples drawn from the trajectory at the distances d=0 m, d=50 m, d=100 m and d=150 m. It has to be mentioned that the autocorrelation functions were obtained for a BPSK modulated signal, with an infinite bandwidth as mentioned in the introduction of this section. On these examples, 5 multipaths are estimated by SAGE with 20 Hz Doppler resolution.

It can be observed that SAGE optimized the conservation of the autocorrelation function, because the autocorrelation functions of the original and reduced channels overlap almost perfectly. Only an exhaustive study of each autocorrelation corresponding to the impulse response snapshots along the trajectory would prove the well-functioning of SAGE all along the scenario. However, these illustrations confirm the possibility to address this optimization problem using SAGE, even if the initial hypothesis are not fully verified (as mentioned in the previous section).

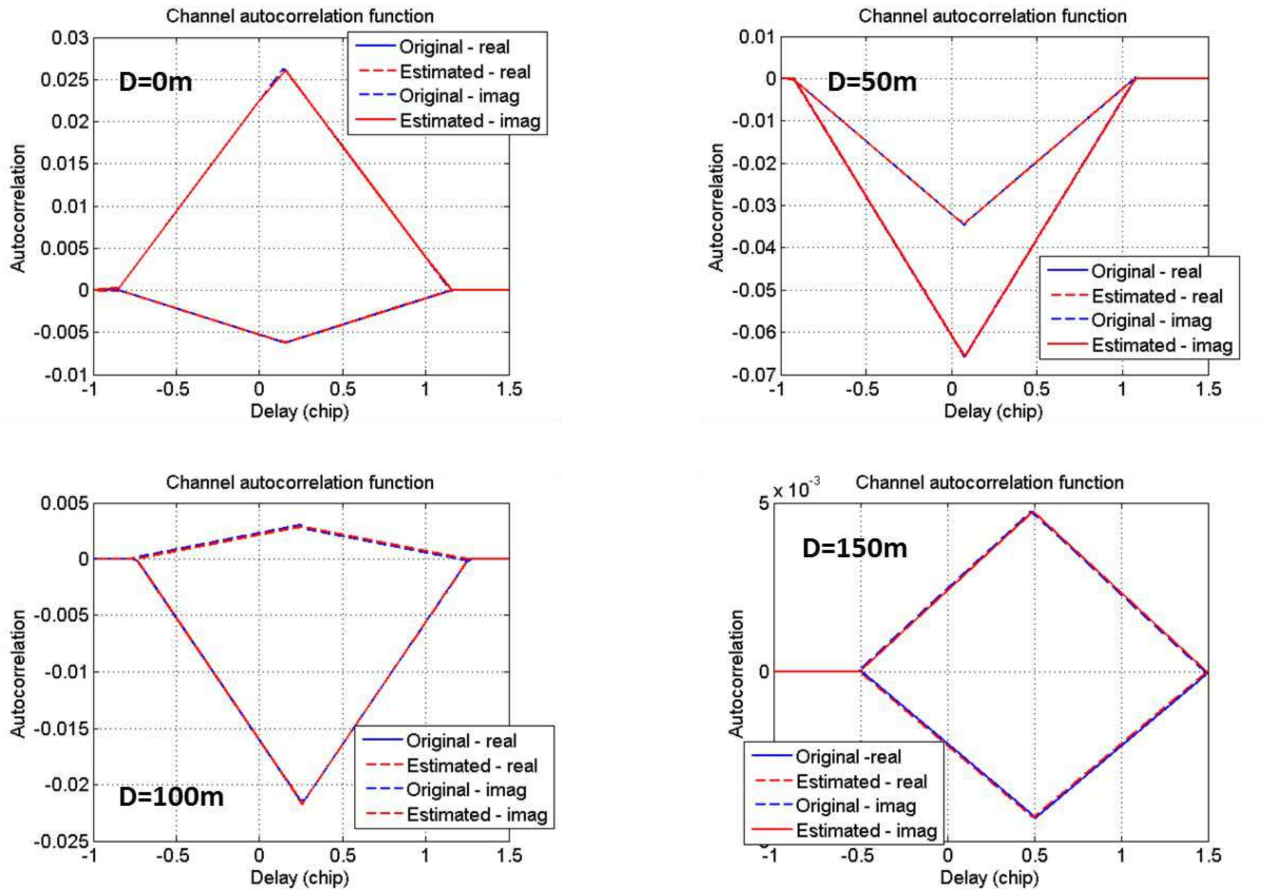

Figure 3.9: Examples of autocorrelation functions comparison corresponding to the original and estimated channels

3.3.4. Synthesis

This section had the double objective to assess the performance of the SAGE with respect to the channel autocorrelation conservation (section 3.3.3) on one side, and to highlight its limits concerning the channel power-delay and Doppler spectrogram preservation (section 3.3.2). These studies have been performed on a canonical scenario to make easier the interpretation of the different results, in particular to highlight the importance of the Doppler resolution of the algorithm.

- In section 3.3.3, 4 examples of channel autocorrelation functions showed the good overlap between original and SAGE reduced channels in terms of autocorrelation function (in real and imaginary domains). It validated the hypothesis made in section 3.2, which stated that the optimization problem of this chapter could be addressed using the SAGE approach.

- In section 3.3.2, the power-delay profiles and Doppler spectrograms of the original and reduced channels were compared with different numbers of multipaths in the reduced channel and different Doppler resolutions of SAGE. The major conclusion of this study was the fact that both delays and Doppler shifts of the reduced channel are impacted by the Doppler resolution of SAGE. This is due to the capacity of SAGE to separate the multipath sources during the *Expectation* phase, which is defined by the Doppler resolution. An inappropriate trade-off between Doppler resolution and number of echoes to estimate leads to the impairment of the original channel characteristics. Therefore, the compromise between number of echoes to estimate and Doppler resolution of SAGE has to be chosen established with respect to the actual number of sources in the original channel.

3.4. Reduction of the reference impulse response using SAGE

In the previous section, it was concluded that SAGE was well suited to estimate the parameters of the reduced channel so as to optimize the conservation of the channel autocorrelation function, despite of a the limitations induced by the Doppler resolution of SAGE. In section 3.2, a few parameters have been identified, for having a significant impact on the performance. Through the study of section 3.3, those parameters have been tuned so as to optimize the trade-off computation time and accuracy of the solution of the optimization problem. The following paragraph summarizes the values chosen for those parameters.

- It is recalled that the cross-correlation between the incoming signal and its local replica, denoted as $r(\tau)$ in Eq. 3.4, corresponds to the autocorrelation function of a BPSK modulated signal with a theoretical infinite bandwidth. In other terms, the shape of this autocorrelation function along the delay domain is a triangle.

- The number of correlators *P* along the delay line of a given correlation sample and the resultant Chip Spacing have been tuned with P=11 and $C_s = \frac{T_c}{5}$, according to section 3.2.2.3.

- The time T_e between two consecutive correlation samples has been set to T_e = 5 ms, which implies a maximum estimable Doppler of 100 Hz.

- The number of correlation samples has been set to N=10, which implies a Doppler resolution of 20 Hz.

3.4.1. Assessment of the delay and Doppler preservation

SAGE has been used to estimate the parameters of the reduced channel all along the trajectory of the reference scenario presented in section 2.2. As previously mentioned, the number of multipaths to estimate has been set to 5, considering 20 Hz Doppler resolution. These estimated multipaths constitute the reduce channel impulse response. It is important to recall that the estimation process is only applied to the multipath channel. The LOS contribution is not considered in this study. Fig. 3.10 illustrates the power-delay profile of the original channel (without LOS), compared to the one of the reduced channel, all along the trajectory.

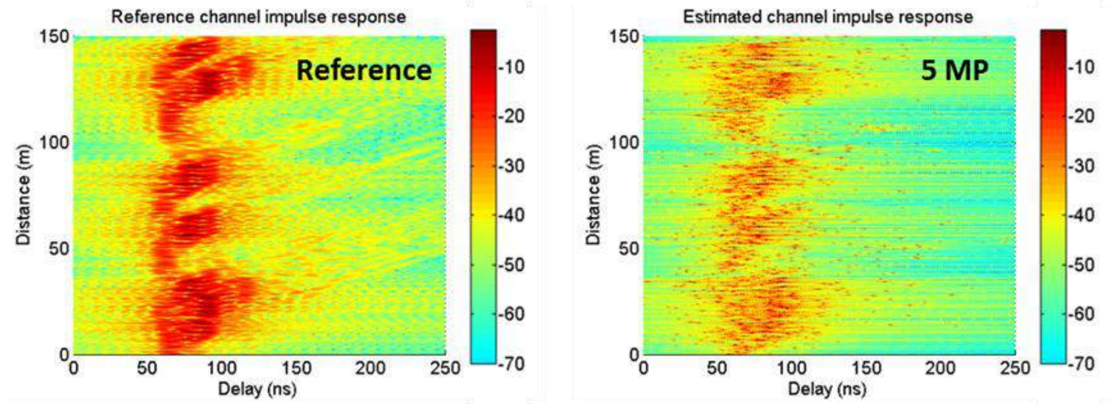

Figure 3.10: Comparison between the reference channel (on the left) and the SAGE reduced channel (on the right) power-delay profiles

It can be observed on the right plot of Fig. 3.10 that the power-delay profile of the reduced channel is very discontinuous as compared to the original one. This result could be expected considering the conclusion of the previous chapter. Indeed, many multipath sources are present in the reference channel environment. Some of them are very close in terms of Doppler. Therefore, the Doppler resolution of 20 Hz is not accurate enough to allow the algorithm to separate the multipaths. No continuous power-delay line corresponding to the motion of the mobile along the buildings is observable, contrary to the reference profile.

In order to have a closer look at the performance of SAGE in terms of delay estimation, 4 impulse response snapshots have been selected along the trajectory, corresponding to d=0m, d=50m, d=100m and d=150m. The comparison between the reference impulse response and the SAGE reduced ones on these samples is displayed on Fig. 3.11. It can be observed that the reduced impulse responses differ significantly from the reference in every case. As a consequence, SAGE has not been able to conserve the delay characteristics of the channel. It can be expected that the reason for that is the Doppler resolution which corrupts the *Expectation* phase of SAGE, as it was highlighted in the previous section. To confirm that, it was decided to investigate the first echo estimated by SAGE isolated.

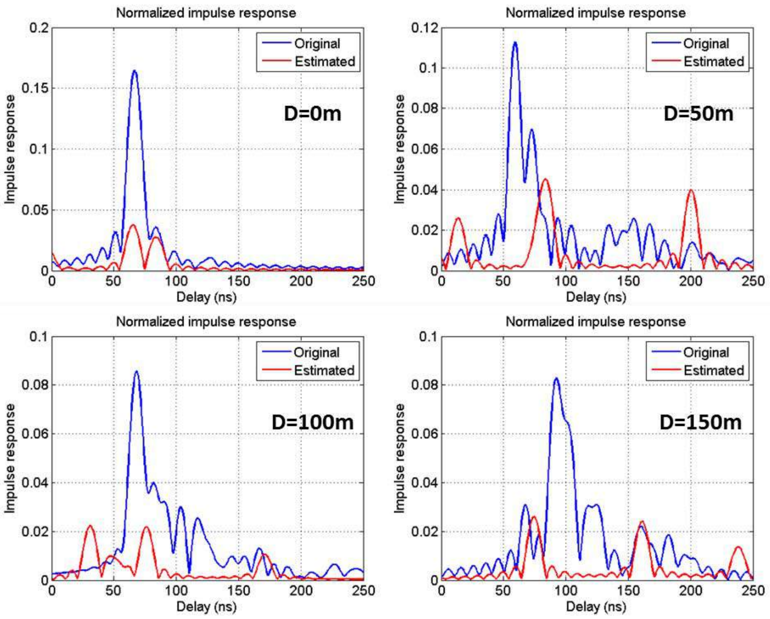

Figure 3.11: Comparison of the estimated channel impulse response with the reference

Fig. 3.12 represents the evolution of the delay of the first multipath estimated by SAGE (first sub-space), on the [0m-25m] segment of the reference scenario. First, it can be observed that its delay corresponds to the delay of high multipath power (between 50 ns and 100 ns). It confirms the statement of the previous paragraph: the poor power-delay conservation is mostly due to the bad estimation of the echoes 2, 3, 4 and 5 by the *Expectation* phase of SAGE. It leads to the instability of the delays and phases of the multipaths 2, 3, 4 and 5, hence the distortion of the impulse responses represented on Fig. 3.11.

However, the delay of echo 1 shows also many discontinuities among the delay interval [50ns, 100ns]. This is due to the fact that the position of the barycenter of the multipaths varies according to the relative phase of these multipaths (because of the dynamic of the scenario). The delay of this barycenter varies, and thus the delay estimated by SAGE.

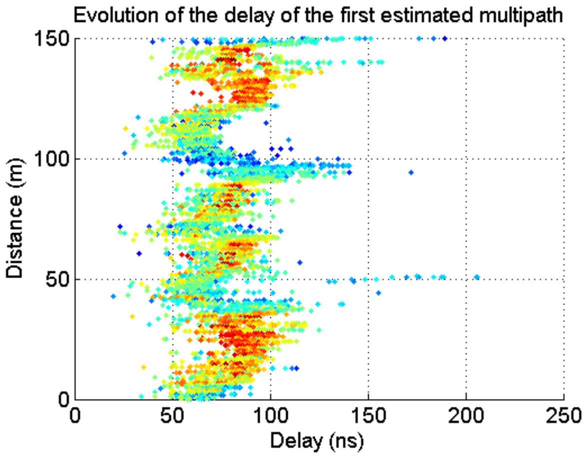

Figure 3.12: Evolution of the delay of the first estimated multipath

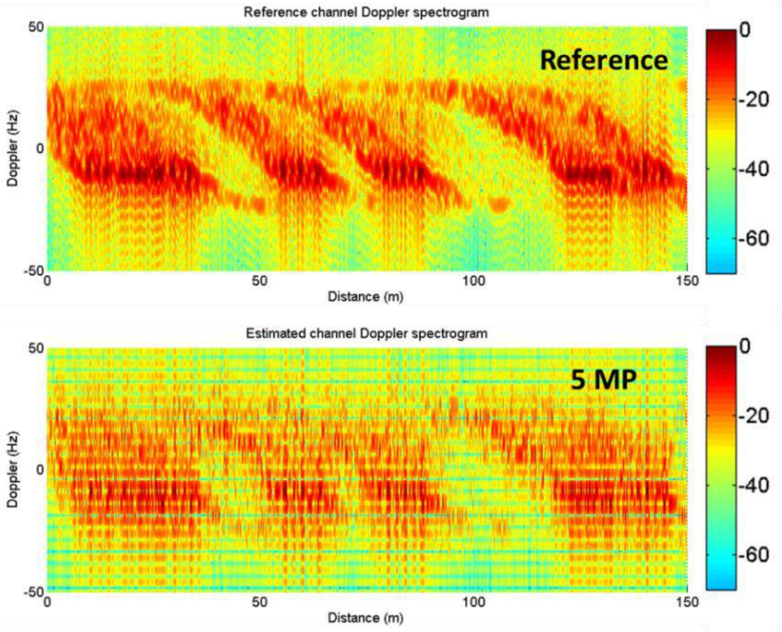

Figure 3.13: Evolution of the reference (on top) and estimated multipath channels (bottom) Doppler spectrograms

Fig. 3.13 represents the comparison between the Doppler spectrograms corresponding to the reference and reduced channels all along the trajectory on the reference scenario. The same conclusions about the discontinuity of the reduced channel can be made as in the case of the power-delay profile.

3.4.2. Influence of the number of echoes on the channel characteristics preservation

The performance of SAGE is strongly impacted by the number of echoes to estimate, as it defines the number of sub-spaces of the optimization problem. This statement was already investigated in section 3.3. However, it has been decided to assess the influence of the number of multipaths on the preservation of the power-delay profile of the reference scenario. Therefore, SAGE has been used to reduce the reference channel of section 2.2.1 with 2, 5 and 10 echoes in the reduced channel. Fig. 3.14 represents the evolution of the power-delay profile in each case.

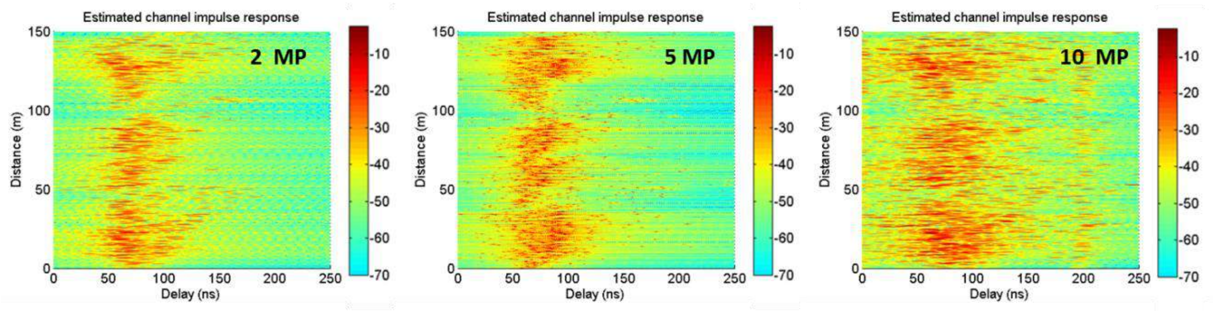

Figure 3.14: Power-delay profile of the estimated channel for 2, 5 and 10 multipaths in the reduced channel

In the case of 2 multipaths only in the reduced channel, the estimated channel delay spread is reduced because of the lack of echoes in the reduced channel. However, the main power contribution is preserved between 50ns and 100 ns delays. It was shown in the previous section that this major power zone is mainly covered by the first echo estimated by SAGE. From the conclusions of section 3.3, it can be deduced that with 20 Hz Doppler resolution, more than 2 multipaths are required.

In the case of 10 multipaths estimated, the delay spread is enlarged with reference to the original channel represented on Fig 3.15. Moreover, an incoherent power peak can be observed at delay 200 ns. It can be deduced that the fact to increase the number of multipaths to estimate tends to decrease the power-delay preservation performance. This is due to the fact that it forces SAGE to divide the optimization problem in more sub-spaces than the actual number of multipaths observable on the scenario. In other terms, the fact to estimate more multipaths than the number of sources identifiable by SAGE (which depends on the Doppler resolution) biases the optimization process. This is one of the conclusions of section 3.3.

In that case, 5 multipaths in the reduced channel appears to be the best compromise to preserve the channel power-delay profile, considering 20 Hz Doppler resolution.

3.5. Complexity of the algorithm

The complexity of the SAGE algorithm is a major limit of this approach. Indeed, it can be deduced from section 3.2 that two major factors have an impact on the computation time of SAGE: the number of correlation samples N and the number of multipaths to estimate L.

- **Dimension of the autocorrelation functions to optimize**

The number of correlation samples N defines the size of the vectors involved in the minimization of the cost function. The bigger those vectors are, the more complex the algorithm is. If P denotes the number of correlators along the delay dimension of the autocorrelation function, the dimension of the vector X_l (using the terminology of Eq. 3.13) is $1 \times NP$. Therefore, the size of this vector is proportional to both the number of correlators P and to the number of correlation samples N. Note that the parameter P has already been set (and minimized) in section 3.2.2.3. Therefore, only the parameter N has an impact on the complexity of SAGE.

- **Number of multipaths to estimate**

The number of multipaths in the reduced channel L sets the number of sub-spaces on which the parametric optimization is processed. It can be expected that the more sub-spaces there are, the larger the computation time of SAGE is.

Therefore, two parameters have an impact on the computation time of SAGE: N and L. It is reminded that N also defines the Doppler resolution of the algorithm. Table 3.1 displays the computation time necessary to perform the reduction of the reference channel on the 150 m of reference scenario using SAGE. This computation time is recorded in terms of N and L, considering the convergence criterion defined in Eq. 3.22. The lines correspond to the Doppler resolution and the columns to the number of multipaths to estimate. It can be observed that the computation time of SAGE can be penalizing, especially if the application requires a high number of multipaths and a good Doppler resolution. As compared to the computation time of the Clustering Weighted presented in the previous chapter, the SAGE computation time is significantly higher.

Table 3.1: Computation time of SAGE to reduce every impulse response samples of the reference scenario

	$L = 2$	$L = 5$	$L = 8$	$L = 10$
50 Hz ⇔ $N = 4$	1h 10min	5h	7h 30min	9h 40min
20 Hz ⇔ $N = 10$	1h 15min	12h	24h	30h
10 Hz ⇔ $N = 20$	1h 33min	17h	38h	48h
5 Hz ⇔ $N = 50$	6h 20min	31h	320h	400h

3.6. Conclusion

In this chapter, the problem of the estimation of the reduced channel according to the minimization of a cost function was addressed. SAGE was used to estimate the delays, Doppler shifts and complex amplitudes of the reduced channel that optimize the conservation of the reference channel autocorrelation function. The Doppler resolution of the algorithm was particularly investigated through the application of SAGE to a canonical scenario. This could explain most of the limitations of SAGE when applied to the reference scenario. Finally, the performance of SAGE have been assessed through the preservation of the reference channel power-delay and Doppler spectrogram, in balance with its computation costs.

In order to consider the channel reduction problem as an optimization problem, it was decided from the literature to build the cost function to minimize according to the difference between the original and reduced channel autocorrelation functions. These autocorrelation functions were sampled both in the delay and in the time domain in order to parameterize the reduced channel along the delay, complex amplitude and Doppler dimensions. This optimization problem is close to the channel estimation problem. From the corresponding literature overview, it has been decided to use the SAGE variant of the Expectation-Maximization algorithm to estimate the parameters of the reduced channel. The hypothesis that SAGE could be used to address this optimization problem was supposed in a first time.

The SAGE approach has been applied to the minimization of the residue of the cost function, which depends on the delays, Doppler shifts and amplitudes of the reduced channel. A few parameters of the algorithm itself were discussed: the number of correlators along the delay line P, the number of correlation samples in time N and the duration between two consecutive correlation samples T_e. The parameters P and T_e were optimized so as to decrease the computation time as much as possible without affecting the performance (according to the literature recommendations). The parameter N was more thoroughly investigated as it defines the Doppler resolution of the algorithm.

A canonical scenario constituted of two distinct multipath sources (two buildings) has been investigated in order to underline the impact of the Doppler resolution on the performance of SAGE. It was observed on both the power-delay profile and the Doppler spectrogram that SAGE was unable to estimate the two multipaths separately on the segments on which they were closer than 20 Hz in terms of Doppler (which corresponds to the Doppler resolution of the algorithm in that case). Therefore, it was concluded that the Doppler resolution has an impact on both Doppler and delay estimations. It could be explained by the fact that the low Doppler resolution impairs the *Expectation* phase of the algorithm, which leads to abnormal algorithm sub-spaces and therefore wrong delay estimations. On the other hand, it was showed that a too high Doppler resolution tended to focus the parameters on one multipath source, which has the effect to cut off the contributions of the second source. Therefore, a compromise has to be established by the user of SAGE between the number of echoes to estimate, the Doppler resolution and the actual number of sources in the environment.

Finally, SAGE has been applied to the reference scenario of this study with 20 Hz Doppler resolution to reduce the multipath channel. The preservation of the power-delay and Doppler spectrogram profiles has been investigated with 5 echoes in the reduced channel. It could be observed a poor preservation of the delay characteristics of the original channel, with many discontinuities along the trajectory. This could be explained by the abundant multipath sources, being given the fact that the mobile is going along a continuous row of buildings. These multipaths are closer in terms of Doppler than the Doppler resolution which impairs the *Expectation* phase of the algorithm. This Doppler resolution would have to be increased in order to achieve a better delay preservation. However, it was previously shown that the number of echoes to estimate has to fit the actual number of multipath sources separately identifiable by SAGE in the environment.

In order to satisfy the specifications of the study which require decreasing the number of multipaths to less than 10, it has been decided to go further in the study of the performance of SAGE with 20 Hz Doppler resolution. Although SAGE showed bad performance in terms of channel delay preservation, it showed to be able to preserve the channel autocorrelation function with success, on Fig. 3.9. Therefore, it can be expected a suitable preservation of the pseudo-range error, which will be investigated in the last chapter of this thesis. Such performance has to be modulated with consideration of the computation costs of SAGE, as compared to the performance of the other approaches.

Chapter 4

4. Reduction of the multipath channel using a Markov process

The method presented in this chapter is another approach to address the channel reduction problem. Indeed, the methods presented in chapter 2 consisted in reducing the multipath channel by aggregating multipaths, aiming at conserving the channel delay and Doppler characteristics. Chapter 3 presented an optimization method to parameterize the multipaths of the reduced channel to preserve the channel autocorrelation function. These two types of reduction methods are both applied directly to the samples of impulse response independently. The third approach, which will be presented in this chapter, computes the variations of the reduced channel parameters as the realization of a stochastic process. Then, this approach consists in reducing the multipath channel focusing on the preservation of the statistical distribution of the parameters and their continuity over time.

Some channel models already proposed the modeling of the multipaths using a stochastic process, as it was presented in the first chapter of this study. The reduction method proposed in [Schu 14] consists in applying those stochastic models to the impulse responses already simulated, so as to decrease the number of multipaths. More specifically, the multipaths of the reduced channel are independent realizations of the stochastic process that will be presented in section 4.2. Section 4.3 will highlight some drawbacks of this approach, when applied to the reference scenario of this study. Therefore, section 4.4 will propose some modifications to improve the performance of the approach with respect to the conservation of the channel impulse response power-delay and Doppler spectrogram.

4.1. Introduction of the problem and literature overview

It was already mentioned in the first chapter of this study that some channel simulators rely on statistical approaches or hybrid statistical-deterministic approaches to model the narrow band/wide band channel. Most of those models are built from data collected during wide band or narrow band measurement campaigns. As mentioned in Chapter 1, the advantage of such approaches is the possibility to adapt it to any scenario, provided to have the same type of environments (urban, sub-urban, forest …). The reduction process introduced in [Schu 14] is an adaptation of those channel simulation issues to the channel reduction problem. The original idea of [Schu 14] is to draw the multipaths of the reduced channel from the pdfs (*probability density functions*) of the samples of original impulse responses.

The reduction method presented in [Schu 14] proposes to draw the reduced channel multipaths from a first order Markov chain, considering the distribution of the multipath delays, amplitudes and phases at the present instant and at the predecessor instant. An overview of the different statistical channel models was already shown in Chapter 1. The state-oriented models have been used in several studies to estimate the different parameters of the channel, and their evolution over time. The most worth mentioning examples are [Pere 01], [Abel 09], [Milo 09] and [Lutz 96]. They all rely on Markov processes to model the evolution of the narrow band channel power. The advantage of the Markov chains is to be fully characterized by the present statistical distribution at the present time (*state vector* P) and by the probability to move from one state to another (transition probability matrix Q). Therefore, the continuity of the different parameters is ensured by the fact that they are drawn considering the history of the transitions from past to present.

For the ease of use of the Markov chains, it has been decided to follow the approach presented in [Schu 14], which will be described in the following section. It has to be mentioned that the statistical approaches presented in [Abel 09], [Milo 09] and [Lutz 96] consider only the evolution of the narrow band channel power (according to Markov chains). In what concerns the wide band models, presented in [Pere 01], only the LOS component follows a stochastic process (the delays and amplitudes are drawn from exponential distributions randomly generated as in [Jahn 01]). The reduction method presented in [Schu 14] extends the Markov chain approach to the estimation of every parameter of the wide-band reduced channel (delay and complex amplitude).

4.2. Description of the CRIME algorithm and adaptation to the channel reduction problem

This section will describe the stochastic process considered in [Schu 14], referred to as CRIME (*Channel Reduction by Independent Markov Estimation*). As mentioned in the previous section, it aims at computing the parameters of the L reduced multipaths, as the realization of independent stochastic processes. More precisely, these parameters follow a first order Markov process, as they depend only on the present instant t_i and the immediate predecessor instant t_{i-1}.

Sub-section 4.2.1 details the formatting of the impulse response samples necessary to build the pdfs of the different parameters (with a suitable quantity of data). Sub-section 4.2.2 gives an overview of architecture of CRIME, with the inter-dependency of the different parameters to estimate and the computation the pdfs. To finish, section 4.2.3 explains how the parameters are drawn from the different distributions.

4.2.1. Data formatting

In this thesis, the statistical distributions from which the multipaths are drawn are built from the reference channel impulse response $h(t)$, which contains $M(t)$ multipaths. Those impulse responses are computed by the SCHUN simulator, as described in chapter 1.

It is important to mention that the original impulse responses on which CRIME is applied in [Schu 14] are computed by the channel model described in [ITU 13], which is different from SCHUN. This model usually generates less than 100 multipaths. In that, the number of echoes in the original impulse responses may not be sufficient to estimate suitable pdfs. Indeed, the more data are available to estimate the distributions of the different parameters, the more accurate the pdfs are. Therefore, [Schu 14] proposes a method to increase the number of data per impulse response sample:

Let us consider a multipath parameter Υ at the time t_i. The idea of [Schu 14] is to use the data of the other impulse responses in the immediate vicinity of t_i. To do so, a sliding window is applied to the impulse response samples at times $T = (t_1, \dots, t_{i-1}, t_i, t_{i+1}, \dots, t_{max})$, weighted as a function of the time distance of the sample to t_i. It has to be mentioned that T is sampled at the sampling period Δt=5 ms, according to the channel coherency time whose computation will be detailed in chapter 5. The weighting coefficient ζassociated to the sample t_j at the time t_i is given by Eq. 4.1.

$$\zeta_{i,j} = \frac{1}{\sigma} \exp\left(-\frac{1}{2} \left(\frac{t_i - t_j}{\sigma} \right)^2 \right) \tag{4.1}$$

The coefficient σ can be tuned in order to ensure enough data samples per impulse response snapshot. In this thesis, it was already mentioned that the impulse responses generated by SCHUN contain usually several thousands of multipaths. It has been considered that it is enough to estimate the pdfs properly. Therefore, no data correction has been applied and the pdfs at time t_i is built directly from the impulse response snapshot at the time t_i only.

The LOS contribution of the impulse response is not considered by CRIME. The direct path remains untouched from the original to the reduced channel. Moreover, the reduced channel multipaths are estimated according to a first-order Markov channel. Therefore, it is necessary to be able to follow the multipaths from one instant to the other on the original channel, in order to build the multi-dimensional pdfs described in the following section. In other terms, the channel model has to provide the signature of the multipaths of the reference channel at each instant. If the channel simulator does not provide these data, an algorithm has been proposed in Annex A to recognize the signature of a given multipath l at the time t_i, with respect to its delay and Doppler at the time t_{i-1}.

4.2.2. Implementation of the CRIME algorithm

4.2.2.1. Architecture of CRIME

The global architecture of CRIME has been schematized on Fig. 4.1. This paragraph details the important steps of the algorithm. Note that each multipath of the reduced channel is computed independently.

- **Initialization :**

The multipaths vary according to a first order Markov process, meaning that their parameters depend on the predecessor instant and of the present instant. Therefore, the initial parameters strongly condition the following parameters, and thus the performance of the algorithm. In order to optimize power-delay and Doppler spectrogram preservation, it has been decided to initialize delay $\tau_l(t_0)$, amplitude module $\gamma_l(t_0)$ and phase $\varphi_l(t_0)$ of the echoes using the Clustering Weighted technique documented in section 2.5.

- **Delay variation :**

At a given instant, the delay of the multipath l (of the reduced channel) is drawn from the reference channel delays at the present time t_i, knowing the delay of l at the predecessor instant t_{i-1}. More specifically, it is drawn from the delay *pdf* at the time t_i of the multipaths which had the same delay as l at t_{i-1}. More details about these 2-dimensional *pdfs* are given in section 4.2.2.2 in the paragraph "*Delays*".

- **Amplitude variation :**

At a given instant, the amplitude module of the multipath l is drawn from the reference channel amplitudes at the present time t_i, knowing the amplitude module of l at the predecessor instant t_{i-1} and the delay of l at t_i. As a consequence, the amplitude of l is drawn from the amplitude *pdf* at t_i of the multipaths which have the same delay as l at t_i and had the same amplitude at t_{i-1}. Therefore, it is important to note that the delay has to be estimated prior to the amplitude. More details about these 3-dimensional *pdfs* are given in section 4.2.2.2 in the paragraph "*Amplitude modules*".

- **Phase variation :**

The phase shift between the two instants t_{i-1} and t_i is computed according to the delay shift, as it is detailed in section 4.2.2.2 paragraph "*Phases*".

- **Post-processing :**

In order to conserve the total energy of the impulse response, the amplitude module of the reduced channel multipaths needs to be adjusted. Indeed, the energy of the multipaths drawn from the amplitude pdfs has the order of magnitude of the energy of a single multipath of the reference channel. Therefore, the total energy of the reduced channel is expected to be significantly lower than the energy of the reference channel. The amplitude correction is displayed by Eq. 4.2. It has been chosen to preserve the narrow-band energy of the channel. L and M denote respectively the number of multipaths in the reduced and reference channels ($L \ll M$). $\tilde{\gamma}_l^{est}$and $\tilde{\gamma}_l^{cor}$ denote respectively the complex amplitude of multipath l estimated by CRIME and the corrected one.

$$\tilde{\gamma}_l^{cor}(t_i) = \tilde{\gamma}_l^{est} \frac{\sum_{k=1}^{M} \widetilde{\gamma_k}}{\sum_{l=1}^{L} \tilde{\gamma}_l} \tag{4.2}$$

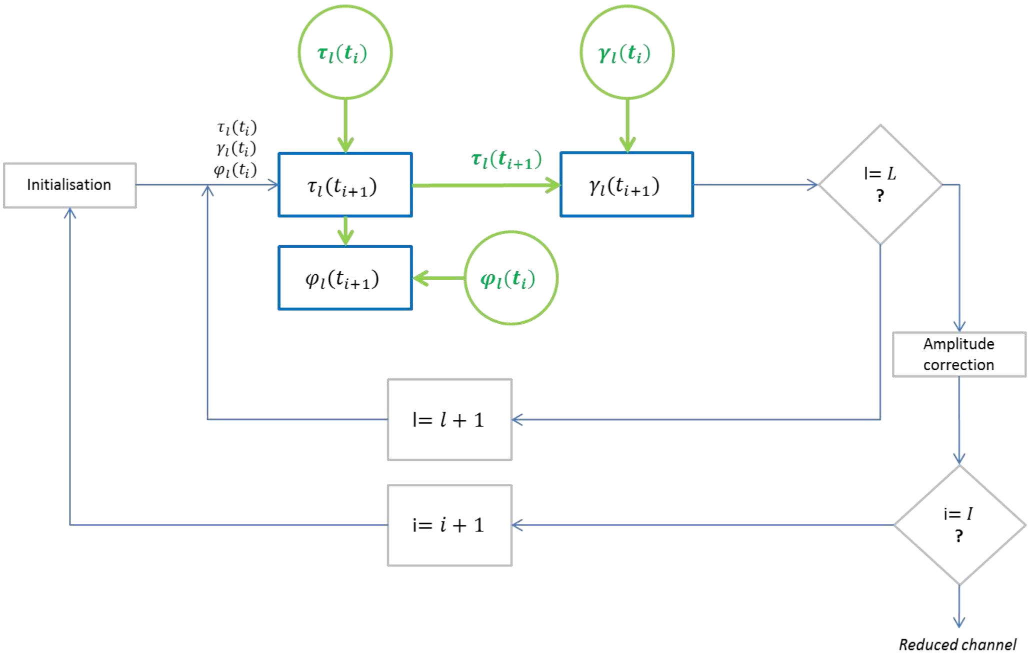

Figure 4.1 : Principle of CRIME scheme

4.2.2.2. Estimation of the parameters of the reduced channel

- **Delays :**

The delays of the reduced channel are supposed to vary according to a first order Markov process. More specifically, the delay $\tau_l(t_i)$ of multipath l at the time t_i is estimated according to the distribution of $\tau(t_i)$ in the original channel, knowing the distribution at the previous instant $\tau(t_{i-1})$. In other terms, $\tau_l(t_i)$ is drawn from the *pdf* associated to $P(\tau(t_i)|\tau(t_{i-1}))$. In order to build a discrete state-discrete time Markov chain, the delay line has been divided in delay bins. The multipaths impinging the receiver within a given delay bin $T_k, k \in [\![1, K^{del}]\!]$, are considered to belong to the state associated to T_k. Those bins T_k are the regular delay intervals: $[k\Delta\tau, (k+1)\Delta\tau]$. The size of the delay bins has been set to Δτ= 2 ns. The Markov chain of the delays of the reduced channel is represented on Fig. 4.2, where q_{mn} denotes the probability $P(\tau(t_i) \in T_n \mid \tau(t_{i-1}) \in T_m)$. At a given instant, this Markov chain is fully characterized by the state probability and transition matrices.

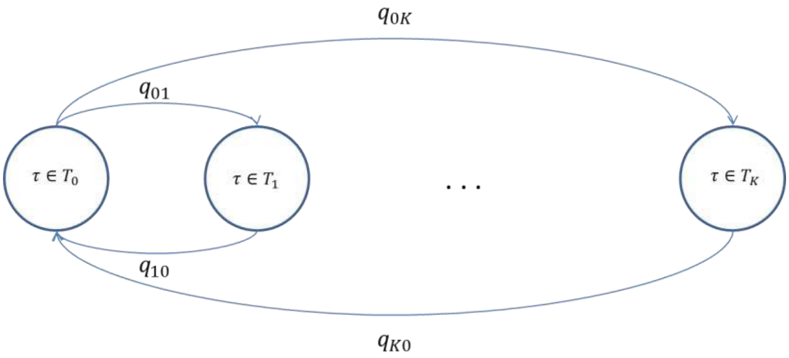

Figure 4.2: Markov chain of the reduced channel delays with K delay states/bins

The state probability of the Markov chain at a given instant is defined by the *pdfs* of the delays in the impulse response sample considered. For example, Fig. 4.3 displays the *pdf* of the channel impulse response at the times t=0 s, t=10 s, t=20 s and t=30 s of the trajectory (of the reference scenario presented in section 2.2.1). Note that in [Schu 14], it is suggested to use the ASH (*Average Shifted Histogram*) technique, described in [Scot 92], with 3 sub-bin divisions (order 3). It has the major advantage to produce more and narrower bins. In that thesis, it has been decided that the original impulse responses contain enough data to build *pdfs* with narrow bins and accurate density estimations. Therefore, the ASHs have not been investigated.

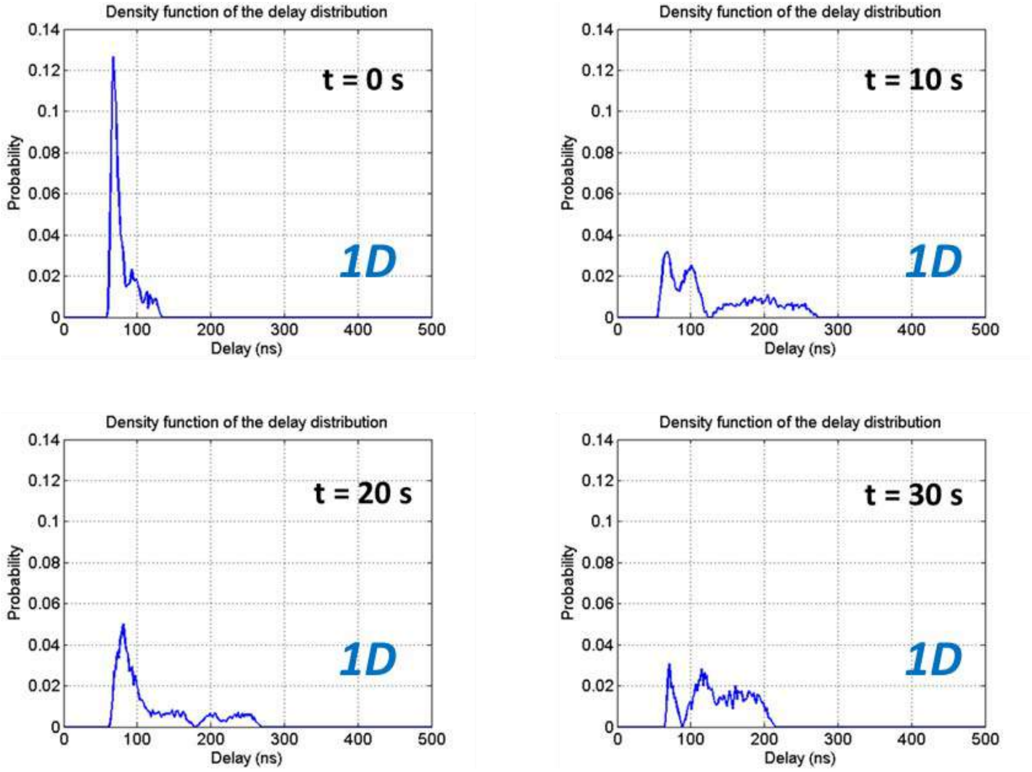

Figure 4.3: Delay *pdf* at the times t=0 s, t=10 s, t=20 s, t=30 s on the reference scenario

The quote "1D" is referred to the 1-dimensional *pdf*. The shape of these different *pdfs* depend on the position of the receiver on the trajectory. At the time t=0 s, no building is located behind the receiver. The multipaths reaching the receiver at t=0 s are all originated from buildings located on the [0 m,50 m] segment of the trajectory (50 m is the multipath influence distance set in section 2.2.1), which explains the high probability to have delays in the low delay zone of the *pdf*. At t=10 s and t=20 s, the multipaths reaching the receiver are originated from buildings located 50 m in front and 50 m behind the receiver. Therefore, the *pdf* shows a significant probability to have low delays and also a significant probability to have larger delays. At t=30 s, only multipaths originated by buildings behind the receiver are considered. As a consequence, the probability to have strong delays is increased as compared to the other instants (they take longer paths from the receiver to the emitter).

Fig. 4.4 illustrates the variations of 3 multipaths of the original channel over 2 s (multipath A, B and C). Multipath A corresponds to a negative Doppler multipath (ϑ=-25Hz). Therefore, its delay is increasing all along the [50 m,60 m] segment of the trajectory. Multipath C has a positive Doppler, thus its delay decreases along the trajectory. Contrary to multipath A and C whose Doppler is almost constant along the trajectory (i.e. the slope of the delay is constant), the Doppler of multipath B varies, because of the proximity of the receiver to the facet emitting the echo. It has to be mentioned that those multipaths delays are represented relatively to the LOS delay for each impulse response snapshot. Therefore, the dynamic of the scenario due to the LOS Doppler is not represented. In other words, those delay variations are represented with respect to the LOS Doppler ($\vartheta_{LOS} \approx$ 10 Hz) and not to their absolute Doppler shift. It explains the fact that the absolute value of the delay slope is not the same for multipath A and multipath B, even if they have the same Doppler shift (in absolute value).

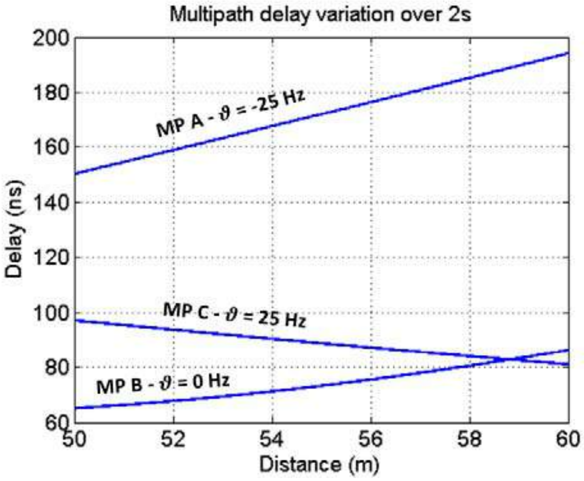

Figure 4.4: Evolution of the delay of 3 multipaths of the original channel on the [50 m, 60 m] segment

The transition probability of the Markov chain is the probability at a given time for a delay to move from one state to another. It depends on the time t_i, on the state of origin $T(t_i)$ and on the state of arrival $T(t_{i+1})$. Let us consider the impulse response sample corresponding to the instant t_i=20 s. Fig. 4.5 illustrates the Doppler-delay profile of this impulse response sample. Two delay bins have been framed on this plot, corresponding to the states $\tau \in$ [68 ns,70 ns] noted $\boldsymbol{T_a}$ and $\tau \in$ [230 ns,232 ns] noted $\boldsymbol{T_b}$. Fig. 4.6 illustrates the delay *pdfs* at the time $t_i + \Delta t$ of the multipaths which belonged to $\boldsymbol{T_a}$ and $\boldsymbol{T_b}$ at the time t_i (Δt denotes the channel sampling period). In other terms, Fig. 4.6 illustrates the conditional probability distribution of the multipath delays at the time $t_i + \Delta t$, knowing their delay at the time t_i. The left plot represents $P(\tau(t_{i+1}) \mid \tau(t_i) \in \boldsymbol{T_a})$ and the right plot $P(\tau(t_{i+1}) \mid \tau(t_i) \in \boldsymbol{T_b})$.

It can be observed on Fig. 4.5 that the maximum Doppler of the channel impulse response is approximately 25 Hz. On the reference scenario, the sampling time is set to 5 ms, which leads to a delay shift of approximately 0.080 ns according to eq. 3.5. This delay increase is negligible as compared to the size of the delay bins. Therefore, only a few multipaths move from one state to another during the 5 ms period. Therefore, in order to illustrate the computation of the transition probabilities, this sampling period has been increased to Δt = 500 ms. Note that this modification is only motivated by the visual ease of illustration for the purpose of this section. The stochastic process described in this chapter will be applied to the reference channel with the original sampling period of 5 ms in the following sections.

The probability distributions of Fig. 4.6 illustrate the probability of transition of the multipaths belonging to the delay states $\boldsymbol{T_a}$ and $\boldsymbol{T_b}$ at the time t=20 s. It can be observed on the left plot of Fig. 4.6 that the multipaths belonging to the delay state $\boldsymbol{T_a}$ at the time t=20 s are all contained in the delay interval [65 ns,80 ns] at the time t=20.5 s. Two major probability peaks can be observed, corresponding to delay zones located after and before the center delay of $\boldsymbol{T_a}$. This is due to the fact that the state $\boldsymbol{T_a}$ contains multipaths with both positive and negative Doppler shifts. It can be deduced from eq. 3.5 that the probability peak located at delay 75 ns corresponds to the negative Doppler multipaths (whose delay increases between t and t+Δt) and the 65 ns peak to the positive Doppler multipaths (whose delay decreases between t and t+Δt). Note that these Doppler shifts are not considered absolute but relative to the LOS Doppler shift.

To the contrary, the state $\boldsymbol{T_b}$ is only composed of negative Doppler multipaths within a short Doppler spread. Therefore, the delays contained in the bin $\boldsymbol{T_b}$ at t=20 s follow have similar delay variations and have similar delays at the time t=20.5 s, hence the single probability peak on the right plot of Fig. 4.6.

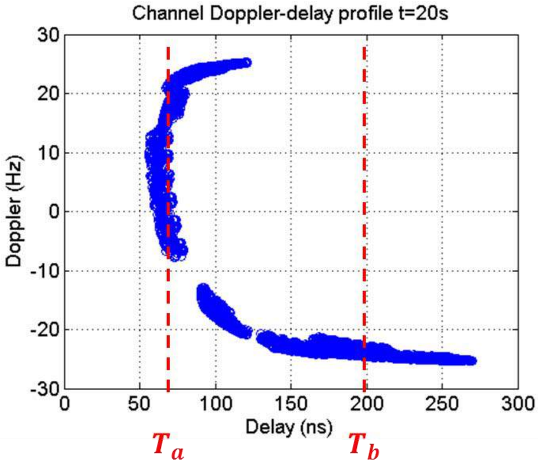

Figure 4.5: Doppler delay profile of the impulse response at the time t=20 s

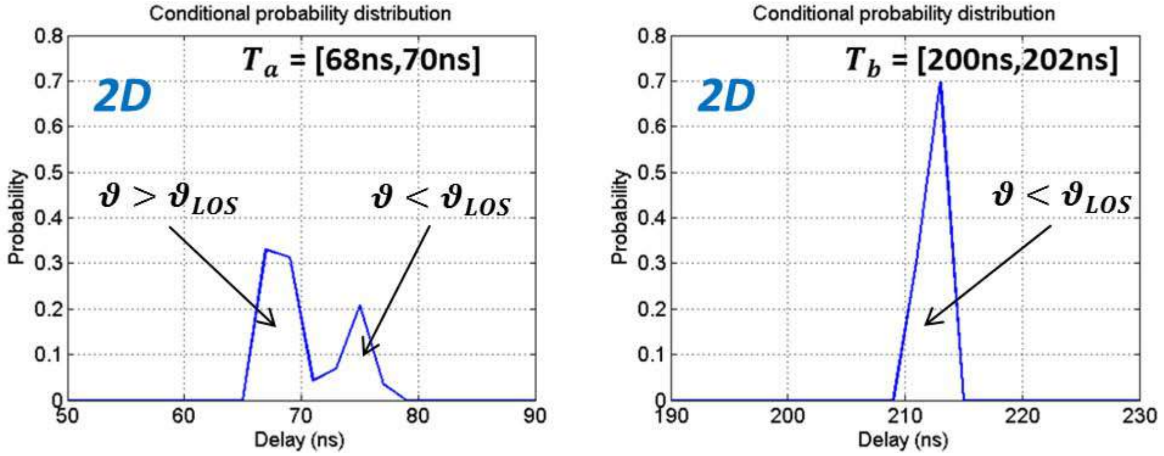

Figure 4.6: Density function of $\boldsymbol{P(\tau(t_i)|\tau(t_{i-1}) \in T_a)}$ on the left and $\boldsymbol{P(\tau(t_i)|\tau(t_{i-1}) \in T_b)}$ on the right

Let us consider that the multipath l belonged to the delay bin T_k at the time t_{i-1}, that is to say $\tau_l(t_{i-1}) \in T_k$. In order to apply the Markov process, CRIME estimates the delay of the reduced channel multipath l at the time t_i according to the following steps:

- First, the multipaths located in the same delay bin as l at the time t_{i-1} are identified: $E_k(t_{i-1}) = \{l\ , \tau_l(t_{i-1}) \in T_k\}$.

- Let us note $\tau_k$the delays of the multipaths belonging to E_k. CRIME estimates the *pdf* of the delays τ_k at the time t_i. It corresponds to the *pdf* of the conditional probability $P(\tau(t_i)|\tau(t_{i-1}) \in T_k)$, that is to say the transition probability from state k to the other states.

- Finally the delay of l at the present time t_i, noted $\tau_l(t_i)$, is drawn from this *pdf*. Examples of taps corresponding to these 2-dimensional *pdfs* are illustrated on Fig. 4.6. A full 2-dimensional *pdf* (with all the delay taps) has been represented in Annex A, on Fig. A.1.

- **Amplitude module :**

The module of the amplitudes of the reduced channel are supposed to vary according to a first order Markov process, considering the prior knowledge of the multipaths delays. In other terms, the variation of the power of a given multipath is provided by a Markov chain, considering only the multipaths located in the same delay state (at the present time). As a consequence, the estimation of the delay is required prior to the estimation of the amplitude. This specificity aims at conserving the power-delay consistency of the original channel.

In order to build the Markov chain of the multipath amplitudes, the amplitude dimension has been divided in amplitude bins. It is important to mention that the amplitude dimension is considered in logarithmic scale, relatively to the LOS amplitude in open sky. The width of the amplitude bins has been set to $\Delta|\gamma|$=1dB. Fig. 4.7 represents the Markov chain defining the variation of the amplitude module of the reduced channel multipaths. Contrary to the delay, the probability of transition from one state to another depends also on the delay of the multipath considered. This specificity has been represented on Fig. 4.7. The amplitude states are noted A_k, $k \in [\![1, K^{amp}]\!]$, considering K^{amp} amplitude bins. This illustration describes the transition probability between the times t_{i-1} and t_i. It can be observed that the probability of transition from state a to state b, noted q_{ab} , is weighted by the probability to be in the amplitude state b knowing the delay $\tau(t_i)$ (conditional probability).

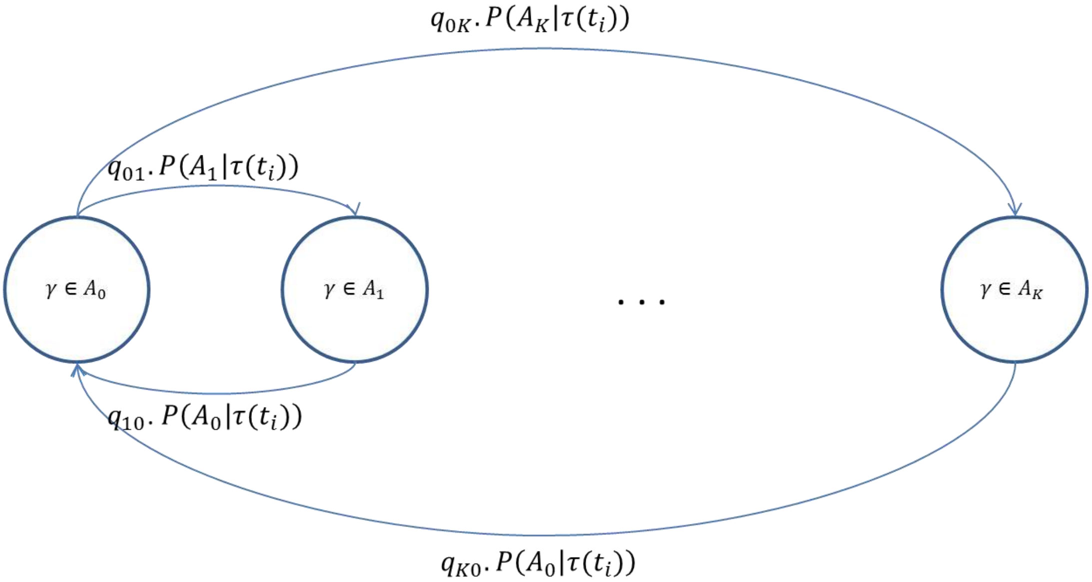

Figure 4.7: Markov chain of the reduced channel amplitudes with the delay dependency with K amplitude states

CRIME computes the amplitude of the multipath l at the time t_i noted $\gamma_l(t_i)$ according to the following steps. It is assumed that l belongs to the delay bin T_j at the time t_i and to the amplitude bin A_k at the time t_{i-1} :

- First, the multipaths located in the same amplitude bin A_k at the previous instant t_{i-1} are recorded as $E_k(t_{i-1}) = \{l\,, \gamma_l(t_{i-1}) \in A_k\}$.

- Then, CRIME identifies the multipaths of $E_k(t_{i-1})$ located in the same delay bin as l at the time t_i: $F_j(t_i) = \{l \in E_k(t_{i-1})\,, \tau_l(t_i) \in T_j\}$.

- Let us note γ_j the set of amplitudes of the multipaths belonging to $F_j(t_i)$. Note that those multipaths belong to $F_j(t_i)$ at the time t_i and to $E_k(t_{i-1})$ at the time t_{i-1}. CRIME computes the *pdf* of the set γ_j at the time t_i. It corresponds to the *pdf* of the conditional probability $P\big(\gamma(t_i) \big| \tau(t_i) \in T_j \ \cap \ \gamma(t_{i-1}) \in A_k\big)$, that is to say the transition probability from the amplitude state k to the other states joint to the probability to have an amplitude in state A_k, knowing that the delay is in T_j at the instant t_i. Finally, the amplitude of l at the time t_i noted $\gamma_l(t_i)$ is drawn from this *pdf*.

Fig. 4.8 illustrates the *pdf* of the power distribution of the reference channel impulse response at different points of the trajectory, corresponding to the instants t=0 s, t=10 s, t=20 s and t=30 s. Contrary to the delay *pdf*, no significant difference can be observed on those plots. It shows that the amplitude *pdf* do not significantly vary from one point of the trajectory to another.

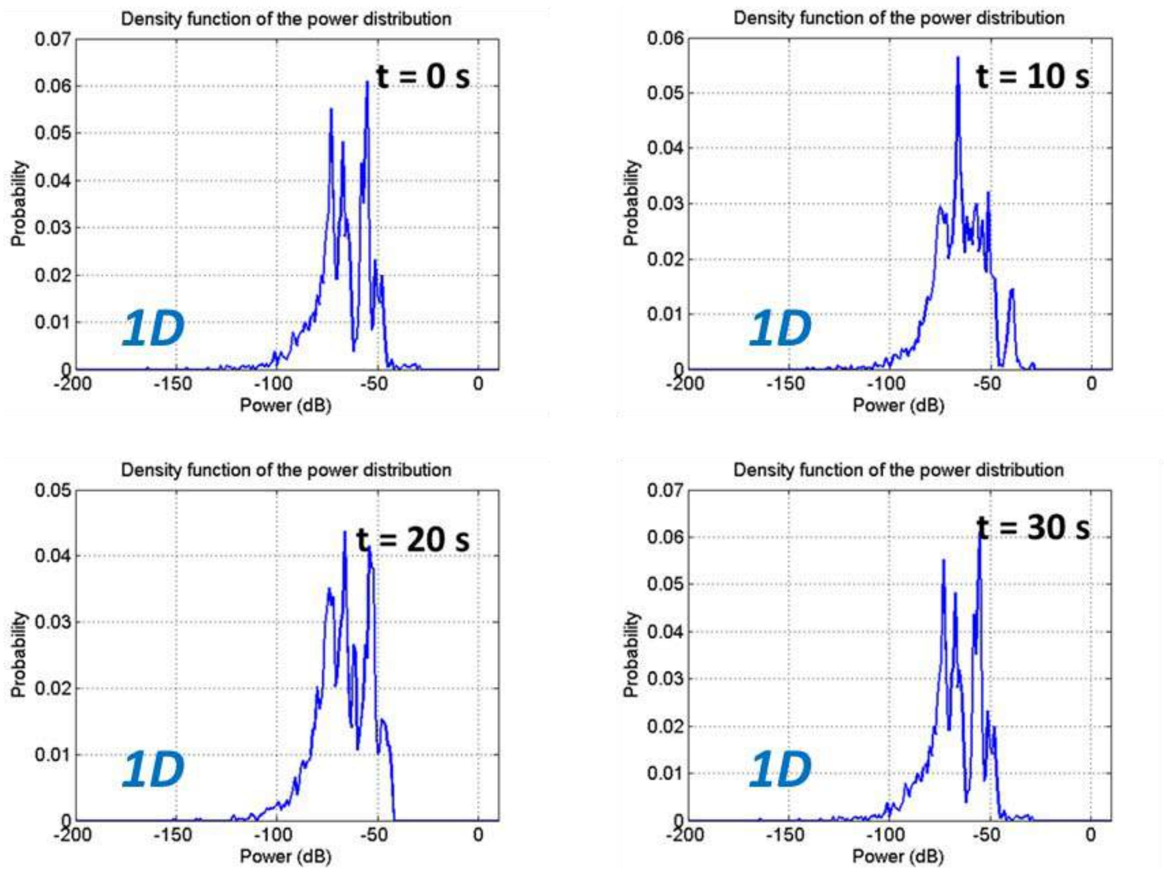

Figure 4.8: Power *pdf* at the times t=0 s, t=10 s, t=20 s, t=30 s on the reference scenario

Fig. 4.9, 4.10 and 4.11 illustrate the different distributions involved in the conditional Markov process illustrated on Fig. 4.7. The example corresponding to two multipaths will be displayed hereafter, referred to as multipath a and multipath b. First, the power-delay profile corresponding to t_i=20 s has been represented on Fig. 4.9. Two amplitude frames have been selected, representing the amplitude states $\gamma \in$[-61dB,-60dB] noted $\boldsymbol{A_a}$ and $\gamma \in$[-101dB,-100dB] noted $\boldsymbol{A_b}$. At the time t_i, multipath a is supposed to be in the amplitude state $\boldsymbol{A_a}$ and multipath $\boldsymbol{b}$ in the state $\boldsymbol{A_b}$.

Fig. 4.10 represents the 2-dimensional amplitude *pdfs* at the time t_{i+1}, corresponding to the multipaths which belonged to $\boldsymbol{A_a}$ and $\boldsymbol{A_b}$ at the time t_i. It corresponds to $P(\gamma(t_{i+1}) \mid \gamma(t_i) \in \boldsymbol{A_a})$ on the left plot and $P(\gamma(t_{i+1}) \mid \gamma(t_i) \in \boldsymbol{A_b})$ on the right plot. As shown on Fig. 4.6, the transition probability from one state to another depends on the state of origin $A(t_i)$, on the state of arrival $A(t_{i+1})$ and on the delay state of the multipath $T(t_{i+1})$. Therefore, Fig. 4.11 illustrates the amplitude *pdfs* at the time t_{i+1} of the multipaths which belong to the delay states $\boldsymbol{T_a}$ and $\boldsymbol{T_b}$ at the time t_{i+1}, that is to say $P(\gamma(t_{i+1}) \mid \tau(t_{i+1}) \in \boldsymbol{T_a})$ on the left plot and $P(\gamma(t_{i+1}) \mid \tau(t_{i+1}) \in \boldsymbol{T_b})$. It can be noted that this example considered Δt=0.5 s to increase the probability of change of state in the amplitude domain (in the same way as in the previous paragraph concerning the delay).

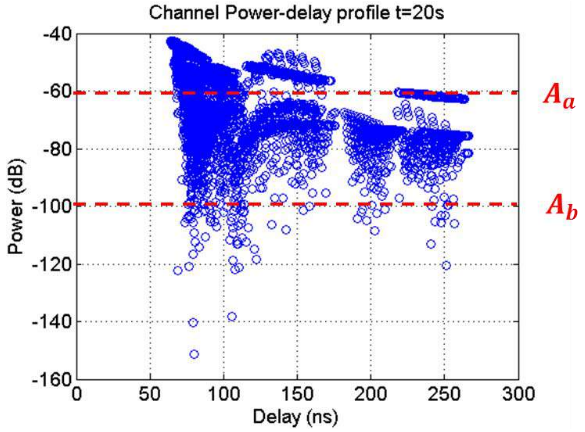

Figure 4.9: Power delay profile of the impulse response at the time t=20 s

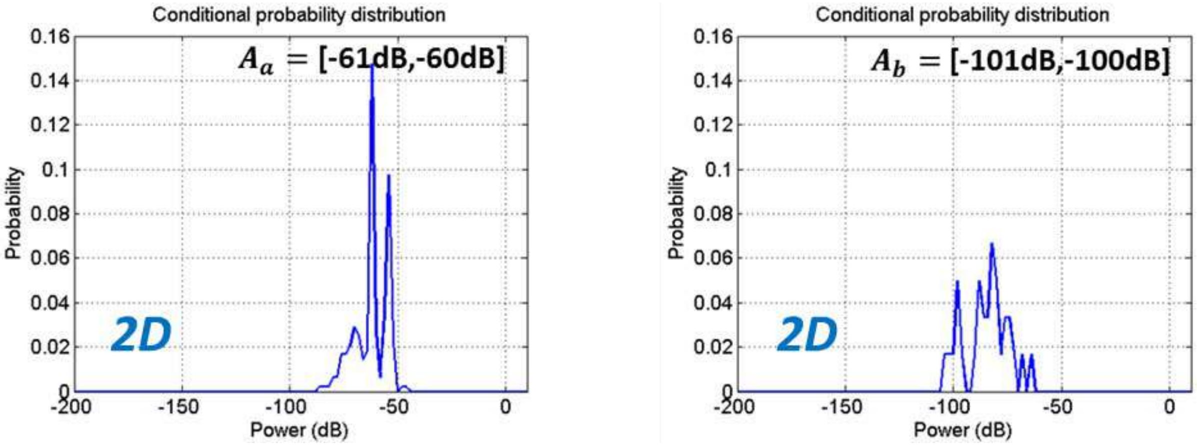

Figure 4.10: Density function of $\boldsymbol{P(\gamma(t_{i+1}) \mid \gamma(t_i)} \in \boldsymbol{A_a})$ (left) and $\boldsymbol{P(\gamma(t_{i+1}) \mid \gamma(t_i)} \in \boldsymbol{A_b})$ (right)

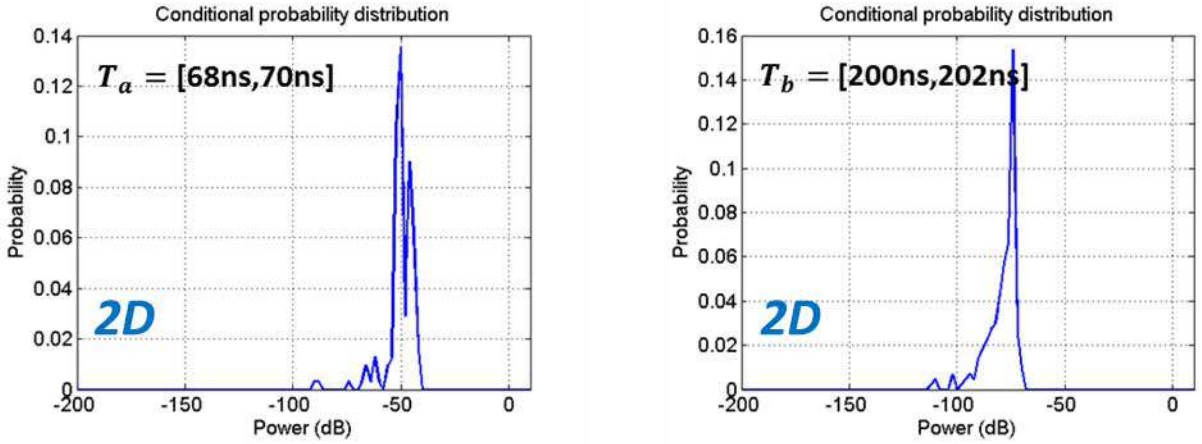

Figure 4.11: Density function of $\boldsymbol{P(\gamma(t_{i+1})\mid\tau(t_i)\in T_a)}$ (left) and $\boldsymbol{P(\gamma(t_{i+1})\mid\tau(t_i)\in T_b)}$ (right)

Finally, CRIME draws the amplitude of the multipath a from the 3-dimensional *pdf* corresponding to the probability$P(\gamma(t_{i+1})|\tau(t_{i+1})\in T_a\ \cap\ \gamma(t_i)\in A_a)$. Fig. 4.12 represents this joint *pdf* for the multipaths a and b considered in this section. It is built as the intersection between the *pdfs* of Fig. 4.9 and 4.10.

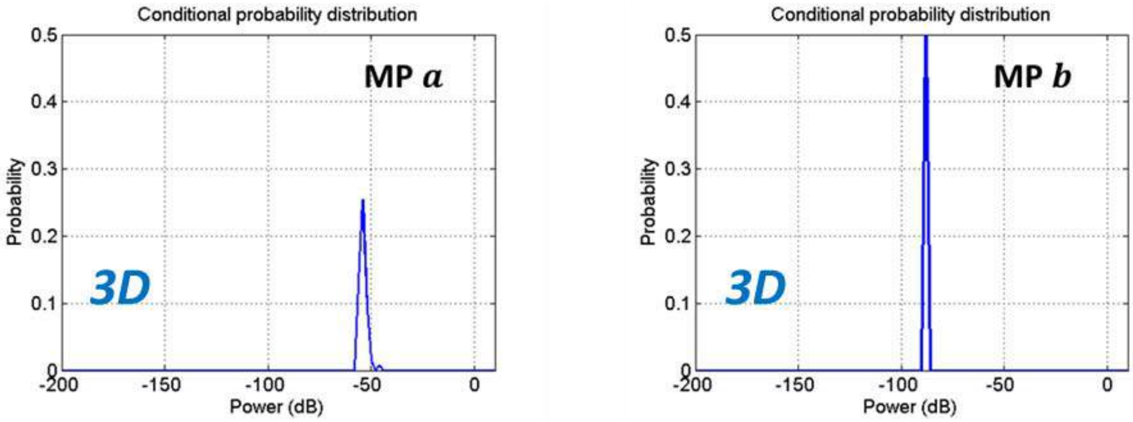

Figure 4.12: Density function associated to $\boldsymbol{P(\gamma(t_{i+1})|\tau(t_{i+1})\in T_a\ \cap\ \gamma(t_i)\in A_a)}$ (left) and $\boldsymbol{P(\gamma(t_{i+1})|\tau(t_{i+1})\in T_b\ \cap\ \gamma(t_i)\in A_b)}$ (right)

- **Phases :**

It is proposed in [Schu 14] to compute the relative phase shifts of the reduced channel according to the delays. To do so, it has been decided to compute the phase $\varphi_l(t_{i+1})$ of multipath l as the propagation of the phase $\varphi_l(t_i)$ along the time Δt using the delay $\tau_l(t_{i+1})$. Eq. 4.3 displays the literal expression of $\varphi_l(t_{i+1})$ where f_0 denotes the carrier central frequency. This method aims at preserving the physical consistency between the delay and phase shifts of the reduced channel multipaths.

$$\varphi_l(t_{i+1})=\varphi_l(t_i)+2\pi f_0(\tau_l(t_{i+1})-\tau_l(t_i)) \tag{4.3}$$

4.2.2.3. Drawing of the multipath parameters from the *pdfs*

The method used to draw the delays and amplitudes from the *pdfs* of Fig. 4.6 and 4.12 has not been described yet. It is proposed in [Schu 14] to use the RNG (*Random Number Generator)*, described in [Scot 92].

Let $F(x)$ denote the *cdf* (*Cumulative Density Function*) of the distribution of a random variable X. Let $f(x)$ denote the corresponding density function. Let us consider $(x_1, \dots, x_n)$, n realizations of X. The RNG technique draws realizations of X, according to the probability distribution defined by F. It processes as follow:

- A value $u \in [0,1]$ is drawn from the random variable uniformly distributed on interval [0,1].
- Let i be the index so that $x_i = \min_{k \in [\![1,n]\!]} |u - x_k|$.
- The sample x drawn from the *cdf* of X is given by Eq. 4.3:

$$x = x_i + \frac{u - F(x_i)}{f(x_i)} \tag{4.4}$$

Fig. 4.13 represents the *cdf* of the distributions corresponding to the delay probability at t=20,5 s of multipaths a (left plot) and b (right plot), knowing that they belonged respectively to T_a and T_b at the instant t=20 s. Note that this illustration takes back the same example as subsection 4.2.2.1. These cumulative distributions correspond to the primitive functions of the *pdfs* represented on Fig. 4.6. The *RNG* method has been applied to these two *cdfs* to draw five random delay samples from the probability distributions considered on Fig. 4.13. The different values of u and the corresponding delays are recorded in Tab. 4.1.

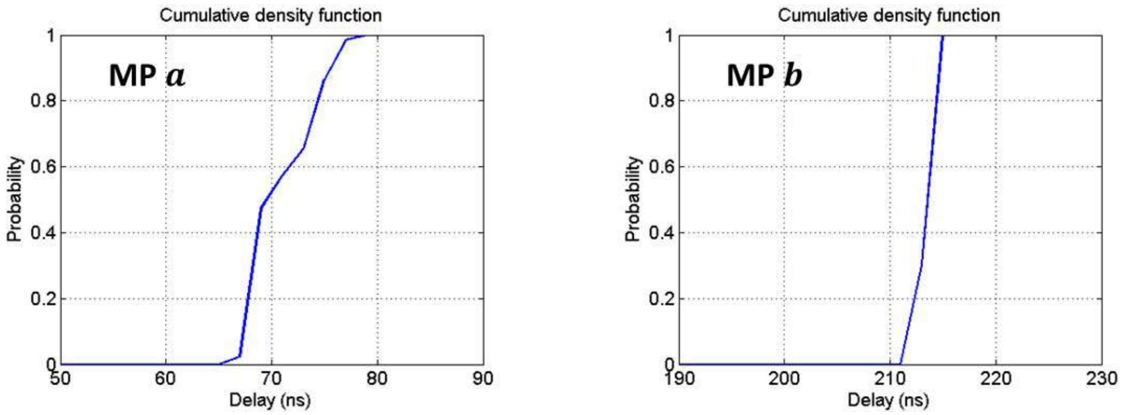

Figure 4.13: Cumulative density function of $\boldsymbol{P(\tau(t_i)|\tau(t_{i-1}) \in T_a)}$ on the left and $\boldsymbol{P(\tau(t_i)|\tau(t_{i-1}) \in T_b)}$ on the right

Table 4.1 : Example of 5 realizations of the RNG process applied to the present delay distribution conditioned by the previous delay

	1	*2*	*3*	*4*	*5*
u	0.95	0.23	0.60	0.48	0.89
τ_a	78.0 ns	68.4 ns	70.9 ns	70.1 ns	76.8 ns
τ_b	215 ns	212 ns	214 ns	213 ns	215 ns

Fig. 4.14 represents the *cdf* of the distributions corresponding to the amplitude probability at the present time (t=20,5 s) of multipaths a (left plot) and b (right plot) knowing that their delays belong respectively to T_a and T_b at the present time and their amplitudes to A_a and A_b at the previous instant (t=20 s). It corresponds to the primitive functions of the *pdfs* represented on Fig. 4.12. Once again, the *RNG* process has been applied to these *cdfs* to display 5 random realizations of the multipath drawing technique that will be used in the following sections. The amplitudes drawn for multipaths a and b have been recorded in Tab. 4.2.

Table 4.2 : Example of 5 realizations of the RNG process applied to the present amplitude distribution conditioned by the present delay and the previous amplitude

	1	*2*	*3*	*4*	*5*
u	0.76	0.45	0.01	0.82	0.44
γ_a	-54.5 dB	-55.5 dB	-71.8 dB	-54.4 dB	-54.5 dB
γ_b	-88.4 dB	-89.1 dB	-90.0 dB	-88.3 dB	-89.1 dB

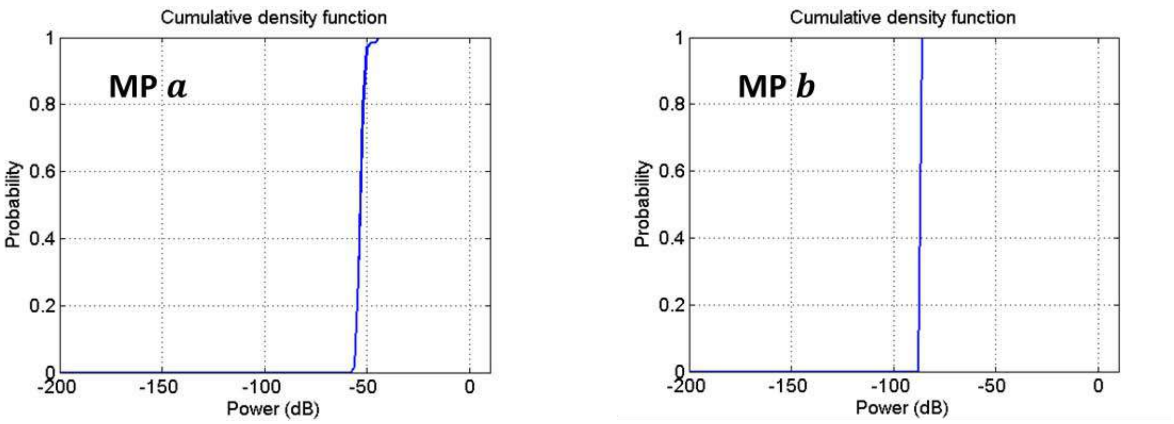

Figure 4.14: Cumulative density function associated to $\boldsymbol{P(\gamma(t_{i+1})|\tau(t_{i+1}) \in T_a \cap \gamma(t_i) \in A_a)}$ (left) and $\boldsymbol{P(\gamma(t_{i+1})|\tau(t_{i+1}) \in T_b \cap \gamma(t_i) \in A_b)}$ (right)

4.3. Application of CRIME to the reference scenario

The algorithm CRIME presented in the previous section has been applied to the reference scenario of section 2.2, considering $\Delta\tau$ = 5 ms between two impulse response samples. In a first time, this paragraph will present the evolution along the trajectory of the different parameters drawn by the algorithm. In as second time, the conservation of the reference channel delay and Doppler characteristics will be investigated through the comparison of the power-delay profiles and Doppler spectrograms. To finish, the limitations of CRIME will be underlined and explained in the last section.

4.3.1. Evolution of the delay and amplitude parameters

4.3.1.1. Delays

Fig. 4.15 illustrates the evolution of the delays of the 5-multipath reduced channel. The parameters are drawn from the different *cdfs* using the RNG technique. Therefore, different realizations of this stochastic process lead to different impulse responses. To illustrate the phenomenon, Fig. 4.15 displays the delay evolution of 4 different realizations of CRIME on the [75m,100m] segment of the reference scenario (the process was initialized at t=0 s). Note that the delay evolution is represented relatively to the LOS delay at each instant. It means that the LOS dynamic is not represented on these plots and the multipath dynamics are represented relatively to the LOS dynamic. It is reminded that the LOS Doppler shift (due to the motion of the receiver) is approximately 10 Hz on the reference scenario.

The first observation that can be made from Fig. 4.15 is the diversity of the impulse response delays on the different realizations of CRIME. For example, only one multipath is located in the delay interval [50 ns,150 ns] at the distance d=100 m on realization 3 whereas 4 multipaths are located in this delay zone on realization 4. This phenomenon highlights the randomness of the CRIME process.

It can also be observed that the delays are continuous, which is ensured by the stochastic estimation of the multipaths (as described in the previous section). The location of the multipath with respect to the receiver can be deduced from its delay dynamic on the trajectory. Indeed, increasing delays correspond to multipaths with negative Doppler according to Eq. 3.6, which means that it is originated behind the receiver. On the other hand, some multipaths show almost constant delays, which correspond to multipaths whose Doppler shift is close to the LOS Doppler shift. It means that CRIME drew those multipaths among the contributions located in the specular direction. This multipath Doppler characteristic illustrates also the randomness of the CRIME process. Indeed, on realization 3, it can be observed that the stochastic process drew 4 multipaths from the backscattering zone (negative Doppler, increasing delay) whereas on realization 1, 2 and 4, only 2 multipaths correspond to backscattering contributions. It means that the proportion between specular, backscattering and incoherent scattering contributions varies according to the realization considered.

On realization 1, the disappearance of multipath 2 can be observed at the distance d=87 m. This is due to the fact that the group of multipaths among which CRIME draws the delay of multipath 2 disappears because it comes out of the 50 m influence length. In that case, CRIME has been designed to re-initialize the parameters of the multipath considered and to start the stochastic process over.

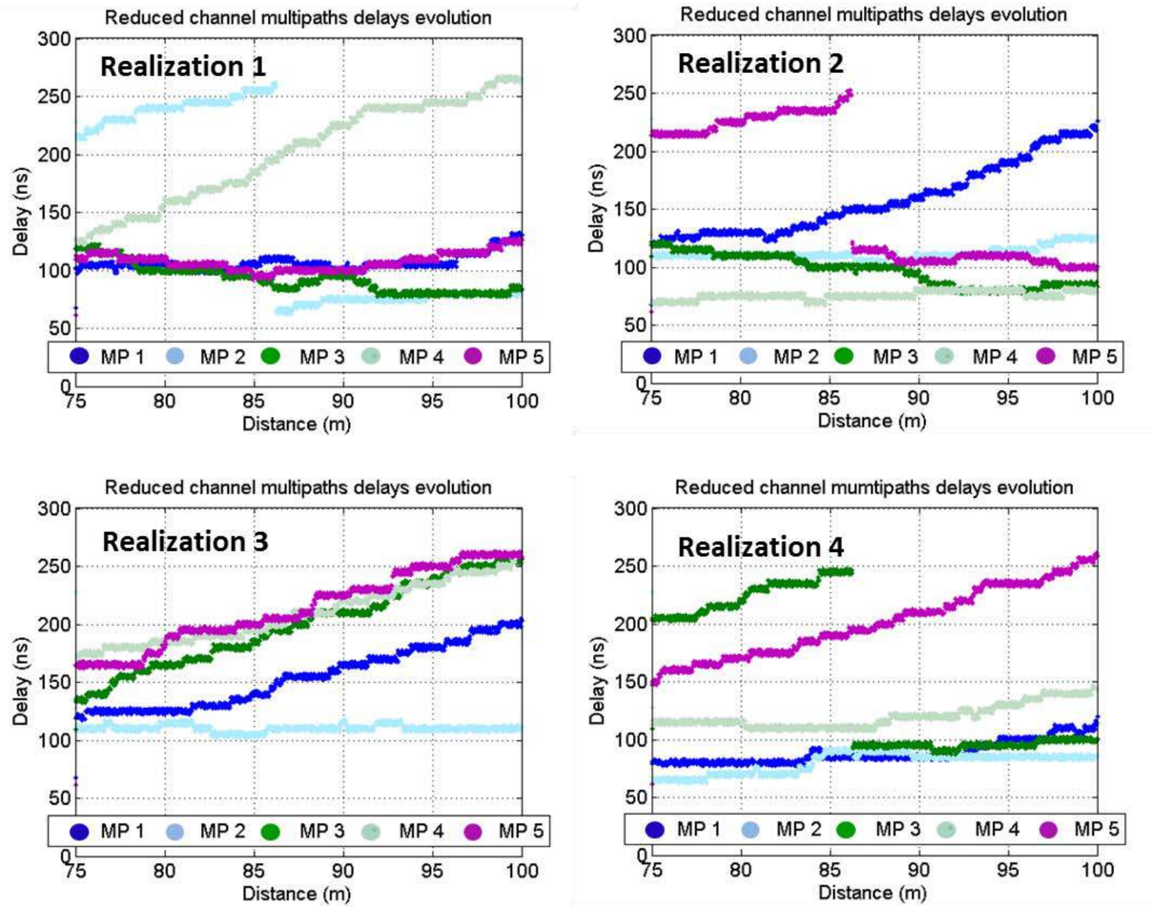

Figure 4.15: Delay evolution of the reduced channel multipaths of 4 realizations of the CRIME process along the [75m,100m] segment of the trajectory

4.3.1.2. Amplitudes

Fig. 4.16 represents the evolution of the amplitude of the reduced channel multipaths along the segment [75m,100m]. These multipaths presented here correspond to the multipaths whose delays were represented on Fig. 4.15. Note that this amplitude is represented in dB relatively to the LOS amplitude.

It can be observed that this amplitude is mostly continuous for each realization of CRIME. However, the power of each multipath present many oscillations due to the amplitude correction displayed on Eq. 4.4. Indeed, the frequency of these oscillations are is similar to the frequency of the reference channel narrow-band power (which is due to the multipath channel dynamic).

Fig. 4.8 showed that multiple power contributions could be associated to a given delay, that is to say that multipaths with very diverse amplitudes could reach the receiver during the same delay interval. Therefore, the link between multipath delay and multipath amplitude is not obvious from the comparison of Fig. 4.15 and 4.16. However, it can be noticed that the multipaths with large delays have lower amplitudes, which is physically relevant.

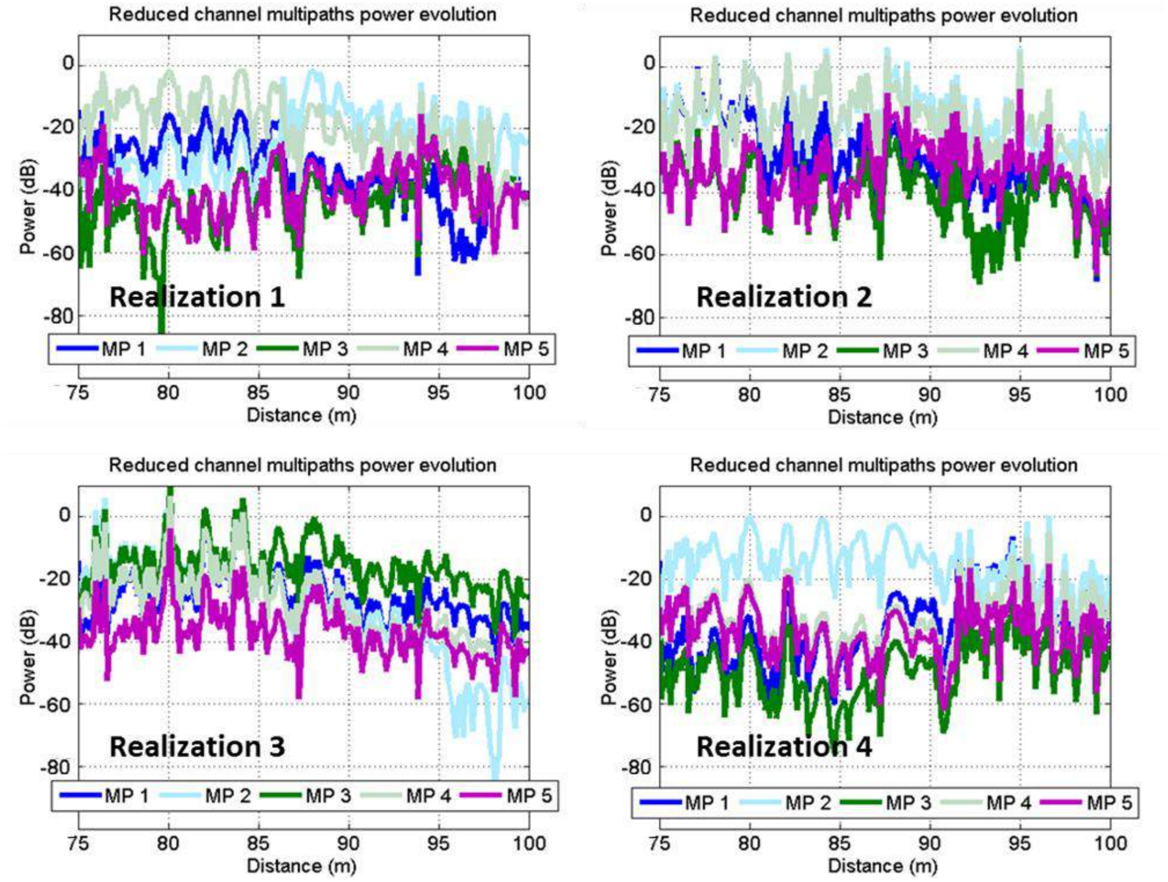

Figure 4.16: Power evolution of the reduced channel multipaths of 4 realizations of the CRIME process along the [75 m,100 m] segment of the trajectory

4.3.1.3. Synthesis

The study of the delay and amplitude profiles allowed identifying two major characteristics of the channel reduction approach using CRIME:

- A major advantage of this method is the continuity of the different parameters composing the reduced impulse response. Contrary to the SAGE parametric method presented in the previous chapter, the continuity of the reduced channel parameters allow an easier physical interpretation of the multipaths especially in terms of delay, phase and Doppler shift.

- A drawback was also identified as the amplitude and delay parameters vary strongly from one realization to another. This characteristic of the CRIME stochastic process can lead to various performance of the reduction method in terms of conservation of the power-delay and Doppler spectrogram preservation.

4.3.2. Study of the delay preservation by CRIME

This sub-section investigates the impact of the channel reduction using CRIME on the power-delay profile of the reference channel. Fig. 4.17 represents the evolution of the impulse response power-delay profile all along the reference scenario on the right plot. The power is normalized by the LOS power. The LOS contribution is not represented on this profile in order to focus on the multipath channel. The left plot represents the reference channel impulse response.

As comparing the reference impulse response to the CRIME reduced impulse response, a few inconsistencies can be observed. First, the reference impulse response maximum power zone is located at delay τ=80 ns on the [0m,40m] and [110m,140m] intervals of the trajectory. No maximum power can be observed in those delay zones on the reduced channel impulse response, on which power is spread uniformly on the [60ns,110ns] delay interval. The same observation about maximum power delays dissimilarities can be made on the [50 m,100 m] trajectory segment.

Moreover, the delay spread has not been preserved all along the trajectory. For example, on the interval [40m,75m], only one power peak is observable on the reduced channel, located approximately at delay τ=60 ns, whereas the reference channel presents a 50 ns large power zone on this interval. Similar differences can be observed on intervals [80m,110m] or [130m,150m]. Therefore, it can be considered that the CRIME reduction impairs the impulse response power-delay profile.

It was already mentioned in the previous sub-section that those results can vary from one realization to another, because of the *RNG*. However, the significant lack of preservation of power-delay profile illustrated on Fig. 4.17 shows the limitations of the original version of CRIME to be adapted to such impulse responses, which will be discussed in the following sub-section.

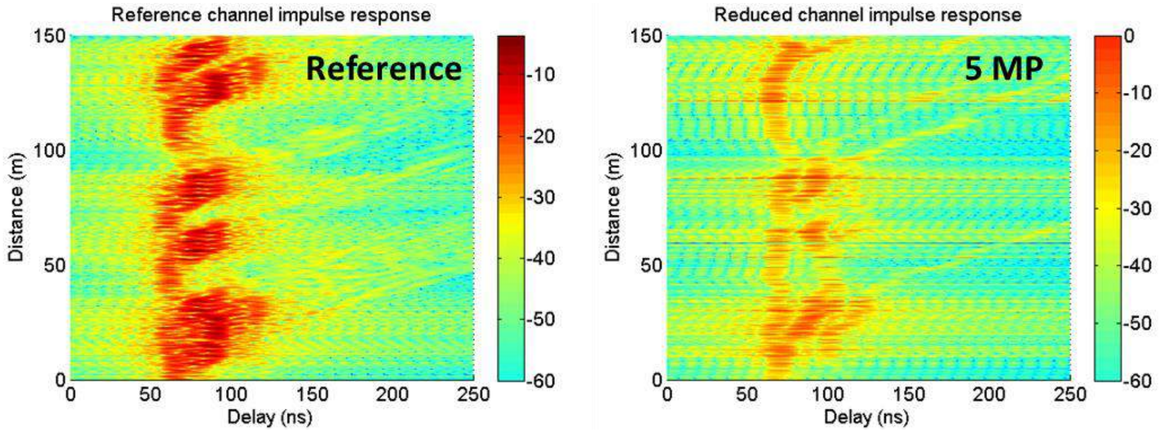

Figure 4.17: Power-delay profile of the reference channel (left) and the CRIME reduced channel (right)

4.3.3. Identification of the limitations of CRIME

In the previous sub-section, the lack of delay and Doppler preservation of the CRIME reduction process questioned the ability of CRIME to address the channel reduction problem. Therefore, this subsection aims at identifying the causes of those limitations in order to design an enhanced version of CRIME.

The principle of CRIME is to draw multipaths among the most probable parameters. However, the impulse response power-delay snapshots of SCHUN are composed both of a small number of high amplitude multipaths and a high number of small amplitude multipaths. This statement has been illustrated on Fig. 4.18 which displays an example of impulse response power-Doppler and power-delay snapshots, corresponding to the instant t=5 s. The high amplitude zones have been framed in red. In such conditions, CRIME will most likely draw the reduced channel parameters from the delay and amplitude zones composed of a high number of multipaths, as the *cdfs* are computed according to the number of contributions in the different delay and amplitude bins. The few high amplitude multipaths have no significant impact on the *pdfs* and *cdfs*. Therefore, they are unlikely to be represented in the reduced channel.

The drawback identified in the previous paragraph leads to two major approximations which impair the original impulse responses. They concern respectively the delay and amplitude.

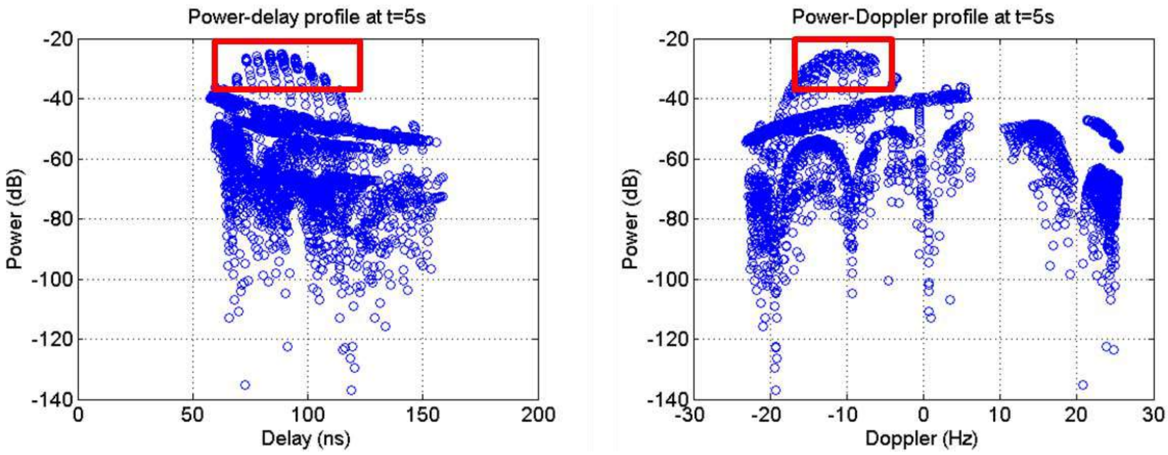

Figure 4.18: Power-delay profile (left) and power-Doppler profile (right) at t=5 s

- **Delay computation:**

Fig. 4.19 and Fig. 4.20 illustrate two examples of the delay drawing process from the *pdf*s corresponding to the instants t=5 s and t=25 s. Both the density function of the delay distribution and the impulse response power-delay profile are represented. The *RNG* has been run 10 times to obtain 10 realizations of the delay drawing process. The delays obtained have been recorded in Tab 4.3 and have been represented by the red dots on both plots of Fig. 4.19 and 4.20.

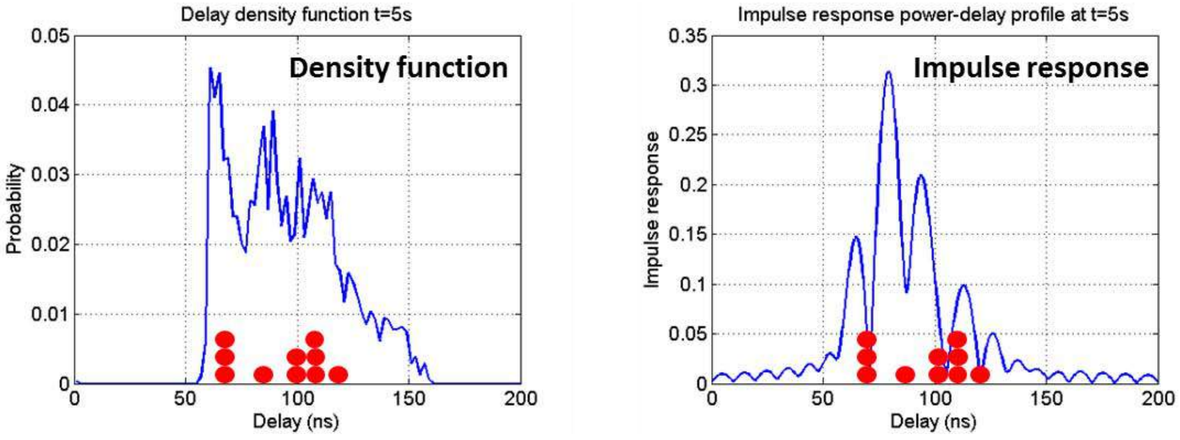

Figure 4.19: Density function of the delays and impulse response power-delay profile at t=5 s

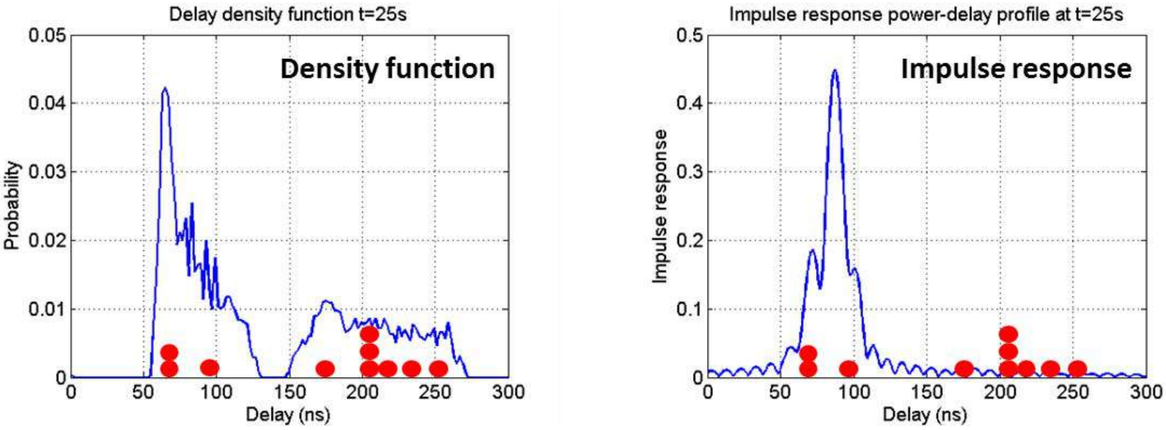

Figure 4.20: Density function of the delays and impulse response power-delay profile at t=25 s

Two important remarks have to be made about these illustrations:

- First, CRIME draws the multipaths from the conditional *pdfs* that were described in section 4.2.2 (2-dimensional *pdf*). On these examples, the multipath delays are drawn from the simple *pdfs* of the delay distribution at the considered time (1-dimensional *pdf*). Therefore, this example is not exactly representative of CRIME. This choice was made to make more obvious the problem caused by drawing multipaths from large impulse response *pdfs*. However, this analysis is directly transposable to multi-dimensional *pdfs*.

- Secondly, the multipaths drawn by the RNG have been spotted on the pdf figures, whereas it is actually drawn from the cdfs, as explained in section 4.2.3. This choice only stands for the fact that more pdfs are more convenient than cdfs for visual interpretation. Those results of Tab. 4.3 were obtained with the regular RNG processed on the cdfs.

Table 4.3 : 10 realizations of the delay drawing process on the pdfs at t=5s and t=15s

	1	**2**	**3**	**4**	**5**	**6**	**7**	**8**	**9**	**10**
t=5s	112ns	103ns	109ns	83ns	116ns	100ns	66ns	111ns	67ns	69ns
t=15s	237ns	223ns	252ns	176ns	63ns	65ns	209ns	213ns	209ns	100ns

At t=5 s, it can be observed on Fig. 4.19 that the impulse response power-delay profile has a major power peak located at delay τ=80 ns. However, it can be observed that no delay drawn from the *pdf* represented on the left plot corresponds to this value. This is due to the fact that the shape of the impulse responses and density functions do not coincide. Indeed, the impulse response is composed of three major power-peaks whereas the density function shows an equivalent probability of the delay bins in the interval [60ns,110ns]. As mentioned in the beginning of this sub-section, the most probable delays do not coincide with the most powerful, which leads to such divergences.

The same conclusion can be made from the observation of Fig. 4.20, as 70% of the delay drawn from the *pdf* are located in the interval [150ns,250ns], whereas no power is observable in this delay zone on the reference impulse response. It means that many multipaths are located in the [150ns,250ns] delay interval but because they are incoherent and have low amplitudes, they have no significant impact on the impulse response. Once more, this statement has a strong impact on the delay profile preservation by the reduced channel.

- **Amplitude estimation:**

The amplitudes of the reduced channel drawn by CRIME is impacted by a similar phenomenon. In order to illustrate it, the right plot of Fig. 4.21 displays the distribution of the amplitudes in dB relative to LOS of the multipaths located in the [70ns,80ns] delay interval at the instant t=5 s, that is to say $P(\gamma_l|\tau_l \in [70ns, 80ns])$. In other terms, it is supposed that the delays have been chosen among the most significant delay zone of the channel impulse response in terms of power, as it can be observed on the right plot of Fig. 4.19. The distribution shown on Fig. 4.21 corresponds to the amplitude density function of those multipaths considering the impulse response snapshot at t=5 s (from which the power of the estimated multipath is drawn). Once more 10 realizations of the amplitude drawing process have been performed, and spotted on the *pdf* of the amplitude distribution. The left plot of Fig. 4.21 represents the power-delay profile of the reference channel at the instant t=5 s. The red frame identifies the multipaths involved in the amplitude distribution on the right plot. The same situation has been represented on Fig. 4.22 concerning the instant t=15 s. The amplitudes drawn for the different realizations have been recorded in Tab. 4.4. Note that like in the paragraph "*Delays*", the multipaths are plot on the *pdf* figure whereas it was actually drawn from the cdfs.

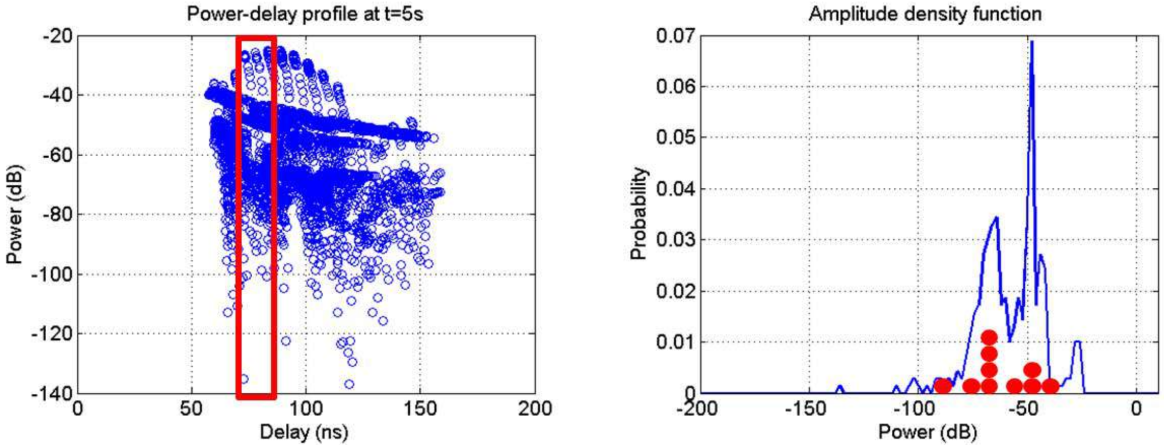

Figure 4.21: Density function of the amplitudes of the multipaths whose delay is tapped into the frame of the left plot at t=5 s

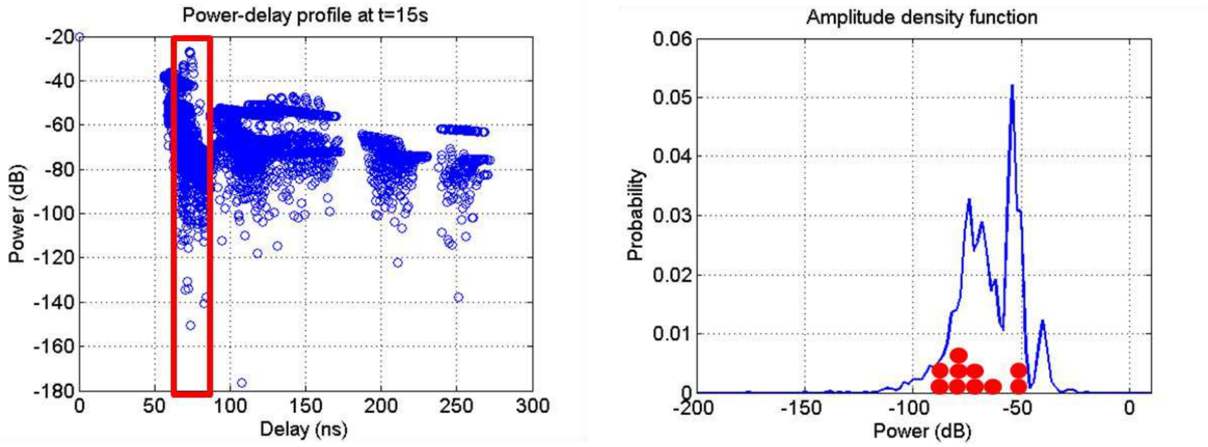

Figure 4.22: Density function of the amplitudes of the multipaths whose delay is tapped into the frame of the left plot at t=15 s

Table 4.4 : 10 realizations of the amplitude drawing process on the pdfs at t=5 s and t=15 s

	1	**2**	**3**	**4**	**5**	**6**	**7**	**8**	**9**	**10**
t=5s	-65dB	-67dB	-91dB	-47dB	-57dB	-68dB	-67dB	-40dB	-76dB	-48dB
t=15s	-72dB	-76dB	-80dB	-76dB	-75dB	-50dB	-72dB	-80dB	-66dB	-48dB

On both Fig. 4.21 and 4.22, it can be observed that only a few multipaths in the considered delay frame have power superior to -40 dB, and they are not observable on the *pdfs*. Therefore, no multipaths are drawn from these power zones, in any realizations. However, it could be observed on the impulse responses of Fig. 4.21 and 4.22 that those multipaths have a strong influence on the power-delay profile. Therefore, the CRIME reduction method is likely to impair the channel impulse response.

- **Synthesis:**

In order to improve the performance of CRIME, it has been decided modify the algorithm. This sub-section has identified two major drawbacks of this stochastic process, concerning the drawing of amplitude and delay parameters. From those ascertainments, it has been decided to investigate two axes of amelioration:

- First, it was shown that high amplitude multipaths were unlikely to be drawn by CRIME because of the low quantity of such multipaths, leading to the impairment of the impulse response power-delay profile. Therefore, the delay *pdfs* should take into account the amplitude of the multipaths, in order to increase the similarity between delay *pdfs* and impulse responses and increase the probability to draw delays from the high power zones of the impulse response.

- Secondly, one of the characteristics of SCHUN is to provide a large quantity of low amplitude multipaths as compared to the high amplitude ones, meaning that the *RNG* process is unlikely to draw high amplitude multipaths. Therefore, the amplitude estimation should be computed from the impulse response amplitude depending on the delay instead of the amplitude distribution.

4.4. Modification of CRIME and application to the reference impulse response

This section will present the different enhancements that have been brought to the original version of CRIME. These modifications are motivated by the different statements of the previous section. Then, the modified version of the CRIME will be applied to the reference impulse response in order to investigate its performances in terms of power-delay profile preservation.

4.4.1. Modification of CRIME

As mentioned in the previous sub-section, the major limitations of CRIME concern the delay and amplitude computations. Moreover, it can be noted that CRIME did not consider the Doppler shift of the multipaths. The possibility to estimate the Doppler shifts of the reduced channel will also be discussed. To finish, the multipath lifespan will be investigated in order to define the behavior of the algorithm in case of “disappearance” or “appearance” of multipaths.

- **Delay :**

It has been decided to modify the distribution from which the multipath delays are drawn, in order to improve the consistency between delay *pdfs* and power-delay profile. To do so, the amplitude of the multipaths have been taken into account to build the density function. In other terms, the delays will not be drawn from the basic delay *pdf* any more (noted f_{CRIME}), but from a new density function that will be noted f_{new}. The following notations will be used to describe this process:

- M denotes the number of delay samples in the impulse response (the outputs of SCHUN).
- $\left[\tau^{(1)}, \dots, \tau^{(i)}, \dots, \tau^{(max)}\right]$ denotes the sampled delay line, represented by the center delays of the delay bins i.
- $\left[V^{(1)}, \dots, V^{(i)}, \dots, V^{(max)}\right]$ denotes the number of multipaths in the different delay bins.

In the original version of CRIME, the density function from which the delays are drawn is given by:

$$f_{CRIME}(\tau^{(i)}) = \frac{V(i)}{M} \tag{4.5}$$

In the new version of CRIME, the multipaths are weighted by their absolute amplitude:

$$f_{NEW}\left(\tau^{(i)}\right) = \frac{1}{M}\frac{\sum_{l,\tau_l \in i}|\widetilde{\gamma}_l|}{\sum_{l=1}^{M}|\widetilde{\gamma}_l|} \tag{4.6}$$

Note that the function f_{new} is still homogenous to a density function. Therefore, it has been decided to compute the cumulative function associated to f_{new}, noted F_{new}, as the primitive function of f_{new}:

$$F_{NEW}(\tau^{(i)}) = \int_{-\infty}^{\tau^{(i)}} f_{NEW}(\tau)\, d\tau \tag{4.7}$$

The *RNG* process is then applied to the *cdf* F_{NEW} instead of F_{CRIME}. Note that this modification of density function can be applied to the conditional distributions, in any dimension.

Fig. 4.20 highlighted the limitation of CRIME concerning the delay estimation. Therefore, it has been decided to represent on Fig. 4.23 the exact same situation at the instant t=25 s, except that the delays are drawn from the modified version of the *pdf* described in the previous paragraph. This new density function has been represented on the left plot, while the right plot still represents the impulse response snapshot at the instant t=25 s. Once again, 10 realizations of the *RNG* have been performed to draw 10 delays on the new density function. The drawn delays are represented in red dots on both plots. Note that this time again, the process has been illustrated with 1-dimensional *pdfs* for visual convenience, whereas it is actually processed on the 2-dimensional delay *pdfs*.

The first observation that can be made from Fig. 4.23 is the closer similarity between density function and power-delay profile. As a consequence, the delays drawn from the new *pdf* are closer to the high power zones of the power-delay profile than with the previous version of CRIME. Therefore, this modification of CRIME is likely to improve the preservation of the channel delay characteristics. This example validates the choice of the new density function on which the RNG is applied.

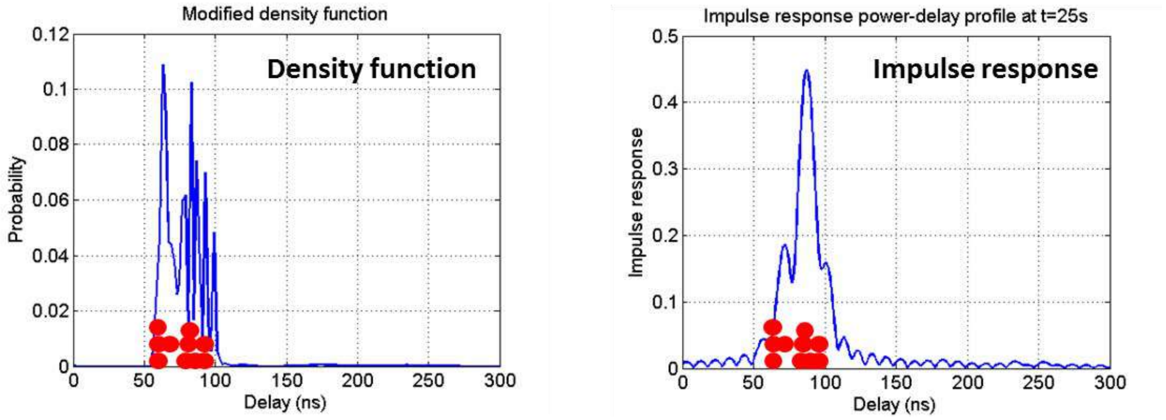

Figure 4.23: New version of the density function of the delay distribution (left) and impulse response power-delay profile at t=25 s

- **Amplitude :**

In what concerns the estimation of the amplitudes of the reduced channel, it has been decided to change the structure of the algorithm presented on Fig. 4.14. Indeed, the stochastic process of the reduced channel amplitudes has been given up, in order to optimize the preservation of the link between power and delay of the echoes. In the modified version of CRIME, only the delays are considered to vary according to a first order Markov process.

The complex amplitude of a given multipath of the reduced channel is deduced from the power-delay profile, knowing the delay of the multipath. Note that the power delay profile is complex, meaning that both amplitude module and phase are computed in the same move.

Let h denote the complex impulse response of the multipath channel at the time t_i (continuous power-delay profile). The complex amplitude of the multipath l is given by Eq. 4.8, knowing that the delay of l is τ_l at the instant t_i.

$$\widetilde{\gamma_l}(t_i) = h(\tau_i, t_i) \tag{4.8}$$

Note that this technique is likely to imply big amplitude modules. Therefore, the same amplitude correction as the one described on Eq. 4.4 has to be performed. An example of such an amplitude estimation process has been illustrated on Fig. 4.24 (in dimension 1), corresponding to the instant t=25 s. The five delays represented have been drawn by the RNG, their amplitude module and phase are estimated using the module and argument of the impulse response. They are respectively represented on the left and right plots of Fig. 4.24.

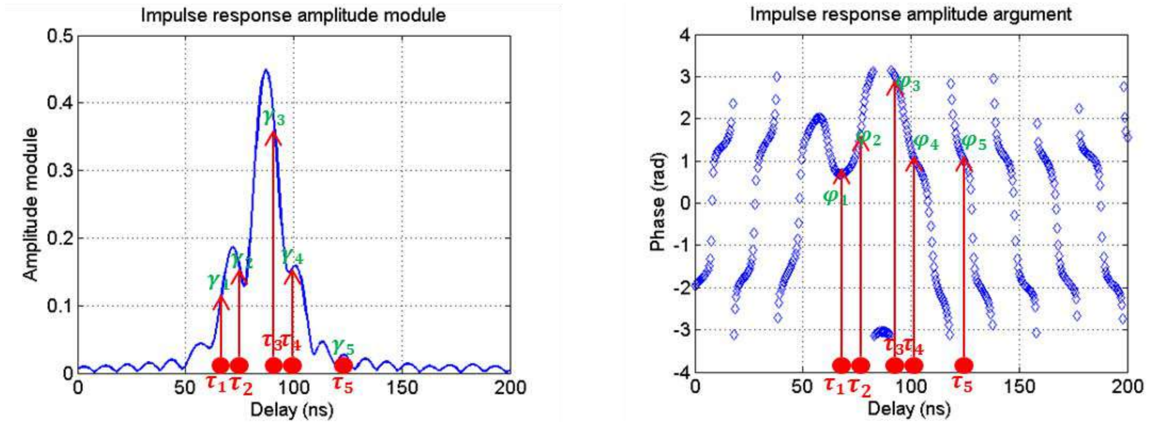

Figure 4.24: Illustration of the complex amplitude estimation process at t=25 s

- **Doppler :**

As shown on Eq. 3.6, the Doppler shift is responsible for the delay shift of the multipaths between two instants t_i and t_{i+1}. Therefore, the Doppler can be deduced from this delay shift using Eq. 4.9, which takes back the notations of Eq. 3.6:

$$\vartheta(t_{i+1}) = \frac{f_0}{T_e}(\tau_{i+1} - \tau_i) \tag{4.9}$$

It can be deduced from Eq. 4.9 that two multipaths with close delays at t_{i+1} and close delays at t_i have similar Doppler shifts. Therefore, it has been decided to draw $\vartheta(t_{i+1})$ from the *pdfs* of the Doppler distribution with the prior knowledge of $\tau(t_{i+1})$ and $\tau(t_i)$. In other terms, the Doppler is drawn from the *pdf* associated to the distribution of $P\big(\vartheta(t_{i+1})\big|\tau(t_{i+1}), \tau(t_i)\big)$.

- **Multipath lifetime :**

It could be observed on realizations 1 and 2 of Fig. 4.15, at the respective distances d=86 m and d=87 m, a strong discontinuities of one echo of the reduced channel. This is due to the disappearance of the echo, caused by the fact that the corresponding cluster of multipaths of the original channel comes out of the multipath influence zone. Therefore, no more multipath with similar delay can be found in the impulse response data set. No more delay *pdf* can be built and the stochastic process stops.

Let us consider that multipath l disappears at the time t_{stop}. In such a case, it has been decided to restart the delay stochastic process, with a new initialization. In other terms, the delay $\tau_l(t_{stop+1})$ is estimated from the *pdf* associated to the distribution of $P(\tau_l(t_{stop+1}))$. Note that technic is likely to generate discontinuities. However, such discontinuities are rare as compared to the duration of the scenario. Secondly, the echo which disappears is supposed to have a low power, as the corresponding multipath cluster is located far from the specular zone of the scenario.

Fig. 4.25 schematizes the modified version of CRIME that was described in this sub-section.

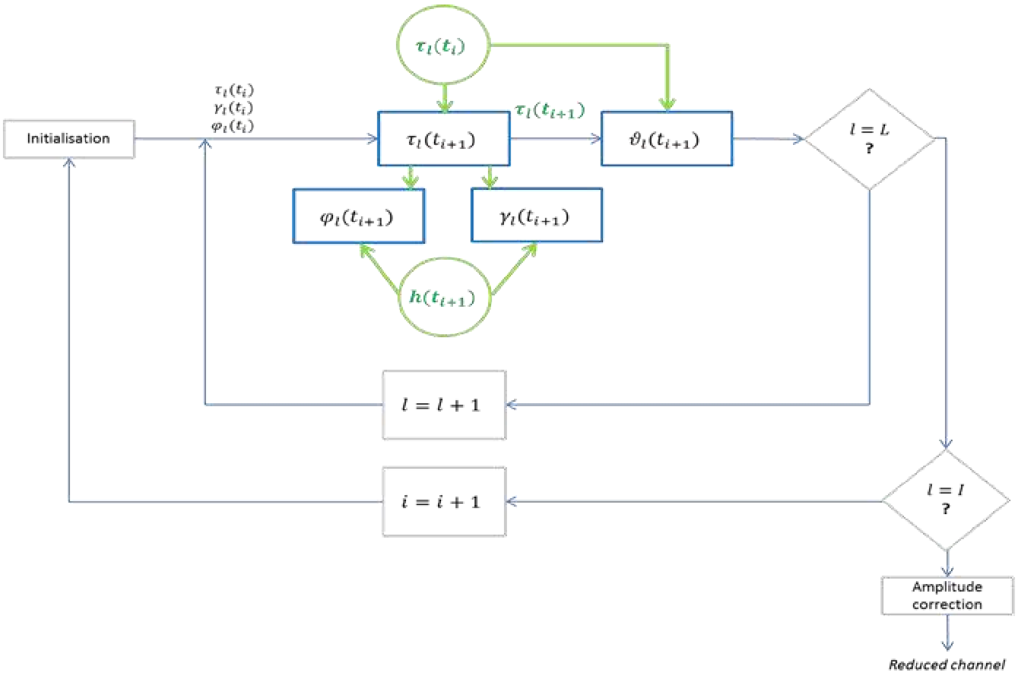

Figure 4.25: Principle of the modified version of CRIME

4.4.2. Application of the modified version of CRIME to the reference scenario

Tis new statistic algorithm has been applied to the reference scenario with 200 Hz channel sampling rate. This sub-section will investigate its performance in terms of power-delay and Doppler spectrogram conservation.

Fig. 4.26 illustrates the evolution of the reference channel power-delay profile and the one corresponding to the new statistic method, considering 5 multipaths in the reduced channel. Note that only the multipath channel is represented (no LOS) relatively to the LOS power.

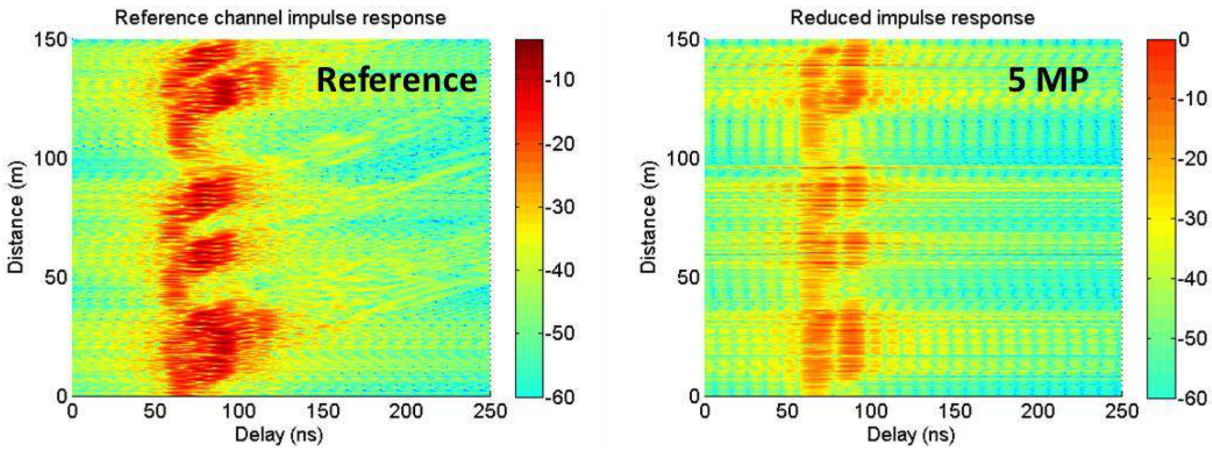

Figure 4.26: Illustration of the impulse response power-delay profile for the original (left) and reduced (right) channels along the trajectory using the new statistic method

As comparing the plots of Fig. 4.26, it can be noted that the delay spread of the original impulse response has been slightly reduced. Indeed, on the [120 m, 140 m] segment of the trajectory, the reference impulse response shows significant power peaks between 50 ns and almost 150 ns whereas the reduced impulse response shows a strong power decay for more than 100 ns. The same observation can be made on the segment [10 m, 30 m]. From a general point of view, it can be noted that the delay spread remains constant on the reduced channel, whereas the reference channel shows some higher delay spread zones (segments [10 m, 30 m] and [120 m, 140m]). Moreover, no power can be observed beyond 150 ns delays on the reduced channel. Those remarks are most likely due to the new delay drawing process. Indeed, the multipath delays have been drawn from the high power zones of the impulse response, which increases the probability to draw lower delays. Therefore, it has to be noted that this choice of implementation impairs the original delay spread.

However, the high power zones of the reduced impulse response overlap the reference impulse response better than with the original version of CRIME, as comparing Fig. 4.26 with Fig. 4.17. Indeed, the main power contributions along the trajectory on the reference channel (around 80 ns delays) are well reproduced by the reduced channel. Moreover, the disappearance of these power contributions on the [40 m, 50 m] and [90 m, 120 m] segments is also reproduced by the new version of the statistic reduction method.

As a conclusion, contrary to the original version of CRIME, the main power contributions have been well preserved by the new reduction method. It was the main motivation of the modification presented in this sub-section, because the location of the main power zones on the delay line has a major impact on the pseudo-range error. However, a slight reduction of the delay spread has to be noted, which may have an impact on performance in terms of pseudo-range error conservation.

Fig. 4.27 illustrates the Doppler spectrogram of the reference channel (above) and reduced one (below) all along the trajectory. Once more, no LOS has been represented in order to focus on the multipath channel and the power is represented relatively to the LOS power.

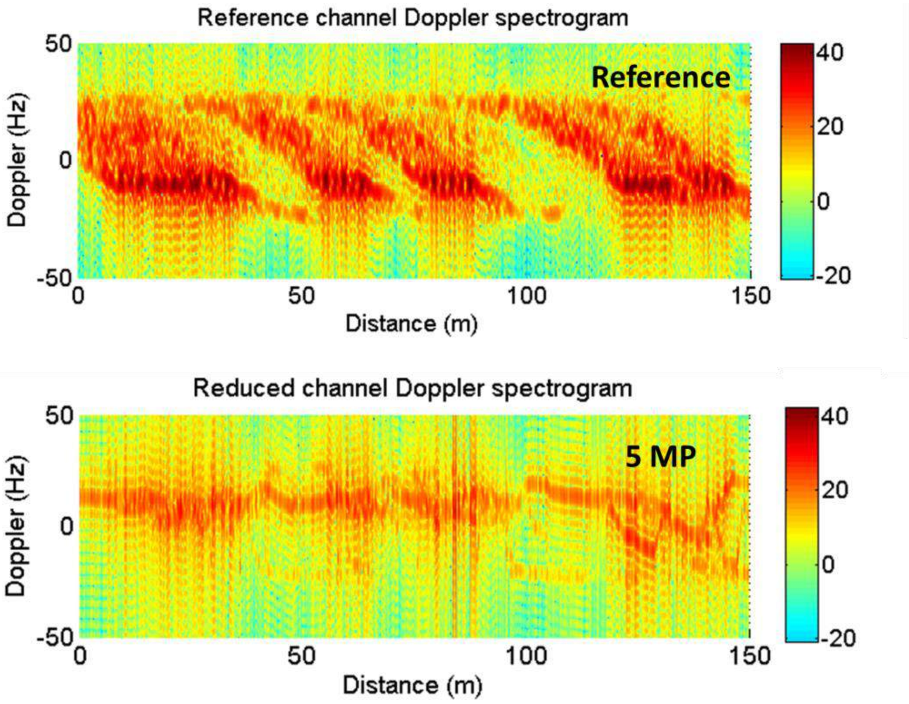

Figure 4.27: Illustration of the Doppler spectrogram of the original (above) and reduced (below) channels along the trajectory using the new statistic method

The reduced channel shows a poor preservation of the reference Doppler spectrogram. First, the Doppler spread is highly reduced (from 40 Hz on the reference channel to a few Hertz on the reduced one). Secondly, the high power zone of the reduced channel Doppler spectrogram (located around 10 Hz on the [0 m, 120 m] segment), does not match the reference channel power zone (located in the negative Doppler). It reveals the fact the Doppler computation, which was explained in the previous paragraph, is not efficient enough. This is due to the fact that the Doppler estimation is based on the prior delay estimation. The delays of the reduced channel echoes show some fluctuations from one instant to the other due to fact that the delay resolution limited to the bin size. Therefore, the delays successively increase and decrease between two consecutive instants, within the interval $\left[\tau - \frac{h}{2}, \tau + \frac{h}{2}\right]$ (where h denotes the bin size). This statement is observable on Fig. 4.15. For that reason, if the Doppler is estimated considering the delay shift between two consecutive instants, it will go from positive to negative successively all along the trajectory. The Doppler 10 Hz identifiable on Fig. 4.27 corresponds to the dynamic of the scenario (i.e. LOS Doppler), which is the mean variation of such a Doppler shift.

In order to adapt the Doppler estimation to this constraint, a possibility is to post process the delay estimation of the total scenario by filtering it, in order to remove the fast fluctuations (using a sliding window for example). The Doppler could be computed along those filtered delays to remove the positive-negative oscillation effect. This method has not been illustrated on this scenario.

4.5. Conclusion

This chapter investigated a new approach to reduce the multipath channel, differing significantly from the two previous methods of chapters 2 and 3. Indeed, instead of applying a reduction algorithm to each impulse response sample independently, the reduction method considered in this chapter consists in drawing statistically the parameters of the reduced channel from the data sets of the original impulse response samples. Moreover, in order to ensure the continuity of the reduced channel echoes, those parameters were supposed to vary according to a stochastic process, more specifically a first-order Markov chain. The reduced channel echoes are independent realizations of this stochastic process.

The technique referred to as CRIME in [Schu 14] was the starting point of this reflection. After describing its principle, this chapter presented the different techniques used to draw the parameters from the statistical distributions in section 4.2. This point was critical for two reasons: first the delay is computed according to the prior knowledge of the delay of the previous instant. Secondly, the amplitude is computed according to the knowledge of the delay at the present time and amplitude at the previous instant. This leads to 2-dimensional and 3-dimensional *pdfs*, whose computation had to be commented.

After presenting the global architecture of the algorithm, the original version CRIME has been applied to this reference scenario with 5 echoes in the reduced channel. The preservation of the channel power-delay profile was investigated all along the trajectory. The conclusion of this comparison was a poor preservation of the delay, with many incoherent power peaks on the reduced impulse response. Two explanations have been proposed to explain such a result. The first one concerned the computation of the delays. More specifically, there is a strong probability to draw delays from the numerous low amplitude delay zones of the delay *pdfs*, systematically occulting the few high amplitude delays. Those ones have a major impact on the impulse response power-delay profile. For the same reason, the amplitudes are systematically drawn from the low amplitude multipaths, because they are more numerous. This leads to a global impairment of the relative power of the reduced channel echoes. It means that the original approach of CRIME is designed for impulse responses with fewer multipaths, like on the scenario presented in [Schu 14]. It appears that large sized impulse responses cannot be reduced using the original version of CRIME.

Starting from these conclusions, a few modifications of CRIME have been proposed in section 4.4. First, the delay drawing process has been modified. Instead of drawing the delays from the delay pdfs, it has been decided to draw them from a new density function. This density function corresponds to the delay distribution weighted by the respective power of the delays. It aimed at increasing the probability of drawing the multipath delays from the high power zones of the power-delay profile. Secondly, the stochastic evolution of the amplitudes has been given up. Instead of drawing the multipath power from the 3-dimensional *pdfs*, it has been decided to deduce it from the impulse response power-delay profile, with the prior knowledge of the delay of the echo considered. It aimed at increasing the correspondence between multipath delay and multipath amplitude. To finish, the treatment of the disappearance of a multipath was detailed, in order to complete the description of the new version of the statistic reduction method.

This new technique was also applied to the reference scenario. It could be observed a better preservation of the original channel power-delay profile. Indeed, the major power peaks of the reduced impulse response overlap the ones of the reference channel better than in the case of the original version of CRIME. This validates the modification of CRIME mentioned previously. However, the Doppler spectrogram comparison revealed a poor Doppler estimation. It was explained by the multiple fast fluctuations of the delays due to the limitation of the delay resolution to the bin size, which made impossible the estimation of the Doppler from the delay shift between two consecutive instants.

The complexity of the algorithm has not been mentioned yet. First, the multipaths of the reduced channel are drawn as independent stochastic processes. Therefore, the computation load is proportional to the number of multipaths in the reduced channel. Secondly, the construction of the *pdfs* can be optimized so as to build only the density functions necessary to the delay estimation, avoiding full 2-dimensional *pdf* computations. In such conditions, the computation load of the statistical method is close to the one of the aggregation methods (around 1 min to estimate 5 multipaths along the reference scenario).

As a conclusion, the modifications brought to the statistical method of section 4.4 were validated by the better preservation of the power-delay profile. Therefore this version of the algorithm will be used to compare the statistical methods performance with the parametric and aggregation methods according to the pseudo-range error conservation in chapter 5.

Chapter 5

5. Comparison of the reduction methods according to the pseudo-range error preservation

This chapter investigates the impact of the reduction methods (presented in chapters 2, 3 and 4) on the pseudo-range error of a GNSS receiver. Indeed, it was already mentioned that the urban channel models are usually used in the navigation context to assess the impact of the multipath channel on GNSS receivers, depending on the environment considered. Therefore, the major performance criterion of the reduction techniques is the preservation of the positioning error before and after the impulse response reduction. The reduction methods must have only a minimal impact on the receiver testing campaigns.

In this chapter, three of these methods will be considered. Their implementations have been documented respectively in chapter 2, 3 and 4. They are listed below:

- The Weighted Clustering method described in chapter 2.
- The SAGE optimization method adapted to the channel reduction problem with the algorithm optimized in chapter 3.
- The modified version of the algorithm CRIME [Schu 14], which computes the reduced channel echoes using a statistical approach, explained in chapter 4.

A few more details about the methods that will be compared are given in section 5.1, which also relates the state of the art concerning pseudo-range error preservation of different reduction methods. Those methods will be applied to a same reference scenario, representing a trajectory in an urban environment, which has been implemented for the purpose of this work. The scenario will be presented in section 5.2. The open loop error of the receiver, referred to as discriminator error, will be investigated on every impulse response sample of this scenario, considering the original and reduced channels. The comparison of the discriminator open loop errors along the trajectory will be displayed in section 5.3, as a preliminary assessment of the impact of the reduction methods on the pseudo-range error. In section 5.4, their impact on a realistic receiver simulator will be investigated, through the tracking error preservation. Section 5.5 and 5.6 will study the impact of the signal parameters (such as the modulation of the signal or the presence/absence of additional noise), receiver parameters (such as RF bandwidth or discriminator) and emitter position on the results presented in sections 5.3 and 5.4. Section 5.7 will finally synthesize this study.

5.1. Introduction of the study and literature overview

5.1.1. Methods to compare

The reduction methods developed in chapter 2 used an aggregation approach to reduce the multipath channel. All along this chapter, a few enhancements have been proposed to overcome the limitations in terms of power-delay and Doppler spectrogram preservation. Finally, the Weighted Clustering technique appeared to preserve the power-delay and Doppler spectrogram profiles at best. Therefore, the Weighted Clustering method has been considered as the best reduction method among the multipath aggregation approaches. It has been chosen to be a part of the comparison of the pseudo-range error preservation in chapter 5. To the contrary, the other methods presented in chapter 2 are considered to be overcome by the Clustering Weighted technique and will not be considered in chapter 5. This method will be simply referred to as Clustering in the following, as no more ambiguity subsides.

In chapter 3, the SAGE optimization method has been adapted to address the problem of the minimization of the cost function considered. This cost-function is the difference between the original and reduced channel autocorrelation functions. The parameters of the SAGE algorithm have been tuned so as to optimize the tradeoff between Doppler resolution and the number of echoes to estimate, as presented in section 3.3. With 5 echoes in the reduced channel, 20 Hz Doppler resolution appeared to be a realistic choice. This specific algorithm will be used to compare the parametric optimization approach to the other approaches in terms of pseudo-range error preservation in this last chapter.

In chapter 4, a statistical approach has been considered to reduce the number of multipaths of the original channel. It considers that the echoes of the reduced channel are the realizations of a stochastic process, as described in [Schu 14]. The original CRIME algorithm of has been modified in order to improve the power-delay profile preservation. The last method presented in section 4.4, which is the modified version of CRIME will be compared to the two other approaches (mentioned in the previous paragraphs) according to the pseudo-range error preservation in this last chapter.

5.1.2. Literature overview

A few studies in the literature have already assessed the preservation of the pseudo-range error of different reduced channel models.

- **Aggregation methods :**

The comparison between the pseudo-range error caused by a reference channel (several thousands of multipaths) and the same channel reduced using a Tap Delay Line approach has been presented in [Ait 11]. It is important to mention that the Tap Delay Line channel model presented in [Ait 11] consists in sampling both delay and space in regular taps. Intermediate and minimal Tap Delay Line resolutions have been tested in the context of [Ait 11], corresponding respectively to intermediate (50 ns, 25°) and wide (100 ns, 50°) bins sizes. Moreover, the impact of the channel reduction has been observed on the pseudo-range error caused on a conventional DLL/PLL GNSS receiver, on a CBF (*Conventional Beam Forming*) GNSS receiver and on a SAGE/STAP multi-correlator GNSS receiver [Roug 12b]. The conclusion of [Ait 11] showed a significant impact of the channel reduction on the conventional DLL/PLL receiver in both intermediate and minimal Tap Delay Line configurations. The CBF and SAGE/STAP GNSS receivers appeared to be less impacted by the reduction process.

A similar comparison has been conducted in [Krac 08]. That time, the reduction methods include a selection method (similar to the one described in section 2.3) and a clustering method using the *Single Linkage* approach (similar to the one presented in section 2.5.3). The pseudo-range error caused by both the reference channel and the reduced channel models has been investigated on different types of GNSS receivers, depending on the multipath mitigation technique. A DLL/PLL receiver using the narrow-correlator approach [VanD 92] has been used, as well as a ML (*Maximum Likelihood*) estimator [Kay 93] and MMSE (*Maximum Mean Square Error*) estimator [Lent 07]. Several modulations have been tested: BPSK, BOC(1,1) and CBOC signals. It has to be mentioned that the reference scenario impulse responses were computed using the channel modeling approach of [ITU 13], which synthesizes only a few tens of multipaths. It means that the reduction methods were not challenged as much as in this thesis which uses the SCHUN channel synthesizer (several thousands of multipaths). In what concerns the comparison of the reduction methods, in each case the clustering technique showed better pseudo-range error preservation than the selection method. This statement confirms the observations of chapter 2 and justifies the choice of the clustering technique to assess the performance of the aggregation approach.

Finally, the comparison of different aggregation methods was presented in [Rib 15], including Tap Delay Line (classic and channel re-sampling approaches) and Clustering techniques. The conclusion also recommends the use of the Clustering technique to conserve the pseudo-range error.

- **Parametric methods :**

As it was already mentioned in section 3.1, the SAGE algorithm has been used in [Garc 10] to minimize two cost functions (to conserve the channel and signal autocorrelation functions). These reduction methods have been applied to a reference scenario computed using the channel model [ITU 13] (low number of multipaths compared to this thesis). The pseudo-range error caused on a DLL-based HW GNSS receiver has been computed on the original channel and on both reduced ones in BOC(1,1) modulation. The result of this study showed that both pseudo-range error and Doppler error are better preserved in the case where SAGE is applied to the channel autocorrelation than to the signal autocorrelation. This result validates the choice of implementation of SAGE on the channel autocorrelation function preservation which was made in chapter 3.

It must be mentioned that [Ait 11] also investigated the impact of the channel reduction using the SAGE algorithm on the pseudo-range error preservation. Note that in that case, SAGE was tuned to estimate the reduced multipath channel in the delay, Doppler and AoA (*Angle of Arrival*) dimensions. This method was applied to the same reference scenario as the one used for the Tap Delay Line channel model presented previously. It was concluded in [Ait 11] that SAGE allowed a good pseudo-range and Doppler error preservation in the case of conventional DLL/PLL GNSS receiver as well as CBF. However, no direct comparison with the Tap Delay Line model was performed.

- **Statistical methods :**

The performance of the CRIME approach in terms of pseudo-range error preservation was also investigated in [Schu 14]. In that case, the CRIME statistical method was applied to a channel model synthesized using the approach of [ITU 13]. Therefore, the original number of multipaths has the magnitude of several tens of echoes. The original and reduced channel pseudo-range error was computed using a standard DLL (*Delay-Locked-Loop*) considering a BPSK signal. This simulation was run with and without additional Gaussian noise to the correlator outputs. However, those results were not compared to other reduction methods, preventing an objective comparison with other methods.

- **Synthesis:**

Some literature works already investigated the performance of the different reduction approaches considered in this thesis. However, the overview presented in this sub-section shows that those assessments were usually performed considering the reduction methods individually (no comparison with one-another), on different channel models and considering different GNSS receivers. Therefore, this chapter will aim at:

- Applying the different reduction approaches to a single reference scenario, computed by a single channel model (SCHUN).
- Comparing their performance according to the tracking error preservation considering a single DLL/PLL GNSS receiver model.

5.2. Implementation of the reference scenario

5.2.1. Definition of the environment

The environment implemented to support the comparison of the different methods has been illustrated on the left plot of Fig. 5.1. The receiver is moving along a straight line (y-axis) parallel to a continuous row of buildings, at the speed 5 m.s^{-1}. Different azimuths α and elevations β of the emitter satellite will be considered during the comparison. They will highlight the possible influence of the angle of arrival on the performance of the methods. The reference axes defining the elevation and azimuth angles have been represented on the middle plot of Fig. 5.1. The azimuths α have been chosen such that the impinging wave reaches the receiver from the right side, that is to say -90°$<\alpha<$90°. The considered azimuths are $\alpha=$-30°, 0°, 30° and 60°. They will be associated to the elevations $\beta=$35° and 65°. The buildings are composed of the facades referred to as façade A and façade B in section 2.2.

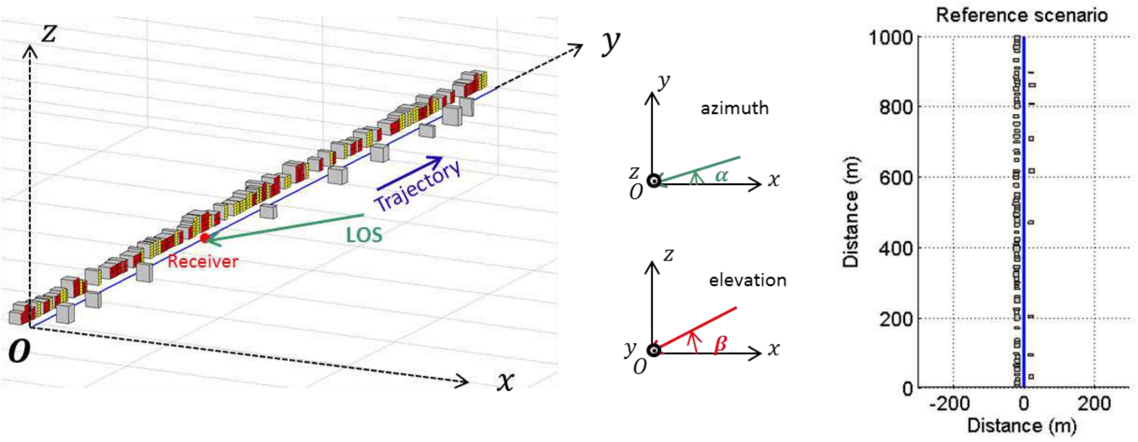

Figure 5.1: Illustration of the reference scenario

As it can be observed, a few isolated buildings have been disposed along the opposite row. Depending on the elevation and azimuth of arrival of the signal, they obstruct the signal on different segments of the trajectory, creating NLOS segments. Note that a simple ON/OFF signal blockage is considered (-20 dB of direct path power if the LOS signal is masked).

The impinging wave is supposed to be RHCP polarized, as any signal from the GPS constellation. Moreover the incoming signal is GPS L1 C/A, BPSK(1) modulated.

The influence length of the multipaths have been set to 50 m. Note that with a BPSK modulated signal, the multipaths with delays $\tau < T_c + C_S/2$ relatively to the LOS delay have an impact on the pseudo-range error [Misr 05]. With $C_S = 1$ chip, it concerns multipaths until approximately 450 m far from the receiver. However, such influence lengths would lead to large impulse responses. It has been chosen to limit the influence length to 50 m in order to limit the computational effort to realize the comparison, even if the environment influence on the pseudo-range error becomes less realistic.

5.2.2. Channel sampling frequency

The channel impulse response has to be generated often enough so that the channel can be considered coherent between two consecutive snapshots. In order to fulfil this statement, the channel coherency time T_{coh} has been investigated. In order to evaluate this distance of correlation, the channel narrow-band autocorrelation function has been computed. It has been considered that the channel can be considered as coherent as long as the normalized autocorrelation function has not decreased by more than 3 dB in magnitude [Skla 97]. Such a study has already been performed in the wide-band channel modeling context using SCHUN in [Rib 15]. This study concluded in a length of 2.5 cm of channel coherency, which is to say $\lambda/7$ (λ representing the carrier wavelength). However, the environment considered in [Rib 15] was different from the reference scenario of this thesis. Therefore, it has been decided to assess the coherency length of the reference channel of the current study. To do so, the reference channel has been computed by SCHUN at a high frequency (10 kHz to guarantee the coherency) and the narrow-band channel autocorrelation function has been plotted in order to identify the distance at which it goes below -3 dB. Note that only the multipath correlation is of interest in this thesis. Therefore, only the multipath channel autocorrelation function is investigated, excluding the LOS component.

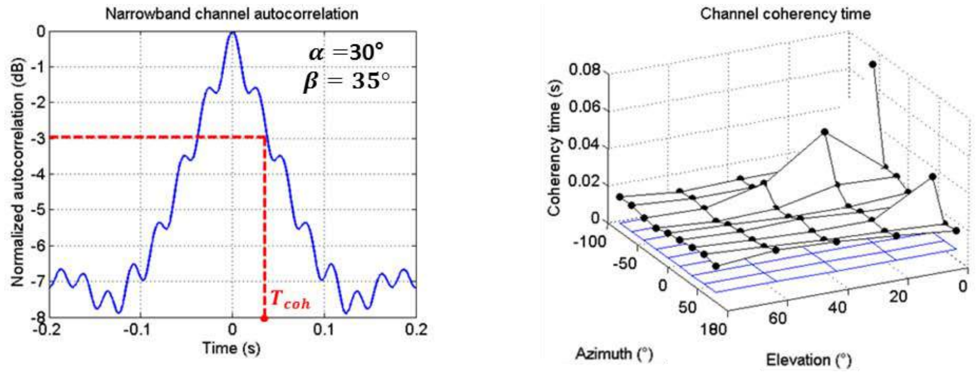

Figure 5.2: Autocorrelation function of the channel (on the left) and coherency time in terms of elevation and azimuth of the incoming signal

The left plot of Fig. 5.2 represents the multipath channel autocorrelation function module along 200 ms, corresponding to azimuth 30° and elevation 35°. In that case, the coherency time is $T_{coh} = 25$ ms, as illustrated in red. It corresponds approximately to $\lambda/2$ considering a speed 5 m.s^{-1}, which is consistent with the theory [Skla 97]. However, the narrowband channel is dependent on the azimuth and elevation of the incoming signal. Therefore, the reference scenario has been computed for different satellite azimuths ($\alpha = \pm 80°$, $\pm 60°$, $\pm 40°$, $\pm 20°$ and 0°) and elevations (β= 0°, 20°, 40°, 60°, 80°) and the corresponding coherency times have been represented on Fig. 5.2 in black dots. The blue grid represents 5 ms coherency time. It can be observed that no signal angle of arrival lead to less than 5 ms coherency time. Therefore, 5 ms may be chosen as the channel sampling period comfortably. Thus, the channel parameters have been computed every 5 ms for the following study, that is to say 200 Hz sampling frequency.

5.3. Open loop discriminator error conservation

First, only the impact on the receiver discriminator error will be investigated. The discriminator error denotes the S-curve deviation caused by the multipaths. Therefore, it can be considered as an open loop error assessment, as no tracking loop is considered. In other terms, the discriminator error corresponding to a given impulse response sample is computed independently from other impulse response samples. The absolute difference between the discriminator error caused by the original channel and the different reduced ones will constitute the comparison set of this section. In the following, it will be referred to as discriminator error difference.

First, sub-section 5.3.1 will detail the computing of the discriminator error caused by a given impulse response snapshot. Sub-section 5.3.2 will show the comparison of the reference and reduced channels in terms of discriminator error preservation, for different signal azimuths and elevations. Finally, sub-section 5.3.3 will investigate the influence of the number of multipaths in the reduced channel on the comparison results.

5.3.1. Open loop discriminator error estimation

The open loop discriminator error denotes the delay between the incoming signal and the local replica for which the discriminator equals 0 (zero of the S-curve). If there is no multipath, this delay is 0. Because of the distortion of the channel autocorrelation function by the multipath channel, this delay is shifted, and this delay shift denotes the pseudo-range error. This sub-section focusses on the discriminator error without considering the tracking and filtering of the DLL along time (open loop error). Therefore, the discriminator error will be considered for each impulse response sample independently (no loop effect). Two correlators are considered, corresponding to the correlation of the incoming signal with an early and a late replica. An EMLP (*Early Minus Late Power*) discriminator has been considered. Eq. 5.1 displays the expression of the EMLP discriminator D in function of the early and late correlator outputs I_e and I_l expressed in Eq. 5.2.

$$D(\tau) = |K_e|^2 - |K_l|^2 \tag{5.1}$$

$$\begin{cases} K_e = R_{s,c*s}(\tau - \frac{C_s}{2}) \\ K_l = R_{s,c*s}(\tau + \frac{C_s}{2}) \end{cases} \tag{5.2}$$

Where :

- $R_{s,c*s}$ denotes the complex correlation function of the incoming signal with the local replica (expressed in Eq. 3.4).
- C_s denotes the chip spacing between the early and late replica.

$D(\tau)$ conctitutes the S-curve as it was already mentioned. If only the LOS contribution reaches the receiver (no multipath), $D(\tau) = 0$ corresponds to $\tau = 0$. As the multipaths distort the channel autocorrelation function, they distort the S-curve as well. The solution of the equation $D(\tau) = 0$ is shifted and the discriminator error p_{de} is given by :

$$p_{de} = c\tau \tag{5.3}$$

Where:

- c denotes the speed of light.
- τ is the solution to the equation $D(\tau) = 0$.

Fig. 5.3 illustrates the distortion of the autocorrelation function caused by the multipath channel (with 3 echoes in the impulse response). The right plot illustrates the resulting distortion of the S-curve, leading to the discriminator error. Note that the discriminator output is normalized on the right plot.

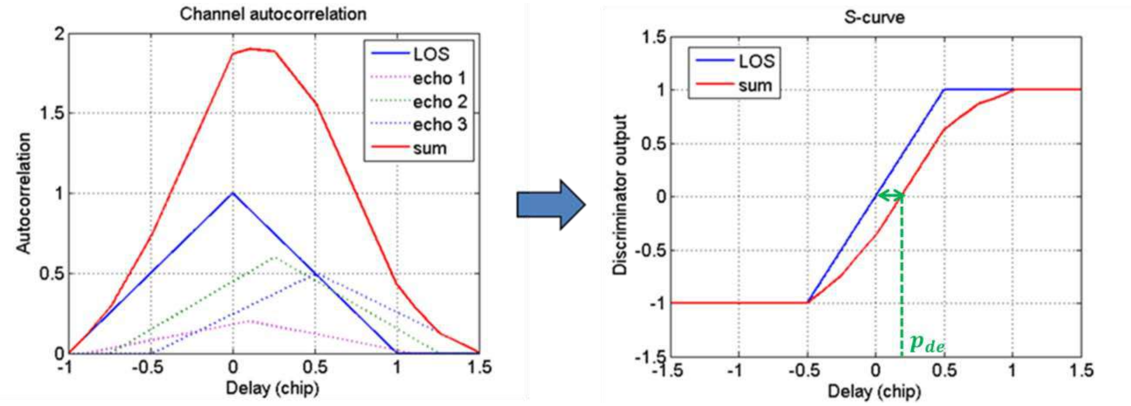

Figure 5.3: Illustration of an autocorrelation function distortion by a multipath channel and of the resulting S-curve

It can be shown that the discriminator error at a given time depends on the channel parameters according to Eq. 5.4, in the case of a BPSK modulated signal with an infinite bandwidth. The different steps of this computation can be found in *Annex B* and has been detailed and validated in [Rib 16a].

$$\begin{cases} p_{de} = c \; * \; \dfrac{\sum_{l=1}^{L} {\Gamma_l}^2 \tau_l + \sum_{i<j=1}^{L} \Gamma_i \Gamma_j \, cos\left(\Phi_i - \Phi_j\right) \left(\tau_i + \tau_j\right)}{\sum_{i,j=1}^{L} \Gamma_i \Gamma_j \, cos\left(\Phi_i - \Phi_j\right)} \\ \Gamma_l = \dfrac{\gamma_l}{\gamma_{LOS}} sinc(\pi(\vartheta_l - \vartheta_{LOS})T_{int}) \\ \Phi_l = \varphi_l - \varphi_{LOS} \end{cases} \tag{5.4}$$

In Eq. 5.4:

- The channel is composed of L paths including the LOS and multipaths.
- $(\tau_l, \gamma_l, \varphi_l, \vartheta_l)$ denote the delay, amplitude module, phase and Doppler of the path l.
- T_{int} is the integration time of the autocorrelation function. In this study, it has been set to T_{int} =1 ms.

Note that the formula of Eq. 5.4 is valid if and only if the assumption Eq. 5.5 is fulfilled. This study was conducted with $C_s = 1$ chip and considering only the influence of the scatterers located 50 m far from the receiver. Therefore, it has been assumed that this assumption has a strong probability to be satisfied (>99.9%), as it has been estimated in Annex B.

$$|p_{de} - \tau_l| < \min\left(\frac{Cs}{2}, T_c - \frac{Cs}{2}\right), \quad \forall\, l \tag{5.5}$$

5.3.2. Discriminator error for the different angles of arrival

Fig. 5.4 illustrates the discriminator error caused by the reference channels all along the [250 m, 500 m] segment of the trajectory. The different azimuths considered have been represented on the different plots. The blue curves represent 35° emitter elevation and the red curved the 65° elevations. A few differences can be noticed, depending on the signal angle of arrival. The following paragraphs aim at giving explanations to such observations.

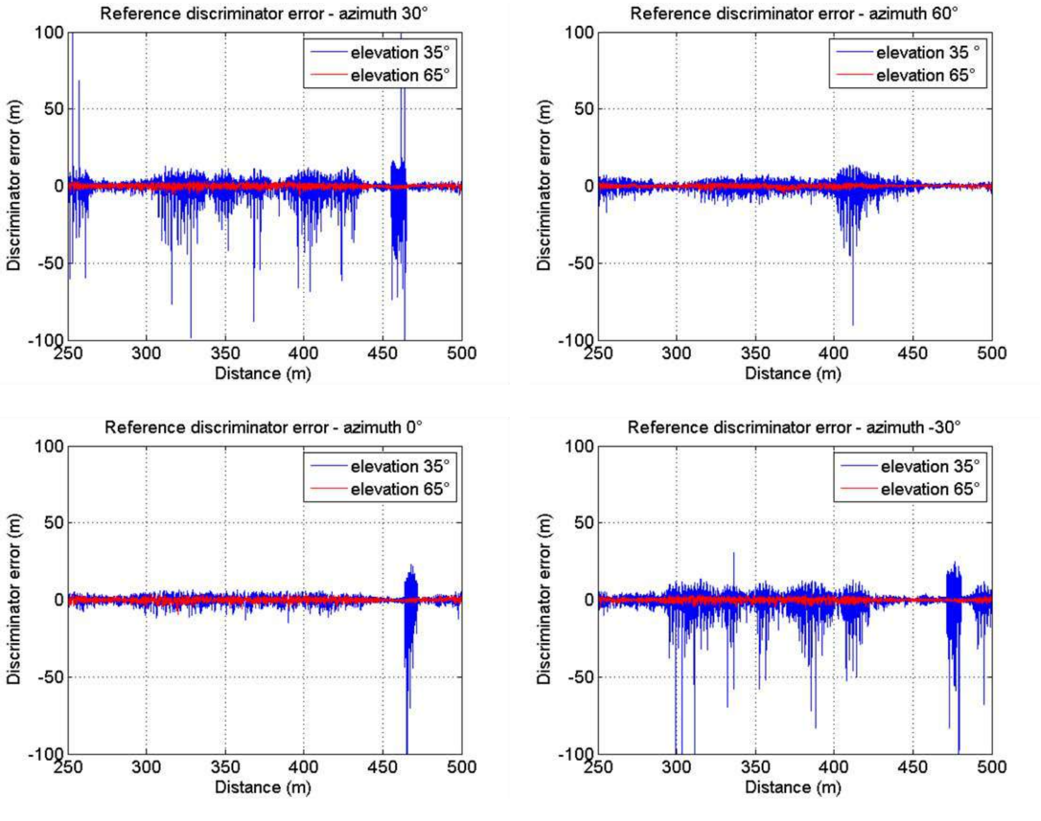

Figure 5.4: Discriminator error along the [250m,500m] of the trajectory for different angles of arrival

- **Impact of the elevations :**

It can be observed on each plot that there is a strong difference between 35° and 65° elevations. Indeed, 65° elevations lead to smaller discriminator errors. There are two explanations to that:

- First, at 65° elevations, the signal is not obstructed by the buildings. Therefore, there is no NLOS segments, which limits the discriminator error. However, at 35° elevation, the signal is masked by the fourth building of the trajectory, located at the distance d=460 m. Strong discriminator errors can be observed on azimuths 30°, 0° and -30° at this location. The NLOS condition increases the power of the multipaths with respect to the direct path, leading to stronger discriminator errors.

- Secondly, the elevation of the incoming signal defines the scattering profile of the specular and backscattering facets [Ait 13]. For high elevations, the receiver is more distant from the principal power lobes than for low elevations. It results in a lower multipath power, especially concerning the specular and backscattering contributions.

- **Impact of the azimuths :**

It can also be observed on Fig. 5.4 that the azimuths have an impact on the discriminator error (for a given elevation). The channels corresponding to 30° and -30° azimuths appear to have similar discriminator errors, which can be explained by the symmetry of those scenarios. However, both 60° and 0° azimuths lead to a lower discriminator error.

- In the case of 0° azimuth, the signal impinges the buildings perpendicularly to the facades. Therefore, no backscattering multipaths are emitted. In the case of a RHCP polarized waves, the backscattering multipaths have a major influence on the impulse response as it was explained in section 2.2. Therefore, the power of the multipath channel is globally reduced and the discriminator error is lower.

- In the case of 60° azimuth, the signal impinges the buildings with a strong incidence angle. It is mentioned in [Ait 13] that the orientation in the horizontal plane of the backscattering facets depends on the emitter azimuth. Therefore, the receiver is more distant from the principal power lobes of the scattering profile of the backscattering facets (specular direction). This leads to a lower overall power of the channel, and thus to lower discriminator errors.

5.3.3. Comparison of the reduction methods according to the open loop discriminator error preservation

This section investigates the impact of the reduction methods on the open loop discriminator error of the receiver. The reduction methods listed in section 5.1.1 have been applied to the reference scenario presented in section 5.1.2. A few remarks can be made before presenting the comparison results.

- First, the channel impulse response depends on the azimuth and elevation of the emitter satellite. Especially, the angle of arrival of the incoming signal has a strong impact on the shadowing of the direct path. Also, the LOS has a strong impact on the discriminator error. Therefore, eight different angles of arrival have been tested and the results of the discriminator error comparison will be presented in function of the azimuth and elevation of the emitter.

- Secondly, the Clustering and SAGE techniques are fully deterministic, meaning that two different realizations of the algorithm lead to the exact same reduced channel. However, the statistical method involves a stochastic process as presented in chapter 4, using the *RNG*. As a consequence, two realizations of the algorithm lead to different reduced channels and thus, different discriminator errors.

- The open-loop error does not directly denote the pseudo-range error of a real receiver, as it bypasses the DLL and PLL tracking loops. This study does not focus on the absolute value of the discriminator error but on the comparison of the discriminator errors of the different reduced channel models.

Fig. 5.5 illustrates the comparison between the different reduced channels with the original one, depending on the emitter azimuths α and elevations β. The results have been presented as the cumulative distributions of the absolute difference between the discriminator error of the original channel and of the reduced ones in logarithmic scale. Tab. 5.1 presents the mean (M), standard deviation (STD), 95th and 99th percentiles (95P and 99P) of these distributions.

Table 5.1 : Mean (M), Standard deviation (STD), 95th and 99th percentiles (95P and 99P) of the distributions of the discriminator error difference with the reference channel

$\alpha = -30^\circ$	$\beta = 35^\circ$				$\beta = 65^\circ$			
	M	STD	P95	P99	M	STD	P95	P99
Clustering	0.46 m	1.6 m	1.5 m	4.9 m	0.14 m	0.11 m	0.37 m	0.52 m
SAGE	0.32 m	0.88 m	1.0 m	2.9 m	0.085 m	0.080 m	0.24 m	0.36 m
Statistic	1.4 m	4.8 m	4.9 m	14 m	0.27 m	0.36 m	0.71 m	1.2 m

$\alpha = 0^\circ$	$\beta = 35^\circ$				$\beta = 65^\circ$			
	M	STD	P95	P99	M	STD	P95	P99
Clustering	0.30 m	1.0 m	0.80 m	3.0 m	0.14 m	0.12 m	0.37 m	0.54 m
SAGE	0.24 m	0.72 m	0.67 m	2.4 m	0.095 m	0.088 m	0.26 m	0.40 m
Statistic	0.82 m	2.5 m	2.4 m	8.2 m	0.32 m	0.42 m	0.88 m	1.6 m

$\alpha = 30^\circ$	$\beta = 35^\circ$				$\beta = 65^\circ$			
	M	STD	P95	P99	M	STD	P95	P99
Clustering	0.36 m	0.86 m	1.1 m	2.9 m	0.13 m	0.11 m	0.37 m	0.53 m
SAGE	0.28 m	0.66 m	0.88 m	2.4 m	0.087 m	0.081 m	0.25 m	0.37 m
Statistic	1.2 m	3.2 m	4.1 m	12 m	0.29 m	0.40 m	0.76 m	1.4 m

$\alpha = 60^\circ$	$\beta = 35^\circ$				$\beta = 65^\circ$			
	M	STD	P95	P99	M	STD	P95	P99
Clustering	0.25 m	0.64 m	0.72 m	1.4 m	0.12 m	0.099 m	0.31 m	0.44 m
SAGE	0.24 m	0.50 m	0.71 m	1.3 m	0.067 m	0.064 m	0.18 m	0.28 m
Statistic	1.7 m	3.0 m	5 m	10 m	0.22 m	0.49 m	0.58 m	1.0 m

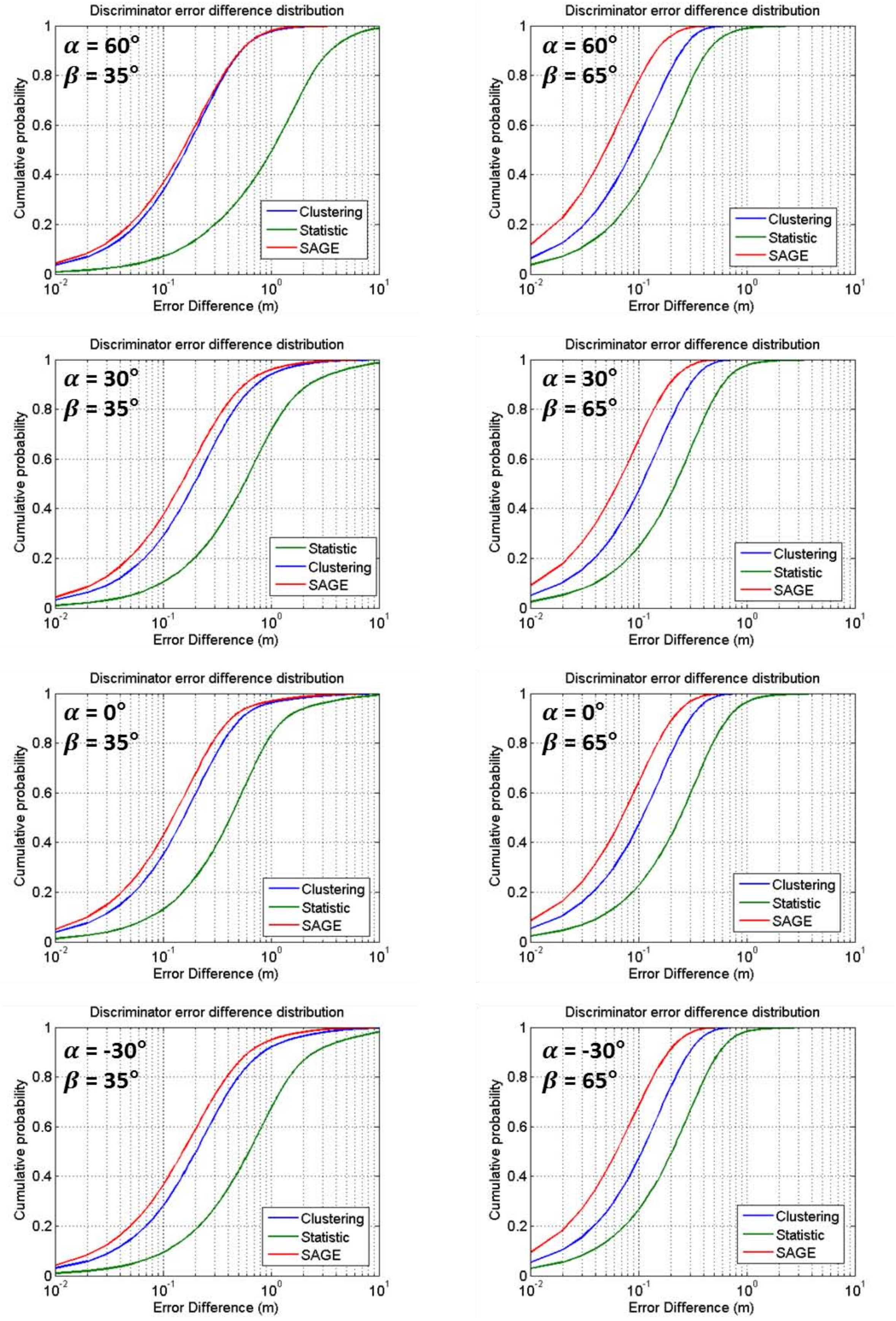

Figure 5.5: Cumulative distribution of the difference between the reference and reduced channel discriminator errors for different emitter azimuths $\boldsymbol{\alpha}$ and elevations $\boldsymbol{\beta}$

Three major conclusions can be drawn from the comparison presented on Fig. 5.5 and Tab 5.1:

- First, a clear hierarchy of the three reduction methods can be established, according to the discriminator error preservation. Every angle of arrival configuration shows the best discriminator error preservation by the SAGE method. Such a result could be expected, being given the fact that SAGE optimizes the preservation of the multipath channel autocorrelation function, which defines the discriminator error.

In second position comes the Clustering technique, whose performance is close to the performance of SAGE in some configurations, like ($\alpha = 60°$,$\beta = 35°$) for example.

To the contrary, the statistical method systematically has the worst performance. Moreover, in some configurations like ($\alpha = 60°$,$\beta = 35°$) for example, its performance is far from the performance of the Clustering and SAGE.

Note that these results are confirmed by the mean difference, 95th and 99th percentiles of the distributions. As a consequence, this study allows establishing a clear ranking of the reduction methods according to the open loop discriminator error preservation: **1°) SAGE** (parametric method), **2°) Clustering** (aggregation method) and **3°) Statistical** method.

- It is reminded that the statistical method is non-deterministic, thus its performance can vary from realization to realization. However, all eight realizations revealed the lower performance of the statistical method. Then, it can be considered that the ranking displayed in the previous paragraph is always valid.

- To finish, it appears that the performance of SAGE and the Clustering technique are closer in $\beta = 35°$ elevation configuration than $\beta = 65°$. This result will be confirmed and clarified in section 5.6.

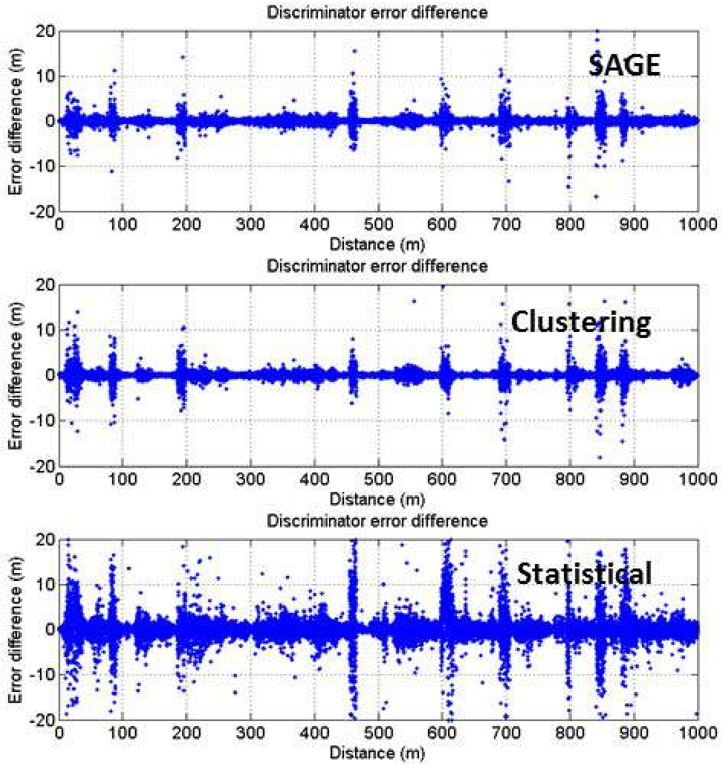

Figure 5.6: Time series of the difference between original and reduced discriminator open loop errors for $\boldsymbol{\alpha} = 30°$,$\boldsymbol{\beta} = 35°$

Fig. 5.6 represents the time-series of the difference between the open loop discriminator error of the reference and reduced channels, for the different reduction methods in the case of $\alpha = 30°$, $\beta = 35°$. The three plots of Fig. 5.7 all represent the discriminator error of the reference channel in grey with the same azimuth and elevation. The red, blue and green curves represent the samples corresponding to the 5% largest difference between original and reduced channel discriminator error, for the SAGE, Clustering Weighted and statistical methods. It can be observed that the large differences correspond to large discriminator errors of the reference channel (Fig 5.6), for all three methods.

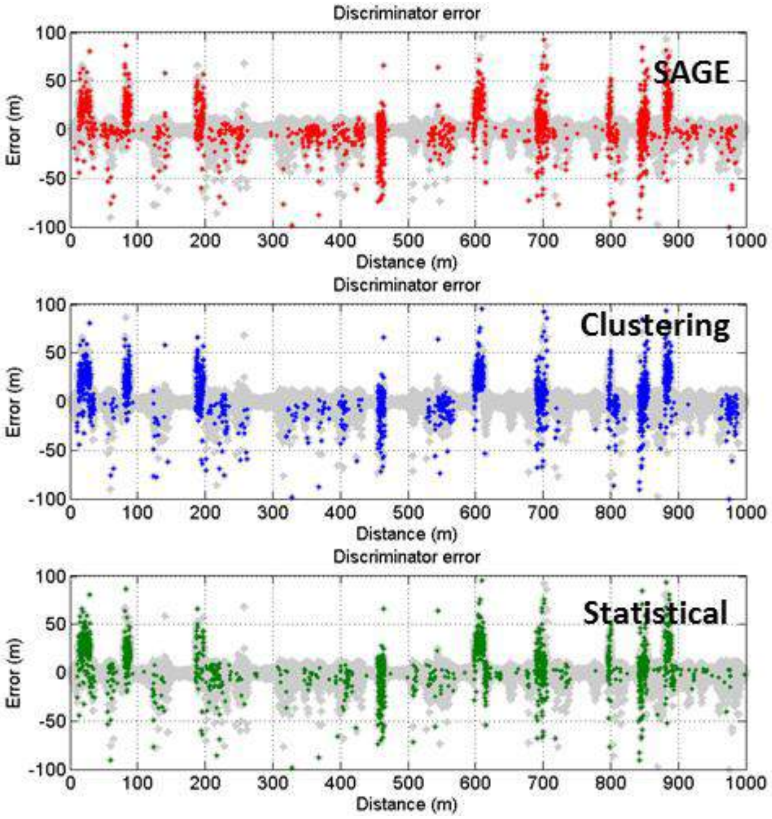

Figure 5.7: Reference channel discriminator error with highlight on the 5% largest difference samples

5.3.4. Influence of the number of multipaths in the reduced channel

This section will highlight the influence of the number of multipaths in the reduced channel on the performance of the reduction methods in terms of discriminator error preservation. To do so, the three methods have been applied to the same reference channel as in the previous sub-section, in the angle of arrival configuration ($\alpha = 0°$,$\beta = 35°$). The number of multipaths in the reduced channel has been set successively to 3, 5, 8 and 10 multipaths. Fig. 5.8 illustrates the cumulative distributions of the difference between the reference channel and the reduced channels discriminator errors. Tab. 5.2 records the mean (M), standard deviation (STD), 95th (P95) and 99th (P99) percentile associated to the distributions of Fig. 5.8.

The difference between the performance of the different methods seem to vary with the number of multipaths in the reduced channel:

- First, the difference between SAGE and the Clustering technique tends to decrease with the augmentation of the number of multipaths estimated. The 3-multipath reduced channel shows an obvious advantage of the SAGE model. This advantage is still observable with 5 multipaths. However, with 8 and 10 multipaths, no more difference can be observed between the SAGE and Clustering channels according to the discriminator error preservation. This is due to the fact that the performance of the Clustering increases faster than the performance of SAGE with the number of multipaths.

- The performance of the Statistical method do not increase with the number of multipaths. This is a constraint of this method insofar as the discriminator error preservation cannot be improved by increasing the number of multipaths.

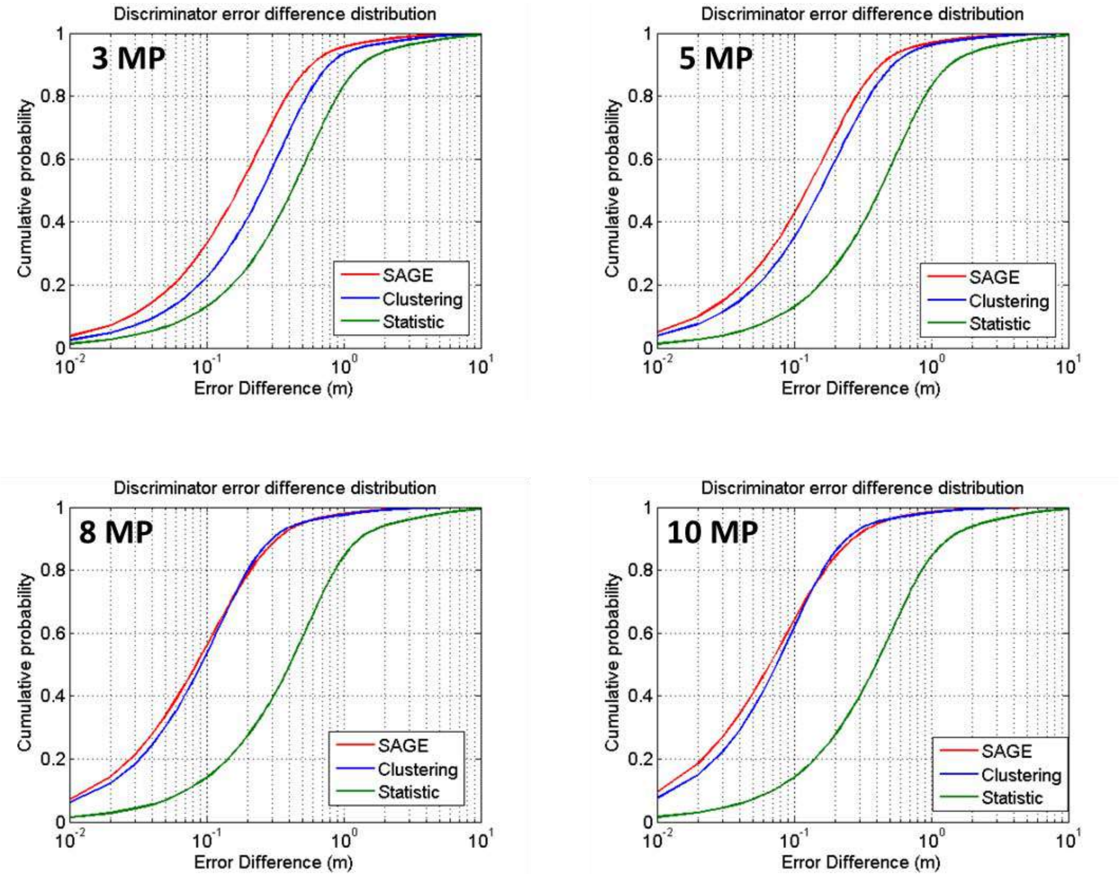

Figure 5.8: Cumulative distribution of the difference between the reference and reduced channel discriminator errors for different numbers of multipaths in the reduced channel

Table 5.2 : Mean (M), Standard deviation (STD), 95th and 99th percentiles (95P and 99P) of the distributions of the discriminator error difference with the reference channel for 3, 5, 8 and 10 MP

3 MP

	M	STD	P95	P99
Clustering	0.47 m	1.4 m	1.2 m	4.7 m
SAGE	0.45 m	0.91 m	0.90 m	3.2 m
Statistic	0.80 m	2.5 m	2.3 m	7.8 m

5 MP

	M	STD	P95	P99
Clustering	0.30 m	1.0 m	0.80 m	3.1 m
SAGE	0.24 m	0.72 m	0.67 m	2.4 m
Statistic	0.82 m	2.6 m	2.4 m	8.2 m

8 MP

	M	STD	P95	P99
Clustering	0.18 m	0.64 m	0.50 m	1.9 m
SAGE	0.17 m	0.48 m	0.51 m	1.8 m
Statistic	0.79 m	2.7 m	2.4 m	7.8 m

10 MP

	M	STD	P95	P99
Clustering	0.15 m	0.97 m	0.38 m	1.4 m
SAGE	0.14 m	0.46 m	0.42 m	1.4 m
Statistic	0.78 m	2.3 m	2.4 m	7.6 m

5.3.5. Synthesis on the preservation of the open loop discriminator error

The discriminator error has been computed on the reference and reduced channels. First, the discriminator error preservation of the different methods has been investigated with 5 multipaths in the reduced channel in section 5.3.3. All the different tested azimuth and elevation configurations of the incoming signal gave the same comparison results: the SAGE method allowed the best discriminator error preservation, followed by the Clustering technique which has close performance. To the contrary, the statistical method systematically shows the worst performance.

Section 5.3.4 modulated the results of the previous sub-section. Indeed, it was shown that the difference between the performance of SAGE and Clustering tended to disappear with the augmentation of the number of multipaths in the reduced channel. From 8 multipaths, no more difference could be observable. It showed that the hierarchy established in section 5.3.3 is preserved with less than 5 multipaths but can change with more than 5 multipaths. It was also showed that the statistical technique performance do not increase with the number of multipaths.

These results only investigated the impact of the reduction methods on the receiver “open loop” pseudo-range error. They have to be consolidated by the investigation of the tracking error preservation in the following section.

5.4. Tracking error conservation

In this section, the preservation of the tracking error of a receiver simulator will be investigated. To do so, the original and reduced multipath channels will be used to compute the tracking error along the reference scenario, using a GNSS receiver simulator, referred to as “GeneIQ” in the following. Then the tracking error conservation will be compared with different azimuths and elevations of the signal and various numbers of multipaths in the reduced channel.

5.4.1. Presentation of the GeneIQ software receiver

GeneIQ is a realistic software receiver developed by ENAC (*Ecole Nationale de l’Aviation Civile,* Toulouse*,* France) [BROC 14]. It consists in modelling the correlator outputs of the DLL/PLL tracking loops. The In-phase (I) and Quadrature (Q) components of the correlators are simulated with respect to the parameters of the multipaths of the LMS channel, and the parameters of the local replica. Eq. 5.6 details the calculation of the prompt correlators I and Q at the instant k. The channel is sampled at the frequency $1/T_s$.

$$\begin{cases} I_P(k) = \sum_{l=1}^{L} \frac{\gamma_l(k)}{2} d\,.\,r(\tau_l(k) - \hat{\tau}(k))\,.\,sinc(\pi(\vartheta_l(k) - \hat{\vartheta})T_s)\,.\cos(\varphi_l(k) - \hat{\varphi}(k)) \\ Q_P(k) = \sum_{l=1}^{L} \frac{\gamma_l(k)}{2} d\,.\,r(\tau_l(k) - \hat{\tau}(k))\,.\,sinc(\pi(\vartheta_l(k) - \hat{\vartheta})T_{int})\,.\sin(\varphi_l(k) - \hat{\varphi}(k)) \end{cases} \tag{5.5}$$

Where:

- d is the value of the bit of the navigation message.
- $(\tau_l, \gamma_l, \varphi_l, \vartheta_l)$ are the delay, amplitude, phase (in the center of the correlation interval) and Doppler shift of the path l (including direct path).
- $(\hat{\tau}, \hat{\gamma}, \hat{\varphi}, \hat{\vartheta})$ are the delay, amplitude, phase and Doppler shift of the local code replica.
- $r(\tau)$ is the correlation function of the PRN code (taking into account the signal modulation and the RF front-end filter).
- T_{int} is the integration time used to compute the correlator outputs.

Many parameters of GeneIQ are tunable in order to reproduce as accurately as possible the behavior of a real receiver. Some of the major possibilities are mentioned hereafter.

First, additional Gaussian noise can be added to the correlator outputs, with a specified C/N0 level. The correlator outputs are filtered in time by PLL, FLL and DLL, with tunable equivalent loop bandwidth. It is possible to choose the modulation of the received signal and local replica (BPSK, BOC and CBOC) as well as the RF bandwidth of the receiver. To finish, the code delay of the signal is estimated using 'EMLP' or 'DP' (*Dot Product*) discriminator and the signal carrier phase is tracked using 'Arctangent' or 'Costas' in the case of a PLL and 'Differential Arctangent', 'Dot Cross' and 'Cross Product' in the case of an FLL. Some of these configurations will be modified along this chapter in order to investigate their impact on the comparison results.

5.4.2. Tracking error for the different angles of arrival

Table 5.3 : Configuration of the GNSS receiver GeneIQ

Parameter	Value
Modulation	BPSK(1)
DLL loop order	2
DLL loop bandwidth	1 Hz
DLL discriminator	'Early Minus Late power'
FLL loop order	2
FLL loop bandwidth	2 Hz
FLL discriminator	'Differential Arctangent'
Integration time	5 ms
RF bandwidth	10 MHz
Noise ON/OFF	'OFF'

The receiver GeneIQ has been used to compute the tracking error all along the trajectory on the reference scenario. The GPS L1 C/A signal has been chosen to test the pseudo-range error. A second order DLL has been used to compute the code error with 1 Hz loop bandwidth and an EMLP discriminator with C_S = 1 chip, in order to increase the impact of the multipaths on the DLL and challenge the reduction methods the most. A second order FLL has been used to track the carrier frequency with 2 Hz loop bandwidth with a '*Differential Arctangent'* discriminator. The RF bandwidth of the receiver has been set to 10 MHz. In a first time, no noise has been added to the correlator outputs in order to consider only the impact of the multipaths on the tracking error. Those parameters are summed up into Tab. 5.3.

Fig. 5.9 illustrates the DLL tracking error of the receiver all along the 1 km trajectory of the scenario. First, the NLOS segments of the different profiles are clearly identifiable by the high absolute pseudo-range error zones. It can be verified on Fig. 5.1 that those sharp peaks correspond to the presence of the buildings on the trajectory. In 35° elevation, the azimuths -30°, 0° and 30° are strongly affected by these LOS masking. However, the 60° azimuth angle is high enough to keep a clear LOS on most of the trajectory. Finally, at 65° elevation, the receiver is always in clear LOS conditions, due to the high elevation angle as compared to the height of the buildings. From a general point of view, the conclusions of section 5.3.2 concerning the open loop discriminator error are respected:

- For a given azimuth, the tracking error envelope is larger with 35° elevation than with 65° elevation, even in clear LOS zones.
- Azimuths 30° and -30° lead to larger tracking errors than 0° and 60°.

The reasons for those observations are the same as the ones of section 5.3.2 concerning the tracking error.

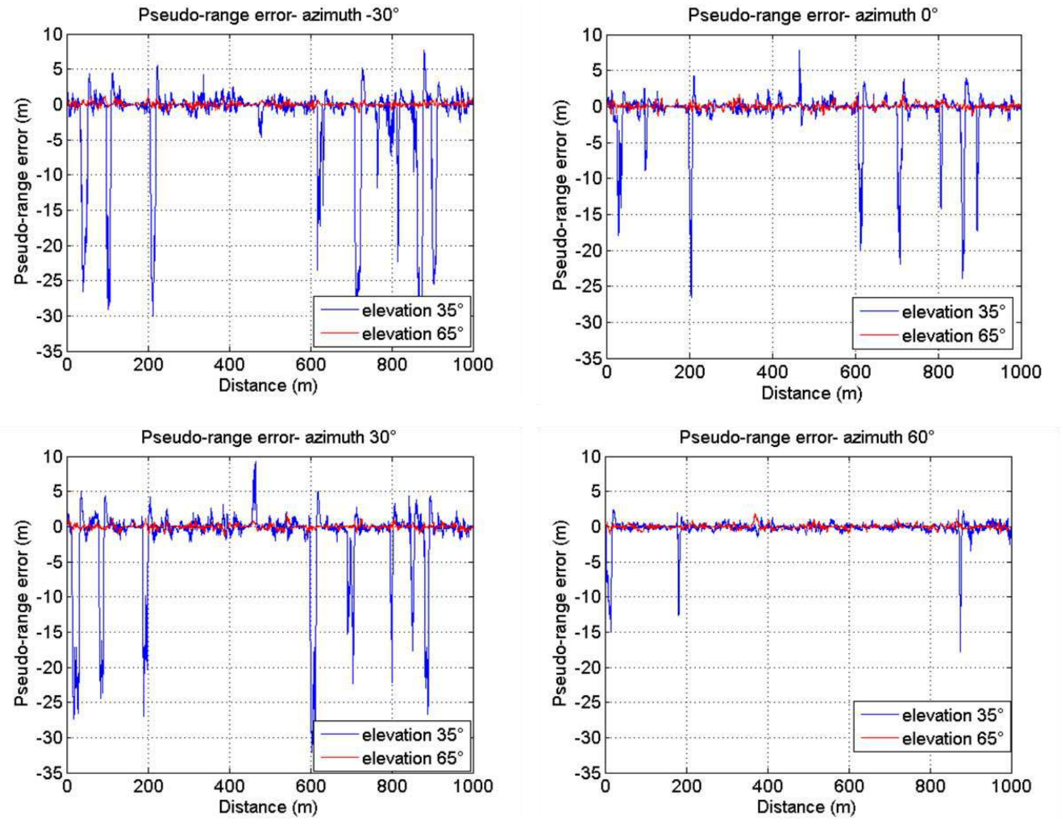

Figure 5.9: Tracking error of the receiver all along the trajectory for the different angles of arrival

5.4.3. Comparison of the reduction methods according to the tracking error preservation

The time series corresponding to the three reduced channel models considered in this chapter, as well as the reference channel have been used to compute the tracking error of the GeneIQ simulator along the trajectory. The number of multipaths in the reduced channels has been set to 5. The difference between the tracking error due to the reference channel and the reduced ones has been recorded for the different angles of arrival of the signal. Note that this study is similar to the one concerning the open loop discriminator error in section 5.3. Fig. 5.10 presents the cumulative distributions of the absolute difference between original and reduced channels tracking errors along the 1 km trajectory, for the different angles of arrival. It will be referred to as tracking error difference in the following.

It can be observed on Fig. 5.9 that the tracking error envelopes are low as compared to the discriminator errors in the previous section. This observation is due to the filtering of the correlator outputs by the DLL, which smooth the open loop error. This leads to low differences between original and reduced channel tracking errors, as it can be read in Tab. 5.4 (a few centimeters only).

It can also be mentioned that the simulations have been run without noise and mostly in clear LOS conditions. It contributes to lower the tracking errors. However, an advantage is the fact that only the multipath channel have an impact on the tracking errors. As a consequence, the tracking error differences displayed on Fig. 5.10 and Tab. 5.4 relate the only impact of the different channel models, isolated from any other parameter. Thus, this study should not focus on the absolute value of these differences but on their comparison. A more realistic configuration will be tested in section 5.5 (with additional Gaussian noise). The statistics recorded in Tab. 5.4 lead to two major comments:

- The comparison of the mean tracking error difference between the different reduced channels and the original one reveals a hierarchy among the reduction methods: **1°) SAGE** (parametric method), **2°) Clustering** (aggregation method) and **3°) Statistical** method. Moreover, this hierarchy is confirmed by the 95th and 99th percentiles. Indeed, the 95th percentile error of the SAGE model is lower than the one of the Clustering, which is lower than the one of the statistical model in every angle of arrival configuration. The same observation can be made concerning the 99th percentile.

- The performance of the SAGE and Clustering models are closer with 35° elevation than with 65°. This statement is conserved by both the mean difference and the 95th and 99th percentiles errors. It will be further investigated in section 5.6.

Those two last results tend to confirm those of the open loop discriminator error. Indeed, the same hierarchy among the methods has been established from the study of Tab. 5.1 (discriminator error) and 5.4 (tracking error). Moreover, in both cases it was observed that the performance of SAGE and the performance of the Clustering method tend to get closer with the decrease of the elevation. This statement proves that the open loop discriminator error is legitimate to assess the performance of the reduction methods. This statement is emphasized by the similarity between the tracking and discriminator errors computation (close code autocorrelation functions, same modulation and same DLL discriminator).

The analysis of the plots of Fig. 5.8 softens these results. Indeed, the distributions of the difference between original and reduced channels tracking errors show that the performance of the Clustering overcome the performance of SAGE in some configurations, like ($\alpha =$ -30°, $\beta =$ 35°), ($\alpha =$ 0°, $\beta =$ 35°) or ($\alpha =$ 30°, $\beta =$ 35°). In those cases, the cumulative probability of the clustering model is higher than the cumulative probability of the SAGE model, for low tracking errors. SAGE keeps an advantage on the Clustering concerning the bigger tracking differences, which explains the favorable statistics in Tab. 5.4. This statement was not observed on the open loop discriminator error in the previous section. It means that the DLL and PLL tracking loops have a slight impact on the comparison of the methods in some cases.

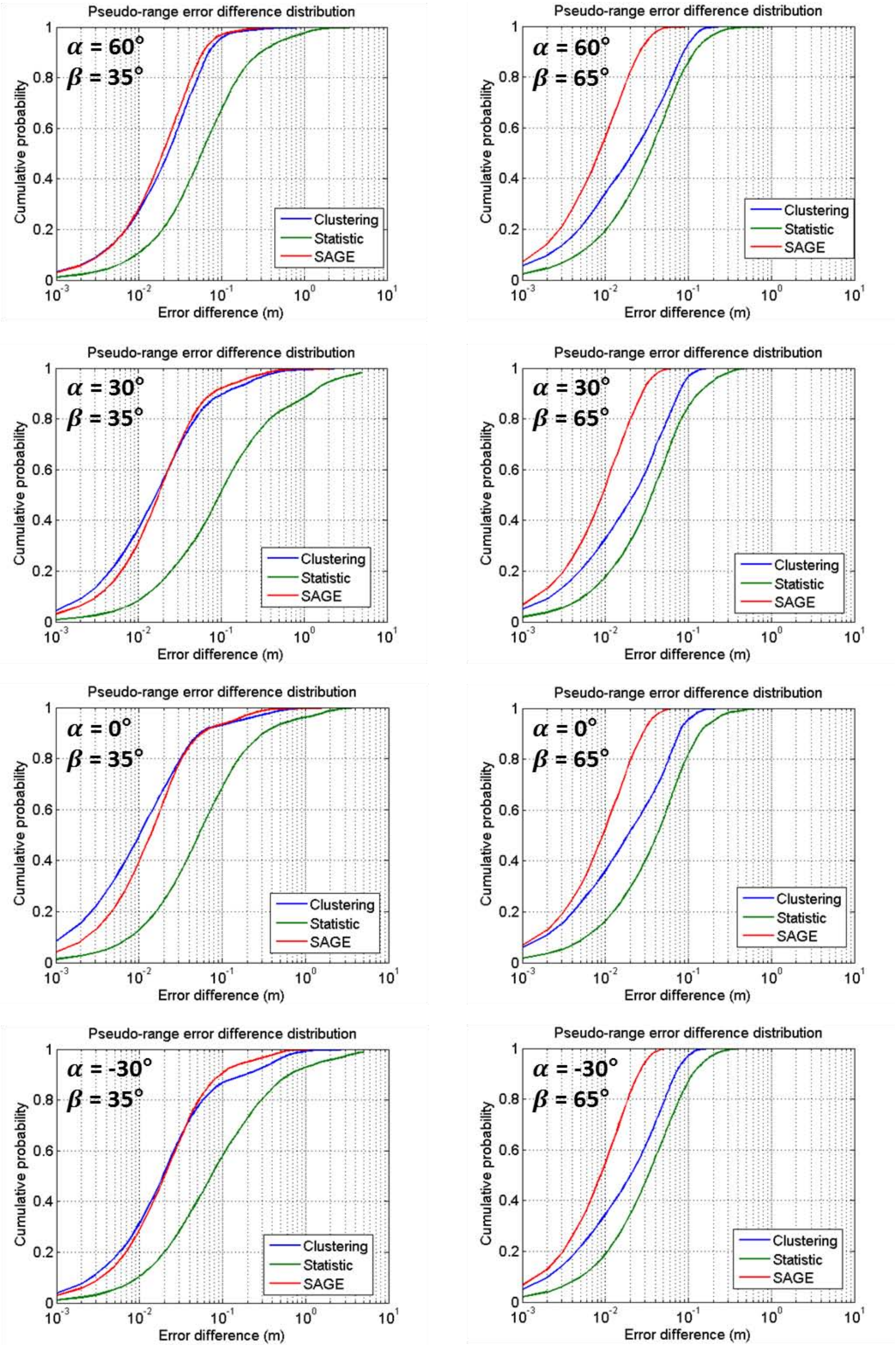

Figure 5.10: Cumulative distribution of the difference between the reference and reduced channel tracking errors for different emitter azimuths α and elevations β

Tab. 5.4 records the mean (M), standard deviation (STD), 95th and 99th percentile associated to the distributions of Fig. 5.10.

Table 5.4: Mean (M), Standard deviation (STD), 95th and 99th percentiles (95P and 99P) of the distributions of the discriminator error difference with the reference channel

$\alpha =$ -30°	**$\beta =$ 35°**				**$\beta =$ 65°**			
	M	STD	P95	P99	M	STD	P95	P99
Clustering	0.078 m	0.22 m	0.42 m	0.93 m	0.030 m	0.029 m	0.088 m	0.12 m
SAGE	0.049 m	0.10 m	0.20 m	0.53 m	0.011 m	0.010 m	0.031 m	0.043 m
Statistic	0.35 m	0.98 m	1.53 m	5.8 m	0.050 m	0.054 m	0.16 m	0.27 m

$\alpha =$ 0°	**$\beta =$ 35°**				**$\beta =$ 65°**			
	M	STD	P95	P99	M	STD	P95	P99
Clustering	0.036 m	0.10 m	0.16 m	0.57 m	0.031 m	0.034 m	0.097 m	0.14 m
SAGE	0.034 m	0.11 m	0.14 m	0.34 m	0.012 m	0.011 m	0.034 m	0.051 m
Statistic	0.16 m	0.39 m	0.71 m	2.3 m	0.063 m	0.077 m	0.20 m	0.42 m

$\alpha =$ 30°	**$\beta =$ 35°**				**$\beta =$ 65°**			
	M	STD	P95	P99	M	STD	P95	P99
Clustering	0.056 m	0.19 m	0.23 m	0.61 m	0.032 m	0.031 m	0.092 m	0.13 m
SAGE	0.046 m	0.14 m	0.17 m	0.47 m	0.012 m	0.011 m	0.034 m	0.048 m
Statistic	0.46 m	1.2 m	2.2 m	6.5 m	0.058 m	0.069 m	0.20 m	0.35 m

$\alpha =$ 60°	**$\beta =$ 35°**				**$\beta =$ 65°**			
	M	STD	P95	P99	M	STD	P95	P99
Clustering	0.036 m	0.064 m	0.095 m	0.27 m	0.035 m	0.038 m	0.11 m	0.15 m
SAGE	0.029 m	0.038 m	0.080 m	0.19 m	0.012 m	0.011 m	0.033 m	0.048 m
Statistic	0.14 m	0.31 m	0.57 m	1.4 m	0.054 m	0.071 m	0.16 m	0.31 m

5.4.4. *Influence of the number of multipaths in the reduced channel*

In order to investigate the impact of the number of multipaths in the reduced channel, the tracking error along the trajectory has been computed for different numbers of multipaths in the reduced channels (3, 5, 8 and 10 multipaths have been tested). This study is similar to the study of section 5.3.4, transposed to the study of the tracking error. The GNSS receiver simulator GeneIQ has been used for this simulation with the same configuration as the one recorded in Tab. 5.3. The scenario configuration corresponds to the case of ($\alpha = 0°$, $\beta = 35°$) angles of arrival.

Fig. 5.11 illustrates the cumulative distribution of the difference between original and reduced channel tracking errors. Each plot represents a different quantity of multipaths in the reduced channel. The Mean (M), standard deviation (STD), 95th (95P) and 99th (99P) percentiles associated to the distributions of Fig. 5.11 are recorded in Tab. 5.5.

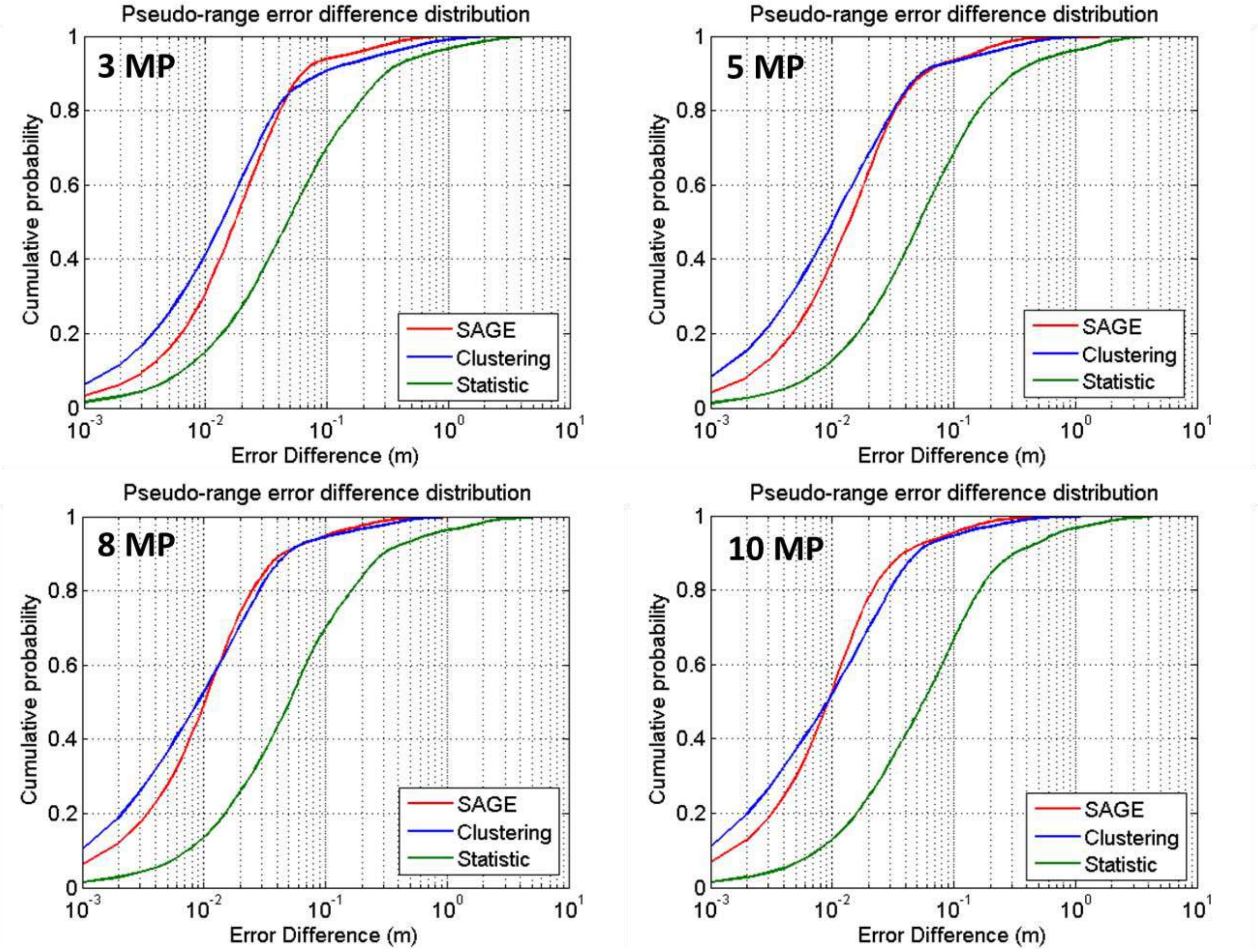

Figure 5.11 : Cumulative distribution of the difference between the reference and reduced channel tracking errors for different numbers of multipaths in the reduced channel

Table 5.5 : Mean (M), Standard deviation (STD), 95th and 99th percentiles (95P and 99P) of the distributions of tracking error (difference with the reference channel) for 3, 5, 8 and 10 MP

3 MP

	M	STD	P95	P99
Clustering	0.059 m	0.18 m	0.28 m	0.97 m
SAGE	0.039 m	0.081 m	0.14 m	0.46 m
Statistic	0.16 m	0.41 m	0.64 m	2.4 m

5 MP

	M	STD	P95	P99
Clustering	0.037 m	0.10 m	0.17 m	0.57 m
SAGE	0.034 m	0.11 m	0.14 m	0.34 m
Statistic	0.17 m	0.39 m	0.71 m	2.3 m

8 MP

	M	STD	P95	P99
Clustering	0.031 m	0.088 m	0.11 m	0.47 m
SAGE	0.027 m	0.077 m	0.10 m	0.33 m
Statistic	0.17 m	0.46 m	0.69 m	2.4 m

10 MP

	M	STD	P95	P99
Clustering	0.030 m	0.086 m	0.11 m	0.41 m
SAGE	0.028 m	0.069 m	0.092 m	0.26 m
Statistic	0.17 m	0.42 m	0.68 m	2.32 m

As it was already mentioned in the previous sub-section, the DLL and PLL tracking loops tend to smooth the difference between the Clustering and SAGE performance. At azimuth 0° and elevation 35°, these two reduced channel models showed the same performance as comparing the cumulative distribution of the tracking error difference on Fig. 5.10, with 5 multipaths in the reduced channel. On Fig. 5.11, it can be observed that the Clustering and SAGE method seem to have similar performance in terms of tracking error preservation. This statement remains the same with 3, 5, 8 and 10 multipaths in the reduced channels.

However, when observing the statistics of the tracking error difference corresponding to the SAGE and Clustering methods in Tab. 5.5, the conclusions of section 5.3.4 are partially conserved (study of the impact of the number of multipaths on the open loop discriminator error). Indeed, the ratio between the mean difference of SAGE and the mean difference of the Clustering gets closer to 1 as the number of multipaths increases. This statement is also true for both 95th and 99th percentiles. Therefore, it can be concluded that the advantage of the SAGE model on the clustering model decreases with the increase of the number of multipaths in the reduced channels.

In what concerns the statistical method, the preservation of the tracking error preservation is not improved by the increase of the number of multipaths from 3 to 10. This statement is shown by both Fig. 5.11 and Tab. 5.5. Note that the same observation was made concerning the open loop discriminator error in section 5.3.4.

5.4.5. Synthesis on the preservation of the tracking error

This section presented the comparison between the preservation of the tracking error by the different reduction methods. The results of this section mostly confirmed the results of section 5.3 about the preservation of the open loop discriminator error:

- The distribution corresponding to the tracking error difference with the original channel of the SAGE model has the lowest mean, as well as the lowest 95th and 99th percentiles. The Clustering method has performance close to SAGE. To the contrary, the statistical technique has the largest tracking error difference with the original channel (with every angle of arrival of the incoming signal).

- The Clustering performance gets even closer to the performance of SAGE as the elevation decreases from 65° to 35°.

- The performance of SAGE as compared to the performance of the clustering tend to decrease with the increase of the number of multipaths in the reduced channel (from 3 to 10 multipaths). The performance of the statistical method are not improved by the augmentation of the number of multipaths.

As a conclusion, these results showed a strong similarity between the discriminator open loop study and the tracking error study. However, it was observed that the difference between the performance of the SAGE and the Clustering models was lower for the tracking error than for the discriminator error. Therefore, this section highlighted the fact that the DLL and PLL tracking loops have a slight smoothing impact on the comparison of the models performance.

5.5. Influence of the parameters of the GNSS simulation on the comparison

In the previous section, the emphasis was put on the tracking error preservation of the different methods in different angle of arrival configurations. As it was already mentioned, these simulations have been run with specific GNSS configurations, summed up in Tab. 5.3. This section aims at assessing the possible impact of some of these parameters on the comparison results. To do so, it has been decided to investigate the tracking error computed by the receiver model GeneIQ along the reference scenario with different simulation parameters (in angle of arrival configuration ($\alpha = 30°$, $\beta = 35°$)). In each case, the r tracking error of the different reduced channels will be compared to the reference channel. The results of this section compared to the results of section 5.4 will highlight the impact of some GNSS parameters on the comparison of the methods. The following parameters will be considered:

- The RF bandwidth of the GNSS receiver GeneIQ has been set to $B = 10$ MHz in section 5.4. This large bandwidth implies a low distortion of the PRN signal, and thus of the signal autocorrelation function. Therefore, other RF bandwidths will be considered: $B = 1$ MHz, $B = 5$ MHz and $B = 10$ MHz in sub-section 5.5.1.

- So far, the tracking error has been computed in noiseless situations. In order to compare the reduction methods in a more realistic environment, a Gaussian noise will be added to the correlator outputs in sub-section 5.5.2, considering a C/N0 of 40 dBHz.

- In section 5.4, the tracking error has been computed on a GPS L1 C/A signal. In the sub-section 5.5.3, it has been decided to consider other signal shapes. Therefore, another modulation will be tested: BOC(1,1) (chosen for its importance in the future GNSS systems: GALILEO, GPS modernization …). With this modulation, another discriminator will be considered to perform the DLL tracking. Indeed, the DP (*Dot product*) will be used instead of the EMLP (*Early Minus Late Power*) discriminator.

5.5.1. Influence of the RF bandwidth

The tracking error has been computed with various RF bandwidths of the GeneIQ simulator: $B = 1$ MHz, $B = 5$ MHz and $B = 10$ MHz. The parameters used to configure this simulation have been recorded in Tab. 5.6. Fig. 5.12 illustrates the cumulative distributions corresponding to the difference between the tracking errors caused by the original channel and the reduced ones on the reference scenario. Tab. 5.7 records the statistics related to these distributions.

Table 5.6 : Configuration of the GNSS receiver GeneIQ

Parameter	Value		
Emitter's position	$\alpha = 30°, \beta = 35°$		
Modulation	BPSK(1)		
DLL loop order	2		
DLL loop bandwidth	1 Hz		
DLL discriminator	'Early Minus Late power'		
FLL loop order	2		
FLL loop bandwidth	2 Hz		
FLL discriminator	'Differential Arctangent'		
Integration time	5 ms		
RF bandwidth	**1 MHz**	**5 MHz**	**10 MHz**
Noise ON/OFF	'OFF'		

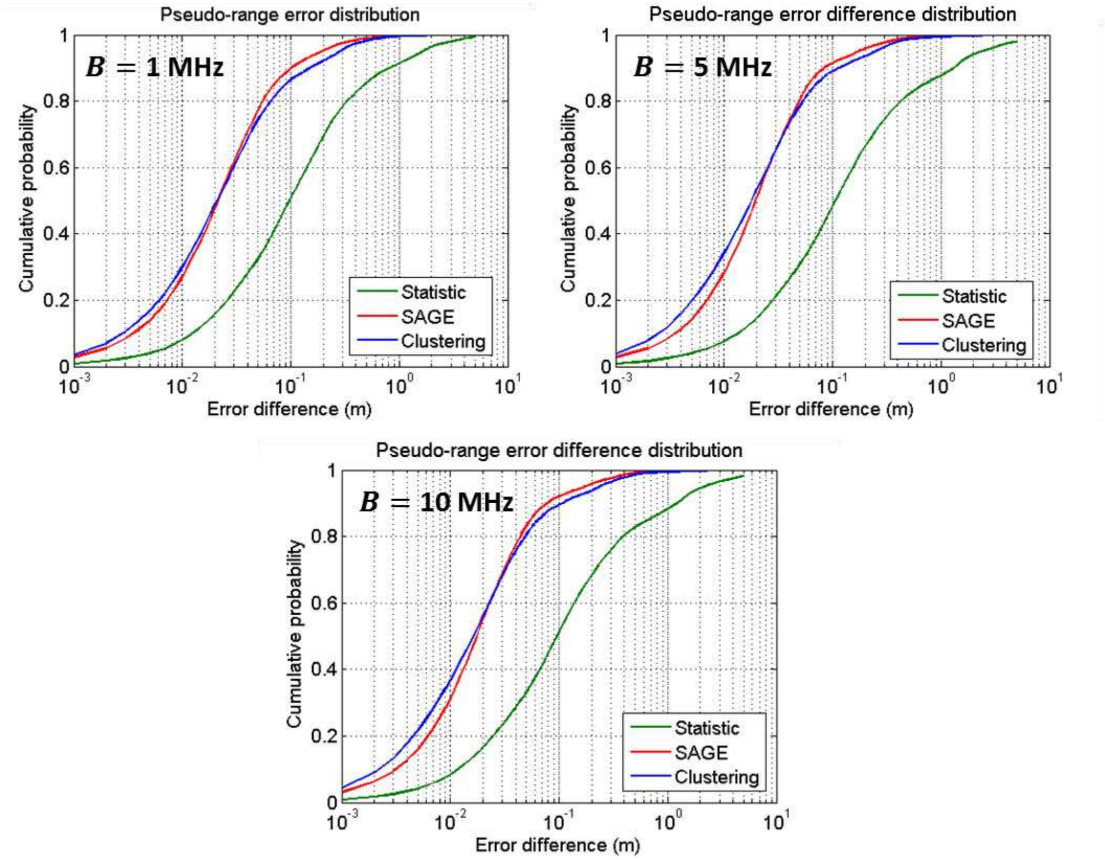

Figure 5.12: Cumulative distributions of the tracking error difference between original and reduced channels for different RF bandwidths

Table 5.7 : Mean, standard deviation, 95th and 99th percentiles corresponding to the tracking error difference distributions for different RF bandwidths

	MEAN			*STANDARD DEVIATION*		
	$B =$ 1 MHz	**$B =$ 5 MHz**	**$B =$ 10 MHz**	**$B =$ 1 MHz**	**$B =$5 MHz**	**$B =$ 10 MHz**
Clustering	0.065 m	0.058 m	0.056 m	0.17 m	0.19 m	0.19 m
SAGE	0.051 m	0.048 m	0.046 m	0.13 m	0.15 m	0.14 m
Statistic	0.34 m	0.51 m	0.46 m	0.78 m	1.4 m	1.2 m

	95th PERCENTILE			*99th PERCENTILE*		
	$B =$ 1 MHz	**$B =$ 5 MHz**	**$B =$ 10 MHz**	**$B =$ 1 MHz**	**$B =$ 5 MHz**	**$B =$ 10 MHz**
Clustering	0.28 m	0.24 m	0.24 m	0.67 m	0.65 m	0.61 m
SAGE	0.19 m	0.17 m	0.17 m	0.51 m	0.46 m	0.47 m
Statistic	1.64 m	2.3 m	2.2 m	4.1 m	7.2 m	6.5 m

It can be observed on both Fig. 5.12 and Tab. 5.7 that the comparison of the reduced channel models lead to the same result with $B = 1$ MHz, $B = 5$ MHz and $B = 10$ MHz. In each case, the Clustering and SAGE models show equivalent distributions of the difference of tracking error with the original channel, even if the statistics of Tab. 5.7 reveal that the mean, 95th and 99th percentiles corresponding to SAGE are slightly lower. The performance of the statistical model are always around 10 times worse in terms of mean and percentiles. It can be concluded that the RF bandwidth has no impact on the comparison of the methods. Note that the mean difference between original and reduced channels tracking errors tends to decrease with the increase of the RF bandwidth, except for the statistical method. This is due to the higher impact of the multipath delays if the RF bandwidth is lower.

5.5.2. Influence of the noise

In order to perform the comparison of the reduction methods on a more realistic scenario, some Gaussian noise has been added to the correlator outputs. The tracking error all along the trajectory has been computed by the GeneIQ simulator in that context. The carrier-to-noise ratio has been set to $CN0 = 40$ dBHz. The other simulation parameters are shown in Tab. 5.8. Note that the same noise-sequence has been used for the reference and the different reduced channels, in order to perform an objective comparison.

Table 5.8: Configuration of the GNSS receiver GeneIQ

Parameter	**Value**
Emitter's position	$\alpha = 30°$, $\beta = 35°$
Modulation	BPSK(1)
DLL loop order	2
DLL Bandwidth	1 Hz
DLL discriminator	'Early Minus Late power'
FLL loop order	2
FLL bandwidth	2 Hz
FLL discriminator	'Differential Arctangent'
Integration time	5 ms
RF bandwidth	10 MHz
Noise CN0	**40 dBHz**

The tracking error caused by the reference channel with and without the noise has been represented on Fig. 5.13 on the segment [250m, 500m] of the trajectory. This figure aims at illustrating the strong impact of the noise on the tracking error (with 40 dBHz CN0). Indeed, major differences between the On and OFF cases are observable on the temporal profile of the tracking error.

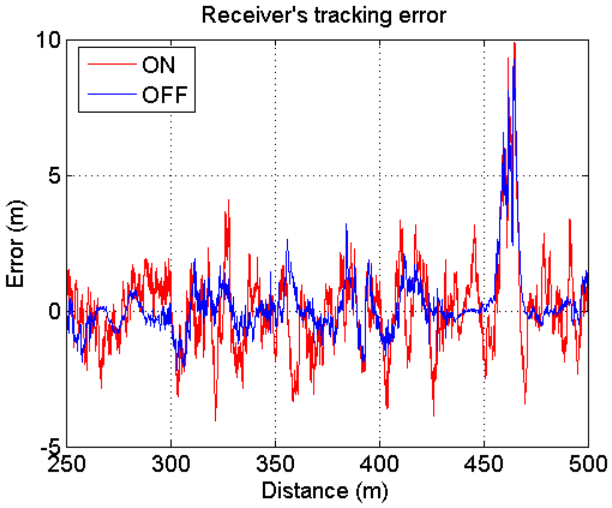

Figure 5.13: Tracking error of the original channel with (ON) and without (OFF) noise on the segment [250m, 500m]

Fig. 5.14 shows the cumulative distributions of the difference between the tracking error of the original channel and the reduced ones with and without noise in the scenario. The statistics corresponding to these distributions are recorded in Tab. 5.9.

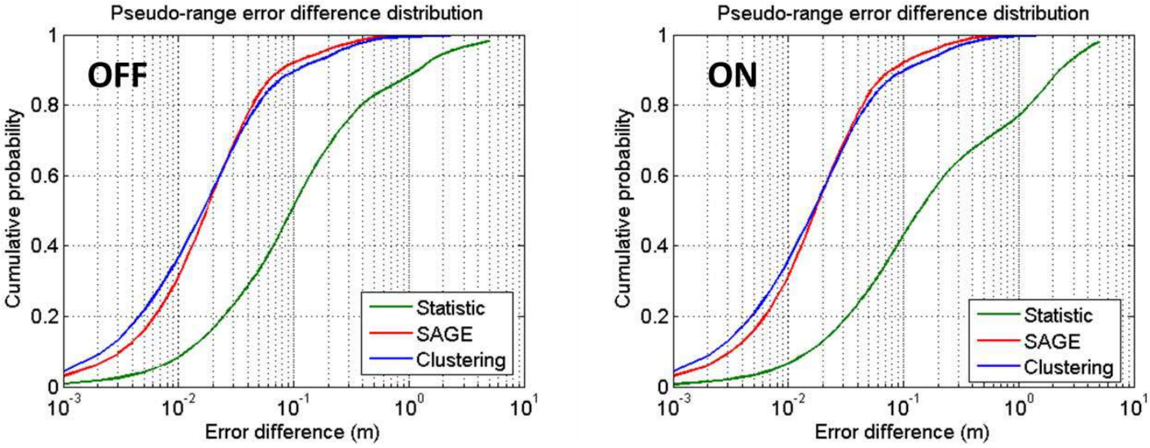

Figure 5.14: Cumulative distributions of the tracking error difference between original and reduced channels with noise (ON) and without (OFF) noise

Table 5.9 : Mean, standard deviation, 95th and 99th percentiles corresponding to the tracking error difference distributions with noise and without noise

	Mean		Standard deviation		95th percentile		99th percentile	
	OFF	**ON**	**OFF**	**ON**	**OFF**	**ON**	**OFF**	**ON**
Clustering	0.056 m	0.052 m	0.19 m	0.12 m	0.24 m	0.22 m	0.61 m	0.59 m
SAGE	0.046 m	0.042 m	0.14 m	0.073 m	0.17 m	0.15 m	0.47 m	0.40 m
Statistic	0.46 m	0.74 m	1.2 m	1.3 m	2.2 m	3.5 m	6.5 m	6.4 m

It can be observed on both Fig. 5.14 and Tab. 5.9 that the difference between the tracking error of the reference and reduced channels has the same order of magnitude with and without noise. Moreover, the comparison of the methods in terms of tracking error preservation has the exact same results. Therefore, it can be deduced that the conclusion of sections 5.3 and 5.4 are still valid even in the presence of noise in the simulations.

5.5.3. Influence of the signal modulation

In the section 5.4, the signal tracking was performed considering a BPSK(1) modulation. This characteristic increased the similarity between the computation of the tracking error and the discriminator error which was also estimated from a BPSK signal. However, the comparison of the reduction models performances according to other signal modulations are of interest. Indeed, other modulations lead to different code's autocorrelation functions and thus to possible modifications in the tracking error caused by the different reduced channel models. Therefore, it has been decided to study the case of a BOC(1,1) modulated signal to run the GeneIQ receiver on the reference scenario. The characteristics of the simulation are summed up in Tab. 5.10.

Fig. 5.15 illustrates the cumulative distribution of the difference between the original and reduced channel tracking errors considering both a BPSK(1) and BOC(1,1) modulated signals. The statistics related to these distributions are recorded in Tab. 5.11.

Table 5.10 : Mean, standard deviation, 95th and 99th percentiles corresponding to the tracking error difference distributions with noise and without noise

Parameter	**Value**	
Emitter's position	$\alpha = 30^\circ$, $\beta = 35^\circ$	
Modulation	**BPSK(1)**	**BOC(1,1)**
DLL loop order	2	
DLL loop bandwidth	1 Hz	
DLL discriminator	'Early Minus Late power'	
FLL loop order	2	
FLL loop bandwidth	2 Hz	
FLL discriminator	'Differential Arctangent'	
Integration time	5 ms	
RF bandwidth	10 MHz	
Noise	No noise	

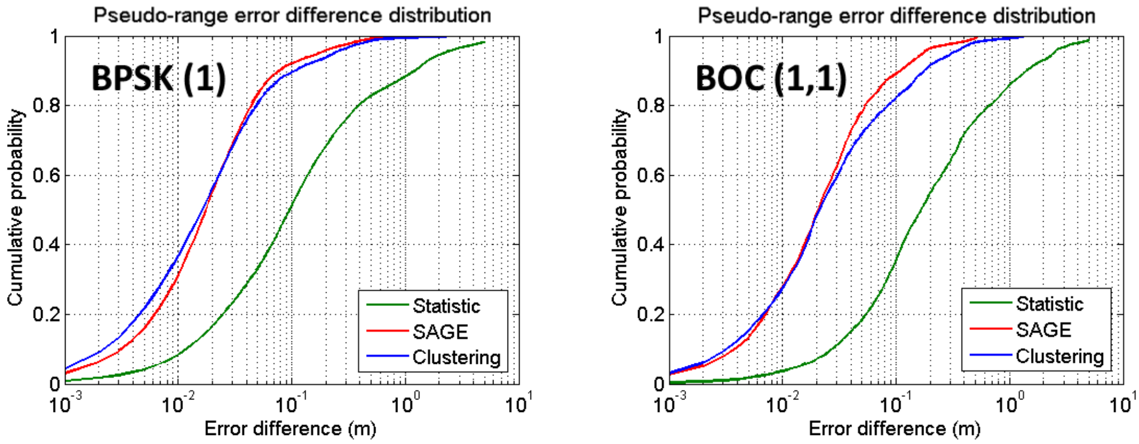

Figure 5.15: Cumulative distributions of the tracking error difference between original and reduced channels considering BPSK (left) and BOC (right) modulated signals

Table 5.11: Mean, standard deviation, 95th and 99th percentiles corresponding to the tracking error difference distributions considering BPSK and BOC modulated signals

	Mean		Standard deviation		95th percentile		99th percentile	
	BPSK(1)	**BOC(1,1)**	**BPSK(1)**	**BOC(1)**	**BPSK(1)**	**BOC(1,1)**	**BPSK(1)**	**BOC(1,1)**
Clustering	0.056 m	0.070 m	0.19 m	0.15 m	0.24 m	0.31 m	0.61 m	0.80 m
SAGE	0.046 m	0.045 m	0.14 m	0.08 m	0.17 m	0.17 m	0.47 m	0.47 m
Statistic	0.46 m	0.53 m	1.2 m	0.98 m	2.2 m	2.4 m	6.5 m	5.4 m

The comparison of the reduction methods according to the preservation of the tracking error lead to the same results in the case of a BOC modulated signal as in the case of a BPSK signal. Indeed, the cumulative probabilities of the tracking error difference on Fig. 5.15 show similar distributions for the SAGE and Clustering methods in both cases of BPSK and BOC modulations. The performance of the statistical model are around 10 times lower in both cases. Moreover, it can be observed in Tab. 5.11 that the relative performance of the different methods in terms of mean tracking error difference, 95th and 99th percentiles remain unchanged from one modulation to another. It can be deduced that the modulation of the signal has no significant impact on the results of this study.

However, it must be mentioned that the SAGE reduction method optimizes the similarity between the channel autocorrelation before and after reduction, considering a BPSK modulated signal. Therefore, the performance of SAGE in terms of pseudo-range error preservation could be slightly increased by changing the cost function to minimize, with autocorrelation functions corresponding to a BOC modulation. The same remark could be made concerning the RF bandwidth, as the autocorrelation functions used in SAGE were obtained with infinite RF bandwidth. An adaptation of bandwidth is likely to improve the pseudo-range error preservation.

5.6. Influence of the emitter position

It has already been observed that the elevation of the signal emitter had an influence on the comparison of the reduced channel models (section 5.3 and 5.4). This section will focus on this problem. To do so, it has been decided to perform the comparison considering more elevation configurations. Therefore, the SCHUN channel model has been used to synthesize the channels corresponding to the reference scenario presented in section 5.2 with the satellite elevations 10°, 30°, 50° and 70°. The azimuth of the satellite has also been expanded to 0°, 20°, 40° and 60° (only positive values for symmetry reasons). In each azimuth-elevation situation, the discriminator error of the reduced channel models will be compared to the discriminator error of the reference channel. Note that it has been decided to investigate the discriminator open loop error instead of the tracking error in order to bypass the impact of the tracking loops on the pseudo-range errors. However, being given the strong similarity between the comparison according to the open loop and tracking errors, the results of this section may be easily transposed to the tracking error.

Fig. 5.16 illustrates the means of the difference between the original and reduced channels discriminator error, for the different angles of arrival. Fig. 5.17 and 5.18 represent respectively the 95th and 99th percentiles associated to those distributions. In each case, the right plot represents the distributions of the Clustering, SAGE and statistical models, whereas the left plot represents only the SAGE and Clustering models in order to make the comparison easier. It has been decided to put the emphasis on the comparison between the Clustering and SAGE models, as the statistical method already proved to have lower performance in every configuration. The statistics associated to those different distributions have been recorded in Tab. 5.12 and Tab. 5.13. The means and standard deviations of the difference between original and reduced channels discriminator error are recorded in Tab. 5.12. The 95th and 99th percentiles are recorded in Tab. 5.13.

Similar observations can be made on Fig. 5.16, 5.17 and 5.18: the performance of the SAGE and Clustering models in terms of discriminator error difference vary in function of the azimuths and elevation of the emitting satellite. The performance of the Clustering tend to overcome the performance of SAGE as the elevation decreases. Indeed, for a given azimuth, SAGE shows clearly a better discriminator error preservation for high elevations (70°, 50°) in terms of mean, 95th and 99th percentiles. However, the mean, 95th and 99th percentiles corresponding to the Clustering model are systematically lower than those corresponding to the SAGE model with 30° and 10° elevation. It can be deduced that the Clustering method preserves the discriminator error better than SAGE for low satellite elevations.

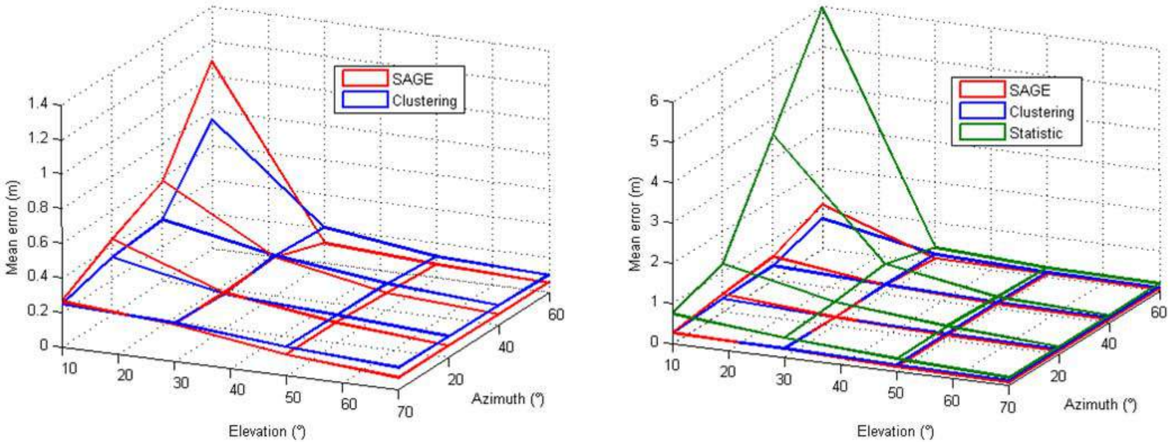

Figure 5.16 : Mean difference between original and reduced channel discriminator error for different azimuths and elevations

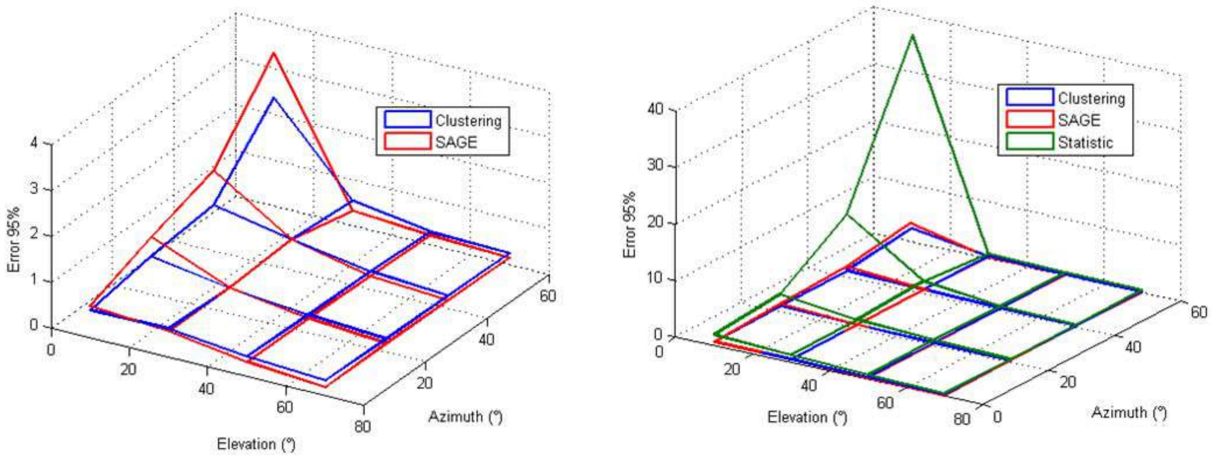

Figure 5.17: 95% discriminator error preservation of the reduction methods for different azimuths and elevations

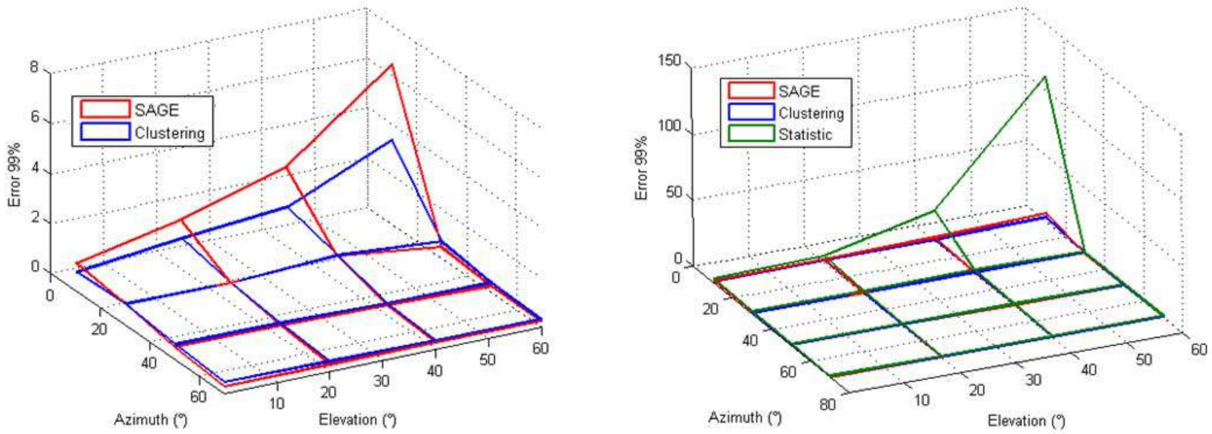

Figure 5.18: 99% discriminator error preservation of the reduction methods for different azimuths and elevations

Table 5.12 : Mean and standard deviations associated to distributions of discriminator error difference for different azimuths and elevations of the emitter

		MEAN				STANDARD DEVIATION			
		$\beta = 10°$	$\beta = 30°$	$\beta = 50°$	$\beta = 70°$	$\beta = 10°$	$\beta = 30°$	$\beta = 50°$	$\beta = 70°$
$\alpha = 0°$	**Cluster**	0.28 m	0.25 m	0.22 m	0.17 m	0.23 m	0.18 m	0.20 m	0.13 m
	SAGE	0.28 m	0.26 m	0.21 m	0.12 m	0.23 m	0.23 m	0.19 m	0.10 m
	Statistic	0.63 m	0.74 m	0.49 m	0.32 m	0.53 m	0.64 m	0.44 m	0.27 m
$\alpha = 20°$	**Cluster**	0.31 m	0.33 m	0.20 m	0.16 m	0.27 m	0.27 m	0.17 m	0.12 m
	SAGE	0.35 m	0.43 m	0.21 m	0.12 m	0.31 m	0.42 m	0.18 m	0.10 m
	Statistic	0.97 m	1.2 m	0.59 m	0.34 m	0.78 m	2.0 m	0.48 m	0.36 m
$\alpha = 40°$	**Cluster**	0.31 m	0.36 m	0.24 m	0.16 m	0.24 m	0.32 m	0.22 m	0.12 m
	SAGE	0.45 m	0.58 m	0.22 m	0.10 m	0.41 m	0.69 m	0.21 m	0.088 m
	Statistic	2.9 m	3.6 m	0.75 m	0.28 m	6.8 m	6.8 m	0.73 m	0.57 m
$\alpha = 60°$	**Cluster**	0.66 m	0.75 m	0.21 m	0.13 m	0.68 m	0.88 m	0.16 m	0.094
	SAGE	1.0 m	1.1 m	0.12 m	0.080 m	1.1 m	1.7 m	0.11 m	0.070 m
	Statistic	14 m	6.0 m	0.38 m	0.23 m	32 m	22 m	0.13 m	0.19 m

Table 5.13 : 95th and 99th percentiles associated to distributions of discriminator error difference for different azimuths and elevations of the emitter

		95th PERCENTILE				99th PERCENTILE			
		$\beta = 10°$	$\beta = 30°$	$\beta = 50°$	$\beta = 70°$	$\beta = 10°$	$\beta = 30°$	$\beta = 50°$	$\beta = 70°$
$\alpha = 0°$	**Cluster**	0.78 m	0.60 m	0.63 m	0.33 m	1.0 m	0.74 m	0.84 m	0.59 m
	SAGE	0.69 m	0.69 m	0.57 m	0.32 m	1.1 m	1.01 m	0.82 m	0.48 m
	Statistic	1.7 m	1.9 m	1.3 m	0.78 m	2.4 m	2.7 m	2.1 m	1.1 m
$\alpha = 20°$	**Cluster**	0.81 m	0.83 m	0.55 m	0.39 m	1.23 m	1.22 m	0.80 m	0.56 m
	SAGE	0.98 m	1.2 m	0.57 m	0.32 m	1.4 m	2.0 m	0.80 m	0.44 m
	Statistic	2.3 m	3.0 m	1.5 m	0.84 m	3.1 m	4.6 m	2.0 m	1.2 m
$\alpha = 40°$	**Cluster**	0.78 m	0.98 m	0.65 m	0.39 m	1.1 m	1.6 m	1.0 m	0.48 m
	SAGE	1.3 m	1.7 m	0.66 m	0.28 m	1.9 m	3.2 m	0.99 m	0.38 m
	Statistic	8.5 m	11 m	2.1 m	0.67 m	19 m	24 m	3.2 m	0.59 m
$\alpha = 60°$	**Cluster**	1.9 m	2.4 m	0.55 m	0.30 m	3.1 m	3.4 m	0.70 m	0.42 m
	SAGE	3.2 m	3.4 m	0.34 m	0.22 m	4.8 m	6.4 m	0.47 m	0.28 m
	Statistic	40 m	36 m	0.94 m	0.61 m	98 m	110 m	1.32 m	0.79 m

Two explanations can be given concerning the observations of Fig. 5.16 to 5.18:

- It was already shown in section 5.3 that the open loop discriminator error increases as the elevation of the emitter satellite decreases (Fig. 5.4). As it was mentioned, when the EM wave impinging the façade is close to the horizontal plane, the power of the reflected ray in the direction of the receiver is large, because the receiver in the specular zone of the façade. Therefore, the channel autocorrelation function is more distorted by the multipath channel, which impairs the performance of SAGE. To the contrary, the Clustering technique gives more weight to the high power multipaths (modified *K-Means*). Therefore, this method is less impacted by the presence of powerful echoes than SAGE. Hence the better conservation of the discriminator error. This statement has been illustrated on Fig. 5.19, which represents an example of power-delay profile (corresponding to the distance d=125 m) at elevations $\beta = 30°$ and $\beta = 60°$ at azimuth $\alpha = 30°$. The high power multipaths are framed in green on the 30° elevation profile. It is not present on the 60° profile. The Clustering (blue dots) and SAGE (red dots) have been applied to these impulse responses. Three echoes of the Clustering channel are located in the delay zone of the high power multipaths. To the contrary, the echoes of the SAGE model are more remote from this delay zone. Thus, the Clustering model is more faithful to the original model than the SAGE model, in the case of low elevations.

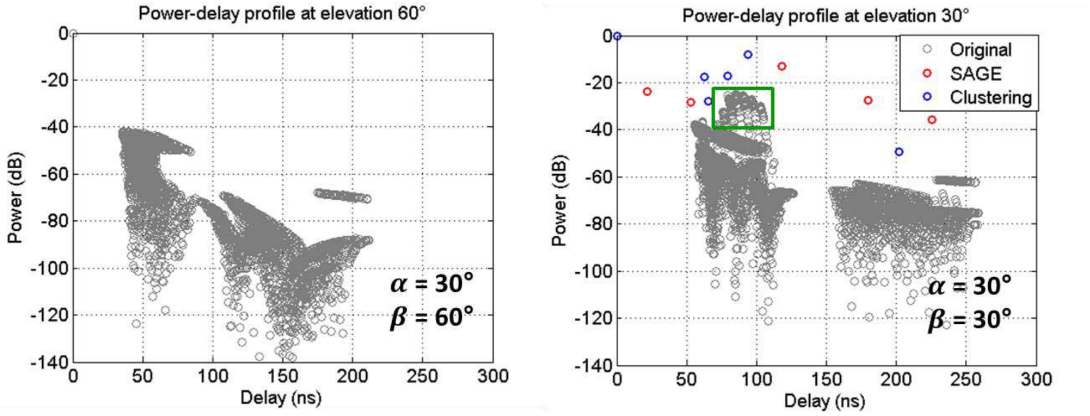

Figure 5.19: Influence of the elevation on the power-delay profile conservation at d= 125 m

- As the elevation of the emitter increases, the difference between the delays of the multipaths originated at the top of the buildings and the delay of the multipaths originated at the bottom of the same building increases. It results in wider delay profiles, as illustrated on Fig. 5.20, which represents the Doppler-delay profile of the impulse response at the distance d=125 m with elevations $\beta = 30°$ and $\beta = 60°$ at azimuth $\alpha = 30°$. Therefore, it is harder for the Clustering to reproduce the original channel. As a consequence, the performance of the Clustering tend to decrease with the augmentation of the elevation.

These statements are emphasized by the combination high azimuth-low elevation. This is due to the geometrical system implied by such angles of arrival, which increases the delay spread of the impulse responses and then, the distortion of the signal autocorrelation. This is illustrated by Fig. 5.21 which represents the Doppler-delay profile at the distance d=500 m at elevation $\beta = 30°$ for the azimuths $\alpha = 10°$ and $\alpha = 70°$. The increase of the delay spread is obvious on this plot. Moreover, the impulse response contains some multipaths with delays close to the LOS delay, which increases the distortion of the signal autocorrelation.

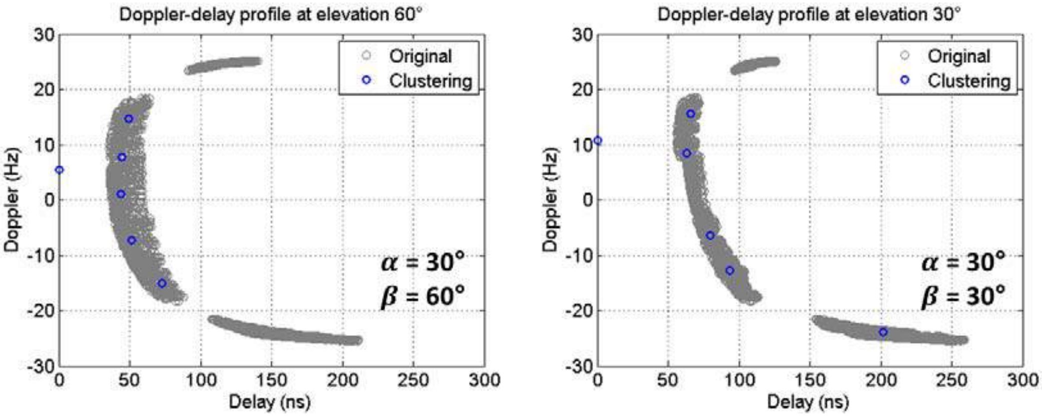

Figure 5.20: Influence of the elevation on the multipath delay at d= 125 m

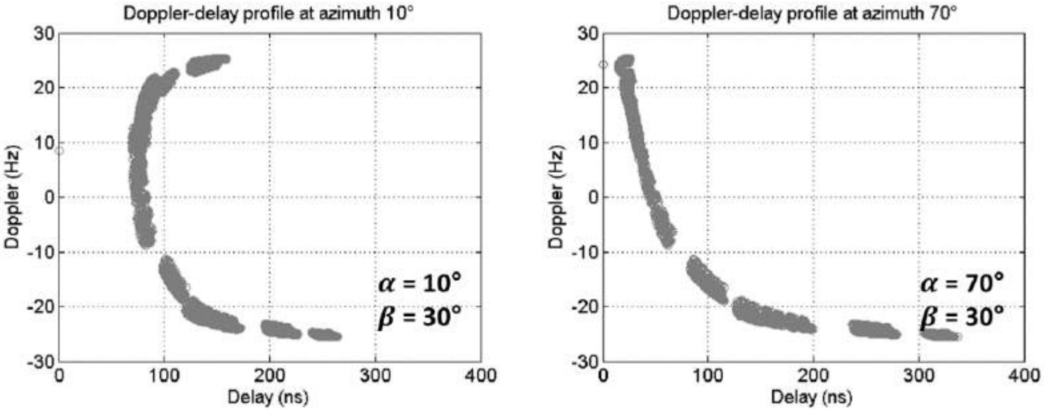

Figure 5.21: Influence of the azimuth on the delay spread at d= 500 m

5.7. Conclusion

This chapter has presented the comparison of the different reduction methods according to the pseudo-range error preservation. The reduction methods considered are the Clustering Weighted, SAGE and the statistical method. The impact of the reduction process on the pseudo-range error of the receiver has been investigated through the discriminator and tracking errors. The discriminator error consists in an open-loop model of pseudo-range error, which quantifies the delay shift of the discriminator output with respect to the LOS delay, caused by the multipath channel (for each instant independently). The tracking error is computed by a real DLL/PLL loop system, using a GNSS receiver model.

After presenting an introduction of the study in section 5.1, a reference scenario has been implemented in section 5.2. The reference multipath channel have been computed using the simulator SCHUN (documented in chapter 1), all along the trajectory. It has been chosen to compute the channel parameters at the sampling rate 200 Hz, according to the channel coherency time, which has been investigated in section 5.2. Different azimuths and elevations of the incoming signal have been tested. The reduction methods have been applied to the reference channels in every configuration to assess their impact on the pseudo-range error in the following sections.

As a first step, the reduction methods were compared according to the open loop discriminator error, in section 5.3. The performance of the methods in terms of discriminator error preservation have been represented by the difference between the discriminator error caused by the reference channel and the reduced ones all along the trajectory. The comparison of the cumulative probabilities corresponding to these distributions made appear a clear hierarchy among the methods: SAGE shows the best preservation performance. The Weighted Clustering has performance close to SAGE, whereas the statistical method has clearly the worst. Note that those results confirm those presented in [Rib 16b]. The fact that SAGE has the best pseudo-range error preservation could be expected, being given the fact that it is dedicated to the conservation of the channel autocorrelation function (from which the discriminator error is deduced). This hierarchy has been observed for every azimuth and every elevation. Although, it appeared that lower elevations tend to smooth the difference between SAGE and the Weighted Clustering. Therefore, it has been decided to dedicate section 5.6 to the thorough assessment of the impact of the carrier angle of arrival on the comparison results.

In the second part of section 5.3, the impact of the number of multipaths in the reduced channel has been considered. Different numbers of echoes have been tested. The comparison of the difference between original and reduced channels showed that the performance of the Weighted Clustering overcome the performance of SAGE for more than 8 echoes in the reduced channel. To the contrary, the performance of the statistical method do not increase with the number of echoes.

In section 5.4, a real GNSS receiver simulator has been considered, referred to as GeneIQ, in order to investigate the possible impact of the DLL/PLL tracking loops on the pseudo-range error conservation. The tracking error difference between original and reduced channels has been investigated following the same process as for the open loop discriminator errors. Globally, the comparison of the methods led to the same results as the previous section. However, in some cases, the tracking loops seem to smooth the difference between SAGE and Weighted Clustering (for low elevations for example). The study of the impact of the number of multipaths in the reduced channel confirmed the results of section 5.3 that is to say that the Clustering Weighted has better performance than SAGE if there are more than 8 echoes in the reduced channel.

So far, GeneIQ was tuned with a BPSK modulated signal, with 10 MHz receiver RF bandwidth and an EMLP discriminator for the DLL. It has to be noted that those parameters tend to optimize the similarity between discriminator and tracking errors. Therefore, the GNSS configuration of the simulation has been varied in order to highlight its possible impact on the comparison of the methods. It was observed that neither the receiver RF bandwidth nor the signal modulation influence the hierarchy of the methods established in the previous sections. The presence of an additional Gaussian noise to the correlators output has no impact either.

To finish, section 5.6 investigated the impact of the azimuth and elevation of the incoming signal on the discriminator error preservation. By testing several angles of arrivals, it was shown that the Weighted Clustering overcomes the performance of SAGE for low elevations. The elevation from which the Clustering is better than SAGE was estimated around 30° (regardless of the azimuth).

This study motivated some recommendations, about the use of reduction methods and their impact on the pseudo-range error:

- First, for every angle of arrival of the incoming signal or GNSS configuration, for any number of echoes in the reduced channel, the statistical model always showed the worst performance both in terms of open loop discriminator error and tracking error preservation. In some cases, its performance is more than 10 times worse than the Clustering or SAGE methods, in terms of mean error, 95% and 99% error margins. Therefore, it can be excluded from the solutions of the channel reduction problem (because it has a major impact on the pseudo-range error).

- As compared to the statistical model, the performance of the Weighted Clustering and SAGE can be considered as similar. It showed to vary depending on different parameters of the simulation :
  - If the elevation is superior to 30° and/or the number of multipaths in the reduced channel is inferior to 8, SAGE has slightly better performance than the Clustering Weighted according to both discriminator and tracking error preservation.
  - If the elevation is inferior to 30° and/or the number of multipaths in the reduced channel is superior to 8, the Clustering Weighted method has slightly better performance than SAGE according to both discriminator and tracking error preservation.

These conclusions are confirmed by the mean and the error margins corresponding to the distributions of discriminator and tracking error difference between original and reduced channels. It was shown in chapters 2 and 3 that SAGE presents more constraints of implementation than the Weighted Clustering, mostly in terms of computational effort. Therefore, the use of the Clustering Weighted to reduce the multipath channel could be recommended, specifying that the SAGE model can improve the tracking error preservation in high elevation configuration or with restrictive echo limitations (inferior to 8 multipaths). Note also that the absolute difference between the tracking error of the reference and the Clustering reduced channel is of the order of 5 cm average and 20 cm 95th percentile (without noise). It has been considered that this difference between the original channel (thousands of echoes) and the reduced channel (5 echoes only) was low enough to consider that the tracking error is well preserved by the Weighted Clustering. The use of this method is likely to impair only very slightly the pseudo-range error of the receivers

A good correlation between the comparison results concerning the open loop discriminator and tracking errors was observed. Therefore, the open loop discriminator error, easier to compute, could be sufficient to assess the performance the reduction methods. It could be used as a tool to quantify the pseudo-range error preservation, as a representativeness index.

Conclusion

This PhD presents the implementation of three algorithms dedicated to the reduction of the multipath channel. The literature concerning multipath channel models showed that large impulse responses are necessary to simulate complex environments using accurate deterministic methods. It is a major limitation to the realistic testing of GNSS receivers. In particular, the hybrid physical-statistical channel simulator SCHUN (*Simplified Channel for Urban Navigation*) is considered as a good tradeoff between channel accuracy and computational effort. However, the high number of multipaths generated prevents the testing of software receivers in real time and even more the use of channel emulators (in the case of hardware receivers). Several methods of channel reduction have been found in the literature and could be divided in three main families: aggregation methods, parametric optimization methods and statistical methods. It has been decided to investigate each approach in order to cover all the channel reduction possibilities. Starting from these three approaches, three original reduction methods have been implemented in this thesis. They have been defined so as to optimize the conservation of the wide-band parameters of the original channel (delay, Doppler shift and complex amplitude). At the end, one reduction method per type of approach has been implemented. They are all considered as optimal within their own family (aggregation, parametric, statistical). Then, these methods have been compared according to their ability to conserve the pseudo range of GNSS receivers. This study showed a hierarchy of methods, which does not depend on the signal characteristics or tracking loops configuration. In particular, it has been shown that the multipath aggregation method implemented in this thesis, namely Clustering Weighted, is able to come close to the performance of parametric optimization methods (referred to as SAGE) and even overcome them in some cases. Therefore, it has proved to be an interesting tradeoff between preservation of the GNSS pseudo range error and low computational effort.

The first three chapters of this thesis are dedicated to the implementation of the three reduction methods considered. Therefore, the results presented by this thesis can be divided in two types. On one hand, three reduction techniques are presented according to three different approaches; with details about the way they manage the reduction process. On the other hand, the study of their impact on the pseudo-range error is performed in the last chapter. This study results in the recommendation of the use of the Clustering Weighted to address the channel reduction problem.

The first result presented in this thesis show the necessity to take into account the delay, phase, amplitude and Doppler shift of the multipaths to realize the aggregation process, in order to preserve the original channel wide-band parameters (power-delay profile and Doppler spectrogram). Indeed, the commonly used Tap Delay Line technique is performed first, considering several enhancements to the basic method (mobile taps along the delay line and channel re-sampling technique). It shows to be shortcoming in terms of Doppler spectrogram preservation, since multipaths with various Doppler shifts are aggregated. Therefore, clustering techniques along delay and Doppler dimensions are considered. It shows that the fact to weight the multipaths by their complex amplitude during the assignment phase of the clustering optimizes the preservation of both power-delay and Doppler spectrogram of the original channel. This study results in the implementation of the Weighted Clustering technique, low demanding in terms of computational resources and offering a good preservation and continuity of the wide-band parameters of the multipath channel.

The following method implemented in this thesis aims at optimizing the conservation of the pseudo-range error. To do so, the optimization algorithm SAGE ("Space Alternating Generalized Expectation-Maximization) is used to minimize the difference between the original and reduced channels autocorrelation functions. In other terms, SAGE parameterizes the delay, Doppler shift and complex amplitude of the reduced channel multipaths, so as to optimize the conservation of the channel autocorrelation function. First, this thesis proves that SAGE is well-suited to address this optimization problem. Then, the importance of the Doppler resolution of the algorithm on its performance is emphasized on a canonical scenario. A suitable Doppler resolution with respect to the number of multipaths in the reduced channel is estimated, so as to implement an efficient optimization method. However, it must be mentioned that some major drawbacks of this method can be identified, such as the delay discontinuity of the reduced channel and the significant computational effort required. These limitations question the ability of this method to address the channel reduction problem.

This thesis also presents the implementation of a statistical method to compute the reduced channel. In that case, the parameters of the multipaths are supposed to evolve according to a first order Markov chain. It is shown that the application of such a stochastic process to the delay and amplitude of the multipaths leads to a severe impairment of the original channel power-delay profile. Therefore a new semi-statistical reduction method is implemented. In this new approach, only the delay evolves according to a first order Markov process whereas the complex amplitude is deduced from the impulse response power-delay profile. This method shows good results in terms of preservation of the power-delay profile of the original channel, with a good continuity of the delays and phases of the reduced channel echoes, in a reasonable computation time.

The originality of this thesis relies also in the comparison that is performed in chapter 5 so as to know which approach is the most convenient to be applied to the realistic testing of GNSS receivers. The three aforementioned reduction methods are applied to a single reference scenario (simulated by SCHUN). It consists in the trajectory of a receiver through a reference urban scenario. In a first time, the reduced channel models are compared to the original channel in terms of open loop discriminator error (considering no tracking loop effect). A close formula computing the open loop discriminator error depending on the impulse response wide-band parameters is presented. This comparison results in a hierarchy of reduction methods in terms of pseudo-range error preservation. As expected, the SAGE parametric method has the best performance. However, it is shown that the Weighted Clustering technique comes close to the performance of SAGE in specific simulation conditions. In particular, it is shown that the Clustering Weighted tends to overcome SAGE while the number of echoes in the reduced channel is increased (that is to say decrease the multipath restriction). As compared to the two other approaches, the statistical method impairs the reference discriminator error severely, which discredits its use in the context of testing of GNSS receivers.

In order to investigate the impact of the tracking loops on the previous results, the same comparison was performed on a software receiver simulator, tracking the signal with a DLL and an FLL. The previous conclusion of the open loop study is almost integrally confirmed, even if the difference between the SAGE and Clustering Weighted methods is slightly smoothed. Also, the investigation of various signal models (modulations and RF bandwidths) has no impact on these conclusions.

To sum up, two main results may be underlined in this thesis. First, an innovative comparison of different reduction approaches was performed, including simple multipath aggregation, parametric optimization and statistical estimation. It results in a hierarchy of methods, according to the conservation of the GNSS performance, which can be extended to various simulation configurations (tracking loops, RF bandwidth, signal modulation, noise). Therefore, the discriminator open loop error is a good indicator of the performance of the methods. The second result is the implementation of an innovative aggregation method, referred to as Clustering Weighted method, which shows to be able to preserve the channel wide-band parameters well with less than 10 multipaths in the reduced channel, with almost real-time computation efficiency. More specifically, this method comes close to the performance of SAGE (accurate but heavy method) in terms of pseudo-rang error preservation. Therefore, the use of the Clustering Weighted method is recommended to answer the channel reduction problem. It seems to be well suited to adapt channel simulators like SCHUN to the receiver testing applications, including the use of hardware signal emulators (less than 10 echoes in the reduced channel).

Further works in the scope of this study may include further development of the reduction methods and further validation of the comparison results. On one hand, the performance of the statistical method appear to be significantly worse than the Clustering Weighted method. Further development of the stochastic process (in the continuity of the work performed in this thesis) may improve this approach, to make it applicable to the satellite navigation context. On the other hand, possible further validation includes the application to these reduction methods to other wide-band channel models, considering a wider bench of simulation configurations (such as other modulations for example), in order to use it for the assessment of the new generation of GNSS signals.

However, the major perspective concerning these results would be the transposition of those reduction techniques to other channel models, including deterministic models like SE RAY-EM FERMAT or hybrid physical-statistical models like the model of the DLR [Lehn 07]. First, this comparison would allow the assessment of the reduction approaches according to different reference channel models, and consolidate the results. Secondly, the comparison of the channel models through reduced impulse responses would offer a new critical comparison of the different physical approaches.

Finally, the possibility to integrate such a method in hardware devices such as RF test benches should be discussed, taking into account the different technological constraints. It could result in the validation of the association of the SCHUN simulator to the reduction methods, considering the assessment of a real GNSS system.

A. Annex A: Proposition of a method to follow the signature of the multipaths along consecutive impulse response samples

A.1. Introduction of the problematic

In chapter 4, a statistical model of channel reduction is presented. The reduced channel delays are estimated from 2-dimensional *pdfs*: distribution of the delays of the original channel at the present and previous epochs. It corresponds to the transition probability from one delay bin to another. Fig. A.1 represents an example of such a 2-dimensional *pdf* distribution, for two consecutive snapshots on the reference scenario represented on Fig. A.2. The x-axis represents the delay bins of the multipaths at time t (spotted B on Fig. A.2). The y-axis represents the delay bins at $t + \Delta t$. The color of the plot represents the *pdf* of the delays at $t + \Delta t$, depending on their delay at t.

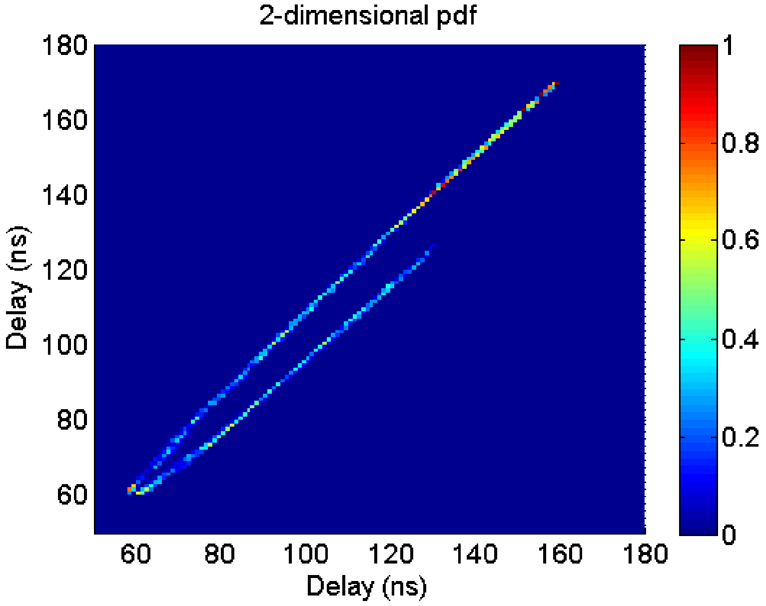

Figure A.1 : Illustration of a 2-dimensional *pdf*

In order to build these 2-dimensional *pdfs*, the delay variation of the multipaths from one instant t to the following one $t + \Delta t$ has to be known. Therefore, the reduction algorithm needs to recognize the multipaths along the consecutive impulse response samples, so as to be able to follow each echo individually. However, the SCHUN software as it was implemented in [Ait 13] does not provide the signature of the multipaths. Therefore, an algorithm has been implemented for the purpose of this thesis in order to be able to follow a given multipath along time. This annex describes this process, as it played a major role in the implementation of the statistical channel model presented in chapter 4.

This algorithm relies on the estimation of the multipath delay at the following epoch knowing their delay and Doppler shift (or angle of arrival) at the present time. Note that a few modifications in the implementation of SCHUN could link each multipath to the facet from which it was emitted, allowing to follow this multipath along time. However, it has been decided to develop an algorithm applicable to any wide-band channel model.

Fig. A.2 represents the reference scenario used to illustrate this annex. Note that it is the same reference scenario as the one used in chapters 2, 3 and 4, illustrated in section 2.2. The exact same simulation configuration is considered (30° azimuth and 35° elevation, 5m.s^{-1} speed and RHCP polarization). The three spots A, B and C will be used for illustration purposes in the following of the annex.

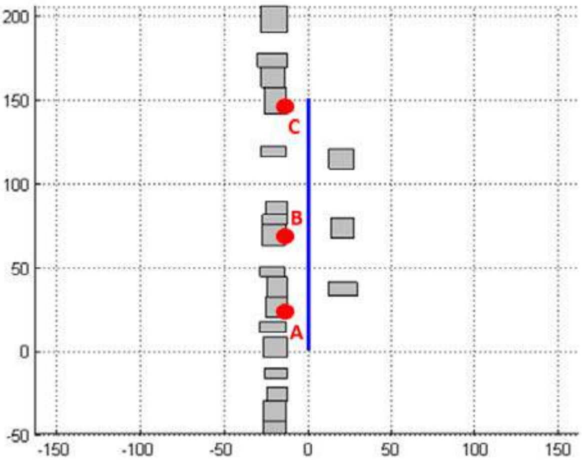

Figure A.2 : Reference scenario

A.2. Presentation of the algorithm

In order to run this algorithm, the delay and Doppler shift of every multipath of channel has to be known (the Doppler shift may eventually be deduced from its angle of arrival). Let τ_l and ϑ_l denote the delay and Doppler shift of a given multipath l at the time t. The variations of the delay of l between the times t and $t + \Delta t$ can be estimated by Eq. A.1:

$$\widetilde{\tau_l}(t + \Delta t)_{est} = \tau_l + \frac{f_0}{\vartheta_l}\Delta t \tag{A.1}$$

The principle of the algorithm is to find multipath l among all the multipaths at the time $t + \Delta t$, by searching the echo whose delay is the closest to the estimated value of the delay of l ($\widetilde{\tau_l}(t + \Delta t)_{est}$).

- Let L denote the number of multipaths in the impulse response at $t + \Delta t$. The multipath l is given by the index minimizing Eq. A.2 :

$$\min_{i \in [1,L]} |\widetilde{\tau_l}(t + \Delta t)_{est} - \tau_i(t + \Delta t)| \tag{A.2}$$

- It is reminded that the influence of the environment has been limited to 50 m. For that reason, some multipaths appear and some multipaths disappear at every instant. Therefore, Eq. A.2 may have no solution, which can impair the algorithm. Therefore, it has been decided to put a threshold ε on the Eq. A.2 in order to assure that the algorithm does not confuse the multipath l with another multipath at $t + \Delta t$. The algorithm will consider the solution of Eq. A.2 if and only if :

$$\min_{i\in[1,L]} |\widetilde{\tau_l}(t + \Delta t)_{est} - \tau_i(t + \Delta t)| < \varepsilon \tag{A.3}$$

If there is no solution to Eq. A.3, the algorithm considers that multipath l has disappeared. To the contrary, if a multipath of the channel at $t + \Delta t$ is not a solution of Eq. A.3 (it has no fiber according to Eq. A.3), the algorithm considers that this multipath has appeared at the instant $t + \Delta t$. The threshold has been set to ε =20.10^{-12} s. Indeed, this value is the lowest delay difference between two distinct multipath sources, according to the geometry of the scenario and the size of the facets (50 cm). This algorithm is applied to each multipath of the channel all along the trajectory, in order to draw the life span of the multipaths of the scenario.

Note that a major assumption of this algorithm is the fact that the Doppler can be considered as constant between two consecutive instants. In order to verify this assumption, Fig. A.3 represents the variation of the Doppler shift of the multipath source B spotted on Fig. A.2. Three different elevations of the source have been considered: 0°, 40° and 80°. Note that the position 0 of the trajectory has been set at the location of B. It can be observed on Fig. A.3 that the largest Doppler variations happen in the vicinity of the multipath source, with 0° elevation. Therefore, the maximum Doppler variation has been estimated in that worst case. With a channel sampling period of Δt =5 ms, the maximum Doppler shift variation is approximately 35 mHz. The resulting delay shift has an order of magnitude of 10^{-13} s (using Eq. A.1). This error on the delay estimation is much lower than the ε threshold. Thus, it can be considered that the assumption of stationary Doppler is always fulfilled for this application.

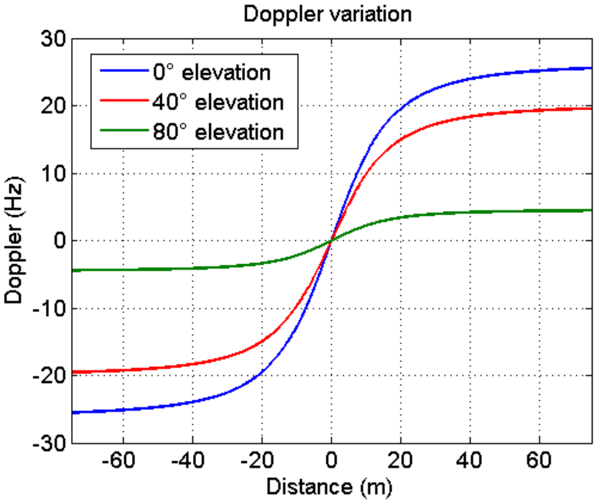

Figure A.3 : Variation of the Doppler of source B considering three elevations

A.3. *Results of the algorithm*

This algorithm has been applied to the reference scenario. The evolution of the parameters corresponding to the three multipath sources A, B and C has been illustrated. Fig. A.4 represents their delay along different segments of the trajectory and Fig. A. 5 represents their Doppler shifts. The continuity of these delays and Doppler shifts shows that the algorithm has succeeded in following the signature of those echoes. Note that the delays are represented normalized by the LOS delay. Therefore, the variation of the delay is related to the Doppler shift of the LOS and not the absolute Doppler shift of the echoes. According to the position of the satellite set in section 2.2, the Doppler shift of the LOS is approximately 10 Hz. Therefore, the delays of the scatterers are supposed to decrease as long as their absolute Doppler shift is above 10 Hz, and decreases under 10 Hz. This statement is confirmed by the consistency between the delay variations of the echoes with their corresponding Doppler shifts. It also comforts the well-functioning of the algorithm.

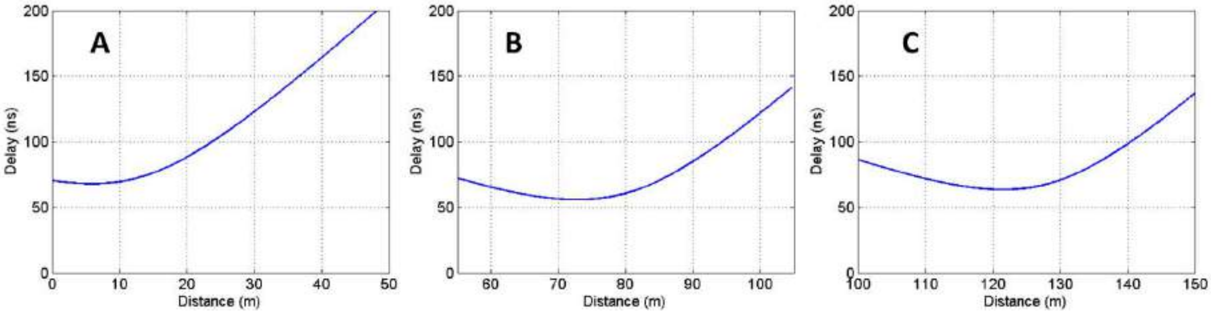

Figure A.4 : Evolution of the delays of the sources A, B and C

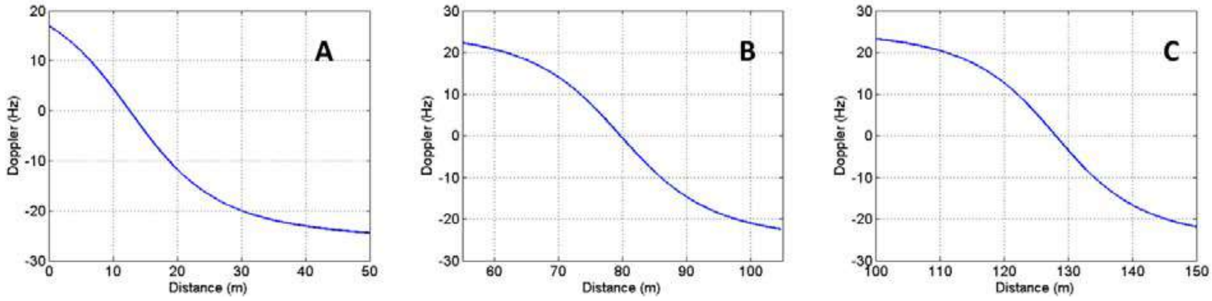

Figure A.5 : Evolution of the delays of the sources A, B and C

B. Annex B: Demonstration of the discriminator error open loop close formula

B.1. Definition of the discriminator open loop error

The open loop discriminator error has been used in chapter 5 to assess the performance of the different reduction methods. This approach was chosen because the discriminator error quantifies the impact of the multipath channel on pseudo-range error of GNSS systems. Moreover, the open-loop characteristic allows investigating the impact of the multipaths separately from any loop effect.

The hierarchy of the reduction methods established in the study of the discriminator open-loop error preservation has been confirmed by the further assessments of different simulation configurations: addition of tracking loops, addition of noise and changes in signal modulation and bandwidth. Therefore, the discriminator error showed to be a relevant comparison criterion to assess the performance of the reduction methods. However, it has to be mentioned that the absolute value is meaningless, since the useful pseudo-range error of the GNSS systems must be considered with the tracking loops effects, which have a major impact on the pseudo-range error (chapter 5). Thus, the discriminator open loop error has to be considered with respect to a reference open loop error. For example, the ratio between the discriminator errors caused by two different channel models may quantify the difference between these models, as it was performed to compare the reduced channel models with the reference channel in section 5.3.

The discriminator error in the delay dimension is computed as the delay shift of the S-curve caused by the distortion of the autocorrelation function by the multipath channel. Fig. B.1 illustrates this principle using an EML (*Early Minus Late*) discriminator with C_S =1 chip (*Chip Spacing*). Considering a given signal modulation and bandwidth and a noiseless simulation, the distortion of the correlation function is fully determined by the channel impulse response. Therefore, it has been decided to implement a close formula to express the value of the discriminator error in terms of the channel power and delay characteristics.

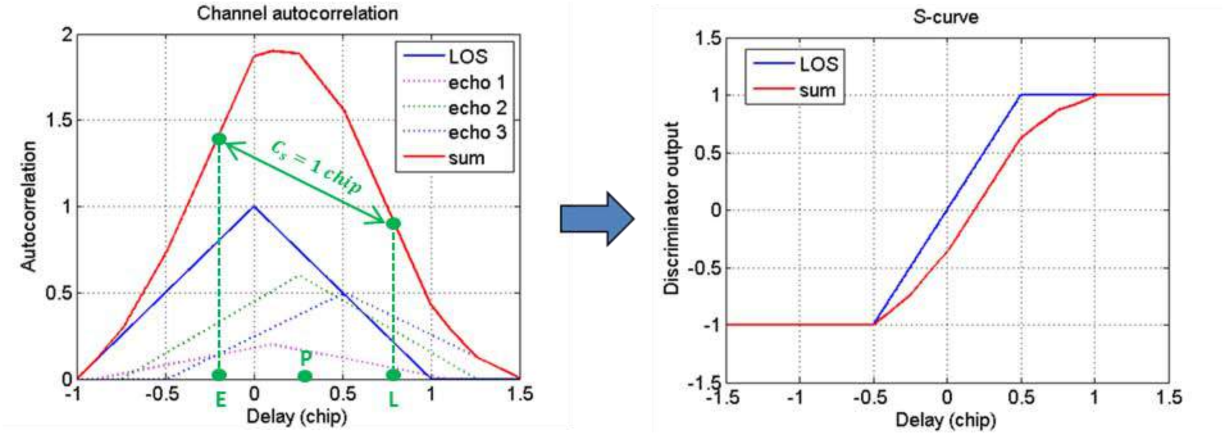

Figure B.1 : Illustration of an autocorrelation function distortion by the multipath channel the resulting S-curve

B.2. *Development of the formula*

B.2.1. Hypothesis:

Before going further in the development of the formula, a few hypotheses will be made. Indeed, the shape of the channel autocorrelation function is defined by the modulation and the bandwidth of the signal. Moreover, the estimation of the delay corresponding to the 0 of the discriminator depends on the type of discriminator considered and on the chip spacing. To finish, a few assumptions will be made on the channel parameters.

- **Signal characteristics:**

The signal is a simple BPSK signal, meaning that the autocorrelation function is a single peak lobe of width $2T_c$ (T_c denotes the chip duration). The shape of this lobe is smoothed by the RF bandwidth of the receiver: from a perfect triangle in case of infinite bandwidth to rounded profiles with lower RF bandwidth. Fig. B.2 represents the impact of the RF bandwidth on the signal autocorrelation function. In this section, an infinite bandwidth is considered. Indeed, the properties of the triangle function will be necessary for the development of the formula.

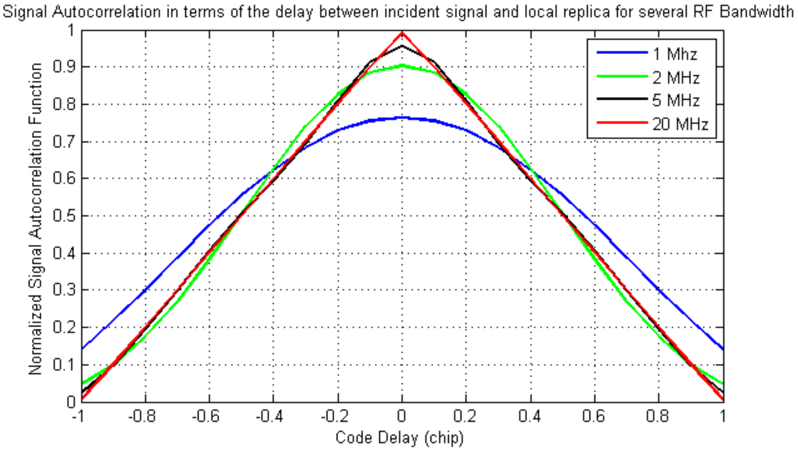

Figure B.2 : Autocorrelation Function of the Signal for different RF Bandwidth

- **Discriminator characteristics:**

The discriminator is an EMLP discriminator, with C_s =1 chip. The value of the discriminator output depending on the delay τ between the LOS signal and its local replica is given by Eq. B.1, where the terms r_l denote the correlation function of the L replicas of the channel (multipaths + LOS). Note that the discriminator is supposed to be synchronized with the LOS signal.

$$D(\tau) = \left|\sum_{l=1}^{L} r_l(\tau - \frac{C_s}{2})\right|^2 - \left|\sum_{l=1}^{L} r_l(\tau + \frac{C_s}{2})\right|^2 \qquad \text{(B.1)}$$

- **Impulse response parameters:**

It can be deduced that the autocorrelation function r_l of a signal replica of delay τ_l and complex amplitude $\widetilde{\gamma_l}$ is a triangle function of width $2T_c$, centered on τ_l:

$$r_l(\tau) = \begin{cases} \widetilde{\gamma_l}.(1 - \left|\frac{\tau - \tau_l}{T_c}\right|)\ if - T_c < \tau < T_c \\ 0\ if\ |\tau| > T_c \end{cases} \tag{B.2}$$

Let t_e denote the discriminator error in the delay dimension ($D(t_e) = 0$). The major assumption on the channel parameters relies on the simplification of Eq. B.2:

$$\forall l, \quad \begin{cases} \left|\frac{t_e - \frac{C_s}{2} - \tau_l}{T_c}\right| = -\frac{t_e - \frac{C_s}{2} - \tau_l}{T_c} \\ \left|\frac{t_e + \frac{C_s}{2} - \tau_l}{T_c}\right| = \frac{t_e + \frac{C_s}{2} - \tau_l}{T_c} \end{cases} \tag{B.3}$$

In other words, when the prompt correlator is located at t_e, the late correlator must be located on the decreasing slope of the correlation function (for each signal replica). Similarly, the early correlator must be located on the increasing slope of the correlation function (for each signal replica). This leads to hypothesis 1:

$$\forall l, \begin{cases} t_e - \tau_l \le C_s/2 \\ t_e - \tau_l \ge -C_s/2 \end{cases} \tag{B.4}$$

Moreover, both early and late correlators must not be located at delays corresponding to zeroes of the correlation function (for each replica), in order to stick to the assumption of triangle function:

$$\forall l, \begin{cases} 1 - \left|\frac{t_e - \frac{C_s}{2} - \tau_l}{T_c}\right| \ge 0 \\ 1 - \left|\frac{t_e + \frac{C_s}{2} - \tau_l}{T_c}\right| \le 0 \end{cases} \tag{B.5}$$

This leads to hypothesis 2:

$$\forall l, \quad \begin{cases} t_e - \tau_l \leq T_c - \frac{C_s}{2} \\ t_e - \tau_l \geq \frac{C_s}{2} - T_c \end{cases} \tag{B.6}$$

The two hypotheses of Eq. B.4 and B.6 can be combined into Eq. B.7:

$$\boxed{\forall l, \ |t_e - \tau_l| \leq \min(\frac{C_s}{2}, T_c - \frac{C_s}{2})} \tag{B.7}$$

B.2.2. Calculation and result

The starting point of the computation of the discriminator error is the fact that t_e is the solution of:

$$D(t_e) = 0 \tag{B.8}$$

Let $\tau_l, \gamma_l, \varphi_l$ denote the delay, amplitude module and phase of the contribution l (all normalized by the LOS parameters). By injecting Eq. B.2 into Eq. B.8, and considering that both terms of the equation are squared modules that can be split into their real and imaginary parts:

$$\begin{aligned} &Re\left(\sum_{l=1}^{L} \gamma_l \left(1 + \frac{te - \frac{Cs}{2} - \tau_l}{T_c}\right) e^{j\varphi_l}\right)^2 + Im\left(\sum_{l=1}^{L} \gamma_l \left(1 + \frac{te - \frac{Cs}{2} - \tau_l}{T_c}\right) e^{j\varphi_l}\right)^2 \\ &= Re\left(\sum_{l=1}^{L} \gamma_l \left(1 + \frac{te + \frac{Cs}{2} - \tau_l}{T_c}\right) e^{j\varphi_l}\right)^2 + Im\left(\sum_{l=1}^{L} \gamma_l \left(1 + \frac{te + \frac{Cs}{2} - \tau_l}{T_c}\right) e^{j\varphi_l}\right)^2 \end{aligned} \tag{B.9}$$

Then, by splitting the exponential terms into real and imaginary parts, Eq. B.9 becomes:

$$\begin{aligned}\left(\sum_{l=1}^{L}\gamma_l\left(1+\frac{te-\frac{Cs}{2}-\tau_l}{T_c}\right)\cos(\varphi_l)\right)^2+\left(\sum_{l=1}^{L}\gamma_l\left(1+\frac{te-\frac{Cs}{2}-\tau_l}{T_c}\right)\sin(\varphi_l)\right)^2 \\ =\left(\sum_{l=1}^{L}\gamma_l\left(1+\frac{te+\frac{Cs}{2}-\tau_l}{T_c}\right)\cos(\varphi_l)\right)^2 \\ +\left(\sum_{l=1}^{L}\gamma_l\left(1+\frac{te+\frac{Cs}{2}-\tau_l}{T_c}\right)\sin(\varphi_l)\right)^2\end{aligned} \quad \text{(B.10)}$$

Eq. B.10 can be developed, in order to isolate t_e. The final expression of the discriminator error is displayed on Eq. B. 11. Note that t_e has been converted in the distance dimension (c denotes the speed of light). Finally, $p_e$denotes the discriminator error, depending on the channel parameters (delay, amplitude and phase):

$$\boxed{pe = c\,\frac{\sum_{l=1}^{L}{\gamma_l}^2\tau_l+\sum_{i<j=1}^{L}\gamma_i\gamma_j\cos\left(\varphi_i-\varphi_j\right)\left(\tau_i+\tau_j\right)}{\sum_{i,j=1}^{L}\gamma_i\gamma_j\cos\left(\varphi_i-\varphi_j\right)}} \quad \text{(B.11)}$$

It can be observed that the close formula of Eq. B.11 does not depend on the chip spacing. Actually the chip spacing has an influence on the hypothesis of this equation only. Indeed, it can be observed on Eq. B.5 and B.7 that C_s has an impact on hypothesis 1 and hypothesis 2. The narrower the chip spacing is, the more limited the domain of validity of the formula is.

B.3. Validation of the formula

In order to validate the formula, the discriminator open loop error has been computed along a reference scenario using the formula on one side, and a dedicated algorithm on the other side. This algorithm has been implemented for the purpose of this study and estimates the prompt position on the channel correlation function corresponding to the zero of the S-curve. To do so, a segment search approach along the delay dimension of the correlation function has been processed, in order to estimate the minimum absolute value of the S-curve. The chip spacing considered for this segment search is tunable. In order to minimize the computational cost all by conserving a suitable accuracy, the grid search is processed four consecutive times, each time increasing the sampling rate of the code delay axis. First, the location of the minimum discriminator is searched with a grid size of $T_c/10$. Then the delay bin containing this minimum is sampled at $T_c/100$ and this operation is repeated three times, meaning that approximately 3 cm resolution is reached. The reference scenario along which the discriminator open loop error has been computed is represented on Fig. B.3. The emitter is located azimuth 30° and elevation 35°, while the receiver is moving at 5 m.s^{-1} along its 150 m long trajectory.

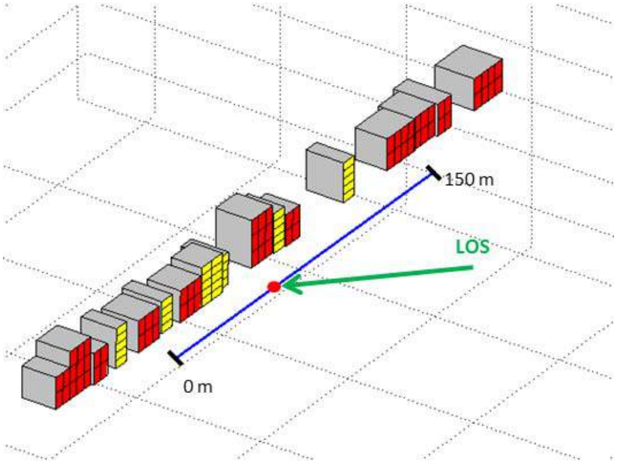

Figure B.3 : illustration of the reference scenario

The discriminator error has been computed with three different chip spacings, T_c, $T_c/2$ and $T_c/5$. The difference between the discriminator error computed with the formula and with the algorithm has been represented on Fig. B.5 all along the reference scenario, considering the three different chip spacings.

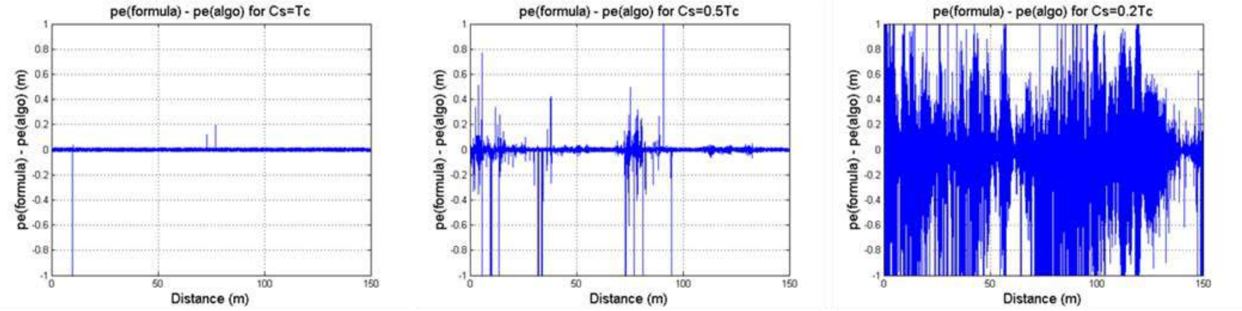

$C_s = T_c$ $\quad$ $C_s = T_c/2$ $\quad$ $C_s = T_c/5$

Figure B.4 : Discriminator error difference between formula and algorithm for different chip spacings

It can be observed on the left plot of Fig. B. 4 that with large chip spacings, the correspondence between the formula and the algorithm is almost perfect. Indeed, the formula computed the exact value of the discriminator error for more than 99.9% of the error samples (the fluctuations lower than 3 cm are due to the resolution of the algorithm). However, with lower chip spacings, more singularities appear. This is due to the fact that low chip spacings make the assumptions of the formula more stringent. In the case of $C_s = T_c/2$, the valid samples are only 92%, and less than 50% with $C_s = T_c/5$.

As a conclusion, the formula of Eq. B. 11 has been validated by this test scenario. Indeed, the formula is able to compute the open loop discriminator error perfectly as long as the assumptions of Eq. B.7 are respected (left plot of Fig. B. 4).

However, these assumptions restrict the domain of validity of the formula significantly in the case of low chip spacings ($C_s < T_c$). Moreover, it can be observed on Eq. B.7 that the position of the prompt correlator itself has an impact on these assumptions. The higher the discriminator error is, the narrower is the domain of validity of the formula. Therefore, the formula is likely to be unsuited for highly degraded environments, in NLOS conditions for example. Therefore, it has been decided to lead the reduction methods comparison of section 5.3 using the algorithm described above, even if it increases the computation load of the study.

Introduction en français

a. Contexte et motivations de la thèse

Le développement de la constellation GPS au cours des années 90 a rendu de plus en plus accessible les systèmes de navigation par satellite. En effet, le besoin d'obtenir un signal direct et correctement synchronisé afin de fournir une navigation fiable tire un avantage considérable des larges étendues terrestres couvertes par les satellites MEO (*Medium Earth Orbit*). Plus récemment, les avancées dans le domaine de la navigation concernent majoritairement l'implémentation de signaux plus complexes afin d'améliorer la précision de la navigation et augmenter leur résistance aux perturbations dues aux interférences, au bruit, aux perturbations ionosphériques ou à l'environnement du récepteur. Dans cette optique, le projet européen GALILEO a mené au cours des dernières années sera intégralement déployé à horizon de 2020.

Actuellement, le développement des systèmes de navigation par satellite est motivé par un intérêt croissant pour le positionnement à haute précision, tout publique et appliqué dans des environnements urbains où la quantité d'obstacles au signal mène à des pertes de LOS (*Line Of Sight*) et à l'apparition de multitrajets qui se combinent au signal utile. De nombreuses applications bénéficieraient de l'amélioration du positionnement en milieu urbain, incluant les services de géolocalisation, les systèmes de transport intelligent ou la réalité augmentée. Il est évident que l'impact des multitrajets sur les récepteurs GNSS (en particulier pour les futurs récepteurs multi-constellation GALILEO) est d'un intérêt primordial, et l'utilisation de ce type de ce type de récepteurs dans des environnements de plus en plus contraints nécessite un test préalable approfondi, tout comme le test d'éventuels algorithmes de réjection de multitrajets.

Les multitrajets sont en effet l'une des plus sérieuses menaces sur la précision des systèmes GNSS. Il s'agit du phénomène par lequel le signal arrive au récepteur accompagné de multiples échos dus à la réflexion et à la diffusion de l'onde électromagnétique par l'environnement urbain. Les échos arrivent au récepteur par un chemin plus long que le signal direct, impliquant une distorsion de la porteuse et du code du signal GNSS, d'où la dégradation des performances GNSS du système. L'effet des multitrajets est prédominant en environnement contraint tel que les canyons urbains, dans la mesure où les antennes réceptrices sont entourées par de multiples structures et réfléchissantes (murs, arbres, véhicules, etc.). Dans certaines configurations, une partie des multitrajets peut-être causée par la plateforme support des antennes réceptrices.

Dans tous les cas, les caractéristiques principales du canal de multitrajets peuvent être décrites par la réponse impulsionnelle, composée de la somme des différents échos constitués de leur amplitude, phase, retard, angle d'arrivée et décalage Doppler.

Ainsi, des modèles de canal large-bande ont été implémentés parallèlement au développement du secteur GNSS, dans le but de synthétiser des environnements réalistes afin de tester les nouveaux modèles de récepteur. Deux principaux types d'approche peuvent être distingués: modèles statistiques et modèles déterministes. Comme de nombreuses variétés de canaux GNSS peuvent être rencontrées, il reste difficile de construire des modèles statistiques ou empiriques à la fois précis et adaptables. De même, des géométries d'environnement très complexes peuvent être rencontrées (par exemple en environnement), ce qui rend les modèles purement déterministes lourds en termes de charge calculatoire. Ainsi, des modèles hybrides ont été développés récemment, mélangeant approche statistique et déterministe. Ces simulateurs de canal constituent un bon compromis entre précision du modèle, adaptabilité et temps calculatoire acceptable. E particulier, le simulateur SCHUN (*Simplified Channel for Urban Navigation*), développé à l'ONERA au cours de la thèse de Mehdi Ait-Ighil (Ait 12), a montré qu'il était capable de synthétiser les phénomènes de masquage et de multitrajets de façon déterministe à travers le concept de ville virtuelle, avec des performances proches des modèles purement physiques avec une efficacité calculatoire proche du temps réel.

Cependant, bien que le modèle de bâtiments développé sous la référence « 3CM » (*3 components Model*) reproduit de façon très précise l'effet des multitrajets sur les systèmes GNSS, le grand nombre d'échos générés par le modèle (plusieurs milliers à chaque instant) empêche son application directe à la problématique de test de récepteurs en environnement réaliste. En effet, ces modèles sont destinés à être implémentés dans des simulateurs GNSS logiciels ou hardware. En pratique, les applications logicielles et hardware souffrent toutes deux de la trop grande quantité de multitrajets des modèles de canal. Pour les simulateurs logiciels, le temps de traitements des échos devient rapidement critique. Pour les simulateurs hardware, chaque écho généré requière son propre canal, augmentant ainsi rapidement la complexité et le coût de l'équipement. Pour ces raisons, la taille des réponses impulsionnelles doit être réduite. Les techniques de réduction doivent être appliquées au modèle de canal afin de limiter le nombre d'échos sans porter atteinte à la représentativité du canal en termes de performances GNSS.

b. Objectifs de la thèse

Pour cette raison, il a été décidé de consacrer cette thèse sur l'analyse des différentes solutions pour réduire le nombre de multitrajets des réponses impulsionnelles, tout en préservant la précision d'origine du modèle SCHUN en termes d'erreur de pseudo-distance des récepteurs GNSS. Dans la lignée de (AIT 13), il a été décidé d'implémenter des techniques de réduction afin de rendre le modèle SCHUN adaptable à la problématique de test de récepteurs GNSS via des émulateurs hardware, respectant les contraintes de précision et une implémentation réaliste (faible temps de calcul).

L'approche choisie afin d'aborder ce problème peut être divisée en deux étapes majeures. D'un côté, différentes méthodes de réduction vont être implémentés et commentées et d'un autre côté, elles vont être comparées à travers le critère de préservation de l'erreur de positionnement du récepteur. Trois différents modèles de réduction ont été considérés. Parmi ces modèles, deux approches peuvent être identifiées. En effet, les deux méthodes « Clustering Weighted » et « Satistical Method » cherchent à conserver les caractéristiques du canal (retard, Doppler, amplitude) en premier lieu. Elles reposent respectivement sur l'agrégation de multitrajets et la sélection statistique des multitrajets les plus importants, les deux méthodes étant peu gourmandes en termes de temps de calcul. Au contraire, la méthode « Parametric Optimization » cherche à préserver la fonction d'autocorrélation du canal, en optimisant mathématiquement les paramètres des multitrajets du canal réduit. Elle est plus coûteuse en termes de temps de calcul. La comparaison des approches selon la préservation de l'erreur de pseudo-distance étudie les performances des méthodes peu coûteuses, en comparaison de la méthode d'optimisation paramétrique.

c. Organisation de la thèse

Le chapitre 1 introduit la problématique de modélisation de canaux de multitrajets réduits. La première section présente différents modèles de canal, extraits de la littérature, divisés en trois groupes: statistique, déterministe et hybride physico-statistique. Puis, une section est dédiée à la présentation et la validation d'un modèle hybride spécifique, le modèle SCHUN, car il sera utilisé comme modèle de référence tout au long de la thèse. Finalement, les difficultés rencontrées pour adapter ce modèle à la problématique du test de récepteurs GNSS motive le sujet de cette thèse.

Le chapitre 2 est consacré à l'implémentation de méthodes d'agrégation de multitrajets. La question à laquelle ce chapitre répond progressivement est « quels facteurs de proximité entre les échos sont à prendre en compte pour effectuer l'agrégation ? », et « quel formalisme rendrait l'algorithme le plus efficace en termes de temps de calcul ? ». En étude préliminaire, une simple méthode de sélection de multitrajets selon leur puissance est essayée. Puis, afin d'optimiser la préservation de l'étalement retard des multitrajets, différents modèles de Tap Delay Line ont été implémentés. Dans les sections suivantes, la possibilité d'ajouter le paramètre Doppler au processus d'agrégation a été testé via les algorithmes de Clustering. Finalement, la méthode « Clustering Weighted » est proposée, visant à préserver au mieux les caractéristiques retard-puissance au mieux en un temps de calcul négligeable, tout en prenant en préservant les Doppler des multitrajets, afin d'améliorer la stabilité du canal réduit.

Le chapitre 3 présente l'implémentation d'un procédé d'optimisation paramétrique, visant à déterminer les paramètres optimaux des multitrajets du canal réduit (retard, amplitude complexe et Doppler) pour préserver au mieux la fonction d'autocorrélation du canal. Après avoir introduit la fonction coût associée au problème, l'optimisation des différents paramètres est présentée, ainsi que l'architecture de l'algorithme SAGE choisi pour résoudre ce problème d'optimisation. Une importance particulière est apportée à la résolution Doppler de l'algorithme, qui a un fort impact sur ses performances. Plus précisément, le compromis optimal entre résolution Doppler et nombre de multitrajets dans le canal réduit est recherché, afin d'implémenter une méthode de paramétrisation optimale.

Le chapitre 4 étudie la possibilité de sélectionner les multitrajets du canal réduit à partir de leur distribution statistique, en considérant que chaque multitrajet évolue selon une chaîne de Markov du premier ordre. Une analyse critique de la méthode CRIME présentée dans (Schu 14) est proposée. En particulier, l'impact de l'estimation d'amplitude et de phase sur la réponse impulsionnelle est souligné, ce qui permet d'implémenter une méthode de réduction semi-statistique innovante. Cette méthode repose sur la sélection statistique des retards des multitrajets, tandis que l'amplitude complexe est déduite du profile retard-amplitude de la réponse impulsionnelle.

Le chapitre 5 présente la comparaison des performances des méthodes de réduction en termes de préservation de l'erreur de pseudo-distance. Dans un premier temps, un état de l'art des différentes études comparatives de méthodes de réduction est présenté. Puis, l'impact des méthodes de réduction sur l’erreur du discriminateur en boucle ouverte est présenté. Une hiérarchie des méthodes est établie selon les résultats de cette comparaison. Cette simulation est transposée dans différents cas de figure d'angle d'arrivée du signal et différents nombre d'échos dans le canal réduit, afin de tester l'impact de ces paramètres sur les performances des algorithmes. Puis, l'impact des boucles de poursuite DLL et PLL est étudié, avec l'aide du récepteur logiciel GeneIQ, qui est brièvement présenté dans le chapitre 5. Par cette comparaison, une autre hiérarchie de méthodes est établie. Différents paramètres du signal sont étudiés, afin d'élargir la validité des résultats.

Finalement, la conclusion de la thèse décide de la méthode à utiliser pour résoudre au mieux le problème de réduction du canal de multitrajets, en mettant en balance le temps de calcul nécessaire à chaque méthode.

d. Contributions de la thèse

Cette thèse analyse la méthode la plus efficace afin de réduire la taille de la réponse impulsionnelle. Tout au long de l'étude, différents résultats seront présentés:

– Implémentation de la méthode Clustering Weighted, qui montre une grande efficacité en termes de préservation du retard et Doppler avec un faible temps de calcul. L'erreur de pseudo-distance du canal d'origine est également bien préservée (presque aussi bien que des méthodes d'optimisation paramétrique).

– Développement d'une méthode de paramétrisation des multitrajets du canal réduit, visant à conserver au mieux la fonction d'autocorrélation du canal, à l'aide de l'algorithme SAGE: détermination du compromis idéal entre résolution Doppler et nombre de multitrajets dans le canal réduit, afin d'optimiser l'efficacité de l'algorithme.

- Implémentation d'une méthode statistique, afin de sortir les multitrajets du canal réduit de la distribution statistique correspondant à un processus stochastique prédéfini. Ce modèle est alors modifié afin d'améliorer les performances en termes de préservation des caractéristiques du canal.
- Comparaison de ces trois méthodes selon la préservation de l'erreur de pseudo-distance du récepteur, en considérant différents paramètres du signal et configurations de poursuite. Détermination de la méthode la plus adaptée à répondra à la problématique de réduction du canal en prenant en compte leur charge calculatoire.
- Implémentation du critère d'erreur discriminateur en boucle ouverte, permettant de comparer rapidement les performances des méthodes de réduction. Développement de la formule de calcul de ce critère.

Conclusion en français

Ce travail de thèse présente l'implémentation de trois algorithmes de réduction du canal de multitrajets. A partir d'une revue de la littérature concernant l'application de différents modèles de canaux au test de récepteurs GNSS, le grand nombre de multitrajets présents dans les réponses impulsionnelles apparaît comme une majeure limitation à des campagnes de tests réalistes. En effet, le simulateur de canal hybride physico-statistique SCHUN (*Simplified Channel for Urban Navigation*) est considéré comme un bon compromis entre précision du modèle et charge calculatoire. Cependant, le grand nombre de multitrajets simulés empêche les récepteurs logiciels d'être testés en temps réel et d'autant plus les générateurs de canaux hardware pour le test de récepteurs physiques. Différentes approches pour réduire le canal ont été identifiées dans la littérature et ont pu être classées en trois familles: méthodes d'agrégation, méthodes d'optimisation paramétriques et méthodes statistiques. Il a été décidé de considérer chaque approche individuellement afin de couvrir l'ensemble des possibilités de réduction. Ces trois approches constituent le point de départ pour l'implémentation de méthodes innovantes, développées dans l'optique de la préservation des paramètres large-bande du canal (retard, Doppler et amplitude complexe). Après avoir abouti à une méthode spécifique par approche, toutes considérées comme optimales au sein de leur propre famille, ces méthodes ont été comparées selon leur capacité à préserver l'erreur de pseudo-distance du récepteur de navigation. Cette étude a permis d'établir une hiérarchie des méthodes, indépendantes des caractéristiques du signal et des boucles de poursuite. En particulier, il a été montré que la méthode d'agrégation implémentée durant cette thèse, nommée Clustering Weighted, est capable d'approcher les performances des méthodes paramétriques et même les dépasser dans certaines situations. Ainsi, elle constitue un compromis intéressant entre préservation des performances GNSS et faible temps de calcul.

Les trois premiers chapitres de la thèse sont dédiés à l'implémentation des trois principales méthodes de réduction considérées. Ainsi, les résultats présentés tout au long de cette thèse peuvent être divisés en deux types. D'un côté, trois méthodes de réduction sont présentées selon les trois approches; avec des détails concernant le procédé de réduction, élaborées de façon à minimiser l'impact sur les paramètres large bande du canal d'origine. D'un autre côté, une étude comparative de leur impact sur l'erreur de pseudo-distance du récepteur selon le canal d'origine, ce qui a permis de préconiser l'utilisation de la meilleure méthode au détriment des autres.

Le premier résultat présenté dans cette thèse concerne la nécessité de prendre le retard, la phase, l'amplitude et le Doppler des multitrajets dans le procédé d'agrégation de façon à préserver le paramètre large bande du canal d'origine. En effet, la méthode usuelle Tap Delay Line a été étudiée, en ajoutant différentes améliorations (Taps mobiles le long de la ligne de retard, méthode de ré-échantillonnage du canal), mais a montré ses limites en termes de préservation de la diversité Doppler du canal d'origine. Ceci est dû au fait que des multitrajets avec des Dopplers différents sont agrégés. Ainsi, des méthodes de clustering selon les dimensions du retard et du Doppler ont été testées. Il a été montré que le fait de pondérer les multitrajets par leur amplitude durant la phase « d'allocation » de l'algorithme optimise la préservation à la fois du profile puissance-retard et puissance-Doppler du canal d'origine. Cette étude a mené à l'implémentation de la méthode « Clustering Weighted », efficace en termes de temps de calcul et offrant une bonne préservation des paramètres du canal et de sa continuité.

Cette thèse présente également le développement d'une méthode d'optimisation des paramètres des multitrajets du canal réduit pour préserver au mieux l'erreur de pseudo-distance du récepteur. Pour ce faire, il a été décidé de minimiser la différence entre les fonctions d'autocorrélation du canal avant et après réduction, en utilisant l'algorithme d'optimisation SAGE (« Space Alternating Generalized Expectation-Maximization »). Il s'applique au retard, à l'amplitude complexe et au Doppler des multitrajets du canal réduit. Après avoir prouvé que l'algorithme SAGE était bien choisi pour répondre à la problématique, l'importance de choisir une résolution Doppler adéquate en fonction du nombre de multitrajets à estimer a été mise en évidence. Cependant, un inconvénient majeur de cette méthode a été identifié: la discontinuité des paramètres du canal réduit. Ceci remet en cause la possibilité d'utiliser cette méthode pour réduire le canal de multitrajets.

Cette thèse présente également l'implémentation d'une méthode statistique de calcul des multitrajets du canal réduit, dont les paramètres sont supposés évoluer selon une chaîne de Markov du premier ordre. Il a été montré que l'application d'un tel modèle stochastique impacte fortement le profile puissance-retard du canal d'origine. Ainsi, une nouvelle approche semi-statistique a été proposée. Dans cette approche alternative, seul le retard des multitrajets évolue de façon stochastique tandis que l'amplitude complexe des multitrajets est déduite du retard sur la réponse impulsionnelle continue. Cette méthode donne de bons résultats en termes de préservation du profile puissance-retard du canal d'origine, avec une bonne continuité des retards et phases des multitrajets, avec un temps de calcul raisonnable.

Cependant, l'originalité de cette thèse réside également dans la comparaison des méthodes effectuées dans le but de juger la meilleure méthode en termes de préservation des performances GNSS. Les trois approches considérées ont été appliquées à un même scénario de référence généré par le simulateur SCHUN. Dans un premier temps les modèles de canaux réduits ont été comparés selon la préservation de l'erreur discriminateur en boucle ouverte (sans effet de filtrage des boucles de poursuite). Une formule a été établie afin de lier l'erreur discriminateur aux paramètres large bande des multitrajets du canal. Cette première comparaison a permis d'établir une hiérarchie des méthodes de réduction en termes de préservation de l'erreur de pseudo-distance. Comme attendu, la méthode paramétrique SAGE offre la meilleure préservation. Cependant, il a pu être observé que la méthode du Clusetring Weighted approche les performances de SAGE dans certaines configurations. En particulier, il a été montré que le Clustering Weighted dépassait les performances de SAGE après augmentation du nombre de multitrajets dans le canal réduit. Comparée aux deux autres méthodes, la méthode statistique impacte sévèrement l'erreur de pseudo-distance due au canal d'origine, ce qui l'élimine des possibilités de réponse à la problématique de réduction du canal.

Afin d'étudier l'impact des boucles de poursuite sur ces résultats, la même comparaison a été effectuée sur un récepteur logiciel poursuivant le signal à l'aide des boucles FLL et DLL. Les conclusions précédentes concernant le cas boucle ouverte ont presque intégralement été conservées, bien que la différence entre SAGE et la méthode de clustering est diminuée. De plus, l'étude de différentes configurations GNSS (modulation du signal, bande RF du récepteur et bruit) n'a montré aucune influence sur les résultats de la comparaison des méthodes.

En résumé, les résultats présentés dans cette thèse peuvent être scindés en deux parties. Premièrement, une comparaison innovante de méthodes de réduction a été effectuée : d’une simple méthode d’agrégation de multitrajets aux méthodes d’optimisation paramétrique en passant par une méthode statistique. Cette comparaison a permis d’établir une hiérarchie de méthodes de réduction, selon la conservation des performances GNSS du système. Cette comparaison a pu être généralisée à différentes configurations de simulation (boucles de poursuite, bande RF du récepteur, modulation du signal, bruit). Ainsi, l’erreur du discriminateur en boucle ouverte a montré être un bon indicateur de performances des méthodes, pour leur comparaison en tout cas. Le second type de résultat de cette thèse est l’implémentation d’une méthode de réduction innovante, le Weighted Clustering, qui a montré être capable de préserver le profile retard-puissance et retard-Doppler du canal d’origine presque parfaitement avec moins de 10 multitrajets, et ce avec un temps de calcul proche du temps réel. Plus précisément, cette méthode est proche de méthodes paramétriques (précises mais très lourdes en termes de temps de calcul) en termes de performances. Ainsi, l’utilisation du Clustering Weighted est recommandée dans le cadre de la réduction du canal de multitrajets. Elle semble être appropriée pour adapter la sortie de simulateurs de canal précis tels que SCHUN au test de récepteurs

GNSS, y compris dans le cadre de l’utilisation de simulateurs hardware de canal (moins de 10 multitrajets dans le canal réduit).

Des travaux futurs dans la lignée de ce travail pourraient inclure un développement plus approfondi des méthodes de réduction ainsi que des tests de validation plus poussés. D’un côté, les performances de la méthode statistique semblent être bien plus mauvaises que celles de la méthode de clustering. Un travail plus approfondi sur le processus stochastique en question (dans le prolongement des modifications déjà apportées) pourrait améliorer cette approche, afin de la rendre compatible avec le test de récepteurs GNSS. D’un autre côté, d’autres validations pourraient inclure l’application de ces méthodes de réduction à d’autres canaux large-bande, avec un banc de test plus large (autres types de modulations par exemple ou autres environnements), afin de tester les nouvelles générations de récepteur GNSS plus spécifiquement.

Cependant, la perspective principale de cette étude serait l’application de ces méthodes de réductions à d’autres modèles de canal, en particulier les modèles déterministes précis mais très lourds tels que SE-RAY FERMAT d’autres modèles physico-statistiques tels que le modèle du DLR [Lehn 07]. Premièrement, cette étude élargirait les conclusions de cette thèse. Deuxièmement, cela permettrait la comparaison de différents modèles de canal à travers leurs canaux réduits, ce qui offrirait une nouvelle comparaison critique des approches physiques utilisées.

Finalement, la méthode du Clustering Weighted pourrait être intégrée dans des outils hardware, en considération des différentes limitations technologiques que cela implique. Cela permettrait de valider l’utilisation conjointe du modèle SCHUN et du Clustering Weighted par le test de vrais récepteurs GNSS.

Abstract

1. Introduction to the problem

This thesis focusses on the development of multipath channel reduction methods. Being given the major impact of the multipaths on the performances of satellite navigation systems in constraint environments, the calibration of new GNSS receivers requires the simulation of realistic urban propagation channels. The SCHUN simulator (*Simplified Channel for Urban Navigation*), which combines physical and statistical modeling approaches, constitutes a good tradeoff between accuracy of the multipath channel synthesized and suitable computational cost. However, such models relying on a deterministic computation of the multipath channel suffer from the high number of echoes generated to simulate complex environments (several thousand for SCHUN). Large impulse responses constraint the GNSS receivers' testing process. In the case of software receivers testing, the increase of the number of multipaths increases the time necessary to estimate the pseudo-range error induced, improving real time testing. In the case of real receivers testing, hardware signal emulators may be used. Those ones only allow the emulations of a limited number of signal echoes (usually less than 10). Thus, channel reduction methods have been implemented in order to adapt the channel models to realistic receiver's testing. They have the double objective to reduce drastically the number of multipaths of the impulse response (from thousands to less than 10) all by conserving the impact of the channel on the GNSS systems performances.

2. Implementation of multipath aggregation methods

The first considered approach is the selection of the most powerful multipaths and the elimination of the others. This method reduces significantly the delay spread of the impulse response. Therefore, aggregation methods have been investigated. Le first considered approach is the usual Tap Delay Line technique which consists in summing coherently the echoes reaching the receiver within the same delay interval. Even though preserving the channel delay profile, this method has the disadvantage to aggregate multipaths with various Doppler shifts, which may lead to the instability of the reduced channel multipaths. Therefore, it has been decided to investigate a clustering technique over the 2-dimensional delay-Doppler space. Moreover, a weighting of the centroids position depending on the power of the echoes has been added to concentrate the centroids in the high multipath power zones of the reference impulse response. This method shows good performances in terms of preservation of the power-delay and Doppler spectrum profiles. Thus, this method has been proposed to address the channel reduction problem by the multipath aggregation approach.

3. Implementation of parametric methods

Because of the fact that aggregation methods are not oriented toward the preservation of the receiver's pseudo-range error directly, it has been decided to implement a method aiming at preserving the channel correlation function. The optimization method SAGE (Space Alternating Generalized Expectation - Minimization) has been utilized to parameter the delay, Doppler shift, phase and amplitude of the reduced channel's multipaths to minimize the difference between the reference and reduced channel correlation functions. This study has revealed the major importance of the Doppler resolution of the algorithm on its performances. Thus, the Doppler resolution has been adapted to the number of multipaths of the reduced channel to optimize the preservation of the reference channel delay and Doppler characteristics. However, these parameters of the reduced

channel appear to be very discontinuous, which is likely to impact the receiver's pseudo-range error computation.

4. Implementation of a statistical method

Because of the discontinuities produced by the parametric methods, it has been decided to investigate stochastic methods of computation of the reduced channel multipaths, in order to ensure their continuity. A method extracted from the literature has been investigated first, considering that the delays, phases and amplitudes of the reduced channel evolve according to first order Markov chain. However, the application of this method to the reference channel composed of thousands of multipaths showed poor power-delay preservation performances. Thus, the original method has been modified, considering that only the delay evolve according to a first order Markov chain, the complex amplitude being deduced from the impulse response. This modification showed an amelioration of the delay preservation, but seems to be shortcoming in terms of Doppler preservation.

5. Comparative analysis of the methods in terms of GNSS performances preservation

These three types of approaches have been applied to a same reference channel in order to compare their performances in terms of pseudo-range error preservation. As a first comparison, only the impact on the discriminator open loop error has been investigated (without tracking loop and without noise), considering a simple BPSK modulation and an infinite RF bandwidth. As expected, the SAGE optimization method preserved the discriminator error at best. To the contrary, the statistical method shows significantly worst performances as compared to the two others. The clustering method has performances close to those of SAGE. Moreover, the transposition of this study to different satellite angles of arrival shows that low elevations tend to equal the performances of SAGE and clustering. As well, the increase of the number of multipaths in the reduced channel reduces the difference between these methods. The performances of the clustering overcome those of SAGE for more than 8 multipaths. In any condition, the statistical method has the worst performances according to the discriminator error preservation.

In order to investigate the impact of the tracking loops on the hierarchy of the methods established according to the discriminator error open loop criterion, the reference channel as well as the reduced ones have been applied to a software receiver simulating the tracking in function of the correlators' outputs. This hierarchy is respected, with the same conclusions concerning the number of multipaths in the reduced channel and the elevation of the emitter satellite. Similarly, other signal models (modulation and signal bandwidth) have been tested with the conservation of the same methods' hierarchy: 1) SAGE, 2) Clustering, 3) Statistical.

6. Conclusion

As a conclusion, three types of methods have been implemented, aiming at covering all possibilities of channel reduction. Even if each of these methods have been developed to optimize the preservation of the reference channel characteristics, the SAGE model still presents the drawback of the delay discontinuity and the statistical model the poor preservation of the Doppler spectrum. Finally, the comparison of the three approaches according to the pseudo-range error preservation allows eliminating the statistical method, whose performances are significantly overcome by those of SAGE and the clustering technique. SAGE has a slight advantage on the clustering. However, this advantage tends to disappear in various simulation configurations: decrease of the emitter satellite's elevation

and increase of the number of multipaths in the reduced channel. Moreover, the clustering technique has the advantage to be more efficient in terms of computational effort as compared to SAGE all by preserving better the delay and Doppler characteristics. Thus, the use of the clustering method implemented in this thesis is preconized to address the multipath channel reduction problem.

Résumé

1. Introduction à la problématique

Ce travail de thèse porte sur le développement de méthodes de réduction du canal de multitrajets. Etant donné l'importance de l'impact des multitrajets sur les performances des systèmes de navigation par satellite en milieu contraint, le calibrage des nouveaux récepteurs GNSS nécessite la simulation de modèles réalistes de canal de propagation urbain. Le simulateur de canal SCHUN (*Simplified Channel for Urban Navigation*), qui allie approche physique et statistique de modélisation, constitue un bon compromis entre réalisme du canal de multitrajets synthétisé et temps de calcul raisonnable. Cependant, de telles modèles reposant sue une modélisation déterministe du canal de multitrajets ont le désavantage de générer de nombreux échos afin de simuler des environnements complexes (plusieurs milliers pour SCHUN par exemple). De trop grandes réponses impulsionnelles sont une contrainte dans la réalisation du calibrage des récepteurs GNSS. Dans le cas du test de récepteurs logiciels, le temps nécessaire à l'intégration de tous les échos du canal pour estimer l'erreur des boucles de poursuite augmente avec le nombre de multitrajets fournis en entrée, empêchant le test en temps réel. Dans le cas du test de récepteurs réels, des émulateurs de signaux « hardware » peuvent être utilisés. Ceux-ci ne permettent de simuler qu'un nombre limité de multitrajets (généralement inférieur à 10). C'est afin de rendre les modèles de réponse impulsionnelle adaptables au test réaliste de récepteurs que des méthodes de réduction du canal ont été implémentées. Elles ont donc le double objectif de réduire drastiquement le nombre de multitrajets des réponses impulsionnelles (de plusieurs milliers à moins de 10) tout en préservant l'impact du canal sur les performances des systèmes GNSS.

2. Implémentation de méthodes d'agrégation de multitrajets

La première approche testée est la sélection des multitrajets les plus puissants et l'élimination des autres. Cette méthode réduit considérablement l'étalement de retard de la réponse impulsionnelle. Ainsi, des méthodes d'agrégation ont été étudiées. La première approche considérée est la méthode usuelle Tap Delay Line, qui consiste à sommer de façon cohérente tous les échos arrivant dans un même intervalle de temps. Cette méthode, si elle conserve bien le profil de retard de la réponse impulsionnelle, a le désavantage d'agréger des multitrajets avec des Dopplers très différents, ce qui a pour conséquence la discontinuité des paramètres des multitrajets du canal réduit. Ainsi, il a été décidé de s'orienter vers une méthode de clustering des multitrajets dans l'espace à deux dimensions retard-Doppler. De plus, une pondération des centroïdes des clusters dépendant de la puissance des échos a été ajoutée pour influencer la concentration des multitrajets du canal réduit dans les zones de puissance du canal de référence. Cette méthode montre de bonnes performances en termes de préservation des profils puissance-retard et spectre Doppler des réponses impulsionnelles. C'est donc cette méthode qui a été proposée pour répondre à la problématique de réduction du canal par l'approche d'agrégation de multitrajets.

3. Implémentation de méthodes paramétriques

Etant donné que les méthodes d'agrégation d'échos sont orientées envers la préservation des caractéristiques de retard et Doppler du canal et non directement l'erreur de pseudo-distance du récepteur, il a été envisagé d'implémenter une méthode orientée envers la conservation de la fonction d'autocorrélation du canal. La méthode d'optimisation SAGE (Space Alternating Generalized

Expectation - Minimization) a été utilisée afin de paramétrer le retard, le Doppler, la phase et l'amplitude des multitrajets du canal réduit pour minimiser la différence entre la fonction de corrélation du canal de référence et du canal réduit. Cette étude révèle la grande importance de la résolution Doppler offerte à l'algorithme d'optimisation et ses performances. Ainsi, cette résolution Doppler a été adaptée au nombre de multitrajets du canal réduit pour optimiser la préservation des profils de retard et Doppler du canal de référence. Cependant, ces paramètres du canal réduit s'avèrent être très discontinus, ce qui est susceptible d'impacter le calcul d'erreur de pseudo-distance du récepteur.

4. Implémentation d'une méthode statistique

Etant donné les discontinuités produites par les méthodes paramétriques, il a été décidé de s'orienter vers des méthodes stochastiques de calcul des paramètres des multitrajets du canal réduit, afin d'assurer leur continuité. Une méthode de la littérature a été étudiée en premier lieu, considérant que le retard, l'amplitude et la phase des multitrajets évoluent selon une chaîne de Markov du premier ordre. Cependant, l'application de cette méthode à un canal de référence composé de plusieurs milliers de sources de multitrajets a montré des limites significatives en termes de préservation du profile de puissance-retard des multitrajets. Ainsi, une modification a été apportée à la méthode d'origine, considérant désormais que seul le retard des multitrajets suit une évolution stochastique, l'amplitude et la phase pouvant être déduites du retard à partir de la réponse impulsionnelle. Cette modification a montré une amélioration de la préservation du profile de retard du canal, mais semble être insuffisante pour préserver les caractéristiques Doppler.

5. Analyse comparative des méthodes en termes de préservation des performances GNSS

Ces trois types de méthodes ont été appliqués à un même canal de référence afin de comparer leurs performances en termes de préservation de l'erreur de pseudo-distance. Dans un premier, le seul impact sur l'erreur du discriminateur en boucle ouverte a été étudié (sans l'effet des boucles de poursuite ni du bruit), considérant une simple modulation BPSK et une bande RF infinie. Comme attendu, c'est la méthode d'optimisation SAGE qui préserve au mieux l'erreur discriminateur. Au contraire, la méthode statistique montre des performances significativement moins bonnes que les deux autres méthodes. La méthode de clustering a des performances proches de celles de SAGE. De plus, la transposition de cette étude sous différents angles d'arrivée du signal satellitaire montre qu'en basse élévation, les performances de ces deux méthodes tendent à converger. De plus, cette étude a été transposée à différents nombre de multitrajets dans le canal réduit. Il apparaît la encore que plus on autorise de multitrajets, moins la différence entre SAGE et clustering est significative, les performances de ce dernier dépassant même celles de SAGE pour plus de 8 multitrajets dans le canal réduit. Dans tous les cas la méthode statistique a les pires performances selon le critère de préservation de l'erreur discriminateur.

Afin d'étudier l'impact des boucles de poursuite sur la hiérarchie des méthodes établie selon le critère de l'erreur discriminateur boucle ouverte, le canal de référence ainsi que les différents canaux de multitrajets réduits ont été appliqués à un récepteur logiciel simulant la poursuite en fonction des valeurs des sorties de corrélateur. Cette hiérarchie semble être respectée, avec les mêmes conclusions concernant le nombre de multitrajets du canal réduit et l'élévation du satellite émetteur. De même, d'autres modèles de signaux (modulation et bande du signal) ont été testés avec toujours la conservation de la hiérarchie des méthodes : 1) SAGE, 2) Clustering, 3) Statistique.

6. Conclusion

En conclusion, trois types de méthodes ont été implémentés, visant à couvrir l'ensemble des possibilités en termes de réduction du canal de multitrajets. Bien que chacune de ces méthodes a été développée dans le but d'optimiser la préservation des caractéristiques du canal de référence, le modèle SAGE présente toujours le désavantage de la discontinuité du retard des multitrajets et le modèle statistique la non préservation du spectre Doppler. Finalement, la comparaison des trois approches selon la préservation de l'erreur de pseudo-distance du récepteur GNSS permet d'éliminer la méthode statistique dont les performances sont largement dépassées par celles du clustering et de SAGE. Cette dernière semble avoir un avantage sur le clustering. Cependant cet avantage tend à se réduire dans certaines conditions de simulation : diminution de l'élévation du satellite émetteur ou augmentation du nombre de multitrajets du canal réduit. De plus, la méthode du clustering a l'avantage d'être significativement plus efficace en termes de temps de calcul que SAGE tout en préservant mieux les caractéristiques retard et Doppler du canal. Ainsi, l'utilisation de la méthode de clustering implémentée dans cette thèse est préconisée pour répondre à la problématique de réduction du canal de multitrajets.

Bibliography

[Abel 08] A. Abele, F. Perez Fontan, M. Bousquet, P. Valtr, J. Lemorton, L. Castanet, F. Lacoste and E. Corbel, "*A physical-statistical model of the propagation channel for land mobile satellite systems*", ESA workshop on propagation, Noordwijk, The Netherlands, Dec. 2008.

[Abel 09] A. Abele, "*Modélisation du Canal de Propagation par Satellite dans les Bandes L, S et C*", PhD thesis, Institut supérieur de l'aéronautique et de l'espace, Dec. 2009.

[Ait 11] M. Ait-Ighil, S. Rougerie, J. Lemorton, G. Carrie, G. Artaud, C. Bourga, and M. Bousquet, "*Channel Modelling in Complex Urban Environments for Testing Multipath Mitigation Methods Enhanced by Antenna Array*". pp. 1-9, ESA/ESTEC, Noordwijk, The Netherlands, Dec. 2011.

[Ait 12] M. Ait-Ighil, J. Lemorton, F. Perez-Fontan, F. Lacoste, G. Artaud, C. Bourga and M. Bousquet, "*Simplifying the Propagation Environment Representation for LMS Channel Modelling*", EURASIP Journal on Wireless Communications and Networking 2012, March 2012.

[Ait 13] Mehdi Ait-Ighil , "*Enhanced Physical-Statistical Simulator of the Land Mobile Satellite Channel for Multipath modelling applied to Satellite navigation Systems*", PhD Thesis University of Toulouse 2013.

[Antr 08] F. Antreich, J. A. Nossek, W. Utschick, "*Maximum likelihood delay estimation in a navigation receiver for aeronautical applications*", Science Direct 2008.

[Arta 08] G. Artaud, L. Ries, Y. Gregoire, M. Jeannot, J. Dantepal, and D. Zobler, "*GNSS receiver test bench*", ENC GNSS, Toulouse Space Show 2008, Toulouse, France, Apr. 2008.

[Arta 10] G. Artaud, A. Latour, J. Dantepal, N. Maury, J.C. Denis, E. Senant, T. Bany, "*A new GNSS multi constellation simulator: NAVYS*", 2010 5th ESA Workshop on Satellite Navigation Technologies and European Workshop on GNSS Signals and Signal Processing (NAVITEC).

[Bala 89] C. A. Balanis, "*Advanced Engineering Electromagnetics*" John Wiley and Sons (WIE), July 1989.

[Bell 63] P. A. Bello, "*Characterization of Randomly Time-Variant Linear Channels*", IEEE 1963.

[Broc 14] P. Brocard, D. Salos, O. Julien, M. Mabilleau, "*Performance Evaluation of Multipath Mitigation Techniques for Critical Urban Applications Based on a Land Mobile Satellite Channel Model",* Position, Location and Navigation Symposium - PLANS 2014, 2014 IEEE/ION .

[Capo 69] J. Capon, "*High-resolution frequency-wavenumber spectrum analysis*", in Proc. IEEE, 01.57, pp. 1408-1418, August 1969

[Chun 01] P. J. Chung, J. F. Bohme, "*Comparative Convergence Analysis of EM and SAGE algorithms in DOA Estimation*", IEEE Transactions on Signal Processing, 2001, vol. 49, no 12, p. 2940-2949.

[Chun 02] P. J. Chung, J. F. Bohme, "*Experimental Study of the EM and SAGE algorithms with application to sonar radar*", in sensor array and multichannel signal processing workshop proceedings. Rosselyn (USA), 2002, p.77-81.

[COST 02] COST255 "*Cost Action 255 - Radiowave Propagation Modelling for SatCom Services at Ku-Band and Above*", R.A. Harris, final report Ed., March 2002.

[Czin 05] N. Czink, P. Cera, J. Salo, E. Bonek, J.P. Nuutinen, J. Ylitalo, " *Automatic Clustering of MIMO Channel Parameters using the Multipath Component Distance Measure* ", WPMC 2005.

[Czin 06a] N. Czink, P. Cera, J. Salo, E; Bonek, J.P. Nuutinen, J. Ylitalo, "*A Framework for Automatic Clustering of Parametric MIMO Channel Data Including Path Powers*", IEEE 2006.

[Czin 06b] N. Czink, P. Cera, J. Salo, E. Bonek, J-P. Nuutinen, J. Ylitalo, "*Improving Clustering Performance using Multipath Component Distance"*, Electronic Letters Vol. 42 No. 1, January 2006.

[Czin 07] N. Czink, et al., "*Tracking Time-Variant Cluster Parameters in MIMO Channel* Measurments", Second International Conference in Communications and Networking in China, 2007.

[Fess 94] J. A. Fessler, "*Space-Alternating Generalized",* IEEE Transactions on signal processing, vol.42, n°10, October 1994.

[Fleu 99] B. H. Fleury, M. Tschudin, R. Heddergott, D. Dahlhaus, K. Ingeman Pedersen, *" Channel Parameter Estimation in Radio Environments using the SAGE algorithm*", IEEE Journal On Selected Areas In Communications, Vol. 17, No. 3, March 1999.

[Garc 10] J. A. Garcia-Molina, F. Zanier, M. Crisci, R. Prieto-Cerdeira, P. Giordano, A. Steingass, A. Hornbostel, "*Land Mobile Multipath Channel Reduction Effects on a Real GNSS Receiver*", Navitech 2010, ESA/ESTEC, Noordwijk.

[ITU 07] ITU, "*ITU-R P.833-6 Attenuation in vegetation*", Attenuation in vegetation ITU-R, P.833-6, ITU, Jan. 2007.

[ITU 13] ITU, "*Report ITU-R P.2145: Model Parameters for an Urban Environment for the Physical-Statistical wideband LMSS model",* in Recommendation ITU-R P.681-686".

[ITU 15] ITU, "Propagation data required for the design of Earth-space land mobile telecommunication systems", in recommendation ITU-R P.681-8, 2015.

[Jahn 96] A. Jahn, H. Bischl, and G. Heiss, "*Channel characterization for spread spectrum satellite communications*". In: Spread Spectrum Techniques and Applications Proceedings, IEEE 4th International Symposium on, pp. 1221-1226 vol.3, 1996.

[Jahn 01] A. Jahn "*Propagation considerations and Fading countermeasures for Mobile Multimedia Services*", International Journal of Satellite Communications, Vol. 19, No. 3, pp. 223-250, 2001.

[Jain 88] A. K. Jain, R. C. Dubes, "*Algorithms for Clustering Data*", Prentice Hall, 1988.

[Jul 13] Olivier Julien, "*Concepts Avancés du GNSS*", IENAC 3rd year lecture 2013/2014.

[Kay 93] S. M. Kay, "*Fundamentals of Statistical Signal Processing – Estimation Theory*". Prentice Hall Signal Processing Series, Prentice Hall, New Jersey, 1993.

[Kolu 03] Janne Kolu, Tomi Jämsä, Ari Hulkkonen, "Real Time Simulation of Measured Radio Channels", IEEE 2003.

[Krac 08] Bernhard Krach, Geraldine Artaud, "*Performance Assessment of Navigation Signals in Realistic Multipath Environment*", 4th ESA Workshop on Satellite Navigation User Equipment Technology-Navitech 2008.

[Laco 10] F. Lacoste, F. Carvalho, F. P. Fontan, A. N. Fernandez, V. Fabbro, and G. Scot, "*MISO and SIMO measurements of the Land Mobile Satellite propagation channel at S-band*". 2010 Proceedings of the Fourth European Conference on Antennas and Propagation (EuCAP), pp. 1 -5, Apr. 2010.

[Lehn 07] A. Lehner and A. Steingass, "*Time Series Multipath Modeling of Suburban Environments in Land mobile Satellite Navigation*", Antennas and Propagation, EuCAP 2007. The Second European Conference on, pp. 1-7.

[Lehn 08] A. Lehner and A. Steingass, "*Differences in Multipath propagation between urban and suburban environments*". 4th ESA Workshop on Satellite Navigation User Equipment Technologies NAVITEC 2008, Noordwijk, The Netherlands,, Dec. 2008.

[Lent 07] M. Lentmaier, B. Krach, P. Robertson, T. Thiasiriphet, "*Dynamic Multipath Estimation by Sequential Monte Carlo Methods*", in Proceedings of the 20th International Technical Meeting of the Institute of Navigation Satellite Division (ION GNSS 2007), Fort Worth, Texas, USA, Sept. 2007, pp. 1712-1721.

[Li 10] X. Li, "*Un modèle hybride statistique-déterministe du canal LMS en environnements complexes*". PhD thesis, University of Poitiers, Poitiers, France, Dec. 2010.

[Lutz 91] E. Lutz, "*The land mobile satellite communication channel-recording, statistics and channel model*", IEEE transactions on Vehicular Technologies, Vol. 40 n°2, May 1991, pp.375-385.

[Lutz 96] E. Lutz, "*A Markov Model for Correlated Land Mobile Land Mobile Satellite Channels*", International Journal of Satellite Communications, Vol. 14, No. 4, pp. 333-339, 1996.

[Maul 12] U. Maulik, "*Performance Evaluation of some Clustering Algorithms and Validity Indices*", IEEE 2012.

[McKa 03] D. J.C. McKay, "Maximum Likelihood and Clustering", Draft 3.1415 January 2003.

[McNa 90] D. A. McNamara and C. W. I. Pistotius, "*Introduction to the Uniform Geometrical Theory of Diffraction*", Artech Print on Demand, Jan. 1990.

[Mehl 08] C. Mehlführer, M. Rupp, "*Approximation and Resampling of Tapped Delay Line Channel Models with guaranteed Channel Properties*", IEEE 2008.

[Milo 09] M. Milojevic, M. Haardt, E. Eberlein, A. Heuberger, "*Channel Modelling for Multiple Satellite Broadcasting Systems*", Broadcasting, IEEE Transactions, Vol.55, No .4, pp. 705-718, 2009.

[Misr 05] P. Misra, P. Enge, "*Global Positioning System: signal, measurement and performance*".

[Mota 10] S. Mota, M. Outeiral Garcia, A. Rocha, F. Pérez-Fontàn, « *Estimation of the Radio Channel Parameters using the SAGE algorithm* », Radioengineering, Vol. 19, No. 4, December 2010.

[Mota 11] S. Mota, M. Outeiral Garcia, A. Rocha, F . Pérez-Fontan, "*Clustering of the Multipath Radio Channel Parameters"* , EuCAp 2011.

[Mota 13] S. Mota, F. Pérez-Fontan, A. Rocha, *" Estimation of the Number of Clusters in Multipath Radio Channel Data Sets* " IEEE 2013.

[Oest 00] C. Oestges, "Propagation Modelling of Low Earth-Orbit Satellite Personal Communication Systems", PhD thesis, Université de Louvain la Neuve, Belgium, Dec. 2000.

[Pede 97] K. Pedersen, B. Fleury, and P. Mogensen, "*High resolution of electromagnetic waves in time-varying radio channels*", in Proc. 8th IEEE Int. Symp. Personal, Indoor and Mobile Radio Communications (PIMRC '97), Helsinki Finland, Sept. 1997.

[Pere 01] F. Perez Fontan, M. Vasquez Castro, C. Cabado, J. Garcia, E. Kubista, "*Statistical modeling of the LMS channel*", Vehicular Technology IEEE Transactions on, Vol. 50, No.6, pp. 1549-1567, 2001.

[Pere 05] F. Perez-Fontan, S. Martinez, B. Sanmartin, C. Enjamio, P. Marino and F. Machado, "*An enhanced Markov chain based model for the narrow-band LMS channel in built up area*", International Journal of Satellite Communication Network, 2005, n°23, pp.111-128.

[Rib 15] F. Ribaud, M. Ait-Ighil, J. Lemorton, O. Julien, F. Perez-Fontan, F. Lacoste, S. Rougerie, "*Comparison of different methods to aggregate multipaths for GNSS receivers performance assessment*", ENC 2015, Bordeaux, France.

[Rib 16a] F. Ribaud, M. Ait-Ighil, S. Rougerie, J. Lemorton, O. Julien, F. Pérez-Fontan, "*Reduction of the Multipath Channel Impulse Response for GNSS applications*", EuCAP 2016, Davos, Switzerland.

[Rib 16b] F. Ribaud, M. Ait-Ighil, S. Rougerie, J. Lemorton, O. Julien, F . Pérez-Fontan, "*Reduced multipath channel modelling preserving representative GNSS receiver testing",* ION GNSS+2016, Portland, USA.

[Roug 12a] S. Rougerie, "*Algorithmes de diversité d'antennes appliqués à la réception des signaux GNSS en environnement urbain et sur terminal mobile*", University of Toulouse PhD Thesis, 2012.

[Roug 12b] S. Rougerie, G. Carrie, L. Ries, F. Vincent, M. Monnerat, "*A new Multipath Mitigation Method for GNSS Receivers based on an Antenna Array*", International Journal of Navigation and Observation, Volume 2012.

[Roy 89] R. Roy, T. Kailath, "*ESPRIT-Estimation of Signal Parameters Via Rotational Invariance Techniques*", IEEE transactions on acoustics, speech, and signal processing. Vol. 37. No. 7, July 1989.

[Ruck 70] G. T. Ruck, D. E. Barrick, W. D. Stuart, and C. K. Krichbaum, "*Radar Cross Section Handbook, Volumes 1 & 2*", Plenum, 1 Ed., Jan. 1970.

[Sale 87] A. Saleh and R. Valenzuela, “*A Statistical Model for Indoor Multipath Propagation*”, Selected Areas in Communications, IEEE Journal on, Vol. 5, No. 2, pp. 128-137, 1987.

[Salo 05] J. Salo, J. Salmi, N. Czink, P. Vainikainen, “*Automatic Clustering of Nonstationary MIMO Channel Parameter Estimates*”, ICT 2005.

[Satn 08] Satnex, “*Influence of the Variability of the Propagation Channel on Mobile, Fixed MultiMedia and Optical Satellite Communications*”, Laurent Castanet, ONERA, France, Jan. 2008.

[Schm 86] R. O. Schmidt, “*Multiple Emitter Location and Signal Parameter Estimation*”, IEEE transactions on antennas and propagation, vol. ap-34, no. 3, March 1986.

[Scot 92] D. W. Scott, “*Multivariate Density Estimation: Theory, Practice and Visualization*”, John Wiley and Sons Inc., 1992.

[Schu 14] F. M. Schubert, M. Heimerl, J. Wendel “*Components Count Decrease of Channel Responses Using Markov Process*”, 7th ESA Workshop on Satellite Navigation Technologies, Navitech 2014.

[Shut 04] D. Shutin, G. Kubin, “*Cluster Analysis of Wireless Channel Impulse Responses with Hidden Markov Models*”, IEEE 2004.

[Silv 03] João Carlos Silva, Nuno Souto, A. Rodrigues, Francisco Cercas, Américo Correia, “*Conversion of the reference tapped delay line channel models to discrete time channel models*”, IEEE 2003.

[Skla 97] B. Sklar, Communication Engineering Services, “*Rayleigh Fading Channels in Mobile Digital Communication Systems Part. 1 : Characterization*”, IEEE Communication Magazine, 1997.

[Soud 02] P. Soudais, P. Leca, J. Simon, and T. Volpert, “*Computation of the scattering from inhomogeneous objects with a discrete rotational symmetry and a non-symmetric part*", IEEE Transactions on Antennas and Propagation, Vol. 50, No. 2, pp. 168-174, Feb. 2002.

[Stei 02] M. Steinbauer, H. Özcelik, H. Hofstetter, C. MecklenbrAûker, E. Bonek, “*How to Quantify Multipath Separation*”, IEICE Trans. Electron., vol. E85, no. 3, pp. 552-557, March 2002.

[Tepe 03] C. Tepedelenlioglu, A. Abdi, G. Giannakis, “*The Ricean K Factor: estimation and performance analysis”*, Wireless communications, IEEE transactions on, Vol. 2, No. 4, pp. 799-810, 2003.

[Tou 74] J. T. Tou, R. C. Gonzales, “*Pattern Recognition Principles*”, Reading: Addison-Wesley, 1974.

[VanD 92] A. J. van Dierendonck, P. Fenton, T. Ford, ‘‘*Theory and Performance of Narrow Correlator Spacing in a GPS Receiver*”, Journal of The Institute of Navigation, Vol. 39, No.3 Fall 1992.

[VanN 94] R.D.J. van Nee, J. Siereveld, P.C. Fenton, R. Townsend, “*The Multipath Estimating Delay Lock Loop: Approaching Theoretical Accuracy Limits*”, Position Location and Navigation Symposium IEEE 1994.

[VanT 04] L. Van Trees, "*Optimum Array Processing, Part IV of Detection, Estimation and Modulation Theory*", 2004.